

AN IN SITU STUDY OF CYTOCHROME BD: A
UBIQUINOL OXIDASE OF 'ESCHERICHIA COLI'

Richard A. Rothery

A Thesis Submitted for the Degree of PhD
at the
University of St Andrews



1989

Full metadata for this item is available in
St Andrews Research Repository
at:

<http://research-repository.st-andrews.ac.uk/>

Please use this identifier to cite or link to this item:

<http://hdl.handle.net/10023/14392>

This item is protected by original copyright

An *in situ* study of Cytochrome *bd*:
A Ubiquinol Oxidase of *Escherichia coli*.

By

Richard A. Rothery

University of St. Andrews
Department of Biochemistry and Microbiology
North Street
St. Andrews
Fife
SCOTLAND



ProQuest Number: 10166387

All rights reserved

INFORMATION TO ALL USERS

The quality of this reproduction is dependent upon the quality of the copy submitted.

In the unlikely event that the author did not send a complete manuscript and there are missing pages, these will be noted. Also, if material had to be removed, a note will indicate the deletion.



ProQuest 10166387

Published by ProQuest LLC (2017). Copyright of the Dissertation is held by the Author.

All rights reserved.

This work is protected against unauthorized copying under Title 17, United States Code
Microform Edition © ProQuest LLC.

ProQuest LLC.
789 East Eisenhower Parkway
P.O. Box 1346
Ann Arbor, MI 48106 – 1346

TK A 978

DECLARATION

I, Richard A. Rothery, hereby certify that this thesis has been composed by myself, that it is a record of my own work, and that it has not been accepted in partial or complete fulfilment of any other degree of professional qualification.

Signed.....Date. 28./04/89

I was admitted to the Faculty of Science of the University of St. Andrews under Ordinance General N^o. 12 on 1st October 1985 and as a candidate for the degree of PhD on 13th February 1986.

Signed.....Date. 28./04/89

CERTIFICATE

I hereby certify that the candidate has fulfilled the conditions of the Resolution and Regulations appropriate to the degree of Ph.D.

Signature of Supervisor.....Date..28/4/89

COPYRIGHT

In submitting this thesis to the University of St. Andrews I understand that I am giving permission for it to be made available for use in accordance with the regulations of the University Library for the time being in force, subject to any copyright vested in the work not being affected thereby. I also understand that the title and abstract will be published, and that a copy of the work may be made and supplied to any *bona fide* library or research worker.

ACKNOWLEDGEMENTS

I would like to thank my supervisor, John Ingledew, for his help and guidance throughout my period of study in St. Andrews. Thanks are also due to my supervisor's other research students, Alan Moodie, Darshan Wariabharaj, and Mark Bacon for helpful discussions during the course of this work. I would also like to thank Professor John Salerno for his help during his stay in St. Andrews in the latter half of 1988. Thanks are also due to Alex Houston for his technical endeavours.

ABSTRACT

An *in situ* study was conducted of the cytochrome *bd* ubiquinol: oxygen oxidoreductase (cytochrome *b₅₅₈-b₅₉₅-d*) of *Escherichia coli* grown anaerobically on glycerol with fumarate as respiratory oxidant.

Nitrite reacts with and is reduced by the oxidase, resulting in the formation of NO adducts to haems *b₅₉₅* and *d*. The kinetics of formation of these species indicate that the affinity of haem *d* for nitrite is higher than that of haem *b₅₉₅*. CO also binds to the oxidase, resulting in the formation of CO adducts to haems *d* and *b₅₉₅*. Binding titrations indicate that the affinity of haem *d* for CO is higher than that of haem *b₅₉₅*. The steady state kinetics of the oxidase reaction in the presence of nitrite or CO are cooperative with respect to oxygen binding, suggesting that both haems *d* and *b₅₉₅* are involved in the reduction of oxygen.

E.p.r. studies of the ferric oxidase indicate the presence of two high spin haem signals, one rhombic and one axial, which are assigned to haems *b₅₉₅* and *d*, respectively. These signals titrate potentiometrically with midpoint potentials similar to those published on the basis of optically followed titrations for haems *b₅₉₅* and *d*. The high spin ferric haem spectra are affected by oxygen, CO, cyanide, and pH. A low spin ferric haem signal is observed at $g=3.3$ and is assigned to haem *b₅₅₈*.

The sidedness with respect to the cytoplasmic membrane of ligand binding haems of the oxidase was determined by investigating the

effect of the exogenous paramagnetic probe DyEDTA on the e.p.r. properties of the ferrous haems *d*-NO and *b*₅₉₅-NO. These haems are located towards the inner aspect of the cytoplasmic membrane at around 8 and 12Å° below the surface, respectively.

Overall, the data supports a functional model for cytochrome *bd* with two oxygen binding sites, haems *d* and *b*₅₉₅, forming the binuclear centre of the oxidase reaction. Possible mechanisms of this reaction are discussed.

ABBREVIATIONS

ATP	-	Adenosine 5'-triphosphate
Bes	-	N,N-bis[2-Hydroxyethyl]-2-aminoethanesulphonic acid
DMSO	-	Dimethyl sulphoxide
EDTA	-	Ethylenediaminetetraacetic acid
E.p.r.	-	Electron paramagnetic resonance
M.c.d.	-	Magnetic circular dichroism
Mes	-	2-[N-Morpholino]ethanesulphonic acid
NADH	-	Nicotinamide adenine dinucleotide
SDS	-	sodium dodecyl sulphate
Tes	-	N-tris[Hydroxymethyl]methyl-2-aminoethanesulphonic acid
TMAO	-	Trimethylamine N-oxide
TMPD	-	N,N,N',N'-tetramethyl-p-phenylene diamine
Tricine	-	N-tris[Hydroxymethyl]-methylglycine

CONTENTS

Declaration.	i
Certificate.	ii
Copyright declaration.	iii
Acknowledgements.	iv
Abstract.	v
Abbreviations.	vii
Contents.	viii
List of figures and tables.	xiv
1. GENERAL INTRODUCTION	1
1.1. The respiratory chain of <i>Escherichia coli</i> .	2
1.2. The ubiquinol oxidases of <i>E.coli</i> .	3
1.3. Distribution of cytochromes <i>bd</i> and <i>b₅₆₂-o</i> in bacteria other than <i>E.coli</i> .	9
1.4. The cytochrome <i>bd</i> complex.	10
1.4.1. Subunit and haem composition.	10
1.4.2. Chemiosmotic aspects.	14
1.4.3. Quinol binding and its oxidation.	15
1.4.4. Orientation of the subunits and haems in the cytoplasmic membrane.	17
1.4.5. Optical spectroscopy.	19
1.4.6. Electron paramagnetic resonance spectroscopy.	24
1.4.7. Ligand binding by cytochrome <i>bd</i> .	26
1.4.7.1. Oxygen and peroxide.	26
1.4.7.2. Carbon monoxide.	29

1.4.7.3.	Low temperature flash photolysis and ligand exchange experiments.	32
1.4.7.4.	Cyanide.	35
1.4.7.5.	Nitric oxide and nitrite.	36
1.4.8.	Redox potentiometry.	37
1.4.9.	The redox cycle of the oxidase reaction.	42
1.5.	The cytochrome $b_5 62-0$ complex.	44
1.5.1.	Subunit and haem composition.	44
1.5.2.	Chemiosmotic aspects.	45
1.5.3.	Optical spectroscopy.	46
1.5.4.	Electron paramagnetic resonance spectroscopy.	47
1.5.5.	Redox potentiometry.	48
1.6.	Research objectives.	48
2.	MATERIALS AND METHODS.	50
2.1.	Organisms.	51
2.2.	Growth media.	51
2.2.1.	Glycerol-fumarate medium.	51
2.2.2.	Sucrose medium.	53
2.2.3.	Nutrient broth and nutrient agar.	53
2.2.4.	Trace elements solution.	54
2.3.	Cell growth.	54
2.3.1.	Anaerobic growth of <i>E.coli</i> EMG2.	54
2.3.2.	Aerobic growth of <i>E.coli</i> FUN4/pNG2.	54
2.3.3.	Aerobic growth of <i>E.coli</i> RG145.	55
2.4.	Cell harvesting.	55

2.5.	Isolation of cytoplasmic membranes.	56
2.6.	Assays.	57
2.6.1.	Determination of protein.	57
2.6.2.	Determination of nitrite reductase activity.	57
2.6.3.	Assay for oxidase activity.	59
2.7.	Spectrophotometry.	60
2.8.	Sample preparation for e.p.r.	60
2.9.	Preparation of DyEDTA/LaEDTA solutions.	60
2.10.	Redox titrations.	61
2.11.	E.p.r. spectroscopy.	62
2.12.	E.p.r. spectra simulation and double integration.	62
2.13.	Chemicals.	63
2.14.	Development of a data collection and analysis system for a Clark type oxygen electrode.	63
2.14.1.	Introduction.	63
2.14.2.	The microcomputer interface.	66
2.14.2.1.	Data collection using the internal ADC.	66
2.14.2.2.	Data collection using the custom built ADC.	68
2.14.3	Calibration of oxygen concentrations.	68
2.14.4.	Simulations of oxygen electrode traces.	69
2.14.5.	Differentiation of progress curves.	70
2.14.6.	Noise.	71
2.14.7.	Data analysis.	75
2.14.8.	Higher derivatives.	80
2.14.9.	Applications of the oxygen electrode interface.	85
2.15.	Other methods.	85

3.	REACTIONS OF THE <i>IN SITU</i> CYTOCHROME <i>BD</i> WITH NITRITE AND OXYGEN.	86
3.1.	Introduction.	87
3.2.	The cytochromes present in membranes from anaerobically grown <i>E.coli</i> EMG2.	88
3.3.	Changes in the optical absorption spectrum of cytochrome <i>bd</i> elicited by nitrite.	90
3.4.	Kinetics of the nitrite induced spectral change at 630nm.	91
3.5.	Kinetics of the nitrite induced Soret change.	95
3.6.	Nitrite reductase activity of membranes containing cytochrome <i>bd</i> .	96
3.7.	The pH dependence of the oxidase reaction.	99
3.8.	The effect of nitrite on oxygen consumption in membranes.	99
3.9.	Conclusions.	108
4.	FORMATION AND SPECTROSCOPY WITH RESPECT TO THE CYTOPLASMIC MEMBRANE OF E.P.R. DETECTABLE NITROSYL CYTOCHROME <i>BD</i> .	115
4.1.	Introduction.	116
4.2.	Formation of nitrosyl cytochrome <i>bd</i> .	119
4.3.	Temperature and microwave power dependence of the nitrosyl cytochrome <i>bd</i> e.p.r. signals.	125
4.4.	Use of dysprosium as an exogenous paramagnetic probe.	132

4.5.	Dysprosium effect on the nitrosyl cytochrome <i>bd</i> spectrum.	137
4.6.	The nitrosyl haem spectrum of nitrite treated whole cells.	143
4.7.	The effect of DyEDTA on the whole cell nitrosyl haem spectrum.	143
4.8.	Conclusions.	147
5.	ELECTRON PARAMAGNETIC RESONANCE SPECTROSCOPY OF THE <i>IN SITU</i> OXIDISED CYTOCHROME <i>BD</i> .	150
5.1.	Introduction.	151
5.2.	E.p.r. of oxidised <i>in situ</i> cytochrome <i>bd</i> .	154
5.3.	E.p.r. spectra of high spin haems.	154
5.4.	Redox potentiometry of the e.p.r. signals.	158
5.5.	Simulation of the anoxically oxidised spectrum around $g=6.0$.	162
5.6.	Effect of oxygen on the high spin ferric haem signals around $g=6.0$.	162
5.7.	Effect of carbon monoxide and cyanide.	166
5.8.	Effect of pH on the high spin spectrum.	168
5.9.	E.p.r. spectra of membranes from <i>E.coli</i> FUN4/pNG2.	168
5.10.	Assignments of the ferric haem e.p.r. signals to the components of cytochrome <i>bd</i> .	173
5.11.	Conclusions.	175

6.	REACTIONS OF THE <i>IN SITU</i> CYTOCHROME <i>BD</i> WITH CARBON MONOXIDE AND OXYGEN.	178
6.1.	Introduction.	179
6.2.	Carbon monoxide binding to cytochrome <i>bd</i> .	180
6.3.	Titration of the optical changes in the haem <i>d</i> alpha region elicited by CO.	182
6.4.	Titration of the optical changes in the Soret elicited by CO.	186
6.5.	Effect of carbon monoxide on oxygen consumption in membranes.	190
6.6.	Effect of CO on the cooperativity of the oxidase reaction catalysed by cytochrome <i>bd</i> .	193
6.7.	Use of higher derivatives of oxygen electrode progress curves to analyse the oxidase reaction catalysed by cytochrome <i>bd</i> .	199
6.8.	Conclusions.	201
7.	DISCUSSION.	207
7.1.	Ligand binding to haems <i>d</i> and <i>b₅₉₅</i> .	208
7.2.	The arrangement of the oxidase in the cytoplasmic membrane.	209
7.3.	Potential models for the oxidase reaction.	211
7.4.	Future prospects.	216
	BIBLIOGRAPHY.	218

LIST OF FIGURES AND TABLES

CHAPTER ONE

Figure 1.1	Aerobic respiration and the mechanism of formation of the proton electrochemical potential in <i>E.coli</i> .	3
Figure 1.2	Structural model of cytochrome <i>bd</i> and the orientation of its components in the cytoplasmic membrane	20
Figure 1.3	Reduced <i>minus</i> oxidised spectra of cells containing cytochrome <i>bd</i> and cytochrome <i>b₅₆₂-o</i> .	21
Figure 1.4	Resolved spectra of the haem components of cytochrome <i>bd</i> .	23
Figure 1.5	Oxygen reduction model for cytochrome <i>bd</i> .	43
Table 1.1	Enzymatic properties of cytochrome <i>bd</i> and cytochrome <i>b₅₆₂-o</i> . I. Substrate affinities.	5
Table 1.2	Enzymatic properties of cytochrome <i>bd</i> and cytochrome <i>b₅₆₂-o</i> . II. Inhibitor affinities.	7
Table 1.3	Molecular weights of cytochrome <i>bd</i> and cytochrome <i>b₅₆₂-o</i> .	11
Table 1.4	Midpoint potentials of the haem components of the <i>E.coli</i> aerobic respiratory chain.	38

CHAPTER TWO

Figure 2.1	Standard curves for protein and nitrite	
------------	---	--

	determinations.	58
Figure 2.2	Noise averaging differentiating algorithm.	72
Figure 2.3	Comparison of the noise limiting properties of the two differentiating algorithms.	74
Figure 2.4	Noise reduction properties of the linear regression type algorithm.	76
Figure 2.5	Distortion of data produced using large differentiating frames.	77
Figure 2.6	Effect of cooperative oxygen binding on Eadie-Hofstee and Hanes plots.	79
Figure 2.7	Effect of cooperative oxygen binding on Hill plots.	81
Figure 2.8	Linear regression type of differentiating algorithm producing second and subsequent derivatives of oxygen electrode traces.	82
Figure 2.9	Higher derivatives of an $n=1$ progress curve.	83
Figure 2.10	Higher derivatives of a cooperative, $n=2$ progress curve.	84
Table 2.1	Characteristics of bacterial strains.	52

CHAPTER THREE

Figure 3.1	Optical difference spectra taken during the reaction of membranes with nitrite.	89
Figure 3.2	Progress curves of the optical changes elicited by nitrite.	92
Figure 3.3	The effect of proton, haem <i>d</i> , and nitrite	

	concentrations on the rate of bleaching of the haem <i>d</i> alpha band.	94
Figure 3.4	Effect of pH on reaction of haem <i>b₅₉₅</i> with nitrite.	97
Figure 3.5	Nitrite reductase activities of membranes and whole cells.	98
Figure 3.6	Effect of pH on cytochrome <i>bd</i> catalysed oxidase activity.	100
Figure 3.7	Effect of nitrite on oxygen electrode progress curves.	101
Figure 3.8	Kinetic analyses of oxygen electrode traces.	103
Figure 3.9	Plots of K_m versus nitrite concentration between pH6 and pH8.	105
Figure 3.10	Effect of pH on the pK_i for nitrite and the apparent number of oxygen binding sites.	107
Figure 3.11	General acid catalysis model for the reaction of cytochrome <i>bd</i> with nitrous acid.	110
Figure 3.12	Electrophilic and general acid catalysis model for the reaction of cytochrome <i>bd</i> with nitrous acid.	112
 <i>CHAPTER FOUR</i>		
Figure 4.1	Formation of nitroxide haem adducts to ferrous cytochrome <i>bd</i> .	120
Figure 4.2	Conformations of Type I and Type II nitrosyl haems.	122

Figure 4.3	Low temperature nitrosyl cytochrome <i>bd</i> spectra.	126
Figure 4.4	Temperature dependence of the nitrosyl cytochrome <i>bd</i> spectrum.	127
Figure 4.5	Effect of increasing microwave power on the e.p.r. spectrum of nitrosyl cytochrome <i>bd</i> .	129
Figure 4.6	Saturation profiles of the three major features of the nitrosyl cytochrome <i>bd</i> spectrum.	131
Figure 4.7	Temperature dependence of the $P_{1/2}$'s of the three major features of the nitrosyl cytochrome <i>bd</i> spectrum.	133
Figure 4.8	E.p.r. spectra of nitrosyl myoglobin and the effect of DyEDTA on these spectra.	136
Figure 4.9	Effect of DyEDTA on the saturation profiles of nitrosyl myoglobin.	138
Figure 4.10	Effect of DyEDTA concentration on the $P_{1/2}$'s of the nitrosyl myoglobin spectral features.	139
Figure 4.11	Effect of DyEDTA on the nitrosyl cytochrome <i>bd</i> spectrum.	140
Figure 4.12	Effect of DyEDTA concentration on the $P_{1/2}$'s of the nitrosyl cytochrome <i>bd</i> spectral features.	142
Figure 4.13	Comparison of the nitrosyl haem spectra of membranes and whole cells.	144
Figure 4.14	Effect of DyEDTA on the $P_{1/2}$'s of the nitrosyl haem spectral features of whole cells.	146

CHAPTER FIVE

Figure 5.1	E.p.r. spectra of air oxidised membranes from fumarate grown cells.	155
Figure 5.2	E.p.r. spectra of redox poised membranes.	157
Figure 5.3	Redox titration of the $g=6$ region of the e.p.r. spectrum	159
Figure 5.4	Redox titration of the $g=3.3$ low spin ferric haem signal.	161
Figure 5.5	Simulation of the anoxically oxidised spectrum in the $g=6$ region.	163
Figure 5.6	Simulation of the oxically oxidised spectrum in the $g=6$ region.	164
Figure 5.7	Effect of cyanide on the anoxically oxidised spectrum in the $g=6$ region.	167
Figure 5.8	Effect of pH on the oxically oxidised spectral lineshape.	169
Figure 5.9	E.p.r. spectrum of membranes from <i>E.coli</i> FUN4/pNG2.	170
Figure 5.10	Effect of cyanide on the low spin ferric haem spectrum of membranes from <i>E.coli</i> FUN4/pNG2.	172

CHAPTER SIX

Figure 6.1	Reduced <i>plus</i> CO <i>minus</i> reduced spectrum of membranes from anaerobically grown <i>E.coli</i> EMG2.	181
Figure 6.2	Effect of CO on the 600-700nm region of the reduced <i>plus</i> CO <i>minus</i> reduced difference spectrum	

	of <i>E.coli</i> membranes.	183
Figure 6.3	Effect of CO concentration on the extent of the absorbance difference between 626nm and 640nm.	184
Figure 6.4	Effect of CO on the Soret region of the reduced <i>plus CO minus</i> reduced difference spectrum of <i>E.coli</i> membranes.	187
Figure 6.5	Effect of CO concentration on the extent of the absorbance changes in the Soret.	188
Figure 6.6	Effect of CO on oxygen electrode progress curves.	191
Figure 6.7	Eadie-Hofstee plots for the inhibition of the oxidase reaction by CO.	192
Figure 6.8	Effect of increasing CO concentration on the kinetic parameters K_m and V_{max} .	194
Figure 6.9	Kinetic analyses of CO inhibition of oxidase activity.	195
Figure 6.10	Effect of CO concentration on the gradient of Hill plots of derivative data.	197
Figure 6.11	Effect of increasing CO concentration on the apparent number of oxygen binding sites, n .	198
Figure 6.12	Higher derivatives of a CO inhibited oxygen electrode progress curve.	200
Figure 6.13	Oxidation-reduction cycle of the reaction between cytochrome <i>bd</i> and oxygen in the presence of CO.	204

CHAPTER SEVEN

Figure 7.1	Arrangement of cytochrome <i>bd</i> in the cytoplasmic
------------	--

	membrane.	210
Figure 7.2	'Bridging oxygen' model for the oxidase reaction.	213
Figure 7.3	'Disproportionation' model for the oxidase reaction.	215

INTRODUCTION

CHAPTER ONE

General introduction.

1.1. The respiratory chain of *Escherichia coli*.

Escherichia coli synthesises two ubiquinol oxidases, cytochrome *b₅₆₂-o* and cytochrome *bd* (Poole & Ingledew, 1987). These catalyse the four electron reduction of oxygen to water and contribute to the proton electrochemical potential produced across the cytoplasmic membrane by the electron transport chain as a whole. In addition to oxygen, *E.coli* is also able to use the alternative respiratory chain oxidants fumarate, nitrate, nitrite, DMSO, and TMAO. Whilst this would appear to suggest a relatively complicated scheme of electron transport, the passage of electrons from respiratory chain reductant to oxidant is uncomplicated compared to that in the mitochondrial system. There are no *c*-type cytochromes associated with the membrane bound respiratory chain; there is no cytochrome *bc₁* complex, and no evidence for a protonmotive Q-cycle.

Dehydrogenases act on respiratory chain reductants and pass the equivalent of two electrons and two protons to one of two quinones, ubiquinone-8 or menaquinone-8, to form the corresponding quinol. These are then oxidised by enzymes specific for the available respiratory chain oxidants. With some exceptions (e.g. formate and NADH dehydrogenase; Poole & Ingledew, 1987), the scalar disposition of these redox reactions across the cytoplasmic membrane is responsible for the maintenance of the proton electrochemical potential. Aerobic respiration and the mechanism of formation of the proton electrochemical potential are illustrated in Figure 1.1.

The aim of this introduction is to review the current status of work on the cytochrome *bd* of *E.coli* and of other organisms in which it

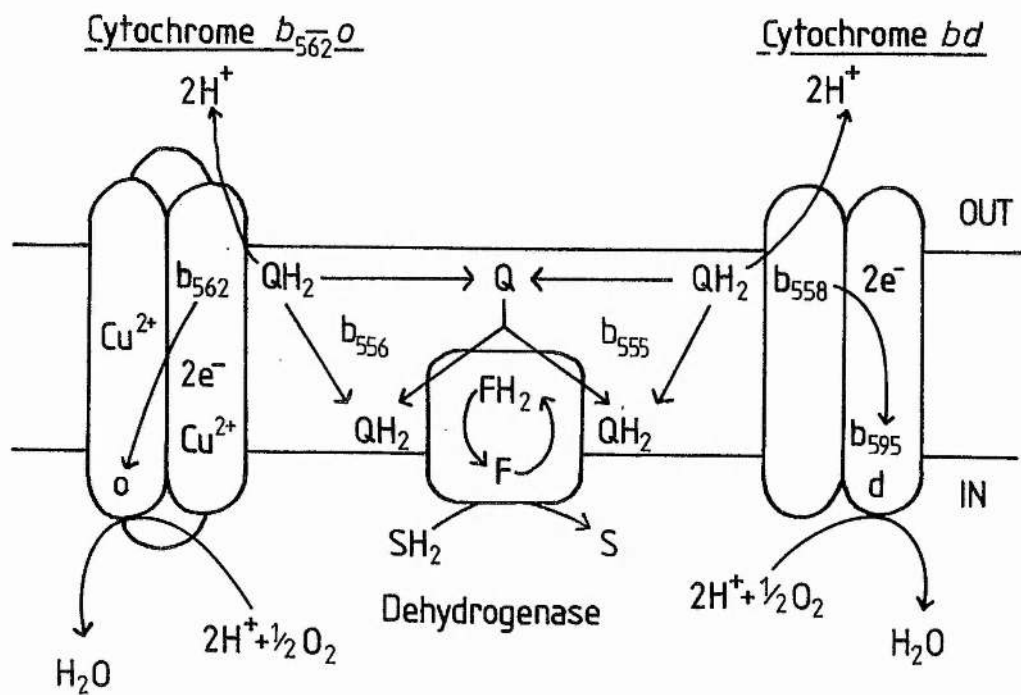
INTRODUCTION

Figure 1.1

*Aerobic respiration and the mechanism of formation of the proton
electrochemical potential in E.coli.*

Illustration of the alternative pathways of electrons in the aerobic respiratory chain. Adapted from Anraku & Gennis (1987).

Symbols used: F, flavin; Q, ubiquinone.



has been studied. In addition, it will briefly review the properties of the alternative quinol oxidase, cytochrome *b₅₆₂-o*.

1.2. The ubiquinol oxidases of *E.coli*.

The two ubiquinol oxidases of *E.coli*, cytochromes *b₅₆₂-o* and *bd*, are intrinsic membrane proteins that are synthesised primarily as a function of growth conditions. Cytochrome *b₅₆₂-o* is the predominant oxidase in cells grown under high aeration, whereas cytochrome *bd* is produced during the late exponential phase of aerobic growth (Shipp, 1972), during growth under low aeration (Rice & Hempfling, 1978), during growth in the presence of cyanide (Ashcroft & Haddock, 1975), and during anaerobic growth (Reid & Ingledew, 1979).

Analyses of the growth of mutants deficient in one of the two ubiquinol oxidases indicate that under laboratory growth conditions in the absence of respiratory inhibitors the two oxidases are mutually redundant (Green & Gennis, 1983; Au *et al.*, 1985). However, their synthesis is regulated so that expression of cytochrome *b₅₆₂-o* is suppressed under growth conditions favouring cytochrome *bd* synthesis (Kranz & Gennis, 1983).

Functionally, one of the major differences between the two oxidases is in their apparent affinities for oxygen (Table 1.1). Kita *et al.* (1984b) found that purified cytochrome *b₅₆₂-o* has a K_m for oxygen of 2.9 μ M, which compares with a value of 0.38 μ M for purified cytochrome *bd*. Other workers (Rice & Hempfling, 1978) have also found an approximate tenfold difference in the K_m for oxygen between the two oxidases. These oxygen affinities compare with values in the range

INTRODUCTION

TABLE 1.1

Enzymatic properties of cytochrome *bd* and cytochrome *bsc2-0*.

I. Substrate affinities

SUBSTRATE	Prep.	<i>bd</i>		<i>bsc2-0</i>		Note
		K_m	V_{max}	K_m	V_{max}	
<u>Kita et al. (1984a/b).</u>						
O ₂	Pure	0.38uM	-	2.9uM	-	[1]
O ₂	Membranes	0.23uM	-	1.4uM	-	[1]
O ₂	Cells	0.27uM	-	1.8uM	-	[1]
Ubiquinol-1	Membranes	0.11mM	20.5 ^a	50uM	15.5 ^a	[1]
Ubiquinol-1	Pure	0.23mM	7.5 ^a	48uM	15.0 ^a	[1]
Menadiol	Membranes	1.0mM	3.29 ^a	-	-	[1]
Menadiol	Pure	1.67mM	7.5 ^a	-	-	[1]
<u>Rice & Hempfling (1978).</u>						
O ₂	Cells	0.024uM	0.7 ^a	0.2uM	1.1-1.5 ^a	[2]

^a - units of (uM O₂) min⁻¹ (nmol cytochrome *bd*)⁻¹.

Notes for Table 1.1.

[1] Oxidase rates were measured using an oxygen electrode, or by following the absorbance change of ubiquinol-1 at 278nm. Experiments with purified oxidase were carried out in the presence of 1mM phospholipid.

[2] Oxidase rates were measured using an oxygen electrode.

INTRODUCTION

0.3-3 μ M and 4-7 μ M for mitochondrial and bacterial *aa₃* type oxidases, respectively (Poole, 1983). Differences also exist in the resistances of the two oxidases to the respiratory chain inhibitors cyanide and azide (Table 1.2). Cytochrome *bd* is more resistant to these inhibitors than cytochrome *b₅₆₂-o*.

Cytoplasmic membranes from cells harvested in the stationary phase of aerobic growth contain higher concentrations of cytochromes, particularly cytochrome *bd*, than membranes from cells harvested in the exponential phase, including cytochromes *bd* and *b₅₆₂-o* (Pudek & Bragg, 1974). However, the NADH oxidase activities of membranes from both sources are similar, indicating that the maximum rate of electron transfer through cytochrome *b₅₆₂-o* is higher than that through cytochrome *bd*. This is supported by the measured turnover rates of the two oxidases reconstituted into proteoliposomes with pyruvate oxidase and ubiquinol-8 (Lorence *et al.*, 1987); these are 150e⁻ sec⁻¹ complex⁻¹ and 550e⁻ sec⁻¹ complex⁻¹ for cytochromes *bd* and *b₅₆₂-o*, respectively. Thus, the presence and ratios of the two terminal oxidases of *E.coli* may represent a trade off between efficiency of respiratory growth, affinity for oxygen in the microaerophilic environment of the gut, and resistance to respiratory inhibitors.

Structurally, the differences between the two oxidases relate not only to the type of redox centres present, but also to their stoichiometry. Cytochrome *b₅₆₂-o* contains two haem components, haems *b₅₆₂* and *b₅₅₅*, and, in addition, it also contains copper (Kita *et al.*, 1984a). The presence of copper is reminiscent of cytochrome *aa₃*, and

INTRODUCTION

TABLE 1.2

Enzymatic properties of cytochrome *bd* and cytochrome *b₅₆₂₋₀*.

II. Inhibitor affinities.

INHIBITOR	Prep.	<i>bd</i>		<i>b₅₆₂₋₀</i>		Note [1]
		<i>K_i</i>	<i>I₅₀</i>	<i>K_i</i>	<i>I₅₀</i>	
<u>Kita et al. (1984a/b)</u>						
KCN	Pure	-	2mM	-	10uM	[2]
NaN ₃	Pure	-	400mM	-	15mM	[2]
HOQNO	Pure	-	7uM	-	2uM	[2]
Piericidin A	Pure	-	15uM	-	2uM	[2]
<u>Matsushita et al. (1984).</u>						
KCN	Pure	-	-	23uM	-	[3]
HOQNO	Pure	-	-	0.8uM	-	[3]
UHDBT	Pure	-	-	0.3uM	-	[3]
<u>Green & Gennis (1983).</u>						
KCN	Mem.	-	1.4mM	-	0.2mM	[4]
<u>Kauffman & Van Gelder (1973b).</u>						
KCN	Mem.	1mM	-	-	-	[5]
<u>Kauffman et al. (1980)</u>						
NaN ₃	Mem.	-	120mM	-	-	[6]
NH ₂ OH	Mem.	-	75mM	-	-	[6]
<u>Pudek & Bragg (1974).</u>						
KCN	Mem.	7.8mM	-	1.4mM	-	[7]

INTRODUCTION

Notes for Table 1.2.

- [1] Inhibitor affinities quoted as the K_i or I_{50} depending on the convention used in the references. It is assumed that this convention is representative of the method of analysis used in the references.
- [2] Oxidase activities were measured using an oxygen electrode. Experiments were carried out in the presence of 1mM phospholipid.
- [3] Oxidase activities were determined spectrophotometrically from the rate of ubiquinol oxidation.
- [4] Oxidase activities were determined using an oxygen electrode using strains with both oxidases present (strain GR19N) and only cytochrome b_{562-o} present (strain GR17N).
- [5] Membranes containing cytochrome bd from *A. vinelandii* were used. The K_i was determined spectrophotometrically from the ratio of the second order k_{on} of cyanide binding to the oxically oxidised haem d to the first order k_{off} for the formation of the reduced, unligated, haem d from cyano-haem d in the presence of NADH.
- [6] Membranes from *A. vinelandii* containing cytochrome bd were used. Oxidase rates were determined using an oxygen electrode.
- [7] The K_i values were determined from analysis of the deceleration of oxidase activity in the presence of cyanide. The value for cytochrome b_{562-o} is derived from membranes containing both oxidases, and therefore is only a rough estimate.

this similarity is supported by amino acid sequence homology studies, which suggest that a significant similarity exists between the two copper containing oxidases (Gennis, R.B.; presentation, 5th EBEC, Aberystwyth, Wales, July 1988). Cytochrome *bd*, on the other hand, contains three haem components, haems *d*, *b₅₉₅*, and *b₅₅₈*, but no copper (Miller & Gennis, 1983). No significant homologies have been found between the amino acid sequence of cytochrome *bd* and those of other haemoproteins with which it has been compared (Gennis, R.B.; presentation, 5th EBEC, Aberystwyth, Wales, July 1988).

1.3. Distribution of cytochromes *bd* and *b₅₆₂₋₀* in bacteria other than *E.coli*.

Kranz & Gennis (1984a) studied the immunocrossreactivity of cytoplasmic membranes from a selection of bacteria with antibodies raised against the two oxidases of *E.coli*. Cytochrome *bd* was identified in a number of strains, including *Serratia marcescens*, *Enterobacter aerogenes*, *Photobacterium phosphoreum*, *Proteus vulgaris*, *Proteus mirabilis*, *Acinetobacter* HO1N, *Salmonella typhimurium*, *Klebsiella pneumoniae*, and *Azotobacter vinelandii*. Cytochrome *bd* type ubiquinol oxidases have been purified from *P.phosphoreum* (Konishi et al., 1986) and *K.pneumoniae* (Smith et al., 1988), and these enzymes are very similar to the purified enzyme from *E.coli*. There is spectroscopic evidence for the presence of cytochrome *bd* in additional bacteria, including *Achromobacter* and *Acetobacter pasteurianus*. Cytochrome *b₅₆₂₋₀* was found by Kranz & Gennis (1984a) to be present in fewer strains, including *K.pneumoniae*, and *S.typhimurium*.

Spectroscopic studies indicate, however, that oxidases of the 'cytochrome *o*' type are the most widespread of bacterial oxidases, occurring in most physiological groups (Poole, 1988), but their subunit composition indicates that they are not all identical to the cytochrome *b_{562-o}* of *E.coli*.

1.4. The cytochrome *bd* complex.

1.4.1. Subunit and haem composition.

Purified cytochrome *bd* contains two subunits, I and II, with molecular weights of 57 000 and 43 000, respectively (Miller & Gennis, 1983; Table 1.3a), and is a heterodimer (Miller *et al.*, 1988). The amino acid sequences of the two subunits are known, and subunits I and II contain 514 and 379 amino acid residues, respectively (Green *et al.*, 1988).

Relatively little is known of the topological arrangement of subunits I and II in the native enzyme. Trypsin digestion of the purified oxidase results in cleavage of subunit I into two proteolytic fragments (Lorence *et al.*, 1988), whilst subunit II remains intact. The proteolytic fragments of subunit I have similar molecular weights (around 25kdal). Antibodies directed towards subunit II do not bind well to the native enzyme (Kranz & Gennis, 1984b). This and the effect of trypsin suggest that subunit I shields subunit II from antibody binding and proteolytic cleavage.

The cytochrome contains three haem components, haems *d*, *b₅₉₅*, and *b₅₅₈* (Lorence *et al.*, 1986). Two of these, haems *d* and *b₅₉₅*, have been reported to interact with ligands (Section 1.4.7). Unlike cytochrome

INTRODUCTION

TABLE 1.3

Molecular weights of the subunits of cytochrome *bd*
and cytochrome *b₅₆₂-o*.

(a) Cytochrome *bd*.

Reference	Molecular weights (kdal)			Growth conditions
	I	II	Native*	
Finlayson & Ingledew (1985)	70	43	113	Anaerobic
Kita <i>et al.</i> (1984b)	51	26	77	Aerobic
Miller & Gennis (1983)	57	43	100	Aerobic

* - sum of detected subunits.

(b) Cytochrome *b₅₆₂-o*.

Reference	Molecular weights (kdal)				
	I	II	III	IV	Native*
Kita <i>et al.</i> (1984)	55	33	-	-	88
Kranz & Gennis (1983)	51	28.5	18	12.7	110.2
Matsushita <i>et al.</i> (1984a)	66	35	22	17	140

* - sum of detected subunits.

INTRODUCTION

aa₃ and cytochrome b₅₆₂-o, there is no copper present in this oxidase (Miller & Gennis, 1983). The porphyrin of haem d is a chlorin (Barrett, 1956; Timkovich *et al.*, 1985), whilst those of haems b₅₅₈ and b₅₉₅ are protoporphyrins IX. The structure of the chlorin of haem d suggests that it may be derived from protoporphyrin IX by reductive dihydroxylation of one of its pyrrole rings (Gennis, 1987).

Haems b₅₉₅ and d are missing from mutant strains lacking subunit II, but haem b₅₅₈ persists, and is therefore located in subunit I (Green *et al.*, 1984). This subunit has been purified from a mutant strain lacking subunit II, and its molecular weight and electrochemical properties of its haem b₅₅₈ appear identical to those reported for the subunit I and haem b₅₅₈ of the native oxidase (Green *et al.*, 1986; Section 1.4.8). The isolated subunit binds and oxidises ubiquinol, and this appears to be its function in the native oxidase (Green *et al.*, 1986; Section 1.4.3). It is not certain whether haem b₅₉₅ and haem d are located in subunit II or in the interface region between the two subunits, as no mutants exist to date that synthesise only subunit II and not subunit I, and it has not been possible to separate the two subunits of the native enzyme without causing their denaturation (Green *et al.*, 1986). In addition to oxidising ubiquinol, the oxidase also oxidises TMPD (Miller & Gennis, 1983) and the site of this oxidation appears to be associated with subunit II (Kranz & Gennis, 1984b).

The native oxidase contains one copy each of haems b₅₅₈ and b₅₉₅, but there is some uncertainty about the number of haems d present. Coulometric and CO-binding titrations have been interpreted to suggest

INTRODUCTION

the presence of two haems *d* per oxidase complex (Lorence *et al.*, 1986), but the data can be reinterpreted to support the presence of a single haem *d*. The coulometric method used overestimated the total haem-*b* content by 0.3 (2.3 ± 0.3), and the estimate of the number of haems *d* present was only 1.4 ± 0.3 . The CO binding data estimated the number of haems *d* as being 1.6 ± 0.1 . The optical changes elicited in the Soret by CO were assumed to be due to the haem *d* with little contribution from haem *b*₅₉₅. However, haem *b*₅₉₅ appears to bind CO (Section 1.4.7.2; Chapter 6), and therefore the haem *d* stoichiometry in the study of Lorence *et al.* (1986) may have been overestimated. Analyses of the total iron content of the purified oxidase are inconclusive in determining the total haem content, and hence the number of haems *d* present. Miller & Gennis (1983) found that the iron stoichiometry was between 2.7 and 3.7 per oxidase complex, depending on the method of determination used. Double integration of e.p.r. spectra of membranes containing cytochrome *bd* from wild type (EMG2) and overexpressing (FUN4/pNG2) strains suggests that the oxidase contains haems *b*₅₉₅ and *d* in a 1:1 ratio (Meinhardt *et al.*, 1989; Chapter 5). Thus, at the present time there is no consensus on the haem *d* stoichiometry of cytochrome *bd*.

In addition to the haem *b*₅₉₅ present in cytochrome *bd*, there is a soluble hydroperoxidase present in *E. coli* with very similar spectral properties. This enzyme, haemoprotein *b*-590 (Poole *et al.*, 1984), contains protoporphyrin IX (haem *b*) and its optical spectrum is almost identical to that of the haem *b*₅₉₅ of cytochrome *bd* (Section 1.4.5). The enzyme has been purified from soluble fractions obtained by high

speed centrifugation of disrupted cells grown anaerobically on glycerol with fumarate as respiratory oxidant. It is a tetramer of total molecular weight 331 000 (Poole *et al.*, 1986). There appears to be one haem *b* present per tetramer. The protein has high catalase and peroxidase activities, and appears almost identical to soluble *E.coli* hydroperoxidase I.

1.4.2. Chemiosmotic aspects.

Cytochrome *bd* is a coupling site in the aerobic electron transport chain. When reconstituted into proteoliposomes, it generates a membrane proton electrochemical potential with ubiquinol-1 (Kita *et al.*, 1984b) as substrate. In addition, the reconstituted enzyme also oxidises TMPD, resulting in a smaller membrane potential consistent with the oxidation of this species not releasing protons on the outside of the proteoliposome membrane (Lorence *et al.*, 1988).

Oxygen pulse experiments with the reconstituted enzyme with ubiquinol-1 as substrate indicate a H^+/O stoichiometry of around 2 (Miller & Gennis, 1985). Concomitant to the acidification of the medium containing the proteoliposomes, alkalinisation of the internal space of the vesicles is also observed, indicating a net consumption of protons within the vesicles. The simplest model of proton translocation consistent with these data is as indicated in Figure 1.1. This simply involves separation of the active sites for the oxidation of quinol and reduction of molecular oxygen by the cytoplasmic membrane, with the ubiquinol oxidation site oriented towards the periplasmic aspect and the oxygen reduction site oriented

towards the cytoplasmic aspect of the cytoplasmic membrane.

The effects of trypsin digestion on the subunit composition of the oxidase have already been covered (Section 1.4.1). In addition, proteolytic cleavage of subunit I results in attenuation of the ability of the oxidase to form a membrane proton electrochemical potential with ubiquinol-1 as substrate, but has little effect on the potential produced with TMPD as substrate (Lorence *et al.*, 1988). The potential produced with the undigested oxidase is 92mV (inside negative, with nigericin present), and the trypsin digested enzyme produces a potential of 35mV. Therefore, quinol oxidation by subunit I of the *in situ* cytochrome *bd* plays a central role in the coupling of electron transfer through the oxidase to the formation of a proton electrochemical potential across the cytoplasmic membrane.

1.4.3. Quinol binding and its oxidation.

Two major quinone species are synthesised by *E.coli*, ubiquinone-8 and menaquinone-8 (Poole & Ingledew, 1987; Wallace & Young, 1977). The ubiquinol species in the mitochondrion is ubiquinol-10 (Nicholls, 1982). During growth of *E.coli* under high aeration, the major species is ubiquinol-8, whilst during anaerobic growth or growth under low aeration, the major species is menaquinol-8. The major difference between these species, apart from the structure of the quinol moiety, is electrochemical; the midpoint potential (E_m') of menaquinone is -74mV, whereas that of ubiquinone is +70mV (Poole & Ingledew, 1987). Ubiquinol-8 is likely to be the preferred substrate for cytochrome *bd* *in vivo*.

INTRODUCTION

The location of the quinol binding site of cytochrome *bd* has been shown to be on subunit I. There are three lines of evidence to support this:

- [1] Proteolysis with trypsin results in cleavage of subunit I and loss of ubiquinol oxidase activity (Lorence *et al.*, 1988), but does not result in loss of TMPD oxidase activity. Trypsin digestion therefore causes the loss or modification of the ubiquinol oxidation site.
- [2] Yang *et al.* (1986) used a radiolabelled azido analogue of ubiquinol to covalently label the subunit of the purified oxidase bearing the quinol binding site. This technique results in subunit I being labelled. As is the case with trypsin digestion, covalent labelling with azido-quinol has no effect on TMPD oxidation, whereas it inhibits quinol oxidation.
- [3] Antibodies raised against subunit I inhibit the rate of ubiquinol oxidation (Kranz & Gennis, 1984b).
- [4] Subunit I purified from an overproducing strain lacking the complete oxidase retains the electrochemical behaviour of the haem *b₅₅₈* of the native enzyme and is reducible by ubiquinol (Green *et al.*, 1986).

Purified subunit I has been reconstituted into proteoliposomes containing ubiquinone (Lorence *et al.*, 1987). Under these conditions the haem *b₅₅₈* appears to be in electrochemical equilibrium with the quinone pool to such an extent that its redox state can be monitored by monitoring the redox state of haem *b₅₅₈* optically. This is surprising in view of the difference between the midpoint potentials of

INTRODUCTION

haem *b₅₅₈* and ubiquinol (180 versus 70mV; Section 1.4.8).

In the purified enzyme, the midpoint potential of haem *b₅₅₈* and the rate of ubiquinol oxidation are dependent on the presence of detergents and pH (Lorence *et al.*, 1984b). The pH optimum for ubiquinol oxidation is around 7.0. In a cytoplasmic membrane preparation, the V_{max} with ubiquinol-1 as substrate is 126 ($\mu\text{mol O}_2$) min^{-1} (nmol haem d) $^{-1}$, whilst it is only 39 ($\mu\text{mol O}_2$) min^{-1} (nmol haem d) $^{-1}$ for the purified enzyme in the presence of 0.05% Tween-20 (Lorence *et al.*, 1984b). The rate of TMPD oxidation is not inhibited in the presence of various detergents (Lorence *et al.*, 1988), confirming that its site of oxidation is not associated with that of ubiquinol (since ubiquinol oxidation is very likely to be associated with a lipophilic region of the oxidase able to interact with detergents). Cytochrome *bd* dissolved in buffers containing octylglucoside or cholate is virtually devoid of oxidase activity with ubiquinol as substrate (Lorence *et al.*, 1984b). Cholate is routinely used in the preparation and storage of the oxidase (Miller & Gennis, 1983), but its inhibitory effects are reversible.

1.4.4. Orientation of the subunits and haems in the cytoplasmic membrane.

Hydropathy profiles of the amino acid sequences of subunits I and II strongly suggest that both of them have multiple membrane-spanning segments. Subunit I has seven and subunit II has eight segments sufficiently long and hydrophobic to span cytoplasmic membrane (Green *et al.*, 1988). Hence, the subunits of the oxidase, unlike the binding

INTRODUCTION

sites for oxygen and ubiquinol are unlikely to be completely oriented towards one side of the membrane or the other.

The effect of antibodies raised against subunit I and trypsin digestion have been used as probes of the orientation of cytochrome *bd* reconstituted into right side out proteoliposomes (Lorence *et al.*, 1988; Kranz & Gennis, 1984b; Miller & Gennis, 1985). These probes are membrane impermeant, and their effects (*viz.*: inhibition of ubiquinol oxidation, and cleavage of subunit I) are observed in reconstituted systems.

Trypsin digestion of cytochrome *bd* reconstituted into proteoliposomes results in incomplete (74%) loss of ubiquinol-1 oxidase activity (Lorence *et al.*, 1988), which contrasts with the complete loss observed in detergent solubilised preparations. Antibodies directed against subunit I also result in incomplete inhibition of ubiquinol oxidase activity in proteoliposomes (Miller & Gennis, 1985). These effects indicate that the cleavage and antigenic sites and therefore the quinol oxidation site are both located on the outer (*i.e.* periplasmic) surface of the cytoplasmic membrane. Their incompleteness is a result of the degree of anisotropy of the method used to prepare the proteoliposomes. Hence, the ubiquinol binding site, haem *b₅₅₈*, and a substantial part of subunit I are oriented towards the outer aspect of the cytoplasmic membrane.

Little is known about the orientation of subunit II, since it is protected against proteolytic cleavage by subunit I, and antibodies directed against this subunit do not bind well to the native oxidase (Kranz & Gennis, 1984b). However, for the model of proton

translocation shown in Figure 1.1 to be valid, the site of the oxygen reduction must be oriented towards the inner aspect of the cytoplasmic membrane. As indicated in Section 1.4.1, the locations of haems *d* and *b*₅₉₅ are either in subunit II or in the interface region between the two subunits. Therefore, a substantial part of subunit II is likely to be oriented towards the inner surface of the cytoplasmic membrane. A structural model of the *in situ* cytochrome *bd* which is consistent with the data discussed above is illustrated in Figure 1.2.

1.4.5. Optical spectroscopy.

Reduced minus oxidically oxidised difference spectra at 77K of cells overexpressing cytochrome *bd* and *b*₅₆₂₋₀ are illustrated in Figure 1.3; the features in these spectra are largely due to the haem components of the oxidases present. The spectrum of cytochrome *bd* is complicated by overlap of the absorbances of its haem components. It has peaks diagnostic for haems *b* (560nm), *b*₅₉₅ (595nm), and *d* (630nm; Miller & Gennis, 1983). The band at 595nm has historically been attributed to cytochrome *a*₁ in membranes or cells containing cytochrome *bd*, but has been found to be due to a high spin haem *b*, haem *b*₅₉₅ (Lorence *et al.*, 1986). The spectrum of haem *b*₅₉₅ (see below) is similar to those of mammalian cytochrome *c* peroxidase (Lorence *et al.*, 1986) and *E.coli* haemoprotein *b*-590 (Poole *et al.*, 1986). Both these latter proteins contain ligand binding high spin haems *b*, indicating that haem *b*₅₉₅ of cytochrome *bd* is high spin and may also be able to interact with ligands.

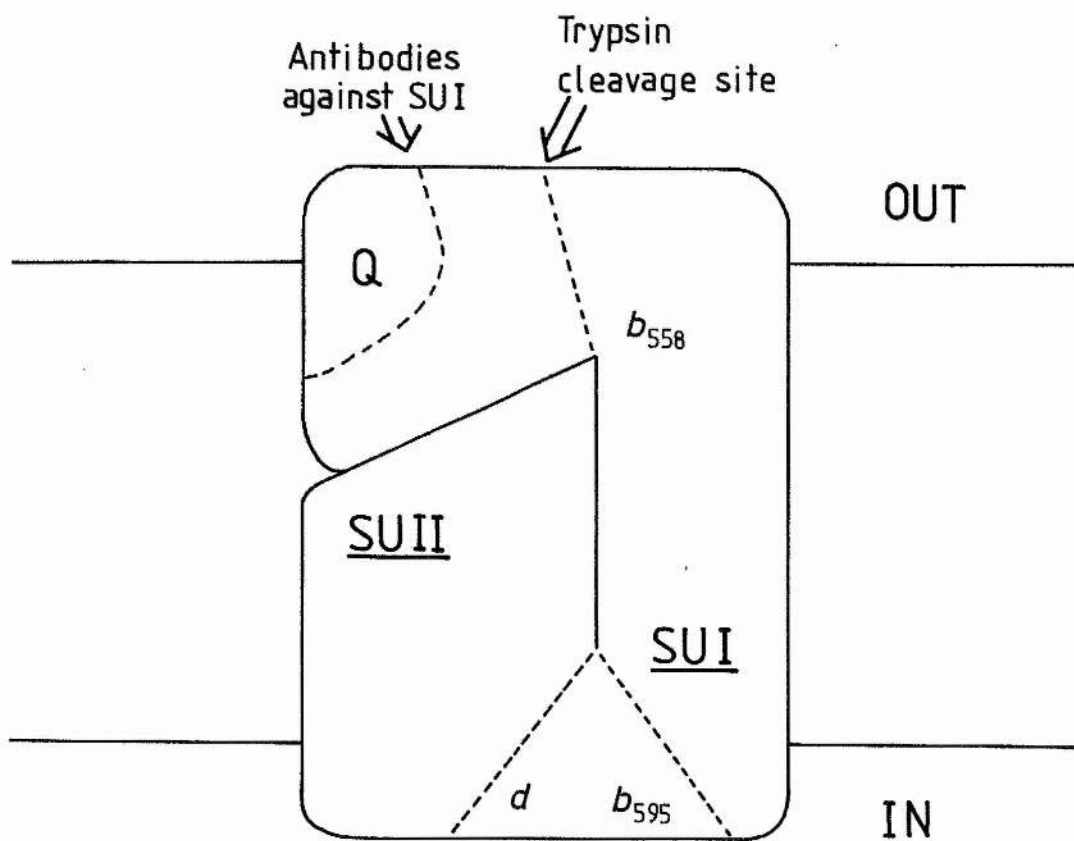
The contributions of the haem components of cytochrome *bd* to the

INTRODUCTION

Figure 1.2

Structural model of cytochrome bd and the orientation of its components in the cytoplasmic membrane.

This is based on the work of Gennis and coworkers. Haems b_{595} and d are shown to be located between two dotted lines. This indicates that they are located either in subunit II or in the interface region between the two subunits. Trypsin and antibodies raised against subunit I selectively inhibit the site of ubiquinol oxidation. See text for details.

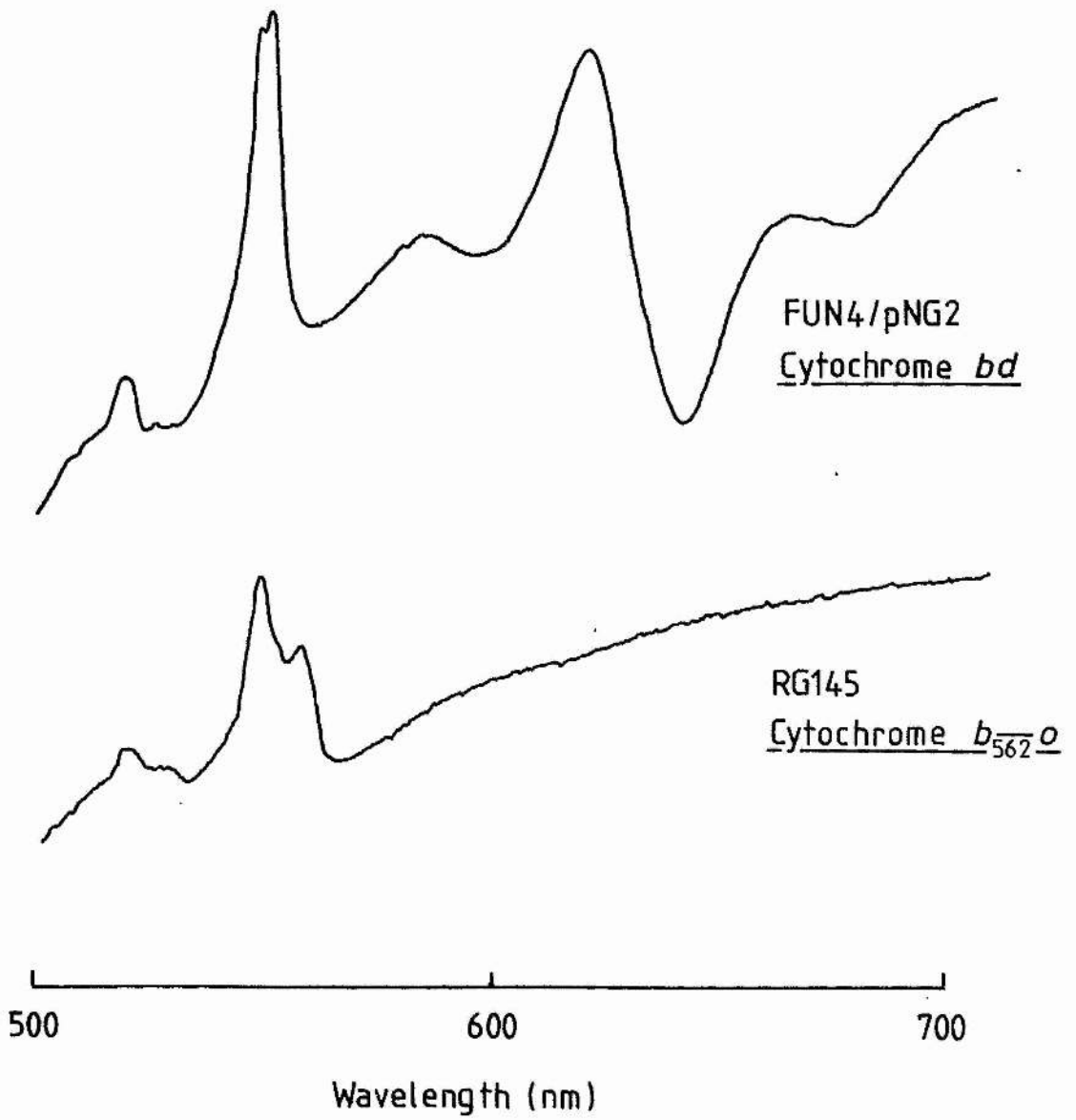


INTRODUCTION

Figure 1.3

Reduced minus oxidised spectra of cells containing cytochrome *bd* and cytochrome *b₅₆₂-o*.

Reduced minus oxidised spectra of mutant whole cells from *E.coli* FUN4/pNG2 (cytochrome *b₅₆₂-o* deficient, cytochrome *bd* overexpressing) and RG145 (cytochrome *bd* deficient, cytochrome *b₅₆₂-o* overexpressing). Spectra were recorded at 77K using a split beam spectrophotometer. Spectral bandwidth, 1nm; scan rate 1nm s⁻¹; protein concentration, 3.5mg ml⁻¹. The reduced and oxidised cuvettes were treated with a few grains of sodium dithionite and 10mM hydrogen peroxide respectively. The mutant strains were a gift of Professor R.B. Gennis of the University of Illinois at Urbana.



INTRODUCTION

500-700nm region of reduced *minus* anoxically oxidised spectra have been deconvoluted (Koland *et al.*, 1984; Lorence *et al.*, 1986; Figure 1.4). The spectrum of haem *b₅₅₈* has alpha and beta bands at 560 and 530nm, respectively, and is typical of a low spin haem *b*. The haem *d* has a major alpha band at 630nm. The haem *b₅₉₅* spectrum is complex, with a beta band at 560nm and an attenuated alpha band at 595nm and a trough at 645nm.

The reduced *minus* oxically oxidised spectrum has troughs at 650 and 680nm, indicating that the oxically oxidised cytochrome *bd* has absorbance bands at these wavelengths, and this is confirmed by analysis of the absolute spectrum of the oxically oxidised enzyme. The 650nm trough is much smaller and the 680nm trough is absent in the reduced *minus* anoxically oxidised spectrum (Koland *et al.*, 1984). The species responsible for the 650 and 680nm bands have been identified as oxygen and peroxide adducts to haem *d*, respectively (Section 1.4.7.1). In the subsequent discussions of these species, reduced, oxygen ligated, and peroxide ligated haems *d* will be referred to as haems *d₆₃₀*, *d₆₅₀*, and *d₆₈₀*, respectively. The oxidised, unligated form of haem *d* will be referred to as haem *d**.

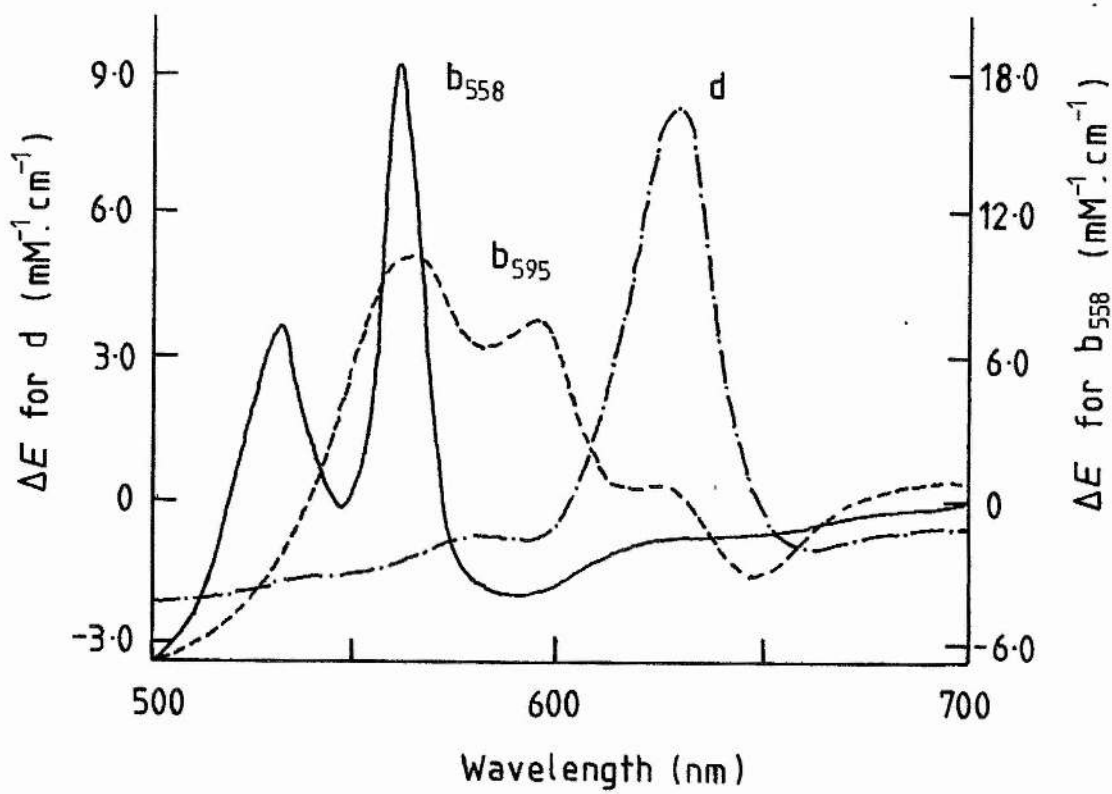
Analysis of the Soret region of low temperature (77K) reduced *minus* oxically oxidised spectrum of cytochrome *bd* is complicated by more extensive overlap of the gamma bands of its constituent haems than in the alpha region. Fourth order finite difference analysis of such spectra of *E.coli* cells grown anaerobically or under conditions of oxygen limitation indicate the presence of three major Soret bands (Scott & Poole, 1982). Major bands can be resolved at 418, 428 and

INTRODUCTION

Figure 1.4

Resolved spectra of the haem components of cytochrome bd.

The reduced *minus* oxidised spectrum of the haem components of cytochrome *bd* deconvoluted from the composite spectrum of the oxidase. The left hand ordinate represents the extinction coefficient of haem *d*. If the haems *b₅₅₈* and *b₅₉₃* are each present in a 1:1 ratio with haem *d*, their extinction coefficients are also represented by the left hand ordinate. If they are each present in a 1:2 ratio with the haem *d*, their extinction coefficients are given by the right hand ordinate. Copied from Figure 5 of Lorence *et al.* (1986).



440nm in such spectra which can be tentatively assigned to *c*, *b* (haems *b₅₅₅* and *b₅₉₅*), and *d* type haems, respectively. Comparison of the optical spectrum of cytochrome *bd* in the Soret region with that of cytochrome *cd₁*, a nitrite reductase of *Pseudomonas aeruginosa* and other bacteria (Barber *et al.*, 1976), indicates that the Soret band of haem *d* is less intense than those of the haems *b* of cytochrome *bd*. The haem *d₁* of cytochrome *cd₁* has a Soret band which occurs at 460nm and is resolved from the Soret absorbance of haem *c*.

1.4.6. Electron paramagnetic resonance spectroscopy.

Relatively little has been published on the e.p.r. characteristics of cytochrome *bd*, and the work reported to date (Hata *et al.*, 1985; Kumar *et al.*, 1985) is in need of clarification. In particular, unequivocal assignments of the e.p.r. signals of preparations containing this oxidase to its haem components are required (Chapter 5).

Hata *et al.* (1985) studied the e.p.r. signals from cytochrome *bd* in a membrane preparation from aerobically grown cells. An axial high spin ferric haem signal at $g=6.0$ was assigned to haem *b₅₅₅*, whilst low spin ferric haem signals at $g=2.5$ and 2.3 were assigned to haem *d*. Under oxidically oxidising conditions, the haem *d* was reported to be present in a diamagnetic oxygen ligated ferrous form (haem *d₅₅₀*). However, Kumar *et al.* (1985) assigned a rhombic high spin ferric haem species with g -values of 6.28 and 5.54 to haem *d* on the basis of triple trapping (low temperature ligand exchange; Section 1.4.7.3) data, whilst an axial high spin ferric haem signal was assigned to *b*

type haems. In a similar study, Hata *et al.* (1987) assigned the rhombic high spin ferric haem species to haem b_{595} . Kauffman *et al.* (1975) studied the e.p.r. properties of a membrane preparation from *A.vinelandii*, and resolved two high spin ferric haem signals, one rhombic and one axial, which were both attributed to the haem d of cytochrome bd . Haem b_{595} was assigned to a low spin ferric haem signal at $g=3.03$, and haem b_{538} (reported as cytochrome b_1) was assigned to low spin ferric haem signals at $g=3.69$ and 3.43 . Both of the published studies on the e.p.r. characteristics of the purified cytochrome bd from aerobically grown (Hata *et al.*, 1985) and anaerobically grown *E.coli* (Finlayson & Ingledew, 1985) report both axial and rhombic high spin ferric haem species. In both cases, the axial species titrated with midpoint potentials of around 180mV. Whilst no low spin ferric haem signals were observed in the preparation of Finlayson & Ingledew (1985), that of Hata *et al.* (1985) had low spin ferric haem signals at $g=2.3$ and 2.5 which titrated with an E_m comparable to the optically determined values for haem d in the purified enzyme (232mV; Koland *et al.*, 1984). Thus, there is no clear consensus on the assignment of e.p.r. resonances to the haem components of cytochrome bd .

On the basis of the precedents of the other oxidases that have been characterised by e.p.r., cytochromes aa_3 (Wikstrom *et al.*, 1981) and b_{562-o} (Section 1.5.4), it would be surprising if the putative ligand binding haems of cytochrome bd don't exhibit ferric high spin haem signals with major features around $g=6.0$. The role of haem b_{538} as the ubiquinol reducible component of cytochrome bd and its optical spectrum suggest that this haem is very likely to be six coordinate

and low spin. Haems *b* from other systems involved in the redox reactions of quinol species such as the haems b_{566} and b_{562} (Salerno, 1984) of mitochondrial complex III, and the haem b_{563} of chloroplast cytochrome b_6f (Salerno *et al.*, 1983), have e.p.r. spectra diagnostic for the presence of low spin ferric haems with features above $g=3.3$.

1.4.7. Ligand binding to cytochrome *bd*.

Optical studies of the effects of ligands on cytochrome *bd* have made a major contribution to delineating the roles of the redox centres present in the oxidase and the sequence of the redox reactions involved in the reduction of oxygen. A model of the oxidation-reduction cycle of cytochrome *bd* based on the published ligand binding data discussed below will be presented in Section 1.4.9.

1.4.7.1. Oxygen and hydrogen peroxide.

A distinct difference is observed between the reduced *minus* oxically oxidised and reduced *minus* anoxically oxidised spectra of cytochrome *bd* in the haem *d* alpha region (600-700nm), with the trough at 650nm being much larger in the oxic spectrum and the trough at 680nm being completely absent in the anoxic spectrum (Koland *et al.*, 1984). The species absorbing at 650nm under oxically oxidising conditions has been attributed to a stable oxygen adduct to ferrous haem *d*, haem d_{650} (Poole *et al.*, 1983a). Resonance Raman spectra of oxically oxidised cytochrome *bd* have oxygen-oxygen stretching bands attributable to oxygen bound to a ferrous haem (Poole *et al.*, 1982a).

INTRODUCTION

Thus, the haem *d* of haem d_{650} is likely to be ferrous. However, redox titrations of haem d_{650} under oxic conditions indicate the possibility of a second, ferric form of haem d_{650} (Section 1.4.8).

Addition of peroxide to anoxically oxidised membranes containing cytochrome *bd*, which have no major 650nm absorbance, results in the formation of a species with an intense absorbance at 680nm, haem d_{680} . Peroxide also causes diminution of the 650nm absorbance when added to oxically oxidised membranes, and is therefore able to displace oxygen from haem d_{650} . On the basis of these results, haem d_{680} has been attributed to a peroxide adduct to ferric haem *d* (Poole & Williams, 1988). Low temperature ligand exchange experiments and optical studies of the oxidase under turnover conditions indicate that this species is an intermediate in the reaction of the oxidase with oxygen, and is derived from haem d_{650} by reduction of the bound oxygen (Section 1.4.7.3).

Under turnover conditions, only haems d_{650} and d_{680} are detectable in the oxidase from *A.vinelandii* (Kauffman & Van Gelder, 1973a) and *E.coli* (Pudek & Bragg, 1976a). Ferrous haem *d*, haem d_{630} , is not detected optically under turnover conditions, indicating that its lifetime is very short, or, more unlikely, that it is not an intermediate in the oxidase reaction. The intensities of the d_{650} and d_{680} species are only 75% of their intensities in spectra of the oxically oxidised oxidase (Kauffman & Van Gelder, 1973a). This indicates the presence of a third intermediate species in the reaction sequence, termed haem d^* (Pudek & Bragg, 1976a; Kauffman & Van Gelder, 1973b). Haem d^* has been identified as the ferric, unligated form of

haem *d* (Poole *et al.*, 1983a).

When allowed to become slowly anaerobic using endogenous substrates, haems d_{650} and d_{680} become undetectable and are replaced by haem d_{630} as the major species (Kauffman & Van Gelder, 1973a). The ratio of haem d_{680} to haem d_{650} increases prior to the full appearance of haem d_{630} . The kinetics of these transitions are consistent with conversion of haem d_{650} to haem d_{630} via haem d_{680} and haem d^* .

There is no evidence similar to that described above for haem *d* to implicate oxygen binding to haem b_{595} . Evidence for this centre being involved in ligand binding is based on the appearance of bands in photochemical action spectra and in reduced *plus* CO *minus* reduced difference spectra (Section 1.4.7.2).

Analysis of the pre-steady state kinetics of the reaction of reduced membranes containing cytochrome *bd* with oxygen has established that electron flow through haem *d* is sufficient to maintain steady state rates of oxygen consumption (Haddock *et al.*, 1976). Haem *d* is thus kinetically competent to function as the terminal, oxygen reducing component of the electron transport chain. Studied independently, haem b_{595} is not competent in this respect. This suggests that it is either a minor terminal branch of the electron transport chain, or that it is rapidly re-reduced during the timescale of stopped flow analyses. The pre-steady state kinetics of the reaction with oxygen have also been analysed using computer simulations of kinetic models of the terminal section of the electron transport chain (D.S. Wariabharaj & W.J. Ingledew, unpublished results). Good fits to experimental data are obtained using models

approximating both of the interpretations of the stopped flow data of Haddock *et al.* (1976) described above.

1.4.7.2. Carbon monoxide.

Cytochrome *bd* binds CO, resulting in perturbation of its absorption spectrum. The inhibition of oxidase activity elicited by this ligand and its photodissociability also enable the recording of photochemical action spectra (Castor & Chance, 1959; Edwards *et al.*, 1981). The photodissociability of CO has also been of major importance in delineating the sequence of redox reactions of oxidases following exchange of oxygen for CO using the low temperature trapping and ligand exchange techniques developed by Chance and coworkers (Chance *et al.*, 1975; Section 1.4.7.3).

In the room temperature reduced *plus* CO *minus* reduced spectrum of purified cytochrome *bd* peaks are observed at 420, 437, and 642nm. Troughs are observed at 430, 440, and 622nm (Miller & Gennis, 1983; Kita *et al.*, 1984b). The features in the 600-700nm region of this spectrum are clearly attributable to CO binding to haem *d*, but the assignments of the features in the Soret are not quite so straightforward.

The spectrum is 'W' shaped in the Soret, indicating CO binding to more than one haem. The peak at 420nm and the trough at 430nm are reminiscent of the Soret features of reduced *plus* CO *minus* reduced spectra of purified cytochrome *b₅₆₂-o* (Matsushita *et al.*, 1984; Kita *et al.*, 1984a), which has a peak at 416nm and a trough at 430nm. This suggests that these features are due to CO binding to a *b* type haem,

INTRODUCTION

probably haem *b₅₉₅*. However, the reduced *minus* oxidised spectrum of this haem (Lorence *et al.*, 1986; Figure 1.4) closely resembles that of haemoprotein *b-590* (Poole *et al.*, 1986). The reduced *plus* CO *minus* reduced spectrum of haemoprotein *b-590* has a peak at 426nm and a trough at 446nm, which suggests that the 442nm trough of the reduced *plus* CO *minus* reduced spectrum of cytochrome *bd* is attributable to haem *b₅₉₅*. However, such an assignment would entail the peak at 420nm and the trough at 430nm being due to denatured haem *b*, possibly haem *b₅₅₈*. Also, there are features in the 500-600nm range of the spectrum of haemoprotein *b-590* (peaks at 539nm and 578nm, and troughs at 560nm and 597nm) which are absent or very small in the spectrum of cytochrome *bd*. Thus, although the alpha bands of haemoprotein *b-590* and haem *b₅₉₅* of cytochrome *bd* appear at similar wavelengths, it is possible that the Soret features of these two ligand binding centres are different.

The contribution of haem *d* to the Soret region of the reduced *plus* CO *minus* reduced difference spectrum has not been clearly resolved. In the low temperature (4K) post photolysis *minus* prephotolysis spectrum of carbonmonoxy cytochrome *bd* in whole cells there is a trough at 638nm and there is a peak at 445nm (Poole *et al.*, 1982b). This suggests that haem *d* is responsible for the trough at 442nm in the CO difference spectrum. Thus, in the work reported herein, it is assumed that the 420-430nm peak-trough is due to CO binding to haem *b₅₉₅*, and that the trough at 442nm is due to CO binding to haem *d*.

In addition to binding to the fully reduced oxidase, CO also

INTRODUCTION

binds to the oxically oxidised enzyme resulting in distinct changes in its absolute spectrum. In the absolute spectrum of the reduced oxidase, CO causes the alpha band of haem *d* to be red shifted by approximately 6nm (Miller & Gennis, 1983; Kauffman *et al.*, 1980), from 630nm to 636nm. The effect of CO on the oxically oxidised enzyme results in displacement of oxygen from haem d_{650} by CO and the appearance of a band attributable to ferrous haem *d*-CO at around 640nm. Thus, there is a 4nm difference in the position of the alpha band of the CO adduct to haem *d* between the spectrum of CO treated reduced and oxidised cytochrome *bd*. Presumably, the other haem components of the oxidase remain ferric when CO is added to the oxically oxidised cytochrome, and an interaction between one of these haems and the CO adduct to ferrous haem *d* may explain the difference in the positions of the haem *d* alpha bands.

Kauffman *et al.* (1980) studied the effect of CO under turnover conditions on the haem *d* alpha region of absorption spectra of cytochrome *bd* in *A.vinelandii*. Under these conditions, haem d_{650} is undetectable, and is replaced by a species with an alpha band at 636nm (CO ligated ferrous haem *d*), and the concentration of haem d_{650} is much lower than in the absence of CO. However, the inhibition of oxidase activity is far from complete. It is possible, given the putative ability of haem b_{595} to bind oxygen, that the oxidase reaction of the CO inhibited oxidase occurs primarily at this centre under conditions of CO inhibition.

Photochemical action spectra have traditionally been used to identify CO binding haemoproteins as functional oxidases. Such spectra

have been recorded of the *E.coli* respiratory chain terminated by cytochrome *bd*. Both haem *b₅₉₅* and haem *d* show bands in photochemical action spectra at wavelengths equal to their alpha absorbances (Edwards *et al.*, 1981; Castor & Chance, 1959), although haem *b₅₉₅* only satisfies this criterion (at its alpha band) when light sources of high intensity such as dye lasers are used. Given that both of these centres are components of cytochrome *bd*, it is possible to speculate that they form the binuclear site of the oxidase reaction itself.

1.4.7.3. Low temperature flash photolysis and ligand exchange experiments.

Cytochrome *bd* exhibits unusual behaviour following photolysis of the CO adduct at low temperatures compared to cytochrome *b₅₆₂-o* and cytochrome *aa₃*. When CO treated cells containing cytochrome *bd* are photolysed in the absence of oxygen, no photolysis of CO from haem *d* is detected (Poole & Chance, 1981) unless the photolysis is carried out at temperatures close to that of liquid helium (<20K; Poole *et al.*, 1982b). A major difference between the oxygen binding site of cytochrome *bd* and those of cytochrome *aa₃* and cytochrome *b₅₆₂-o* appears to be the presence of copper in the latter two oxidases (Wikstron *et al.*, 1981; Kita *et al.*, 1984a; J.C. Salerno, B. Bolgiano, & W.J. Ingledew, unpublished results). Copper present in the ligand binding pocket of cytochrome *aa₃* is able to trap photodissociated CO, and thus slow its recombination with haem *a₃* (Alben *et al.*, 1981).

The sequence and intermediates of the reaction between reduced cytochrome *bd* and oxygen have been studied following flash photolysis

of the carbonmonoxy ferrous oxidase in the presence of oxygen at subzero temperatures. This technique was originally developed by Chance and coworkers (Chance *et al.*, 1975) to study the intermediates in the reaction of cytochrome *aa₃* with oxygen, and has been used to study the intermediates in the oxidase reaction of cytochrome *bd* from *E.coli* (Poole *et al.*, 1983a & b; Poole & Williams, 1987) and *A.pasteurianus* (Williams & Poole, 1987).

The first spectroscopically detectable species in the reaction of cytochrome *bd* with oxygen has an alpha band at 650nm and corresponds to an oxygen adduct to ferrous haem *d*, haem *d*₆₅₀ (Poole *et al.*, 1983a). A species with an absorbance band at 680nm, haem *d*₆₈₀, subsequently appears whilst the concentration of *d*₆₅₀ decreases (Poole *et al.*, 1983b). Oxidation of haem *b*₅₉₅ appears to take place concomitant to the formation of haem *d*₆₈₀ (Poole & Williams, 1987; Williams & Poole, 1987). Williams & Poole therefore proposed that the role of haem *b*₅₉₅ in the redox cycle of the oxidase is direct electron donation to haem *d*. Donation of one electron from haem *b*₅₉₅ and one from the ferrous haem of haem *d*₆₅₀ to the bound oxygen would result in formation of the peroxide adduct, haem *d*₆₈₀. The kinetics of formation of haem *d*₆₈₀ are consistent with it being derived from haem *d*₆₅₀ provided that haem *d*₆₈₀ itself is slowly converted to a third intermediate with no distinct spectrum in the 600-700nm region. This third species is presumably haem *d*^{*}, the unligated oxidised form of haem *d*. Subsequent to the oxidation of haem *b*₅₉₅ and formation of the peroxy haem *d*₆₈₀ species, additional oxidation of *b*-type haem takes place, probably corresponding to haem *b*₅₅₈.

INTRODUCTION

No e.p.r. detectable components corresponding to haem d_{650} are observed when the post photolysis events are followed using e.p.r. rather than optical spectroscopy (Poole *et al.*, 1983a; Kumar *et al.*, 1985; Hata *et al.*, 1987). The haem of this species under these circumstances is therefore ferrous rather than ferric (Poole *et al.*, 1983a). The first e.p.r. detectable intermediate is a rhombic high spin ferric haem with $g_x=6.3$ and $g_y=5.5$ (Kumar *et al.*, 1985; Hata *et al.*, 1987), which has been attributed to haem b_{595} . A second e.p.r. species is subsequently detected which is an axial high spin ferric haem with $g_{xy}=6$, its appearance is concomitant to the major part of haem b oxidation observed in experiments followed optically. Its appearance, however, is also concomitant with the formation of haem d^* from haem d_{680} , as is consistent with the kinetics of the conversion of haem d_{650} to haem d_{680} (see above). Given the probability that haem b_{558} has a low spin ferric haem e.p.r. signal (Section 1.4.6), it is possible that the axial high spin ferric haem signal is due to haem d^* , although it has been assigned to haem b_{558} by Hata *et al.* (1987). Thus, there are two kinetically resolvable high spin haems in cytochrome bd . The sequence of formation of the e.p.r. detectable species following photolysis is consistent with the role of haem b_{595} being the donation of electrons to haem d_{650} (Hata *et al.*, 1987).

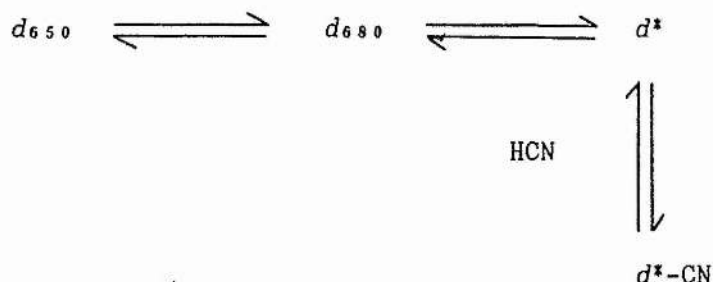
A model of the oxidation reduction cycle based largely on the low temperature ligand exchange data discussed above is presented in Section 1.4.9.

1.4.7.4. Cyanide.

Cytochrome *bd* has a higher resistance to cyanide than cytochrome *b₅₆₂₋₀* (Table 1.2), and cells grown in its presence contain higher concentrations of cytochrome *bd* (Section 1.2). In addition to inhibiting the rate of the oxidase reaction, cyanide also elicits changes in the optical absorption spectrum of the oxidase.

Cyanide reacts slowly with the oxidically oxidised oxidase, resulting in diminution of both the 650nm and 680nm bands (Kauffman & Van Gelder, 1973b). It elicits no changes in the optical spectrum of the reduced oxidase unless oxygen is also present (Pudek & Bragg, 1974). In the aerated reduced *plus* cyanide *minus* reduced spectrum there are major troughs at 628, 442, and 423nm. The former two of these bands are attributable to cyanide binding to the ferric (bleached) form of haem *d* (haem *d*^{*}), whilst the latter may be due to cyanide binding to the ferric (bleached) form of haem *b₅₉₅*. Under turnover conditions, the rate of formation of the cyanide adduct to haem *d* is proportional to the rate of electron flux through the oxidase (Kauffman & Van Gelder, 1974; Jones, 1973). The above data are consistent with cyanide binding to the unligated ferric form of haem *d* (*d*^{*}) which is an intermediate species in the redox cycle of the oxidase reaction (Section 1.4.7.1). The following scheme for cyanide binding to haem *d* can therefore be proposed (based on Pudek & Bragg, 1974):

INTRODUCTION



There has been no thorough study of the effect of cyanide on the haem b_{595} component of the oxically oxidised oxidase or the oxidase under turnover conditions. Some reports indicate that there is no cyanide effect on the optical spectrum of this component (Pudek & Bragg, 1974), whilst others report that cyanide binding to haem d results in reduction of haem b_{595} , but only in membranes containing unusually high concentrations of this haem (Kauffman & Van Gelder, 1973b).

1.4.7.5. Nitric oxide and nitrite.

Nitrite reacts with cytochrome bd , resulting in the formation of distinct optically detectable nitrosyl haem species. Anoxic reaction of the reduced *E.coli* cytoplasmic membranes containing cytochrome bd with nitrite results in bleaching of the 630nm ferrous haem d absorbance (Hubbard *et al.*, 1983; Meyer, 1973). There are also optical changes in the Soret which may be due to reaction of nitrite with cytochrome b_{562-0} or haem b_{595} . Reaction of cytochrome bd with nitric oxide results in optical changes similar to those reported for the reaction with nitrite, indicating that the optical species formed are nitrosyl haems. E.p.r. spectroscopy shows that these nitrosyl haem

species are formed concurrent with the optical changes (Chapter 4).

Nitrite (Arima & Oka, 1965) and hydroxylamine (Kauffman *et al.*, 1980) inhibit the rate of oxygen consumption in membranes containing cytochrome *bd* as the major terminal oxidase.

These reactions of cytochrome *bd* with nitrogen species are distinct from the known *E.coli* nitrite reductase pathways, of which there are three (*viz*: a membrane bound nitrite reductase, a soluble NADPH dependent enzyme which functions *in vivo* as a sulphite reductase, and a soluble NADH dependent enzyme; Lin & Kuritzkes, 1987). The reactions of the *E.coli* electron transport with nitrite and its inhibitory effects are the subject of Chapter 3 of this thesis.

1.4.8. Redox potentiometry.

A selection of the published midpoint potentials (E_{m7} 's) of the components of cytochrome *bd* is presented in Table 1.4. Haem *d* has an E_{m7} of around 250mV and haem *b₅₉₅* has an E_{m7} of around 150mV. These values are approximately the same in membrane bound and purified preparations. However, the E_{m7} of haem *b₅₅₈* appears to be markedly affected by purification (Lorence *et al.*, 1984b). In membrane preparations its E_{m7} is around 180mV, whereas in the purified oxidase it is between 150 and 0mV. The E_{m7} 's quoted in Table 1.4 correspond to one electron oxidations or reductions (Nernstian $n=1$ titrations), unless otherwise stated.

The midpoint potentials of the putative ligand binding haems of cytochrome *bd* (haems *d* and *b₅₉₅*; 250mV and 150mV) are much higher than those reported for the haem *b₅₅₅/b₅₆₂* pair of cytochrome *b₅₆₂-o*

INTRODUCTION

TABLE 1.4

Midpoint potentials of the haem components of the *E. coli*
aerobic respiratory chain.

STRAIN	GROWTH PHASE	CO	Prepn.	b ₅₅₆	o b ₅₆₂ b ₅₅₅	b ₅₅₈	b ₅₉₅	d	Note
<u>Lorence et al. (1984a).</u>									
MR43L(F152)	Sta.	No	Mem.	50	-	182	150	247	[2]
MR43L(F152)	Sta.	Yes	Mem.	20	-	185	125	>400	[2]
MR43L	Sta.	No	Mem.	32	185	185	140	247	[2]
MR43L	Sta.	Yes	Mem.	57	>400	190	175	>400	[2]
GR19N	Sta.	No	Mem.	20	170	-	-	-	[2]
GR19N	Sta.	Yes	Mem.	21	310	-	-	-	[2]
<u>Pudek & Bragg (1976b).</u>									
NRC482	Sta.	No	Mem.	36	-	165	147	260	[3]
<u>Koland et al. (1984).</u>									
MR43L	Sta.	No	Pure	-	-	61	113	232	[4]
<u>Reid & Ingledew (1979).</u>									
EMG2	Exp.	No	Mem.	-	80	-	-	-	[5]
EMG2	Lt.Exp.	No	Mem.	140	-	260	160	260	[6]
<u>Hata et al. (1985).</u>									
MR43L	Sta.	No	Pure	-	-	30	-	240	[7]
MR43L	Sta.	No	Mem.	-	-	140	-	240	[7]
<u>Finlayson & Ingledew (1985).</u>									
EMG2	Sta.	No	Pure	-	-	180*	180*	300	[8]
<u>Kita et al. (1984a).</u>									
KL251/ORF4	Exp.	No	Pure	-	125	-	-	-	[9]
<u>Kita et al. (1984b).</u>									
MR43L	Lt.Exp.	No	Pure	-	-	10	-	240	[10]
<u>Kita et al. (1978).</u>									
MR43L	Lt.Exp.	No	Pure	-45	-	-	-	-	[11]
<u>Green et al. (1986).</u>									
GR84N/pNG10	Lt.Exp.	No	Pure	-	-	160	-	-	[12]
GR84N/pNG10	Lt.Exp.	No	Pure	-	-	90	-	-	[13]

Notes for Table 1.4.

- [1] Haem b_{556} is associated with the succinate dehydrogenase, haems b_{562} and b_{555} are components of cytochrome b_{562-0} , and haems b_{558} , b_{595} , and d are components of cytochrome bd . Midpoint potentials (E_{m7} 's) are quoted in units of millivolts. Haems exhibit $n=1$ behaviour unless otherwise stated.
- [2] Fractional reduction of the cytochromes was determined using the following wavelength pairs: haems b (except b_{595}), A_{560} - A_{579} , haem b_{595} , A_{595} - A_{603} ; haem d , A_{628} - A_{603} . MR43L(F152) overexpresses cytochrome bd two to threefold compared to MR43L and has suppressed cytochrome b_{562-0} expression. GR19N lacks cytochrome bd (Green & Gennis, 1983).
- [3] Redox states of haems b_{595} and d were obtained from the heights of the absorbance peaks at 594 and 628nm relative to an oxidised baseline.
- [4] Fractional reduction of the components were determined by measurement of A_{557} - A_{568} , A_{571} , and A_{628} for the haems b_{558} , b_{595} , and d , respectively. Haem b_{558} exhibited $n=0.8$ behaviour.
- [5] Fractional reduction determined at 559nm.
- [6] Redox states determined at 559nm (haem b), 590nm (haem b_{595}), and 630nm (haem d). Cells grown anaerobically on glycerol and fumarate.
- [7] E.p.r. data. Redox states of haems b_{558} and d determined from intensities of the $g=6.0$ signal, and the $g=2.5$ signal, respectively.
- [8] E.p.r. data. *The axial high spin component at $g=6$ titrated with an E_{m7} of 180mV, so this can be assigned to haem b_{595} or haem b_{558} . The E_{m7} for haem d is based on titrations of the lineshape changes observed on the high field side of the axial peak.
- [9] Redox state determined at 560nm.
- [10] Redox state of haem b_{558} determined as in [9]. Redox state of haem d determined at 630nm.
- [11] As [9].
- [12] The cells used in this study overproduced subunit I of cytochrome bd , but lacked subunit II and haems b_{595} and d . The purified subunit I was reconstituted into proteoliposomes prior to determination of the E_m . Redox state of haem b_{558} determined as in [1].
- [13] As [12], but with purified subunit I solubilised using cholate.

INTRODUCTION

(180mV). These values compare with values between 362 and 375mV for haem a_3 of mitochondrial cytochrome aa_3 (Poole, 1983).

Detergents and lipids influence the electrochemical behaviour of the three haems of purified cytochrome bd (Lorence *et al.*, 1984b). The most dramatic of these effects is a substantial lowering of the E_m of haem b_{558} from, for example, 151mV in the presence of Tween-20 to 0mV in the presence of cholate. The equivalent drops in the E_m 's of haems b_{595} and d are 158 to 74mV, and 263 to 183mV, respectively. Octylglucoside and cholate are most effective at perturbing the midpoint potentials of the haem components of the oxidase. The sensitivity of haem b_{558} to detergents is consistent with this component of the oxidase being associated with the lipophilic transmembranous region of the oxidase.

Surprisingly, the haem b_{558} of purified subunit I when reconstituted into proteoliposomes has an E_m (160mV; Green *et al.*, 1986) comparable to that found in the reconstituted oxidase and in the *in situ* oxidase. Loss of subunit II therefore has little effect on the haem b_{558} , and this suggests that the location of haem b_{558} is relatively far from the subunit I - subunit II interface region of the native enzyme.

In addition to the effects of lipids and detergents, the midpoint potentials of the purified complex are markedly pH dependent (Lorence *et al.*, 1984b). These decrease with increasing pH in an approximately linear fashion. In the case of the haem d , the gradient dE_m/dpH is $-61\text{mV pH unit}^{-1}$, and for the haems b_{595} and b_{558} the gradients are $-41\text{mV pH unit}^{-1}$. These data indicate that protons are taken up by the

complex upon reduction of its haems.

When redox titrations are carried out in the presence of CO the E_{m7} of haem *d* is increased beyond 400mV (Lorence *et al.*, 1984a). Surprisingly, in view of the evidence for CO binding to haem *b₅₉₅* (Section 1.4.7.2), its presence has little effect on the potentiometric behaviour of this centre (Lorence *et al.*, 1984a; Reid & Ingledew, 1979). If CO is able to bind to haem *b₅₉₅*, it either does so with low affinity, or more unlikely, it is also able to bind to the oxidised haem.

Hendler & Schragar (1979) carried out redox titrations of *E.coli* membranes under oxic conditions and found that under these conditions haem *d* exhibits unusual potentiometric behaviour. Titrations carried out in the reducing (from high to low potential) direction indicate that the 630nm band of haem *d* behaves as an $n=4$ species with an E_{m7} of 310mV, suggesting that the 4 electron reduction of oxygen in addition to the redox transition of haem *d* titrates under oxic conditions. The band at 650nm (haem *d₆₅₀*), which is not observed in the anoxic titrations, exhibits even more unusual behaviour. At potentials above around 330mV, its intensity is level at about one third of its maximum. There is a sharp dip to zero intensity at 330mV, and at lower potentials the intensity increases until a maximum is reached at about 100mV. Pudek & Bragg (1976b) noted that the 650nm band of haem *d* could only be observed at high potentials if oxygen was introduced into the titration. The data indicates that there are two forms of haem *d* with absorbance bands around 650nm, one ferrous and one ferric. It is possible that both of the species responsible for the 650nm

absorbances are oxygen adducts to haem *d*. E.p.r. data will be presented in Chapter 5 which is consistent with oxygen binding to fully oxidised cytochrome *bd* (Chapter 5).

1.4.9. The redox cycle of the oxidase reaction.

The spectroscopic and kinetic data discussed above enable a tentative model to be described for the oxidation-reduction cycle of cytochrome *bd*. The intermediates in the reaction of cytochrome *bd* following photolysis at low temperatures of the CO adduct to haem *d* in the presence of oxygen and under turnover conditions have been described (Section 1.4.7). Any model proposed for the redox cycle of the oxidase must take into account the intermediates detected using low temperature ligand exchange techniques and those observed under turnover conditions. Hata *et al.* (1987) proposed a model for the redox cycle of the oxidase under turnover conditions, but whilst their model is consistent with low temperature ligand exchange data, it fails to include the haem *d*^{*} intermediate detected by Pudek & Bragg (1976a) and Kauffman & Van Gelder (1973a).

A tentative model for the redox cycle of cytochrome *bd* is presented in Figure 1.5. The model assumes that the reduction of oxygen proceeds via two 2-electron transfers via a bound peroxide intermediate. Two redox cycles are represented, one corresponding to the reactions leading up to and following photolysis at low temperatures of the fully reduced CO ligated oxidase in the presence of oxygen (Figure 1.5a), and another corresponding to the redox cycle of the oxidase under turnover conditions (Figure 1.5b). These cycles

Figure 1.5

Oxygen reduction model for cytochrome bd.

A tentative model for the redox reactions involved in oxygen reduction following flash photolysis of the CO ligated enzyme at low temperature (a), and under turnover conditions (b). Note that the intermediates d_{630} , d_{650} , d_{680} and d^* are labelled solely on the basis of the redox or ligand binding state of the haem *d*. Multiple forms of these intermediates which are spectroscopically identical in the haem *d* alpha region of optical spectra are therefore possible and some of these are labelled in the model. It is assumed in the model that full reduction of the haems of cytochrome *bd* results in a bound semiquinol radical. Symbols used: QH_2 , ubiquinol-8; $QH\cdot$, semiubiquinol-8; Q , ubiquinone-8; H^+_{OUT} , periplasmic proton; H^+_{IN} , cytoplasmic proton; $h\nu$, photolysing photon.

differ primarily in the redox state of the haem b_{558} and the presence of bound ubiquinol (semiubiquinol) species during the sequence of oxygen reduction. In Figure 1.5a, the enzyme becomes fully reduced prior to photolysis of the CO. In Figure 1.5b, it is assumed that the concentration of ubiquinol and its rate of binding and oxidation are rate limiting, resulting in the enzyme being more oxidised overall during the redox cycle.

Alternative models for the oxidase reaction, catalysed by cytochrome bd are possible, involving different sequences of ubiquinol binding and electron transfer reactions. The mechanism of oxygen reduction may also be different; for example, an alternative mechanism could involve one 2-electron transfer and two 1-electron transfers resulting in reduction of oxygen via a bound peroxide and a ferryl haem intermediate, as has been proposed for the reaction catalysed by cytochrome aa_3 (Naqui *et al.*, 1986).

1.5. The cytochrome b_{562-0} complex.

Having described in some detail the properties of cytochrome bd , which is the subject of this thesis, it is pertinent to briefly review the alternative ubiquinol oxidase, cytochrome b_{562-0} .

1.5.1. Subunit and haem composition.

Cytochrome b_{562-0} is the ubiquinol oxidase synthesised by *E. coli* grown under conditions of high aeration. The enzyme has been purified, and is a heterodimer (Kita *et al.*, 1984a) or heterotetramer (Kranz & Gennis, 1983; Matsushita *et al.*, 1984; Table 1.3b). The subunits have

been labelled subunits I to IV. It contains two protoporphyrins IX, accounting for haems b_{562} and b_{555} (haem o). It has been reported to contain two coppers (Kita *et al.*, 1984a), but e.p.r. data suggests the presence of only a single copper (J.C. Salerno, B. Bolgiano, & W.J. Ingledew, unpublished results; Section 1.5.4). The presence of copper is reminiscent of cytochrome aa_3 , and its functional role in the oxidase reaction may be similar.

The protein subunits of the oxidase have been sequenced (Gennis, R.B.; presentation, 5th EBEC, Aberystwyth, Wales, July 1988), and reveal homologies with both bacterial and mammalian cytochrome aa_3 . Subunit I has extensive regions of homology with cytochrome aa_3 subunit I. This is the subunit of cytochrome aa_3 which contains haems a and a_3 and one of the coppers (Wikstrom *et al.*, 1981). Subunit IV of cytochrome b_{562-o} has a sequence homologous to subunit III of cytochrome aa_3 .

1.5.2. Chemiosmotic aspects.

Like cytochrome *bd*, cytochrome b_{562-o} is a coupling site in the aerobic respiratory chain. A membrane proton electrochemical potential of around 140mV (with nigericin present, inside negative) is formed by the oxidase reconstituted into proteoliposomes with ubiquinol as substrate (Matsushita *et al.*, 1984). Oxygen pulse experiments with these proteoliposomes indicate that the oxidase translocates two protons across the cytoplasmic membrane per pair of electrons used in the reduction of oxygen (a H^+/O ratio of 2; Matsushita *et al.*, 1984; Carter & Gennis, 1985). Similar experiments in whole cells containing

cytochrome b_{562-o} as the major terminal oxidase (Lawford & Haddock, 1973) also indicate a H^+/O ratio of 2. The simplest model of proton translocation consistent with these data is as indicated in Figure 1.1, and is identical to that for cytochrome bd (Section 1.4.2).

1.5.3. Optical spectroscopy.

Optical difference spectra of purified cytochrome b_{562-o} are diagnostic for the presence of b -type haems. In the reduced *minus* oxidised spectrum at room temperature there are major peaks at 560, 530, and 427nm corresponding to the alpha, beta, and gamma bands of b -type haems, respectively (Kita *et al.*, 1984a). At liquid nitrogen temperatures the alpha band at 560nm is resolved into two peaks, at 555 and 562nm (Figure 1.2).

In the absolute spectrum of reduced cytochrome b_{562-o} there are major peaks at 560, 530, and 427nm which correspond to the alpha, beta and gamma bands of b -type haems (Matsushita *et al.*, 1984). In the presence of CO there are minor changes in the alpha and beta regions. In the Soret region (400-500nm), the gamma band of the CO binding haem is blue shifted by 8nm to 419nm, whilst the gamma band of the other haem remains in approximately the same position. In the reduced *plus* CO *minus* reduced spectrum at room temperature there is an intense derivative type feature in the Soret, with a peak at 416 and a trough at 430nm. In the alpha region a trough is observed at 554nm, indicating that the CO and oxygen binding component of the oxidase is haem b_{555} (Kita *et al.*, 1984a). It is this component that has been

traditionally described in the literature as 'cytochrome o'.

1.5.4. *Electron paramagnetic resonance spectroscopy.*

The e.p.r. signals attributable to the haems of cytochrome b_{562-o} in purified and membrane bound preparations have been assigned (Hata *et al.*, 1985; J.C. Salerno, B. Bolgiano, & W.J. Ingledew, unpublished results). Haem b_{555} has an axial high spin ferric haem signal with $g_{xy}=6.0$ (g_z at $g=2$, not observed), and this species appears to be antiferromagnetically coupled to a high potential copper in the fully oxidised enzyme. Potentiometric studies indicate that as the ambient redox potential of the oxidase is increased, the $g=6.0$ signal appears, and then becomes attenuated by antiferromagnetic coupling between the haem and the copper as the latter becomes oxidised. Haem b_{562} has a low spin ferric haem signal with $g_z=3.0$ and $g_y=2.26$ (g_x not observed). No e.p.r. evidence was found for the presence of a second copper in the unpublished study of Salerno, Bolgiano, and Ingledew.

The presence of both high and low spin haems in the oxidase and the g -values of the observed e.p.r. signals are, like the presence of copper, reminiscent of published data on the mitochondrial cytochrome aa_3 system. An additional similarity between cytochromes b_{562-o} and aa_3 is the orientation of the haems with respect to the cytoplasmic or inner mitochondrial membrane. E.p.r. spectra of oriented multilayers containing amplified levels of cytochrome b_{562-o} and no cytochrome bd indicate that the orientation of haems b_{562} and b_{555} are very similar to the orientations of haem a and a_3 in mitochondria (J.C. Salerno & W.J. Ingledew, unpublished results). These haems all have their planes

approximately parallel to the membrane normal.

1.5.5. Redox potentiometry.

Potentiometric analyses of liquid nitrogen optical difference spectra of membranes containing cytochrome *b₅₆₂-o* indicate that the 555 and 562nm bands of the optical spectra are isopotential with an E_{m7} of around 170mV (Lorence *et al.*, 1984a; Table 1.4). The E_{m7} 's of both the haems appear to be raised in the presence of CO to around 350mV, indicating a tight thermodynamic coupling between haems *b₅₅₅* and *b₅₆₂*.

1.6. Research objectives.

It is clear from the above that the two oxidases synthesised by *E.coli* are structurally and functionally distinct. There are clear homologies between cytochrome *b₅₆₂-o* and the familiar cytochrome *aa₃* type oxidase. Cytochrome *bd*, on the other hand, appears very different and yet catalyses the same four electron reduction of oxygen to water. This thesis describes an *in situ* study of cytochrome *bd* in a membrane preparation from *E.coli* grown anaerobically on glycerol with fumarate as respiratory oxidant. Such growth conditions lead to the synthesis of cytochrome *bd* as the major, and perhaps sole, oxidase.

The overall aim of the research reported in this thesis is to gain further information about the nature of the oxidase reaction catalysed by the *in situ* cytochrome *bd* and, in particular, the roles of the two ligand binding haems, haems *d* and *b₅₉₅*. Studies are reported on the reaction of cytochrome *bd* with nitrite

INTRODUCTION

(Chapters 3 & 4) and CO (Chapter 6), and the effects of these inhibitors on the optical and steady state kinetics of the oxidase. The e.p.r. properties of the oxidase are investigated with a view to unequivocally assigning the observed resonances of membranes containing cytochrome *bd* to the haem components of the oxidase (Chapter 5). An investigation of the sidedness of the site of the oxidase reaction is also reported, using the effect of the exogenous paramagnetic probe dysprosium(III) on the e.p.r. spectra of nitric oxide adducts to the ligand binding site of the oxidase (Chapter 4).

MATERIALS AND METHODS

CHAPTER TWO

Materials and methods.

2.1. Organisms.

The *Escherichia coli* strains used in this research are shown with their genotypes in Table 2.1. The bulk of the work reported herein was carried out on material derived from strain EMG2. The other strains were used in preliminary experiments extending this work. Strain FUN4/pNG2 was used to study the ligand binding characteristics of cytochrome bd using e.p.r. spectroscopy. Strain RG145 was used to compare the optical properties of cytochromes bd and b_{562-0} (Chapter 1, Figure 1.2).

All the strains were kept as stock cultures on nutrient agar slopes or plates. Strain RG145 was maintained in the presence of 200mg l⁻¹ ampicillin in the nutrient agar. Strain FUN4/pNG2 was maintained in the presence of 5mg l⁻¹ tetracycline. Liquid media were inoculated by loop-transfer from the stock cultures. For long term storage, cells were stored frozen at -70°C as a suspension in a solution containing 50% nutrient broth, 25% DMSO, and 25% glycerol.

2.2. Growth media.

Strain EMG2 was grown anaerobically in batch culture on glycerol with fumarate as respiratory oxidant. Strain FUN4/pNG2 was grown aerobically on sucrose. Strain RG145 was grown aerobically on nutrient broth. The growth media used are described below.

2.2.1. Glycerol-fumarate medium.

This contained the following: 7.9g l⁻¹ potassium dihydrogen phosphate; 6.1g l⁻¹ fumaric acid; 9.65g l⁻¹ potassium hydroxide;

TABLE 2.1

Characteristics of Bacterial Strains.

Strain	Genotype and Phenotype	Source
EMG2	Prototroph	NCIB, Torry, Aberdeen
FUN4/pNG2	<p><i>Genotype:</i> F⁻, cydA2, cyo, recA, srl, rpsL, gal, menA401, nadA.</p> <p>pNG2: pBR322- derived plasmid containing cloned cyd. Tet^R.</p> <p><i>Phenotype:</i> Cytochrome <i>bd</i> overexpressing, cytochrome <i>b_{562-o}</i> deficient.</p>	Professor R.B. Gennis, University of Illinois, Urbana, USA.
RG145 (RG129/pRG101)	<p><i>Genotype:</i> F⁻, rpsL, thi, gal, nadA, cydA2, lon100(?), cyo, srl::Tn10, recA56.</p> <p>pRG101: Amp^R cosmid containing cloned cyo.</p> <p><i>Phenotype:</i> Cytochrome <i>b_{562-o}</i> overexpressing, cytochrome <i>bd</i> deficient.</p>	As FUN4/pNG2

MATERIALS AND METHODS

2.1g l⁻¹ ammonium sulphate; 5.25ml l⁻¹ glycerol; 1.05g l⁻¹ acid hydrolysed casein; 1.05ml l⁻¹ selenite and molybdate solution containing 50mM sodium biselenite and 50mM ammonium molybdate; 1.05ml l⁻¹ trace metals solution (Section 2.2.4). The pH of this medium was 7.0-7.5. 0.21ml l⁻¹ 1M magnesium sulphate were added after autoclaving.

2.2.2. Sucrose medium.

This contained the following: 7.9g l⁻¹ potassium dihydrogen phosphate; 2.25g l⁻¹ potassium phosphate; 2.1g l⁻¹ ammonium sulphate; 1.05g l⁻¹ acid hydrolysed casein; 5g l⁻¹ sucrose; 1.05ml l⁻¹ selenite and molybdate solution (50mM sodium biselenite and 50mM ammonium molybdate); 1.05ml l⁻¹ trace metals solution (Section 2.2.4); 5mg l⁻¹ thiamine; 12.5mg l⁻¹ nicotinic acid. The pH of this medium was 7.0-7.5. 0.21ml l⁻¹ 1M magnesium sulphate were added after autoclaving. Strain FUN4/pNG2 was grown on this medium in the presence of 10mg l⁻¹ tetracycline which was also added after autoclaving.

2.2.3. Nutrient broth and nutrient agar.

This contained the following: 10g l⁻¹ tryptone; 5g l⁻¹ yeast extract; 12g l⁻¹ dipotassium hydrogen phosphate; 3g l⁻¹ potassium dihydrogen phosphate. The pH of this medium was 7.0-7.5. Antibiotics added to this medium for strains FUN4/pNG2 and RG145 were 10mg l⁻¹ tetracycline and 400mg l⁻¹ ampicillin, respectively. These were added to the medium after autoclaving. Nutrient agar was prepared from nutrient broth by addition of 1% (w/v) bacteriological agar (Oxoid

Agar N° 1) prior to autoclaving.

2.2.4. Trace elements solution.

The trace metals solution contained the following: 3mM iron (III) chloride; 2mM manganese (II) chloride; 2mM calcium chloride; 1.2mM cobalt sulphate; 4.5mM boric acid. A 1 litre stock solution was made to which 1ml chloroform was added and the pH was adjusted to 7.

2.3. Cell growth.

2.3.1. Anaerobic growth of *E.coli* EMG2.

E.coli strain EMG2 was grown anaerobically on the glycerol-fumarate medium described above in 20 litre batches. An inoculum of 500ml was initially grown for 18 hours anaerobically on nutrient broth. Cells were grown at 37°C to the late exponential phase of growth, this was typically achieved 18 to 24 hours after inoculation. When unbroken cells were required, anaerobic growth was in 500ml bottles inoculated with 5mls of the nutrient broth inoculum.

2.3.2. Aerobic growth of *E.coli* FUN4/pNG2.

E.coli strain FUN4/pNG2 was grown aerobically in 20 litre batches at 37°C on the sucrose medium. An inoculum of 500ml was initially grown aerobically in a shaker flask on nutrient broth for 24 hours in the presence of 10mg l⁻¹ tetracycline. The 20 litre batches were sparged vigorously with sterile air during growth to late exponential phase, which typically occurred after 24 to 30 hours growth.

2.3.3. Aerobic growth of *E.coli* RG145.

E.coli strain RG145 was grown aerobically in 500ml shaker flasks on nutrient broth in the presence of 400mg l⁻¹ ampicillin to late exponential phase, which in this medium occurred between 18 and 24 hours. When limited numbers of whole cells were required, *E.coli* strain FUN4/pNG2 was also grown aerobically in 500ml batches as described above, but in the presence of 10mg l⁻¹ tetracycline.

2.4. Cell harvesting.

Cells grown in 20 litre batch culture were harvested by continuous flow centrifugation using either a continuous flow rotor running at 18 000 rpm in an MSE High Speed 18 centrifuge or a Sharples air turbine driven Laboratory Super Centrifuge (Pennwalt) running at 35 000 rpm. When cells or membranes were required for e.p.r. work, it was found that the Sharples was unsatisfactory. Wear of the lower (drag) bearing immediately below the rotor resulted in contamination of the harvested cells with metallic (paramagnetic) material which had been washed into the rotor by the upward throughflow of medium. This problem appeared to be due to a combination of the version, condition, and age of the machine used.

Cells were washed twice in an ice cold 50mM phosphate buffer (pH7) by centrifugation and resuspension. Centrifugation was carried out using a Sorvall RC-5B Superspeed (DuPont) centrifuge operating at 9 000g and 4°C for 15 minutes. When cells or membranes were required for e.p.r. work, the buffer contained 5 or 10mM EDTA (disodium salt).

Cells were frozen by pipetting them as a slurry suspended in buffer dropwise into liquid nitrogen and they were stored at -30°C prior to isolation of cytoplasmic membranes as described below. When unbroken cells were required, all harvesting and centrifugation were carried out using the Sorvall centrifuge.

2.5. Isolation of cytoplasmic membranes.

Frozen cells were thawed and suspended in an equal volume of a 20mM pH7.5 Tes/KOH buffer containing 5mM EDTA at 4°C . Bovine spleen deoxyribonuclease II and lysozyme ($2\mu\text{g ml}^{-1}$ each) were added to hydrolyse any DNA released during cell breakage and to digest the peptidoglycan of the cell wall, respectively. Cell breakage was achieved by passing the suspension of cells twice through a French press operating at between 10 and 15 MPa. Cell debris and residual whole cells were removed by centrifugation of the lysate at 10000g and 4°C for 15 minutes. Membrane fragments from the supernatant were pelleted by centrifugation for 90 min at 125000g in a PrepSpin 50 ultracentrifuge operating at 4°C . This pellet was washed by resuspension in the Tes-EDTA buffer and recentrifugation at 125000g for 90 min. For e.p.r. work the membranes were often subjected to a further wash. Finally, the pellet was suspended in a minimal volume of an appropriate buffer (typically 50mM Tes/KOH, pH7 containing 2mM MgSO_4) and frozen by pipetting dropwise into liquid nitrogen. Membranes were stored under liquid nitrogen until required.

2.6. Assays.

2.6.1. Determination of protein.

Protein determinations were carried out using the method of Lowry *et al.* (1951), modified by the inclusion of sodium dodecyl sulphate (SDS; 1% w/v) in the assay solution to solubilise membrane bound protein. Two reagent solutions, solution A and solution B were prepared. Solution A contained the following: 20g l⁻¹ sodium carbonate, 0.5g l⁻¹ sodium potassium tartrate, and 4g l⁻¹ sodium hydroxide. Solution B contained 1g l⁻¹ copper sulphate. 9 parts of solution A were mixed with 1 part of solution B, SDS was added to 1% (w/v), and this assay solution was incubated at 40°C to solubilise the SDS. Protein to be assayed was added to 3mls of this assay solution in a test tube which was then incubated for 10 minutes at 40°C. 0.3mls of a 1:1 water dilution of Folin and Ciocalteu's Phenol Reagent were then added, and the assay solution was incubated at 40°C for one hour to allow full colour development. The absorbance of the assay solution was then measured at 750nm. Bovine serum albumin (Fraction V) was used as a standard, and a fresh standard curve was constructed for each protein assay. A standard curve is illustrated in Figure 2.1a.

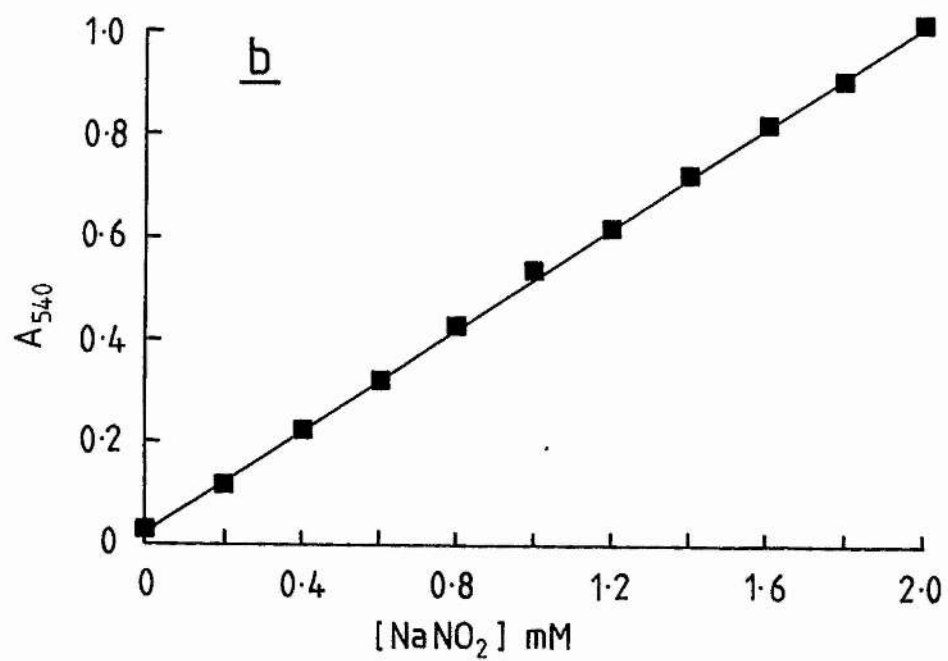
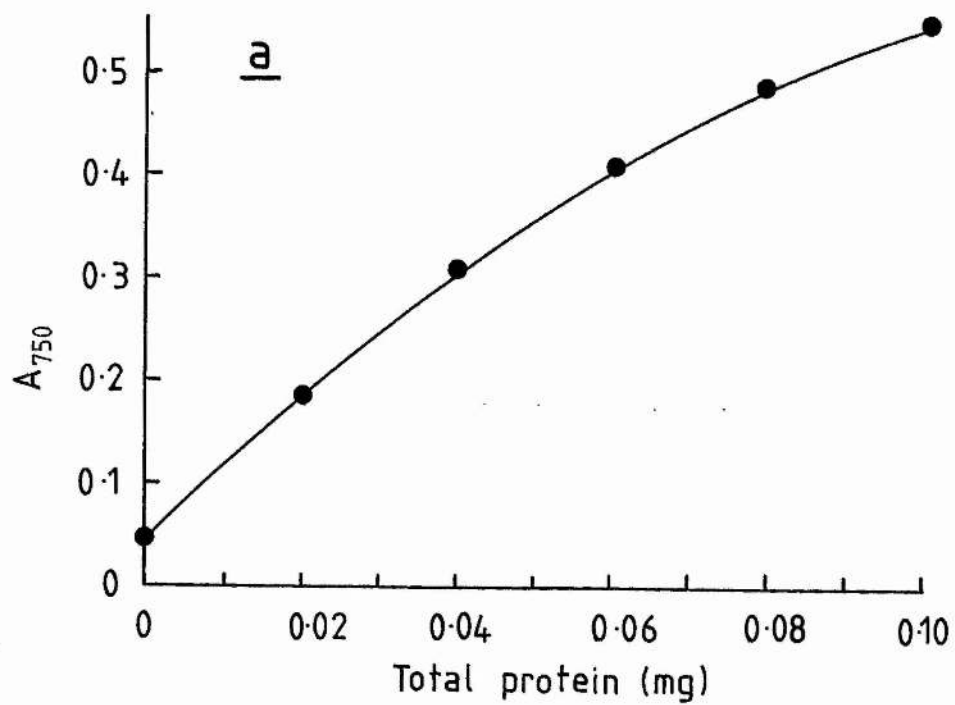
2.6.2. Determination of nitrite reductase activity.

Anaerobic nitrite reductase activity was measured in membranes and whole cells from *E.coli* strain EMG2 by a modification of the method of Wray & Filner (1970). Incubations of cells or membranes in the presence of nitrite were carried out in a redox titration vessel

Figure 2.1

Standard curves for protein and nitrite determinations.

(a) Standard curve for Lowry protein assay. The units on the abscissa refer to the total amount of protein added to the assay as mgs of bovine serum albumin. (b) Standard curve for nitrite assay. The units on the abscissa refer to the known concentration of nitrite in the aliquot (50ul) assayed.



constructed by Mr. C. Smith of the University of St. Andrews Chemistry Department Glass Workshop. This vessel was continuously purged with nitrogen gas which had been passed through a Nil-Ox oxygen scrubbing apparatus (Jencons Scientific) and was water jacketed to maintain a constant temperature of 30°C. Cells or membranes were incubated in a 50mM phosphate buffer (pH7) with sodium lactate (20mM) and sodium nitrite (1-2mM) at 30°C. Samples (50ul) were withdrawn into test tubes containing 3ml distilled water, 1ml 1% (w/v) sulphanilamide in 3M HCl, and 1ml 0.02% N-(1-naphthyl)ethylenediamine dihydrochloride. After 15 minutes, suspended cells or membranes were centrifuged out and the absorbance was measured at 528nm. Sodium nitrite was used to construct a standard curve (Figure 2.1b) and the rate of nitrite reductase activity was determined from plots of nitrite concentration versus time.

2.6.3. Assay for oxidase activity.

Oxidase activities were measured using a Clark type oxygen electrode (Rank Brothers) with a glass incubation vessel incorporating a water jacket (constructed by Mr. C. Smith of the University of St. Andrews Chemistry Department Glass Workshop). The incubation vessel had a volume of 2.55ml and had a ground glass stopper with a capillary portal through which microsyringe additions could be made. The electrode was connected to a resistance box which had the dual function of polarising the electrode (-0.6V) and converting the current flowing through it to a voltage. This type of electrode has a linear concentration-voltage dependence (Lessler & Brierley, 1969).

Voltages were either recorded with a chart recorder, or, where more detailed data analyses were required, to a BBC Model B microcomputer (Acorn Computers; Section 2.14). Oxygen concentrations were calculated using the data of Chappell (1964).

2.7. Spectrophotometry.

Optical difference spectra of *E.coli* cells or membranes were obtained using a split beam spectrophotometer constructed in the workshop of the department of Biochemistry and Microbiology of the University of St. Andrews. Spectra at liquid nitrogen temperatures were recorded using the same instrument incorporating a cryogenic attachment, which was also constructed in the workshop of this department. For the spectrophotometric assays described above, a CE272 single beam spectrophotometer (Cecil Instruments) was used.

2.8. Sample preparation for e.p.r.

Samples for e.p.r. spectroscopy were prepared in 3mm internal diameter quartz e.p.r. tubes as described by Ingledew (1983). Samples were rapidly frozen by immersion of the e.p.r. tubes in a mixture of methylcyclohexane and isopentane (1:4, v/v), cooled to around -80°C with a liquid nitrogen cold finger. Samples were stored frozen in liquid nitrogen until used to record e.p.r. spectra.

2.9. Preparation of DyEDTA/LaEDTA solutions.

Stock solutions of 100mM DyEDTA and LaEDTA were prepared by mixing equal volumes of 200mM DyCl₃ or LaCl₃ and Na₂EDTA and carefully

adjusting the pH to 7.

2.10. Redox titrations.

Potentiometric redox titrations were performed as described by Dutton (1978). The oxidation reduction mediators used, at concentrations of between 25 and 150 μM , were: 2-hydroxy-1,4-naphthoquinone ($E_{m7} = -130\text{mV}$); pyocyanine ($E_{m7} = -30\text{mV}$); duroquinone ($E_{m7} = +10\text{mV}$); 1,4-naphthoquinone ($E_{m7} = +50\text{mV}$); N-methylphenazonium methosulphate ($E_{m7} = +80\text{mV}$); 1,2-naphthoquinone ($E_{m7} = +125\text{mV}$); 2,6-dibromophenolindophenol ($E_{m7} = +190\text{mV}$); 1,2-naphthoquinone-4-sulphonic acid ($E_{m7} = +210\text{mV}$); 2,6-dichlorophenolindophenol ($E_{m7} = +217\text{mV}$); N,N,N',N'-tetramethyl-p-phenylene diamine ($E_{m7} = +260\text{mV}$); tetrachlorohydroquinone ($E_{m7} = +340\text{mV}$). The ambient redox potential (E_h) was adjusted using solutions of sodium dithionite or potassium ferricyanide, and was measured using a combination platinum/reference (Ag/AgCl) electrode purchased from Russell pH-Ltd. The vessel was continuously flushed with nitrogen gas (99.9% v/v) which had been passed through a Nil-Ox oxygen scrubbing apparatus (Jencons Scientific). Membranes were suspended in 100mM Tes/KOH (pH7.0) in the redox titration vessel (at 30°C) and were poised at 0mV to remove all traces of oxygen. The potential was then adjusted to 450mV and the titration was carried out in the reducing direction. Alternatively, after poisoning at 0mV, the titration was done in the oxidising direction. When titrations were carried out in the presence of carbon monoxide, this gas was substituted for nitrogen in the above procedure.

Redox titration data were analysed using a computer program developed by Professor A.R. Crofts of the University of Illinois at Urbana. The program gave best fit data for the experimental points and was able to fit single or multiple components.

2.11. E.p.r. spectroscopy.

E.p.r. spectra were obtained using a Bruker ER200D spectrometer (Bruker Spectrospin) equipped with a liquid helium cryostat (ESR-9, Oxford Instruments) and liquid helium transfer line. The temperature of the cryostat and the helium flow rate through the transfer line was measured and controlled using an Oxford Instruments DTC2 temperature controller.

2.12. E.p.r. spectral simulation and double integration.

Simulation of e.p.r. powder spectra was performed using a computer program developed by Professor J.C. Salerno of the Rensselaer Polytechnic Institute, Troy, New York. This program simulated Gaussian e.p.r. lineshapes and enabled simulated spectra to be plotted out on a Benson B9211 plotter using the GHOST subroutines available on the VAX 11/780 at the University of St. Andrews.

Truncated double integrations of spectra were performed using an electronic spreadsheet programmed to integrate using the trapezoid method. The distance of the e.p.r. spectrum from the baseline was measured every few Gauss over the required spectral range, and these values were entered into a BBC Master Series Microcomputer (Acorn Computers) running spreadsheet software (ViewSheet, Acornsoft).

2.13. Chemicals.

Oxidation reduction mediators were obtained from Aldrich or Koch-Light Laboratories. Nitrogen and CO gases were obtained from BOC. Acid hydrolysed casein and tryptone were obtained from labM. Dysprosium chloride and lanthanum chloride were obtained from Koch-Light. Bacteriological Agar was obtained from Oxoid. All other chemicals were obtained from BDH or Sigma.

2.14. Development of a data collection and analysis system for a Clark type oxygen electrode.

2.14.1. Introduction.

Analysis of the steady state kinetics of enzyme systems usually involves carrying out a large number of almost identical experiments in which there are small variations of, for example, the substrate concentration. It is often not possible to obtain the data necessary to construct standard kinetic plots from a single progress curve because of substrate exhaustion and product inhibition. However, this is not the case for oxidases catalysing the reduction of oxygen to water. Product inhibition is not a problem because the product of the reaction is water. In the case of an intact electron transport chain, such as is found in cytoplasmic membrane preparations of *E.coli*, the problem of substrate (respiratory chain reductant) exhaustion can be overcome by using an excess of the chosen substrate or a combination of substrates. Thus, provided that a viable method of oxygen

concentration determination is available, a great deal of information can be determined from a single experiment by recording the oxygen concentration as it proceeds towards anoxia. All the data required for conventional Michaelis-Menton analysis can be obtained by differentiation of such progress curves with respect to time.

Several methods have been utilised to measure oxygen concentrations in biological systems; these include oxygen binding to myoglobin (Wittenberg & Wittenberg, 1985), oxygen dependent quenching of fluorescence (Knopp & Longmuir, 1972), bacterial chemiluminescence (Oshino *et al.*, 1972), oxygen dependent quenching of phosphorescence (Vanderkooi *et al.*, 1987; Wilson *et al.*, 1988) and oxygen electrodes (Lessler & Brierley, 1969; Lakshminarayanaiah, 1976). Of these methods, the use of oxygen electrodes is by far the most common due to the simplicity of the experimental set up. Oxygen electrodes also have the advantage in that they are non invasive in the sense that they do not involve additions of substances directly to the assay mixture, and therefore there is less scope for the occurrence of artifacts. The most commonly used design of oxygen electrode, and the type used in the work reported herein, is the membrane covered Clark type (for a description see Lakshminarayanaiah, 1976).

Rice & Hempfling (1978) and Kita *et al.* (1984b) used Clark type oxygen electrodes to study the oxidase kinetics of cytochrome *bd* in the absence of inhibitors. However, the high oxygen affinity of cytochrome *bd* makes the Clark type electrode unsuitable for studying oxidase reactions with K_m 's in the sub-micromolar range. This is borne out by the range in the published K_m 's of cytochrome *bd* for oxygen.

The K_m 's reported for cytochrome *bd* in cells range from 0.024 μ M (Rice & Hempfling, 1978) to 0.27 μ M (Kita *et al.*, 1984b).

In the work reported herein a Clark type oxygen electrode was used to study the kinetics of oxygen consumption by a cytoplasmic membrane preparation containing cytochrome *bd*. No effort was made to study the effect of very low concentrations of oxygen on the rate of oxygen uptake. Instead, the oxidase inhibitors nitrite (Chapter 3) and carbon monoxide (Chapter 6) were used to raise the K_m of the cytochrome for oxygen to a level where corresponding oxygen concentrations could accurately be measured using an oxygen electrode. In order to study the oxidase kinetics at concentrations of oxygen in the sub-micromolar range in the absence of inhibitors, it would be necessary to use more sophisticated approaches such as a vibrating oxygen electrode (Longmuir, 1957; Degn & Wohlrab, 1971) or the effect of oxygen on phosphorescence lifetimes (Wilson *et al.*, 1988).

A data collection system was developed which allowed collection, storage, and analysis of oxygen electrode traces using a 64K BBC Model B microcomputer (Acorn). Data could also be analysed using the University's VAX 11/780 minicomputer (DEC). All software was written in either BBC BASIC or VAX-11 BASIC, taking advantage of the ability of both these languages to dispense with software relevant line numbers. It was found that the speed of the BASIC on the microcomputer was sufficient for this particular application, and it was not necessary to resort to the complications of machine code. Graphics were produced using GHOST subroutines running on the VAX and were plotted out on a Benson B9211 electrostatic plotter connected to

the same machine.

2.14.2. The microcomputer interface.

Two oxygen electrode-microcomputer interfaces were developed, one based on the internal analogue to digital converter (ADC) present in the BBC Model B, and one based on a custom built ADC. In both cases the response of the ADC was linear with respect to input voltage. Each oxygen electrode trace consisted of up to 500 data points (stored as time, $[O_2]$). Times were recorded from the internal clock of the microcomputer.

2.14.2.1. Data collection using the internal ADC.

The initial approach to data collection was to read voltages from the oxygen electrode using the internal 8-bit ADC of the microcomputer which is able to read voltages in the 0-1.8V range. This had advantages in terms of cost and simplicity, and its performance also approached that of the custom built ADC. The oxygen electrode was connected to the ADC input via an amplifier (741 operational amplifier, constructed by Mr. C. Armit of the Department of Biochemistry and Microbiology Electronics Workshop), and an analogue port interface (constructed by Mr. A. Young of the University of St. Andrews Computing Laboratory). The latter was originally designed to interface a Gould storage oscilloscope to a BBC Model B and incorporated a 0.9V offset to enable the ADC to record voltages from the 741 operational amplifier in the -0.9 to 0.9V range. However, the oxygen electrode only produced positive voltages, so that the 0.9V

offset of the analogue port interface resulted in a readable range of voltages at the ADC of 0-0.9V, effectively reducing the resolution of this device for this application from 8-bit to 7-bit.

Voltages output from the oxygen electrode were amplified by the operational amplifier (10mV to around 0.8V) and fed into the analogue port interface. The voltage fed into and read by the computer was directly proportional to the voltage applied to the electrode side of the amplifier. The internal ADC of the computer was able to provide a new reading of input voltage every 10msec (Coll, 1982).

Since the timescales of the experiments envisaged for this system were minutes rather than seconds, it was possible to exploit the sampling rate of the internal ADC to filter voltage data concurrent to its collection. This was achieved by using a data collection routine which collected as many voltage samples as possible within a specified timescale. Although the voltage reading from the analogue to digital conversion was updated by the ADC every 10msec, the data collection routine was able to read the current value of the conversion every 2.6msec. This meant that although the apparent sampling rate of the system indicated by the collection routine is once every 2.6msec, new voltage readings were actually recorded once every 10msec. This anomaly introduced no errors into the collected data and was user invisible, so no steps were taken to correct it. The voltage samples collected within the specified timescale were averaged and the result stored to memory along with their mean time of collection. Such filtering results in a reduction in the amount of noise in a recorded voltage by a factor of \sqrt{N}/N , where N is the number of samples taken.

2.14.2.2. Data collection using the custom built ADC.

To enhance the signal to noise ratio of the collected data, an ADC was designed and constructed by Mr. A. Burnley of the University of St. Andrews Psychology Department Electronics Workshop. This device was sensitive enough to measure voltages in the -1 to 9mV range with 8-bit resolution, so no additional amplification was necessary between the oxygen electrode and the ADC. Data was collected and filtered as described above.

A major difference between the custom built and internal ADC's was the ability of the former to sample voltages from the oxygen electrode much more rapidly than the latter (2.5usec conversion⁻¹ compared to 10msec conversion⁻¹). The data collection routine was able to read a new voltage every 3.2msec from the custom built ADC. Each new voltage reading therefore corresponded to a new value for the analogue to digital conversion. The custom built ADC was therefore able to support enhanced levels of digital filtering of the data concurrent to its collection.

2.14.3. Calibration of oxygen concentrations.

The initial oxygen concentration of the contents of the electrode incubation vessel was calculated from the data of Chappell (1964). Of particular importance to the kinetic analyses of oxygen electrode traces was confidence in the voltage corresponding to complete anoxia. Initially, this was calibrated by "shorting" the input to the output from the oxygen electrode and programming the microcomputer to assume

that this corresponded to complete anoxia. However, this only appeared to be satisfactory when the oxygen electrode was new. Spurious positive or negative residual voltages were often subsequently produced when the contents of the incubation vessel were anoxic.

It was found that additions of small volumes (2-3ul) of a freshly prepared saturated solution of sodium dithionite resulted in a stable anoxic baseline. This was exploited by adding dithionite at the end of each progress curve. The microcomputer was programmed to calculate oxygen concentrations from the collected voltage data on the basis of the known initial oxygen concentration corresponding to the voltage at the start of the progress curve and the voltage corresponding to the dithionite induced complete anoxia.

2.14.4. Simulations of oxygen electrode traces.

It was important to test the data analyses described herein (Section 2.14.7), and this was achieved by writing a computer program simulating oxygen electrode traces conforming to Michealis-Menton kinetics using the following rate equation:

$$v = V_{\max} s^n / (K_m^n + s^n) \quad \dots\dots\dots 2.1$$

The simulation was conducted as follows. The concentration of oxygen consumed during a small time interval was calculated from Equation 2.1. This was subtracted from the total concentration and the calculation repeated until the elapsed time corresponded to the chosen interval between data points appropriate for the oxygen electrode

trace. The current substrate concentration and time were stored to memory and these iterations were repeated until 500 data points had been collected.

Computer generated noise could be incorporated into simulations as a percentage of the initial oxygen concentration. The variation in oxygen concentration due to noise remained constant throughout the trace so that its value as a percentage of the oxygen concentration increased as the oxygen concentration decreased. For example, an initial 1% noise (100:1 signal/noise ratio) became the equivalent of 10% noise (10:1 signal/noise ratio) when 90% of the oxygen had been consumed. This approximated the effect of electrical noise in experimental data.

2.14.5. Differentiation of progress curves.

Data collected from the oxygen electrode was analysed in terms of the effect of substrate concentration on the rate of oxygen consumption. In order to determine the rates of the oxidase reaction at different oxygen concentrations it was necessary to differentiate the progress curves collected by the microcomputer with respect to time.

Two differentiating algorithms were developed, one of which is a convolution function based on a non-weighted linear regression through a differentiating frame of data points which moves through the oxygen electrode trace one data point at a time. The estimation of the rate through the frame of points is based on a standard linear regression calculation (Sokal & Rohlf, 1981). The BASIC listing of the linear

regression algorithm is shown in Figure 2.2a. The other algorithm was based on the finite difference type of analysis used to resolve overlapping absorbance bands in optical spectra (Shipp, 1972; Butler, 1979), and its BASIC listing is shown in Figure 2.2b. The figure legend of Figure 2.2 contains a brief description of how these two algorithms function.

2.14.6. Noise.

Addition of a moderate amount of noise to simulated oxygen electrode traces generates an appreciable amount of noise in its derivative. This is most easily understood by considering random noise in an oxygen electrode trace expressed by an amplitude between zero and one. The first derivative of the noise calculated by measuring the gradient between adjacent data points one unit of time apart will give values in the range +1 to -1. Thus, the intensity of noise transferred to the derivative from the progress curve is doubled.

The extent of this problem can be grasped by considering the intensity of noise transferred from a progress curve to its derivative using a simulated oxygen electrode progress curve which approximates one obtained experimentally. For example, consider a progress curve simulated with the following kinetic parameters (Equation 2.1): $K_m=0.001\text{mM}$; $V_{max}=0.0008\text{mM sec}^{-1}$, initial $s=0.22\text{mM}$, $n=1$, and signal to noise ratio at the start of the simulation of 100:1. At the start of the trace the oxygen concentration is 0.22mM and its apparent value varies by 0.0022mM (1% of the $[\text{O}_2]$); that is, between 0.2189 and 0.2211mM . If the first derivative of the simulated progress curve is

Figure 2.2

*Noise averaging differentiating algorithms.**(a) Linear regression algorithm.*

An oxygen electrode trace consisting of M% collected data points is stored in array X as X(time, substrate). The differentiating frame is the variable AV% and represents the number of data points through which the gradient is determined. Since data is collected at a constant rate, the differentiating frame in terms of time remains unaltered through the stored trace. The rate through the frame of points is determined from a calculation of regression coefficient (Sokal & Rohlf, 1981). The value of each regression coefficient calculated is stored to array Y as Y(time, substrate, rate) where the values of time and substrate concentration are the mean values through the frame of points. The frame then moves one point further through array X and the calculation of rate is repeated. The algorithm iterates until all the points in array X have been included in rate determinations and results in AV% fewer points being present in array Y than in array X.

(b) Finite difference algorithm.

The oxygen electrode trace is stored and the differentiating frame is as in (a). The apparent rate of oxygen consumption is calculated simply as the ratio of the difference in oxygen concentration between the two points at each end of the differentiating frame to the respective time difference. Each value of rate is stored in array Y along with the median time and substrate concentration as Y(time, substrate, rate). The frame then moves one point further through array X and the calculation of rate is repeated. The algorithm iterates as for (a).

(a) *Linear regression algorithm.*

```
M%=M%-AV%
FOR B%=1 TO M%
  tend%=B%+AV%-1
  sumX=0
  sumY=0
  sumXY=0
  FOR A%=B% TO tend%
    sumX=sumX+Y(A%,0)
    sumY=sumY+Y(A%,1)
    sumXY=sumXY+(Y(A%,0)*Y(A%,1))
  NEXT A%
  avX=sumX/AV%
  avY=sumY/AV%
  squareX=0
  FOR A%=B% TO tend%
    squareX=squareX+((Y(A%,0)-avX)^2)
  NEXT A%
  sumprod=sumXY-((sumX*sumY)/AV%)
  regco=sumprod/squareX
  Y(B%,0)=avX
  Y(B%,1)=avY
  Y(B%,2)=-regco
NEXT B%
```

(b) *Finite difference algorithm.*

```
M%=M%-AV%
FOR A%=1 TO M%
  Tsub=(Y(A%+AV%,1)+Y(A%,1))/2
  Ttime=(Y(A%+AV%,0)+Y(A%,0))/2
  Trate=(Y(A%+AV%,1)-Y(A%,1))/(Y(A%+AV%,0)-Y(A%,0))
  Trate=-Trate
  Y(A%,0)=Ttime
  Y(A%,1)=Tsub
  Y(A%,2)=Trate
NEXT A%
```

calculated at the start of the trace by measuring the differences between data points one second apart, the noise present will result in a maximum variation of 0.0022mM sec^{-1} in the value of the first derivative. However, the actual oxidase rate at the start of the trace is approximately 0.0008mM sec^{-1} , so clearly in this case the first derivative of the progress curve is swamped by noise having a peak to peak intensity of up to 2.75 times the expected value of the derivative (or a signal to noise ratio of 0.36:1).

Two approaches were used in this work to minimise the amount of noise in collected and analysed data. Firstly, the data was digitally filtered concurrent to its collection (Section 2.14.2.1). Secondly, the differentiating algorithms used were written so as to calculate the rate of oxygen consumption through a 'frame' of points (section 2.14.5). The performance of these algorithms was evaluated using simulated data. Figure 2.3a shows a simulated oxygen electrode trace with a signal to noise ratio of 100:1 at the start of the trace. Figure 2.3b shows how the two algorithms cope with the noise in Figure 2.3a. Clearly, the finite difference algorithm was inferior to the linear regression algorithm. The latter was therefore used in the analyses of data carried out using the VAX. However, data analysis programs running on the BBC Model B were prohibitively slow when running the linear regression algorithm. The simpler finite difference algorithm was therefore used when data was analysed using the microcomputer.

The noise reduction properties of the linear regression type algorithm with respect to its differentiating frame were further

Figure 2.3

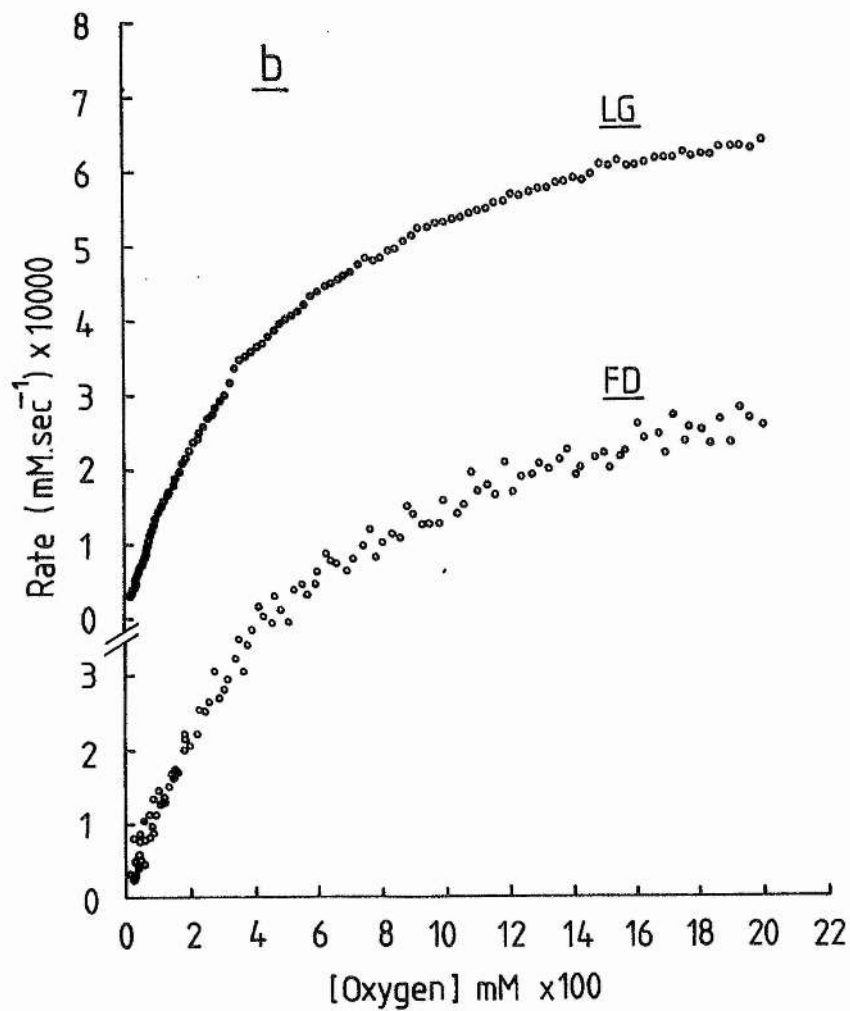
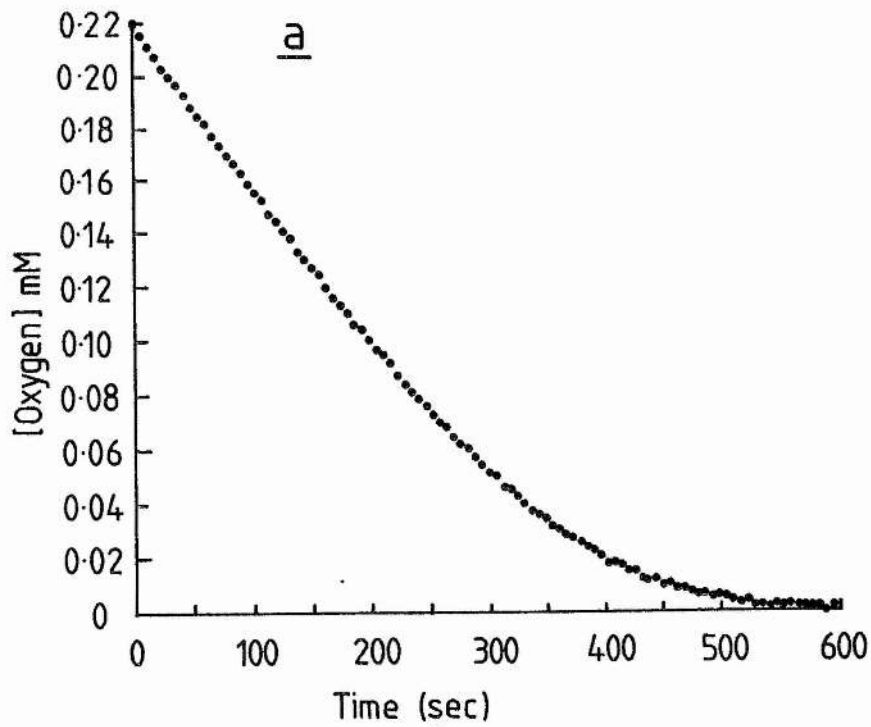
Comparison of the noise limiting performance of the two differentiating algorithms.

(a) Simulated progress curve containing computer generated noise.

An oxygen electrode progress curve was simulated with the following parameters: $K_m=0.05\text{mM}$; $V_{\text{max}}=0.0008\text{mM s}^{-1}$; initial substrate concentration = 0.22mM ; apparent number of sites, $n=1.0$; signal to noise ratio = 100:1; timespan = 600sec. Of the 500 data points simulated, only 100 are plotted in this figure.

(b) Plots of first derivative data versus oxygen concentration.

The progress curve in (a) was differentiated with respect to time using the two differentiating algorithms with differentiating frames of 60sec in each case and the derivatives were plotted as a function of substrate concentration. LG - data differentiated by the linear regression method. FD - data differentiated using the finite difference method. In both cases the differentiation resulted in the loss of 50 data points and, as in (a), only 100 of the data points are plotted.



probed by simulating a constant 'baseline' value of oxygen concentration with a signal to noise ratio of 100:1. Figure 2.4 illustrates qualitatively the effect of increasing the differentiating frame on the amount of noise transferred to the derivative. Clearly, a differentiating frame of 50sec, or one equivalent to 10% of the timescale of the derivative, is sufficient to eliminate most of the noise from the derivative. However, it is of importance to determine if such differentiating frames cause significant distortion of kinetic parameters determined from differentiated progress curves. This issue is addressed in the next section.

2.14.7. Data analysis.

Kinetic parameters were determined from collected progress curves by plotting the v and s data as Eadie-Hofstee (v versus v/s), Hanes (s/v versus s) and Hill plots ($\log v/(V_{max}-v)$ versus $\log s$). That this method of analysis was appropriate was tested by analysing simulated oxygen electrode traces. It was important to determine if the use of differentiating frames sufficiently large to limit the amount of noise in the derivative data could result in distortion of the apparent kinetic parameters. Figure 2.5 illustrates the effect of increasing the differentiating frame on the analysis of a simulated progress curve. The kinetic parameters used in the simulation are indicated in the figure legend. As can be seen, distortion occurs when large differentiating frames are used, particularly when the frame size exceeds about 20% of the time span of the trace. This results in an increase in the apparent K_m (Figure 2.5a), a slight downward curvature

Figure 2.4

Noise reduction properties of the linear regression type algorithm.

A "baseline" with zero rate was simulated with a stable oxygen concentration of 0.22mM and a signal to noise ratio of 100:1, this trace is labelled PC. This data was differentiated using the linear regression algorithm. The times on the right of the individual traces represent the differentiating frames used. In the case of the 2 second derivative, the differentiating frame is the lowest acceptable by the differentiating algorithm, and therefore represents a "worst case". As in Figure 2.3, only 100 points were plotted out of the possible 450-500.

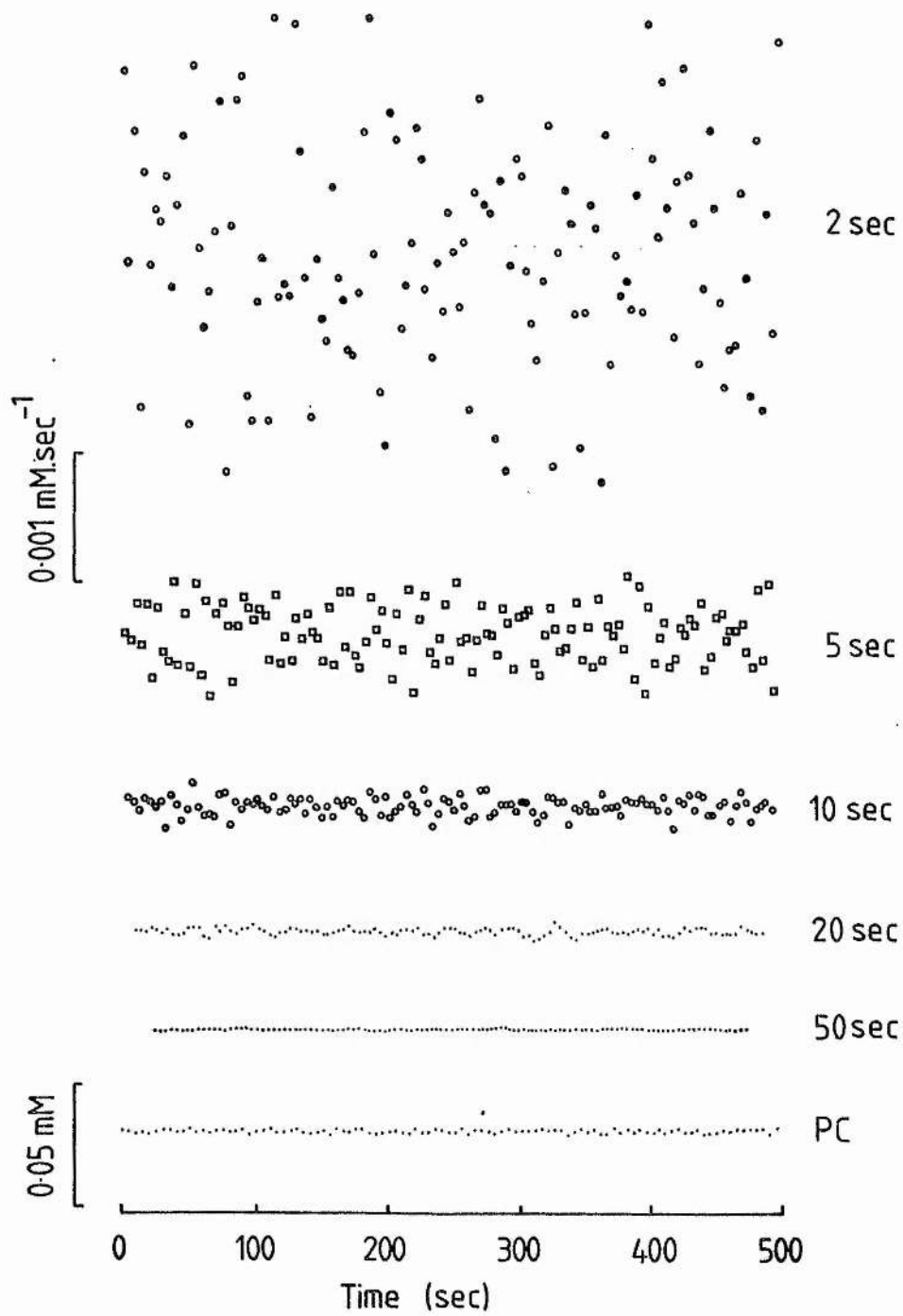
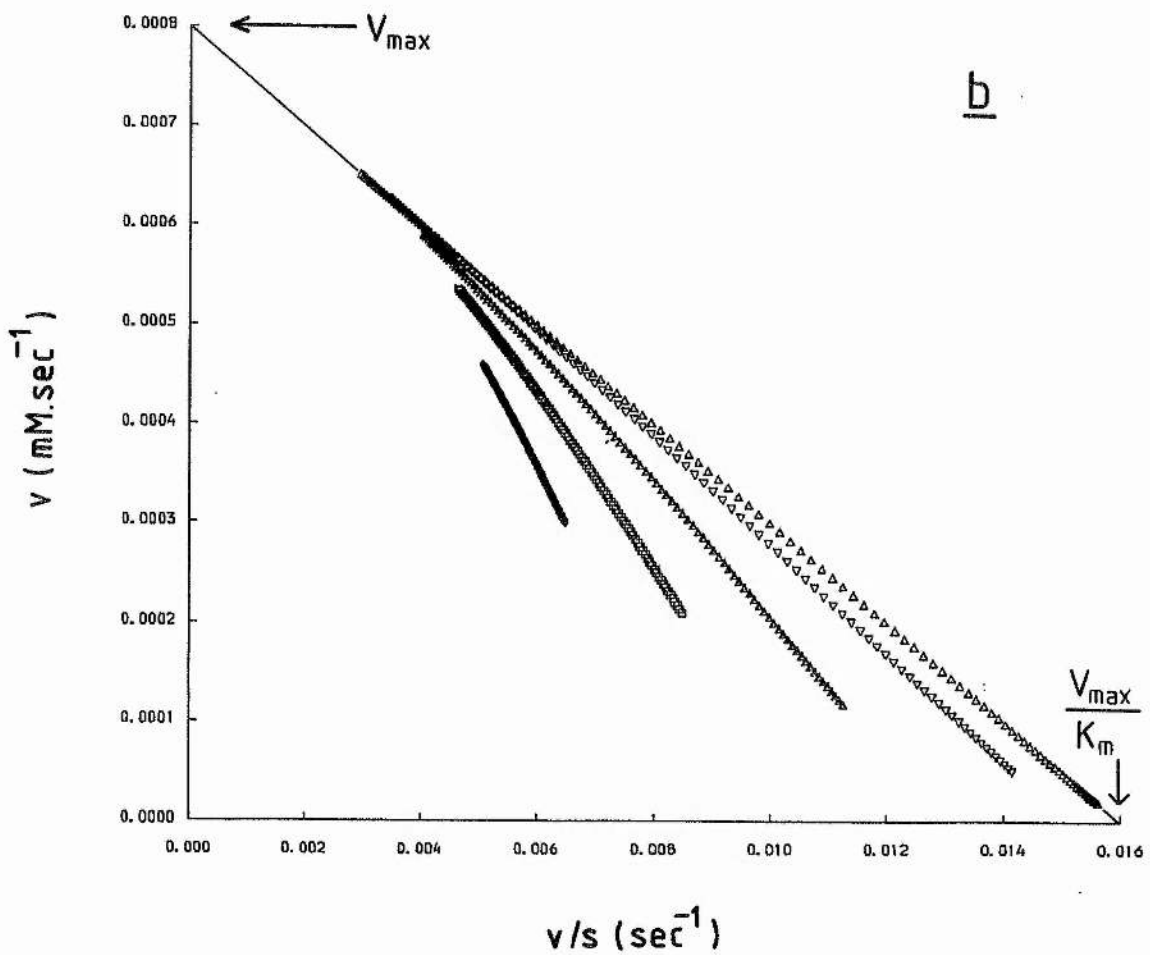
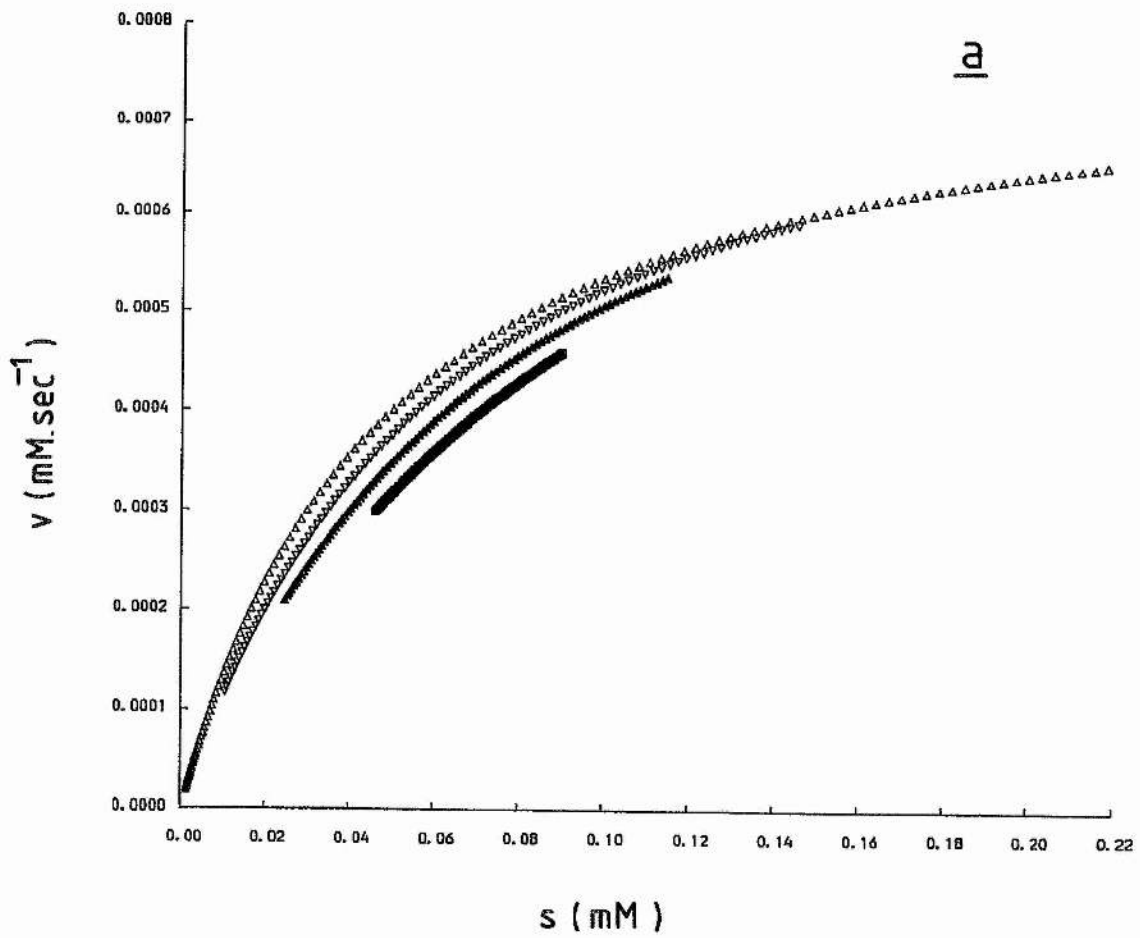


Figure 2.5

Distortion of data produced using large differentiating frames.

A progress curve was simulated with the following parameters: $K_m=0.05\text{mM}$, $V_{\text{max}}=0.0008\text{mM sec}^{-1}$, $n=1.0$, initial substrate concentration = 0.22mM , time span = 600sec . The first derivative data were plotted as v versus s (a), or v versus v/s (b). Increasing the differentiating frames resulted in distortion and 'loss' of data in the derivative. Differentiating frames used in (a) were: \triangle , 2.4sec ; ∇ , 240sec ; \blacktriangle , 360sec ; \square , 480sec . Differentiating frames used in (b) were: \triangle , 2.4sec ; ∇ , 120sec ; \blacktriangle , 240sec ; \square , 360sec ; \diamond , 480sec .



of the Eadie-Hofstee plot (Figure 2.5b), and a slight upward curvature of the Hanes plot (not shown). A good compromise value for the differentiating frame was found to be one equivalent to 10% of the time span of the oxygen electrode trace.

Of particular relevance to the data presented in Chapter 3 and Chapter 6 is the effect of cooperative oxygen binding to an oxidase (cytochrome *bd*) in the presence of inhibitors. Eadie-Hofstee and Hanes plots derived from oxygen electrode traces simulated according to Equation 2.1 are illustrated in Figure 2.6. In the case of the Eadie-Hofstee plot, when $n > 1$, a peak in the direction of v/s is observed, the position of the tip of which can be used to estimate the values of the kinetic parameters K_m and n (Segel, 1975). The coordinates of this peak bear the following relationships to the kinetic parameters:

$$v = ((n-1)/n) V_{max} \dots\dots\dots 2.2$$

$$v/s = \frac{(n-1) ((n-1)/n) V_{max}}{n K_m} \dots\dots\dots 2.3$$

Equations 2.2 and 2.3 can be used to estimate the value of K_m and n provided that an estimate of V_{max} is available. The V_{max} can either be estimated by extrapolation from the upper end of the Eadie-Hofstee curve to the v axis, or by measuring the gradient of the linear region of the equivalent Hanes plot (Figure 2.6b). Alternatively, V_{max} can be estimated as before, and n and K_m obtained from a Hill plot.

Figure 2.6

Effect of cooperative oxygen binding on Eadie-Hofstee and Hanes plots.

Oxygen electrode traces were simulated with the following kinetic parameters: $K_m=0.05\text{mM}$, $V_{\text{max}}=0.0008\text{mM sec}^{-1}$, initial substrate concentration = 0.22mM , time span= 600sec . Apparent number of sites, n variable. \triangle , $n=1$; ∇ , $n=1.3$; \blacktriangle , $n=1.5$; \square , $n=1.7$; \diamond , $n=2.0$. These traces were differentiated using the linear regression algorithm using a differentiating frame equal to 10% of the total time span of the traces (60 sec) and the data were plotted as Eadie-Hofstee (a) and Hanes plots (b).

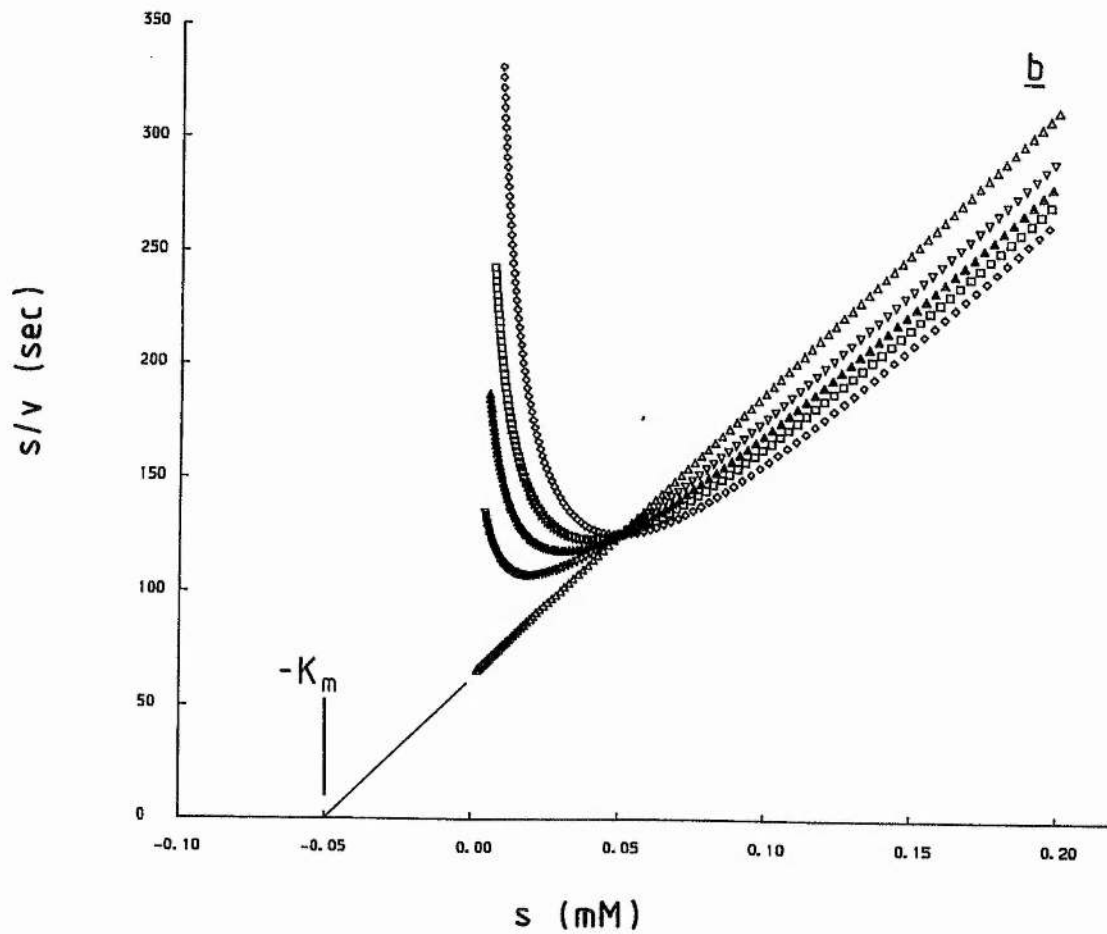
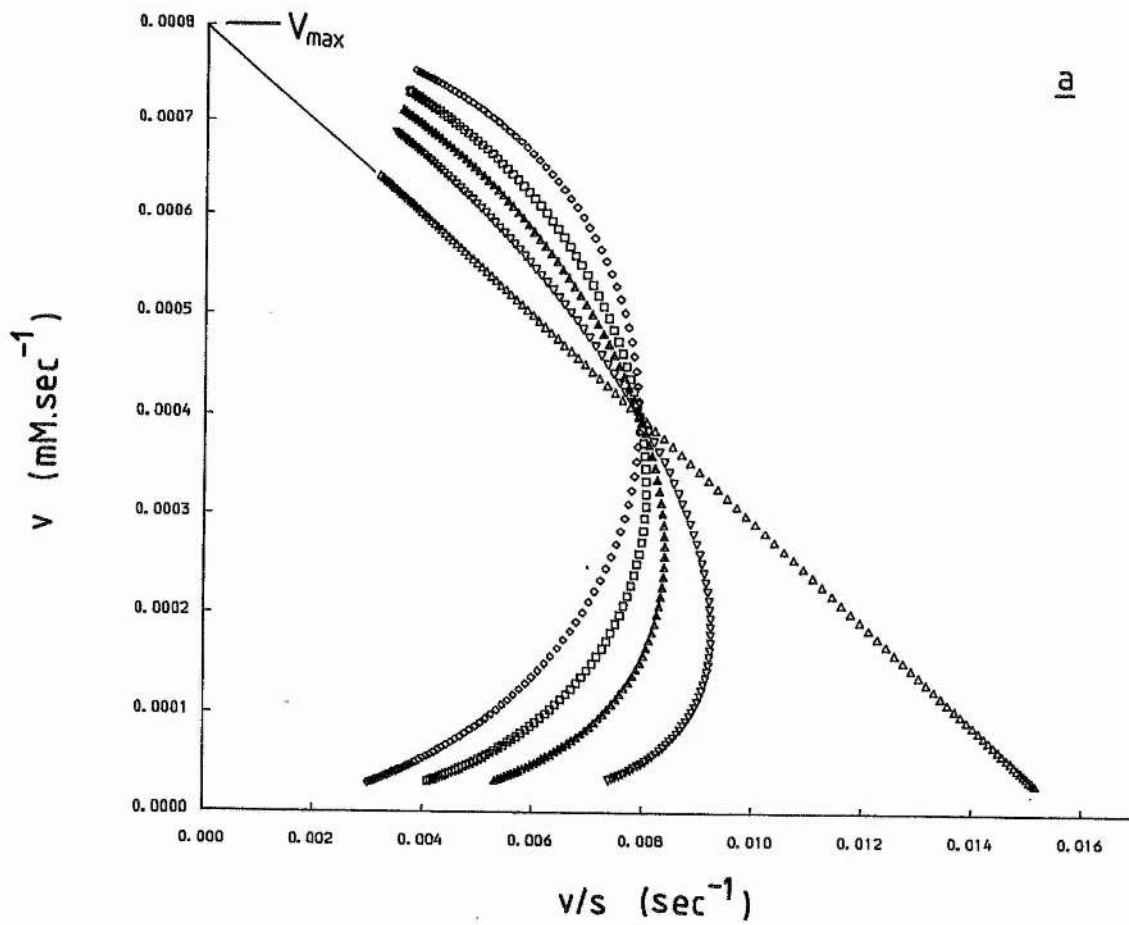


Figure 2.7 shows Hill plots derived from progress curves simulated with identical kinetic parameters, apart from a variation in n .

It is notable that the differentiations of the progress curves used to produce Figure 2.6 and Figure 2.7 were carried out using the 'default' differentiating frame equivalent to 10% of the timescale of each simulation. In all three plots, little or no distortions of the kinetic parameters determined from them were detected.

2.14.8. Higher derivatives.

Higher derivatives of progress curves have been used successfully to determine kinetic parameters. Peterson (1983) showed that analyses of electronically produced derivatives of progress curves can be used to determine values of K_m and V_{max} . The analysis is quite sophisticated, and is not used herein.

Higher derivatives of progress curves could easily be produced by modifying the linear regression type algorithm of Figure 2.2a. The BASIC listing of an algorithm able to produce higher derivatives is shown in Figure 2.8 and the differences between this algorithm and that of Figure 2.2a are described in the figure legend. Figure 2.9 shows an $n=1$ progress curve and derivatives thereof. Peterson (1983) showed that the peak of the second derivative in this case occurs at $v=V_{max}/3$ and used a derivative form of the Michaelis-Menton equation to calculate the K_m . In cases where the reaction is cooperative, the peak of the second derivative occurs at $v=V_{max}/2$ (Figure 2.10). In this case the value of s at the peak of the second derivative corresponds to the K_m of the enzyme.

Figure 2.7

Effect of cooperative oxygen binding on Hill plots.

Oxygen electrode traces were simulated with the following kinetic parameters: $K_m=0.05\text{mM}$, $V_{\text{max}}=0.0008\text{mM sec}^{-1}$, initial substrate concentration = 0.22mM , time span = 600sec . Apparent number of sites, n variable. \triangle , $n=1$; ∇ , $n=1.2$; \blacktriangle , $n=1.4$; \square , $n=1.6$; \diamond , $n=1.8$; \circ , $n=2.0$. These traces were differentiated using the linear regression algorithm with a differentiating frame equal to 10% of the total time span of the traces (60 sec) and the data were plotted as Hill plots with a V_{max} of 0.0008mM sec^{-1} .

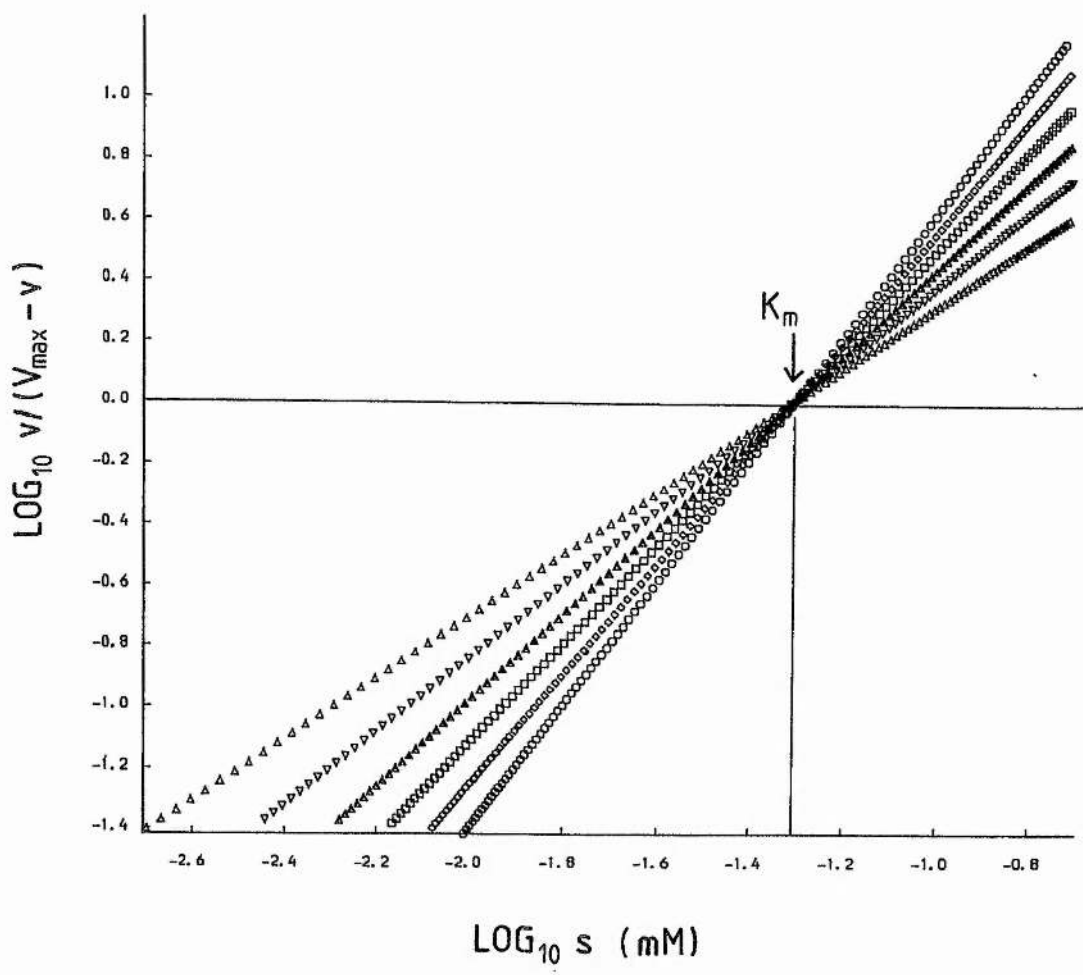


Figure 2.8

Linear regression type differentiating algorithm for producing second and subsequent derivatives of oxygen electrode traces.

This is based on the linear regression differentiating algorithm described in Figure 2.2 with some modifications. The oxygen electrode trace is stored in array Y as Y(time,substrate,substrate). The major difference between this algorithm and the one in Figure 2.2(a) is that the contents of Y(n,2) are differentiated with respect to Y(n,0). Thus, after the calculation of the first derivative, Y(n,2) contains data corresponding to reaction rates. This means that there is no need to copy data between arrays after each derivative is calculated. An additional feature is the provision for averaging of the data between derivatives; this represents an additional filtering of the data. D% is the number of derivatives required, AV% is the differentiating frame, SM% is the size of the averaging frame, and DF is the factor by which AV% is multiplied between each differentiation. For each derivative calculated, the resultant number of data points is decreased by AV%+SM% if SM%>1 or AV% if SM%=1.

(a) Differentiating algorithm for second and subsequent derivatives.

```
FOR C%=1 TO D%
  IF SM%>1
    THEN
      M%=M%-SM%
      FOR A%=1 TO M%
        sumX=0
        sumY=0
        sumZ=0
        tend%=A%+SM%-1
        FOR B%=A% TO tend%
          sumX=sumX+Y(B%,0)
          sumY=sumY+Y(B%,1)
          sumZ=sumZ+Y(B%,2)
        NEXT B%
        Y(A%,0)=sumX/SM%
        Y(A%,1)=sumY/SM%
        Y(A%,2)=sumZ/SM%
      NEXT A%
    END IF
    M%=M%-AV%
    FOR B%=1 TO M%
      tend%=B%+AV%-1
      sumX=0
      sumY=0
      sumZ=0
      sumXY=0
      FOR A%=B% TO tend%
        sumX=sumX+Y(A%,0)
        sumY=sumY+Y(A%,1)
        sumZ=sumZ+Y(A%,2)
        sumXY=sumXY+(Y(A%,0)*Y(A%,2))
      NEXT A%
      avX=sumX/AV%
      avY=sumY/AV%
      squareX=0
      FOR A%=B% TO tend%
        squareX=squareX+((Y(A%,0)-avX)^2)
      NEXT A%
      sumprod=sumXY-((sumX*sumZ)/AV%)
      regco=sumprod/squareX
      Y(B%,0)=avX
      Y(B%,1)=avY
      Y(B%,2)=regco
    NEXT B%
    AV%=INT(AV%*DF)
  NEXT C%
```

Figure 2.9

Higher derivatives of an $n=1$ progress curve.

A progress curve was simulated having the following parameters: $K_m=0.05\text{mM}$, $V_{\text{max}}=0.0008\text{mM sec}^{-1}$, initial substrate concentration = 0.22mM , $n=1.0$, time span= 600sec . All differentiations that were plotted directly were carried out with a differentiating frame of 2.4sec . In (b) the Hanes plot data was differentiated with a differentiating frame of 60sec .

(a) Plots of derivatives versus time.

Progress curve ($\triangle \times 1$), first derivative ($\nabla \times 3.37 \times 10^2$), second derivative ($\blacktriangle \times 1.16 \times 10^5$), and third derivative ($\square \times 2.04 \times 10^7$).

(b) Plots of derivatives versus oxygen concentration.

First derivative ($\triangle \times 4.81 \times 10^5$), second derivative ($\nabla \times 1.65 \times 10^8$), and third derivative ($\blacktriangle \times 2.91 \times 10^{10}$). In addition, a Hanes plot is included on the same axes ($\square \times 1$).

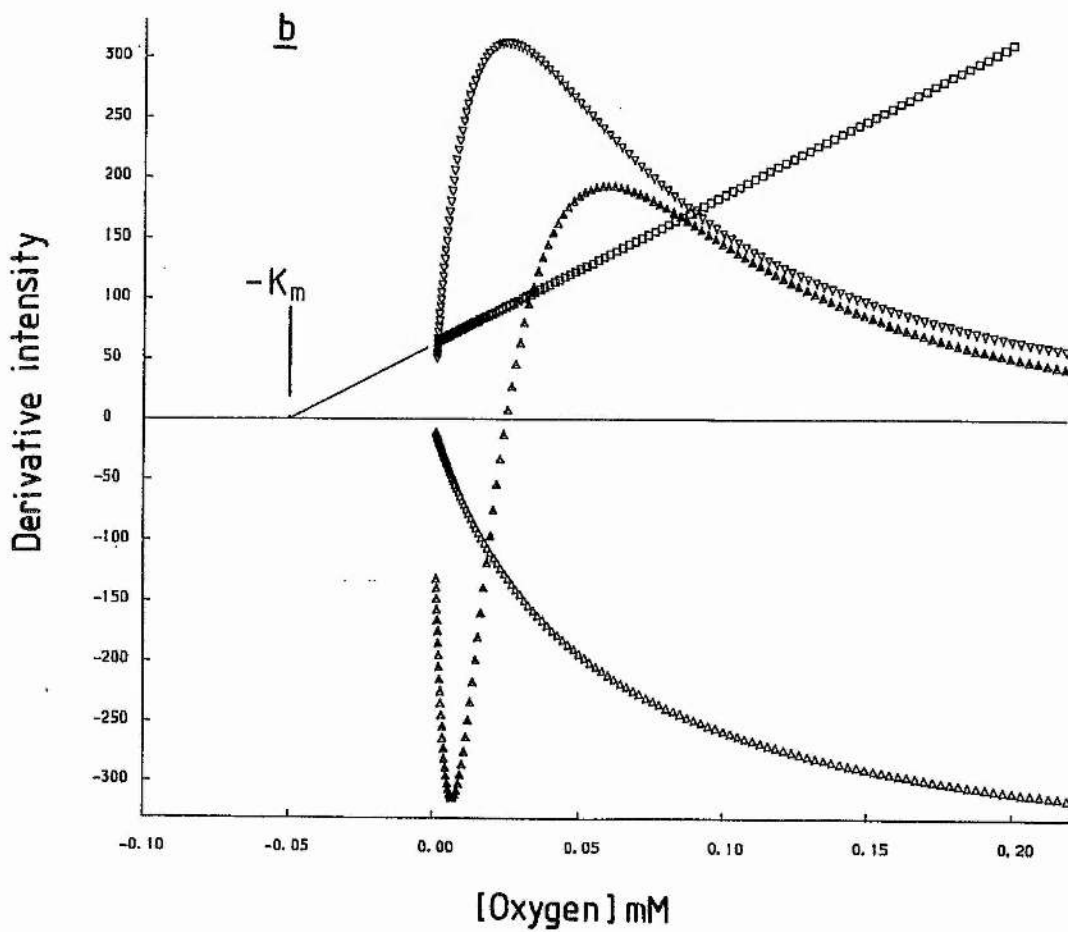
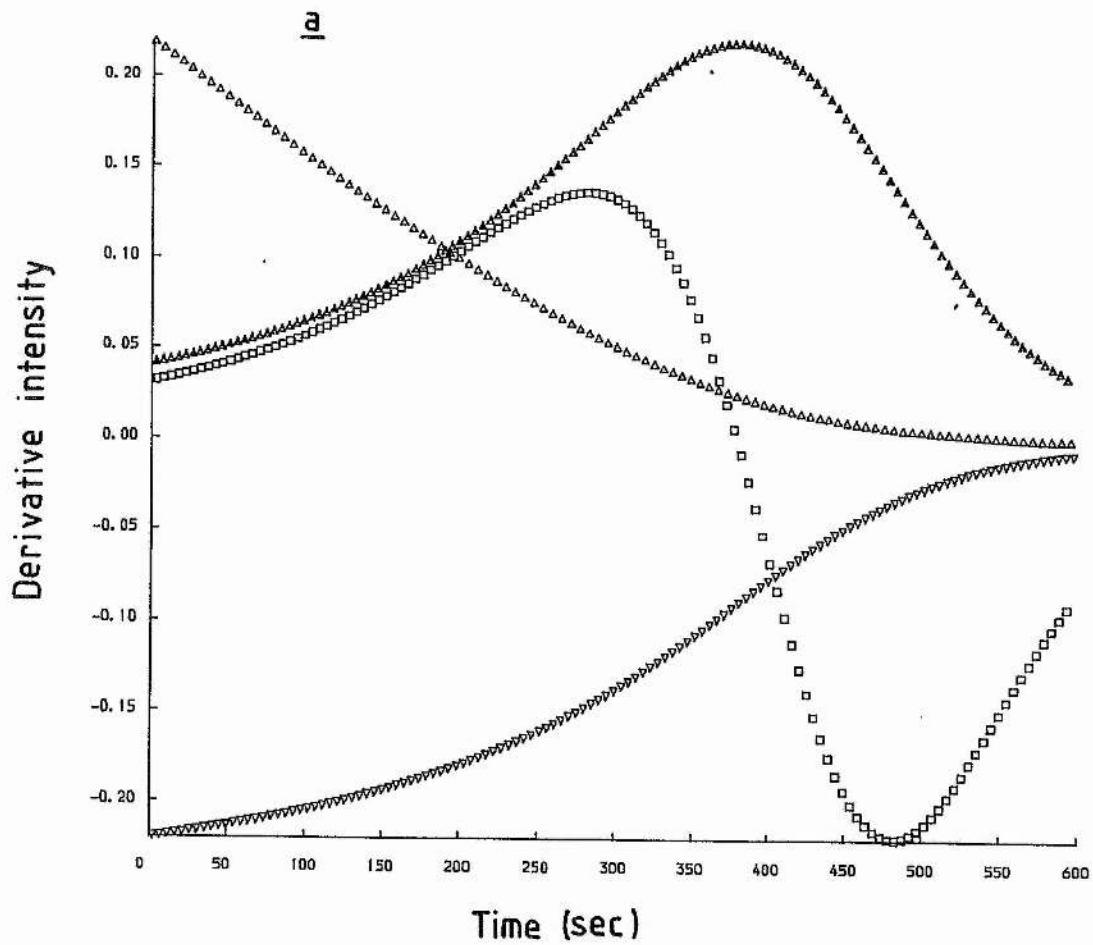


Figure 2.10

Higher derivatives of a cooperative, n=2 progress curve.

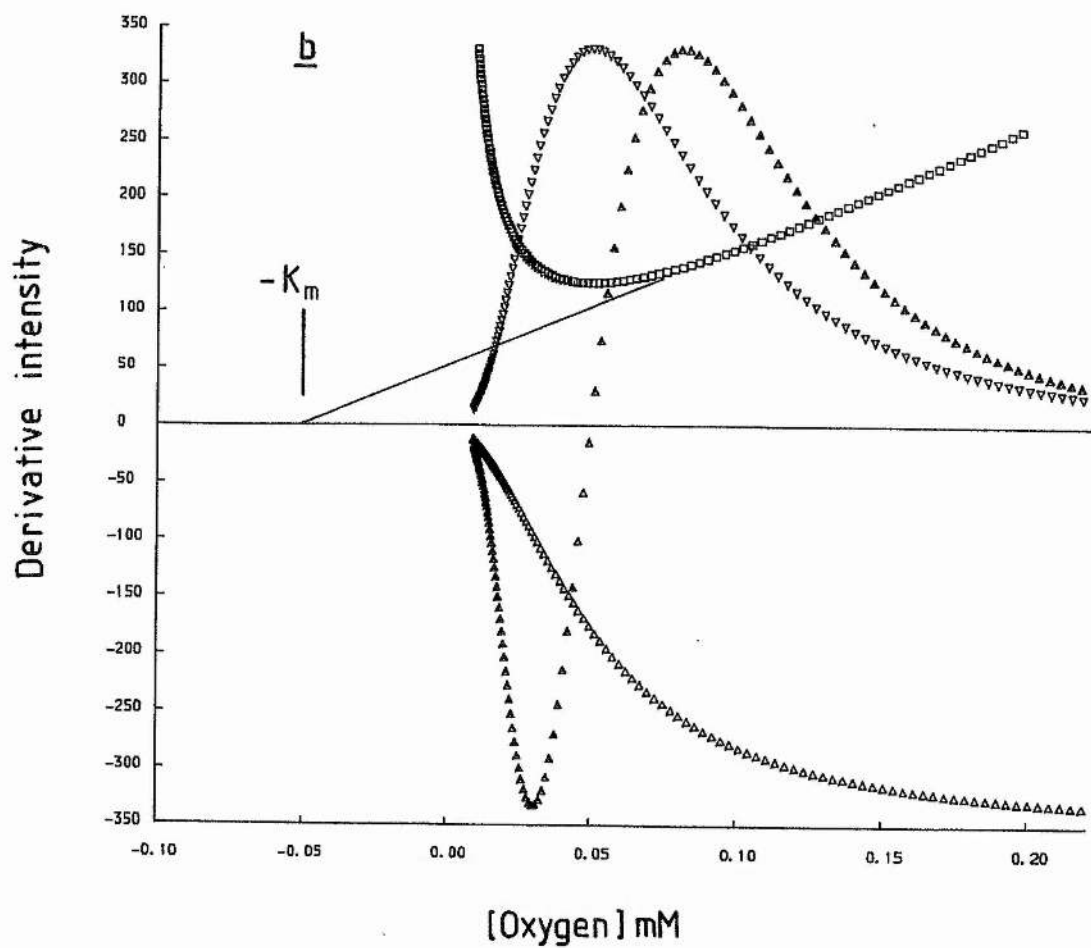
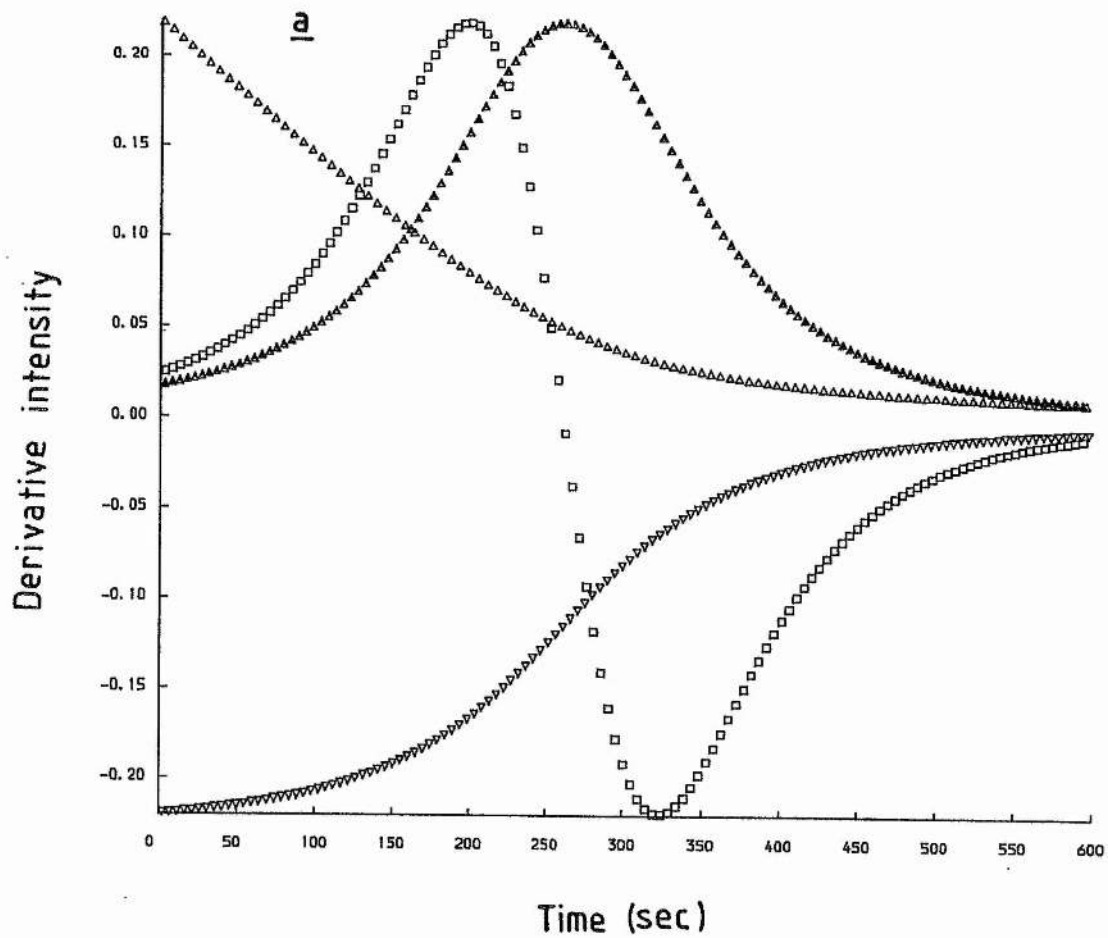
A progress curve was simulated having the following parameters: $K_m=0.05\text{mM}$, $V_{\text{max}}=0.0008\text{mM sec}^{-1}$, initial substrate concentration = 0.22mM , $n=2.0$, time span= 600sec . All differentiations were carried out with a differentiating frame of 2.4sec , except the one used to calculate the data for the Hanes plot of (b) which was carried out using a differentiating frame of 60sec .

(a) Plots of derivatives versus time.

Progress curve (\triangle x 1), first derivative (∇ x 2.88×10^2), second derivative (\blacktriangle x 6.85×10^4), and third derivative (\square x 9.96×10^6).

(b) Plots of derivatives versus oxygen concentration.

First derivative (\triangle x 4.37×10^5), second derivative (∇ x 1.04×10^8), and third derivative (\blacktriangle x 1.51×10^{10}). In addition, a Hanes plot is included on the same axes (\square x 1).



Analysis of data reported herein was not carried out using higher derivatives. The primary reason for this is that excessive amounts of noise were transferred to second and subsequent derivatives resulting in noise-swamping of the data. This problem can easily be understood by extension of the arguments in Section 2.14.6. Only exceptionally 'clean' progress curves could be successfully analysed using higher derivatives.

2.14.9. Applications of the oxygen electrode interface.

The data collection and analysis system described herein has been used to study oxidase kinetics in the presence of the respiratory inhibitors nitrite and CO (Chapters 3 & 6). Its major drawback is its inability to accurately measure the very low oxygen concentrations necessary for it to be used to study oxidase kinetics in the absence of inhibitors. Apart from being used in the studies reported herein, the system has been used to study sulphur and selenium oxidation by *Thiobacillus ferrooxidans* (M.Bacon & W.J.Ingledew, unpublished results) and photorelief of CO inhibition of cytochrome *bd* (Moodie & Ingledew, 1988).

The data collection and analysis software described herein is held in the account on the VAX at St. Andrews of Dr. W.J. Ingledew.

2.15. Other methods.

Descriptions of methods used in the work reported herein which are not described in the above are provided in appropriate figure legends elsewhere in this thesis.

CHAPTER THREE

Reactions of the in situ cytochrome bd with nitrite and oxygen.

3.1. Introduction.

As discussed in Chapter 1 (Section 1.4.7.5), nitrite reacts with reduced cytochrome *bd* and results in bleaching of the Soret and haem *d* alpha bands of its optical absorption spectrum. Meyer (1973) studied the optical changes following reaction of reduced *E.coli* cytoplasmic membranes with nitrite and concluded that the changes in the haem *d* alpha region are attributable to the formation of a nitric oxide adduct to haem *d*, whilst the changes in the Soret are attributable to the formation of nitric oxide adducts to haem *b₅₉₅* or haem *b₅₅₅* (of cytochrome *b₅₆₂₋₀*). The formation of a nitric oxide adduct to haem *d* should also result in minor changes in the Soret. As the cells used by Meyer were grown under conditions of low aeration, they probably contained cytochrome *bd* as the major terminal oxidase. This suggests that the changes in the Soret region of optical spectra following reaction with nitrite are due to the formation of a nitric oxide adduct to haem *b₅₉₅*. Analyses of the optical changes following reaction of nitric oxide with membranes containing cytochrome *bd* confirms that the species detected optically following reaction with nitrite are nitrosyl haems (Hubbard *et al.*, 1983; Meyer, 1973). This chapter includes an optical study of the reaction of nitrite with the *in situ* cytochrome *bd* in a cytoplasmic membrane preparation from anaerobically grown *E.coli* strain EMG2.

The reaction of nitrite with cytochrome *bd* is potentially very interesting. Solutions of nitrite exist as an equilibrium mixture of nitrite and nitrous acid and the concentrations of these species are determined by the pK_a of nitrous acid (3.37). If nitrite is the

species involved in the reaction with cytochrome *bd*, its reduction to nitric oxide involves addition of one electron and two protons, followed by the loss of one molecule of water. If nitrous acid is the reactive species, its reduction to NO involves addition of one electron and one proton. Thus, with respect to the reaction of nitrite being a reduction involving the loss of water, any information obtained about its mechanism may be relevant to an understanding of the oxidase reaction itself.

The reactions of cytochrome *bd* with nitrite described herein are distinct from the known *E.coli* nitrite reducing pathways, of which there are three (Lin & Kuritzkes, 1987; Cole, 1982). The nitrite reductases associated with these pathways include: (i) a soluble NADPH dependent enzyme which functions *in vivo* as a sulphite reductase; (ii) a soluble NADH dependent enzyme which functions during anaerobic growth to regenerate NAD⁺; and (iii) a membrane bound enzyme facilitating respiratory growth with nitrite as terminal oxidant.

In this chapter, the optical changes elicited by nitrite in a membrane preparation from anaerobically grown *E.coli* strain EMG2 containing cytochrome *bd* as terminal oxidase are described. A study of the inhibition of the oxidase reaction catalysed by cytochrome *bd* is also reported.

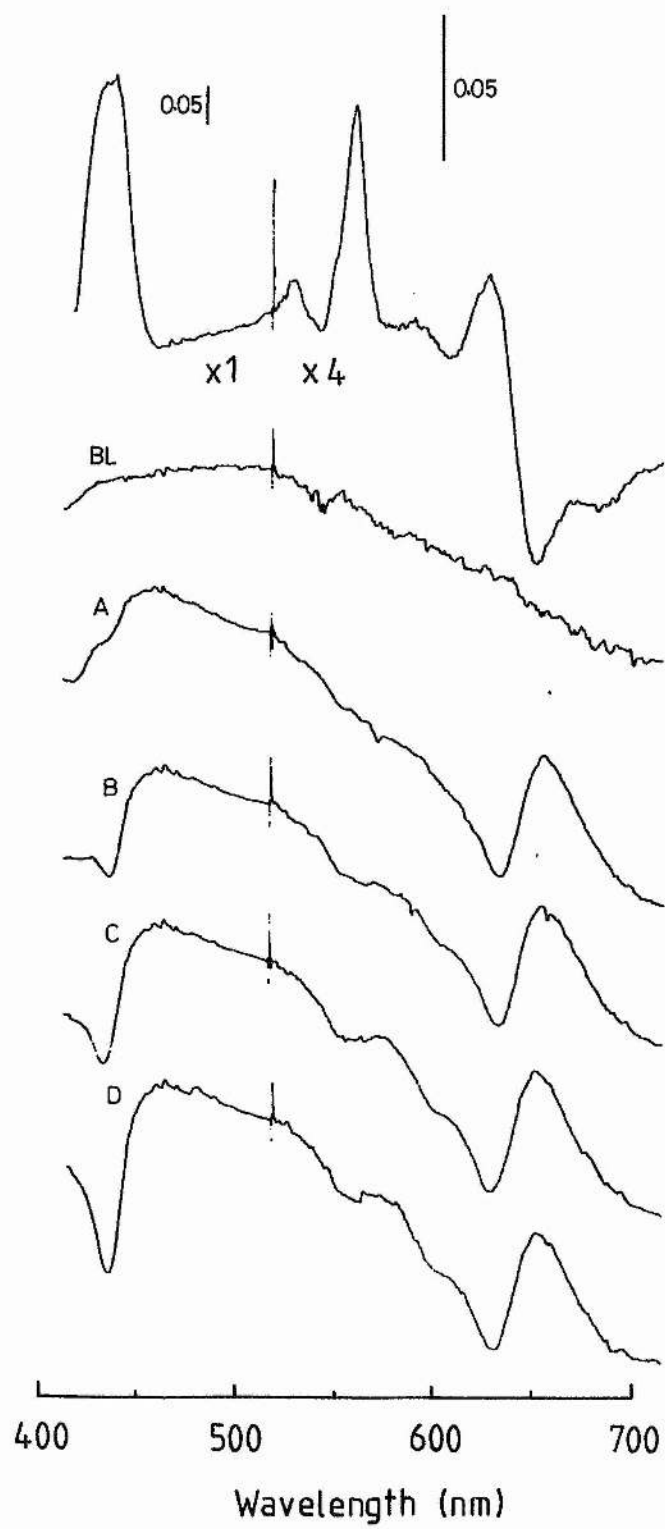
3.2 The cytochromes present in membranes from anaerobically grown *E.coli* EMG2.

Figure 3.1 (top) shows a reduced *minus* oxidically oxidised spectrum of the cytoplasmic membrane preparation used in this work. Noticeable

Figure 3.1

Optical difference spectra taken during the reaction of membranes with nitrite.

Spectra of cytoplasmic membranes showing a lactate reduced minus oxidically (H_2O_2) oxidised spectrum (top), a lactate reduced minus lactate reduced baseline (BL), and reduced plus nitrite minus reduced spectra taken at different times after addition of 1mM nitrite (sodium salt) to 10mM lactate reduced membranes at pH7: A (15 sec), B (14 min), C (21 min), and D (51 min). The reaction with nitrite (A-D) causes absorbance changes in the 438nm, 560nm, 595nm, and 630nm bands of the reduced spectrum of cytochrome *bd*. The change at 630nm appears to be complete within the time taken to record the first spectrum (A). Temperature, 20°C; scan rate, 1nm sec⁻¹; protein concentration, 7mg ml⁻¹. Membranes were suspended in 50mM Tes/KOH, pH7.



therein is a broad absorbance difference in the Soret (around 435nm) and prominent peaks at 530nm (haem b_{558} , beta band), 560nm (haem b_{558} , alpha band and haem b_{595} , beta band) and 630nm (haem d , alpha band). The trough at 650nm arises because oxically oxidised haem d has an absorbance maximum in this region (due to oxygen ligated haem d , haem d_{650} ; Poole *et al.*, 1983a). An additional trough at 680nm is due to an absorbance band of peroxide ligated haem d (haem d_{680} ; Poole & Williams, 1988). The small peak at 595nm is due to the alpha band of haem b_{595} (Lorence *et al.*, 1986). The reduced *minus* oxidised spectrum of Figure 3.1 (top) is very similar to the corresponding spectrum of purified cytochrome *bd* (Miller & Gennis, 1983; Kita *et al.*, 1984b). Cytochrome *bd* is therefore the major haemoprotein present in membranes prepared from anaerobically grown *E.coli* EMG2.

3.3. Changes in the optical absorption spectrum of cytochrome *bd* elicited by nitrite.

The effect of nitrite (sodium salt) on the optical spectrum of membranes containing cytochrome *bd* is illustrated in Figure 3.1A-D. Trace BL is a reduced *minus* reduced spectrum showing the instrument baseline, and traces A-D are reduced *plus* nitrite *minus* reduced spectra taken at successive times after addition of 1mM nitrite (15 sec, 14 min, 21 min, and 51 min respectively). It can be seen that a reaction resulting in an apparent bleaching of the haem d alpha band (inverse of the reduced *minus* oxidised spectrum) goes to completion within the time taken to record spectrum A. This rapid reaction is not accompanied by any other detectable change of comparable rate.

A relatively slow absorption change in the Soret region (at 438nm) can be discerned in the spectra of Figure 3.1 which is quite large compared to the Soret band of the reduced *minus* oxidised spectrum (Figure 3.1, top). Parallel changes are barely discernable at 595nm and 560nm and these can be attributed to bleaching of the haem *b₅₉₅* alpha and beta bands by nitrite. The connection between the optical change at 438nm and those at 560nm and 595nm is strengthened by kinetic analyses of the *E.coli* respiratory chain terminated by cytochrome *bd*; such analyses indicate that haem *b₅₉₅* has a Soret band at 438nm (D.S. Wariabharaj & W.J. Ingledew, unpublished results).

Comparison of the optical spectra of membranes following treatment with nitrite with those reported by Hubbard *et al.* (1983) and Meyer (1973) following treatment with nitric oxide indicates that the species responsible for the optical differences between the nitrite treated and reduced membranes are nitric oxide adducts to the ligand binding haems of cytochrome *bd* (haems *d* and *b₅₉₅*). This is confirmed by analysis of e.p.r. spectra of nitrite treated membranes (Chapter 4).

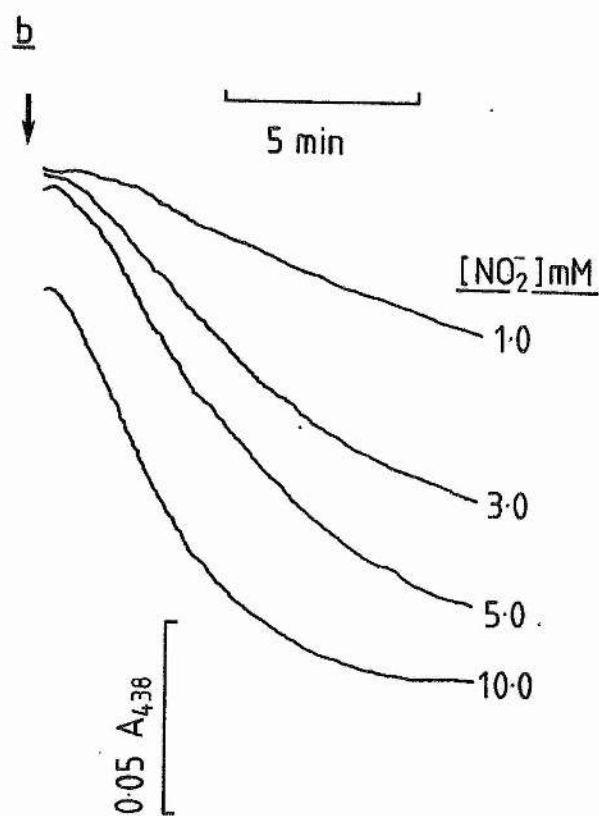
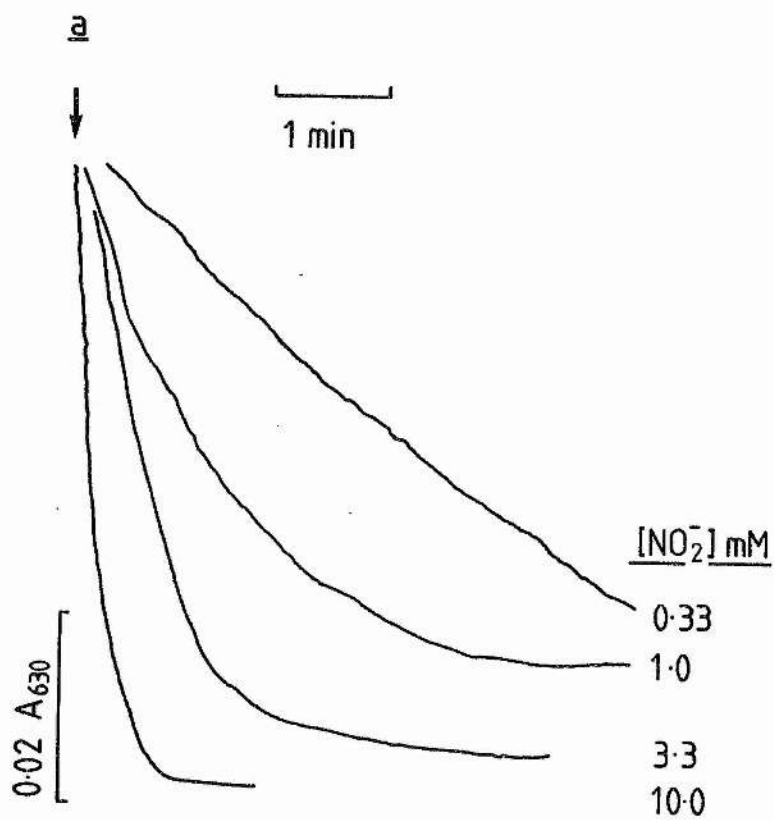
3.4 Kinetics of the nitrite induced spectral change at 630nm.

The time course of the reaction of reduced haem *d* with nitrite was studied in greater detail by monitoring the changes in the haem *d* alpha region at a fixed wavelength (630nm) with reduced membranes in the reference cuvette. Progress curves of the haem *d* reaction at different nitrite concentrations are shown in Figure 3.2a, and such curves were analysed to determine the effect of proton, nitrite, and

Figure 3.2

Progress curves of the optical changes elicited by nitrite.

Nitrite was added to membranes (7mg ml^{-1} protein) which had been reduced with 10mM sodium lactate, and the subsequent optical changes were recorded with lactate reduced membranes in the reference cuvette. The progress of the 630nm (a) and 438nm (b) optical changes are shown. Membranes were suspended in 50mM Tes/KOH (pH7) and the experimental temperature was 25°C .



haem *d* concentrations on the rate of formation of haem *d*-NO. These analyses enabled the apparent kinetic order of the reaction with respect to its reactants to be determined.

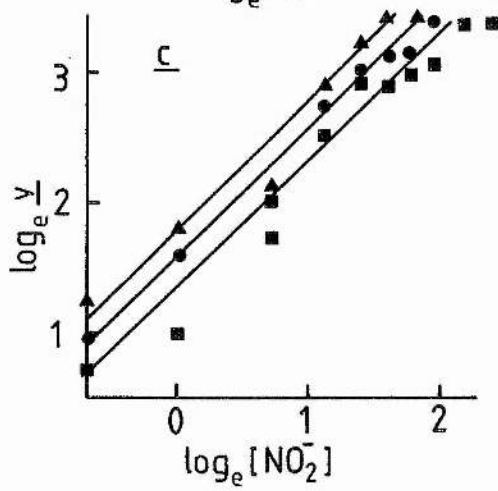
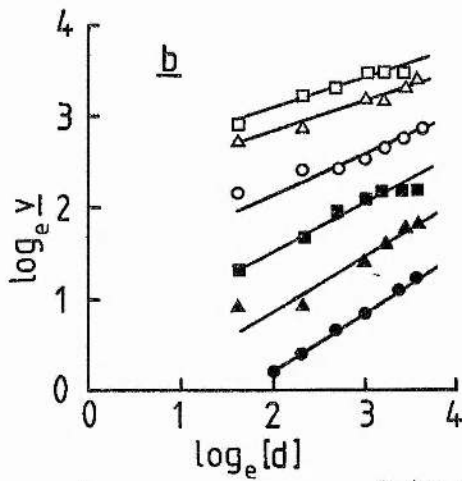
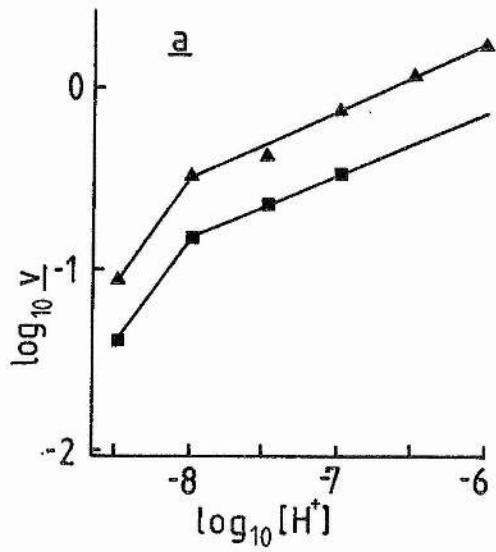
The rate of formation of haem *d*-NO becomes more rapid with decreasing pH. The relationship between the velocity of the reaction and proton concentration at two different concentrations of unreacted haem *d* is shown in Figure 3.3a. The reaction appears to be first order with respect to protons above pH8 and 0.35 order below this pH. However, the order of the reaction with respect to protons depends on whether nitrite or nitrous acid is the reactive species. The concentration of nitrous acid in a 1mM nitrite solution is around 2.3 μ M at pH6 (pK_a of nitrous acid = 3.37) and this decreases by one order of magnitude per unit increase in pH. The data in Figure 3.3a can be corrected for the pH dependence of nitrous acid concentration simply by subtracting one unit of gradient from the plot. Under these circumstances, the reaction order with respect to protons is zero above pH8 and -0.65 order below this pH. Thus, if nitrous acid is the reactive species, protons inhibit the formation of haem *d*-NO below pH8. However, any estimation of the number of protons involved in the reaction of haem *d* with nitrite is likely to be complicated by more general effects of pH on the ligand binding haem pocket of cytochrome *bd*. The pH dependence of the formation of haem *d*-NO and other data presented below indicate that nitrous acid is likely to be the form of nitrite which reacts with haem *d*.

Figure 3.3b shows the relationship between the velocity of the 630nm reaction and the concentration of unreacted haem *d* for a range

Figure 3.3

The effect of proton, haem d, and nitrite concentrations on the rate of bleaching of the haem d alpha band.

Progress curves such as those in Figure 3.2a were analysed to determine the kinetic order of the reaction of haem d with nitrite with respect to protons, haem d, and nitrite. Haem d concentrations were calculated using the extinction coefficient of $5.3\text{mM}^{-1}\text{cm}^{-1}$ for the wavelength pair 630-610nm quoted by Reid and Ingledew (1979). All rates are logarithms (natural or to the base 10) of arbitrary units. Depending on the required pH, membranes were suspended in 50mM Mes/KOH (pH6), Tes/KOH (pH7), or Tricine/KOH (pH8). Intermediate pH's were obtained by using appropriate mixtures of these buffers and adjusting the pH with KOH or HCl prior to use. (a) Velocity of the 630nm reaction versus the concentration of protons. \blacksquare — \blacksquare , log rate of reaction with 0.007 OD₆₃₀ haem d (1.32uM) unreacted; \blacktriangle — \blacktriangle , log rate of reaction with 0.02 OD₆₃₀ (3.77uM) haem d unreacted. Reactions were initiated by adding 1mM nitrite to a suspension of 10mM lactate reduced membranes. Protein concentration, 7mg ml⁻¹. (b) Velocity of the reaction versus concentration of haem d. Determination of reaction order at pH8 at different concentrations of nitrite. Nitrite concentrations: \bullet — \bullet , 0.5mM; \blacktriangle — \blacktriangle , 1mM; \blacksquare — \blacksquare , 2mM; \circ — \circ , 3mM; \triangle — \triangle , 4mM; \square — \square , 10mM nitrite. Protein concentration 7mg ml⁻¹. (c) Velocity of the reaction versus the concentration of nitrite. \blacksquare — \blacksquare , 0.005 OD₆₃₀ (0.94uM) haem d unreacted. \blacktriangle — \blacktriangle : 0.035 OD₆₃₀ (6.60uM) haem d unreacted. \bullet — \bullet : 0.025 OD₆₃₀ (4.72uM) haem d unreacted. Protein concentration: 8.9mg ml⁻¹; pH7.0.



of concentrations of nitrite. The reaction order with respect to haem *d* decreases with increasing nitrite concentration. At low nitrite concentrations, the reaction tends towards first order, and at high nitrite concentrations it approaches 0.25 order. This is consistent with the reaction approaching a haem *d* limited saturated rate at high nitrite concentrations. The data is therefore consistent with a single haem *d* being involved kinetically in the formation of haem *d*-NO.

Figure 3.3c shows the relationship between the concentration of nitrite and the rate of the 630nm reaction. The reaction is first order with respect to nitrite and there is no change in order with increasing nitrite concentration. This is consistent with a single nitrite being involved kinetically in the formation of haem *d*-NO.

Despite the complex effect of protons on the reaction rate and the effect of nitrite concentration on the order of the reaction with respect to haem *d*, the formation of the nitric oxide adduct to the haem *d* is much as expected, and appears to be a monophasic reaction of a single haem *d* with a single nitrite.

3.5 Kinetics of the nitrite induced Soret spectral change.

The reaction of nitrite with haem *b₅₉₅* was monitored in the Soret at a fixed wavelength of 438nm. This reaction is considerably slower than the reaction of nitrite with haem *d*, and appears to undergo a lag phase of initial acceleration. Its initial rate under the conditions used for Figure 3.2b (after the phase of acceleration) at 10mM nitrite was only 0.02 OD units min⁻¹, whilst the rate of the 630nm change was 0.20 OD units min⁻¹ (both rates were measured at pH7).

The rate of the reaction of haem *b₅₉₅* with nitrite increases with decreasing pH, again indicating that nitrous acid is the reactive form of nitrite. The extent of the reaction is also pH dependent. Figure 3.4a shows spectra taken after completion of the reaction at different pH's and Figure 3.4b shows the effect of pH on the extent of the haem *b₅₉₅* reaction. A pH dependent end point is suggested, associated with a pK_a of 7.3. The kinetics of the reaction of nitrite with haem *b₅₉₅* are therefore more complex than those of its reaction with haem *d*.

3.6 Nitrite reductase activity of membranes containing cytochrome *bd*.

The nitrite reductase activities of whole cells and cytoplasmic membranes from anaerobically grown *E.coli* EMG2 are illustrated in Figure 3.5. The activity at pH7 of whole cells is $1.87 \text{ nmol min}^{-1} (\text{mg protein})^{-1}$, whereas that of membranes is $0.068 \text{ nmol min}^{-1} (\text{mg protein})^{-1}$. These values compare with oxidase activities in membranes of around $150 \text{ nmol min}^{-1} (\text{mg protein})^{-1}$ with lactate as substrate. No significant increase in the rate of nitrite reduction by membranes is observed at pH6.

Cytochrome *bd* therefore appears to be unable to function as a nitrite reductase *in vivo*. This is significant because the only other enzyme containing a haem *d* to have been extensively studied is the dissimilatory nitrite reductase cytochrome *cd₁* of *Pseudomonas aeruginosa* and a number of other denitrifying bacteria (Poole, 1983). However, the structures of haems *d* and *d₁* are quite distinct. Haem *d* is a chlorin with one reductively dihydroxylated pyrrole (Timkovich

Figure 3.4

Effect of pH on the extent of the reaction of haem b₅₉₅ with nitrite.

(a) Spectra after completion of the reaction at different pH values. Reduced plus nitrite minus reduced difference spectra are illustrated between pH6.5 and pH8.5. 10mM lactate reduced membranes were reacted with 10mM nitrite and the reaction was allowed to proceed to its end point. Protein concentration, 7.0mg ml⁻¹. (b) The extent of the 438nm reaction versus pH. Temperature, 25°C; scan rate 1nm sec⁻¹. Membranes were suspended in 50mM Mes/KOH (pH6), Tes/KOH (pH7), or Tricine/KOH (pH8). Intermediate pH's were obtained by using appropriate mixtures of these buffers and adjusting the pH with KOH or HCl prior to use.

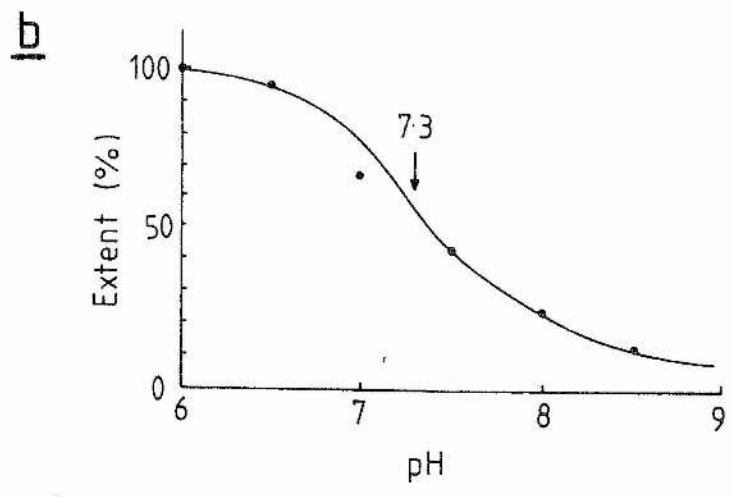
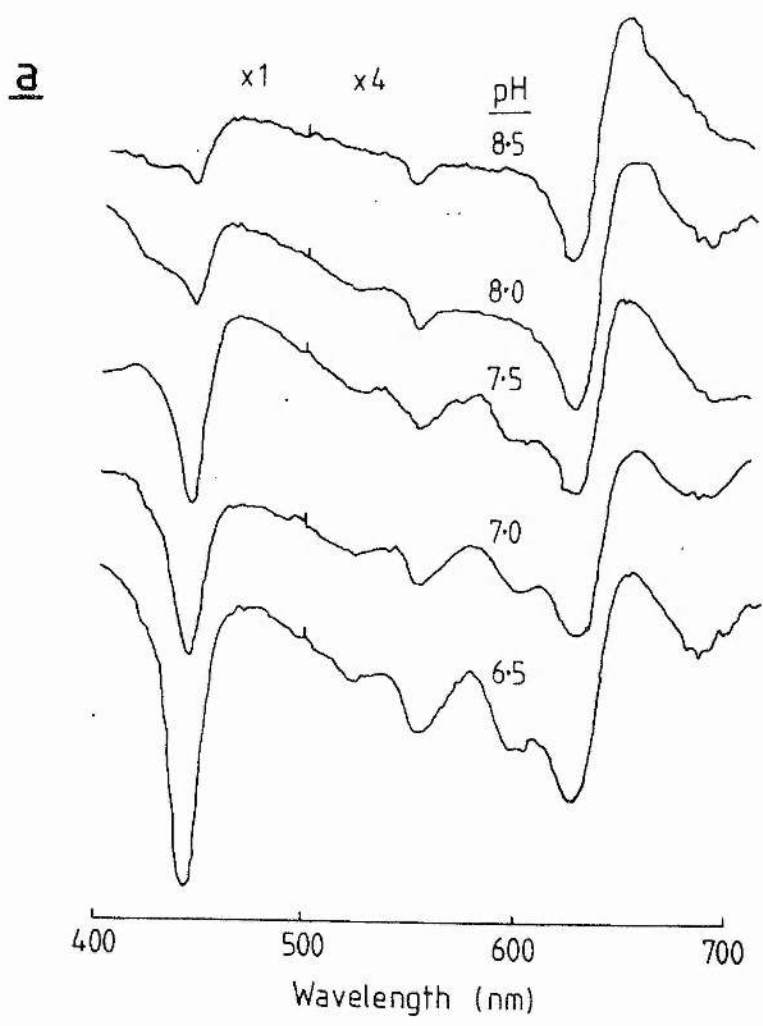
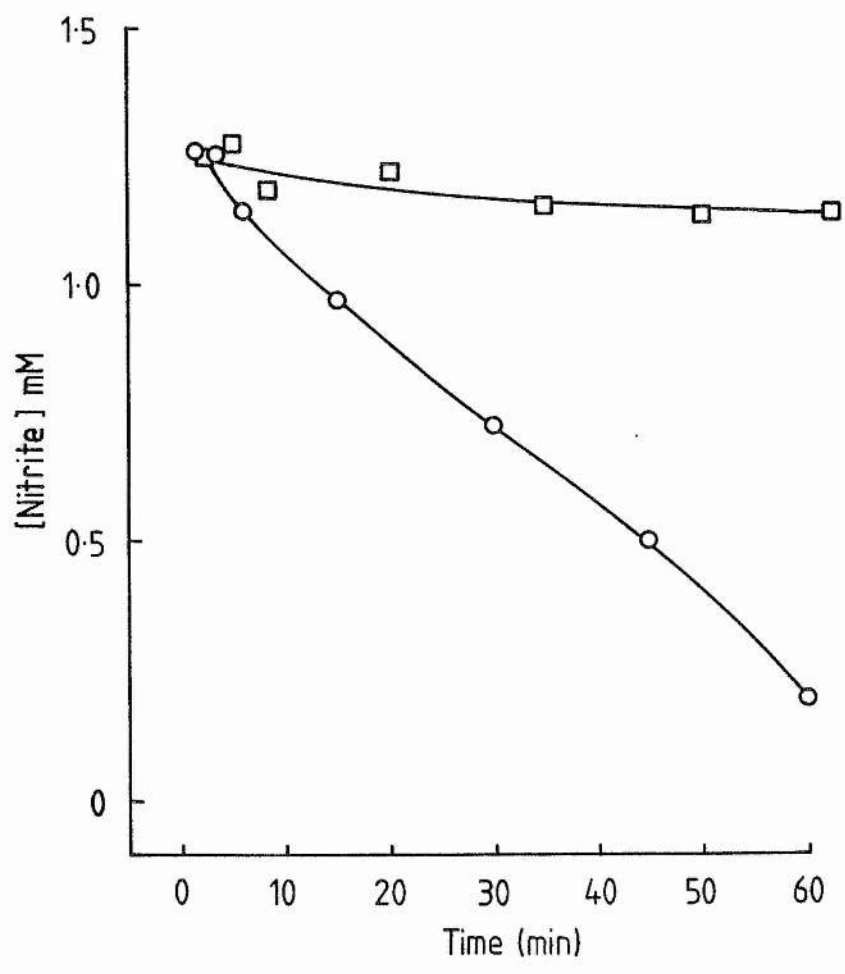


Figure 3.5

Nitrite reductase activities of membranes and whole cells.

Membranes (\square — \square) or cells (\circ — \circ) were incubated anaerobically (in a 50mM potassium phosphate buffer, pH7) in the presence of nitrite with lactate (20mM) as substrate at 30°C. Samples were withdrawn and assayed for nitrite as described in the text. The protein concentration of the incubation with whole cells was 10.7mg ml⁻¹ and that of the incubation with membranes was 29.4mg ml⁻¹.



et al., 1985), whereas haem *d*₁ is a porphyrindione with ketone groups on two adjacent pyrroles (Chang *et al.*, 1986). Whilst cytochrome *cd*₁ functions *in vivo* as a nitrite reductase (Yamanaka, 1964) which is fortuitously able to catalyse the reduction of oxygen (Timkovich & Robinson, 1979), cytochrome *bd* appears to function exclusively as an oxidase.

3.7 The pH dependence of the oxidase reaction.

The pH dependence of the oxidase activity of cytochrome *bd* in cytoplasmic membranes with lactate as substrate is shown in Figure 3.6. A pronounced pH optimum is observed at pH6.8 at an oxygen concentration of 0.1mM. However, this reflects the pH optimum of the entire lactate oxidase system rather than that of cytochrome *bd* itself. Oxidase activity is inhibited by 16mM nitrite and this concentration of inhibitor results in a shift in the pH optimum from pH6.8 to pH7.8 (Figure 3.6). Nitrite becomes a more potent inhibitor with decreasing pH from around pH7.8. However, low concentrations of nitrite (0-20mM) elicit a small activation of the oxidase reaction in the range pH7.8 to pH9.0. The reason for this activation is unknown.

3.8 The effect of nitrite on oxygen consumption in membranes.

The effect of nitrite on oxygen electrode progress curves recorded using the microcomputer interface described in Chapter 2 (Section 2.14) is illustrated in Figure 3.7. Nitrite reversibly inhibits the oxidase reaction and allows analysis of the steady state kinetics of the oxidase reaction by raising the K_m for oxygen to

Figure 3.6

Effect of pH on cytochrome bd catalysed oxidase activity.

pH profile for the consumption of oxygen by membranes with 16mM lactate as substrate. Data were obtained using a Clark type oxygen electrode and chart recorder. Rates were measured at 0.1mM oxygen concentration. \square — \square , pH profile of the oxidase reaction. \circ — \circ , pH profile of the oxidase reaction in the presence of 16mM nitrite. Protein concentration, 0.42mg ml⁻¹; temperature, 30°C. Depending on the required pH, membranes were suspended in 50mM Malonate/KOH (pH5.6), Mes/KOH (pH6), Tes/KOH (pH7), or Tricine/KOH (pH8). Intermediate pH's were obtained by using appropriate mixtures of these buffers and adjusting the pH with KOH or HCl prior to use. The buffers also contained 2mM MgSO₄.

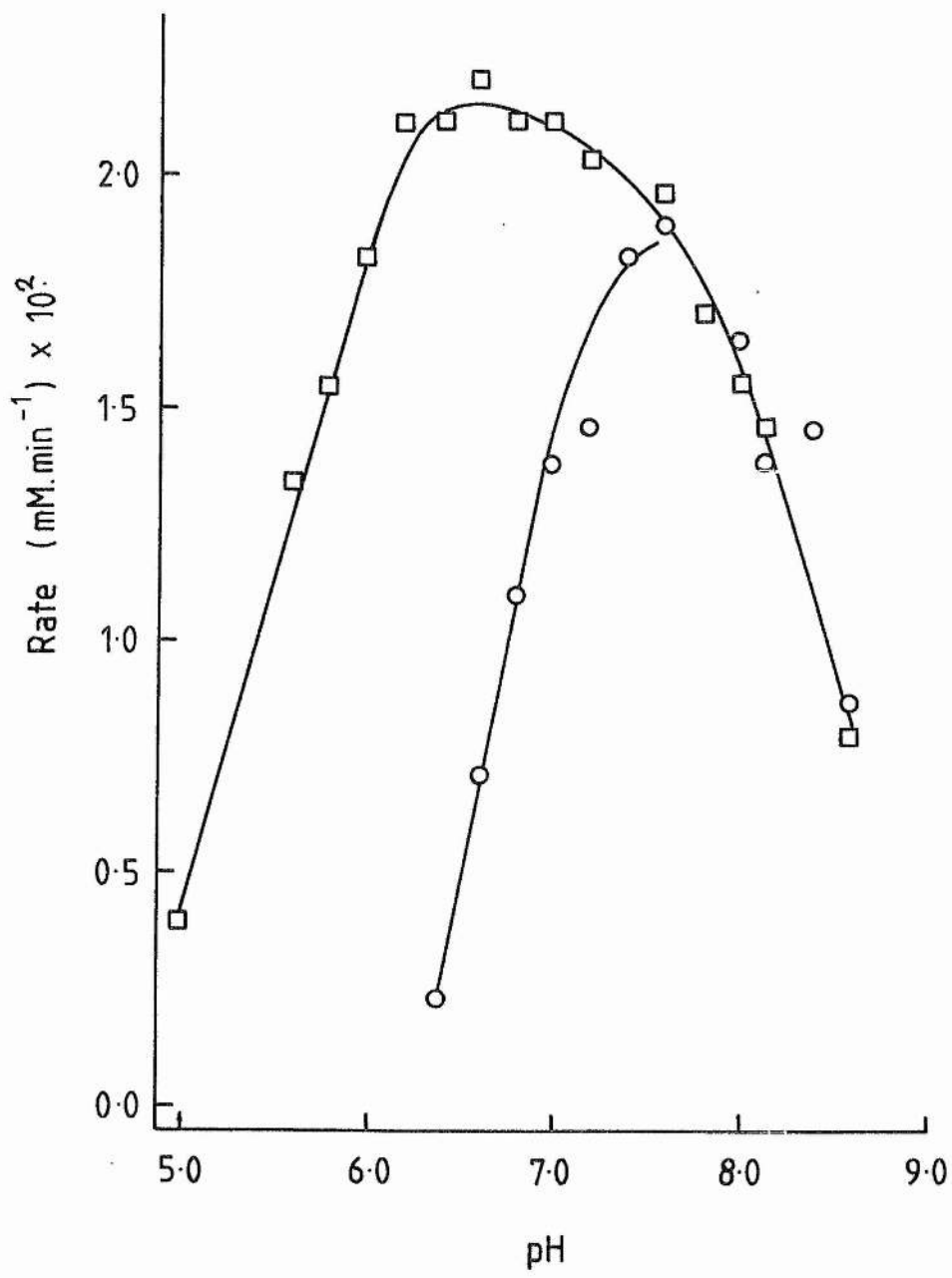
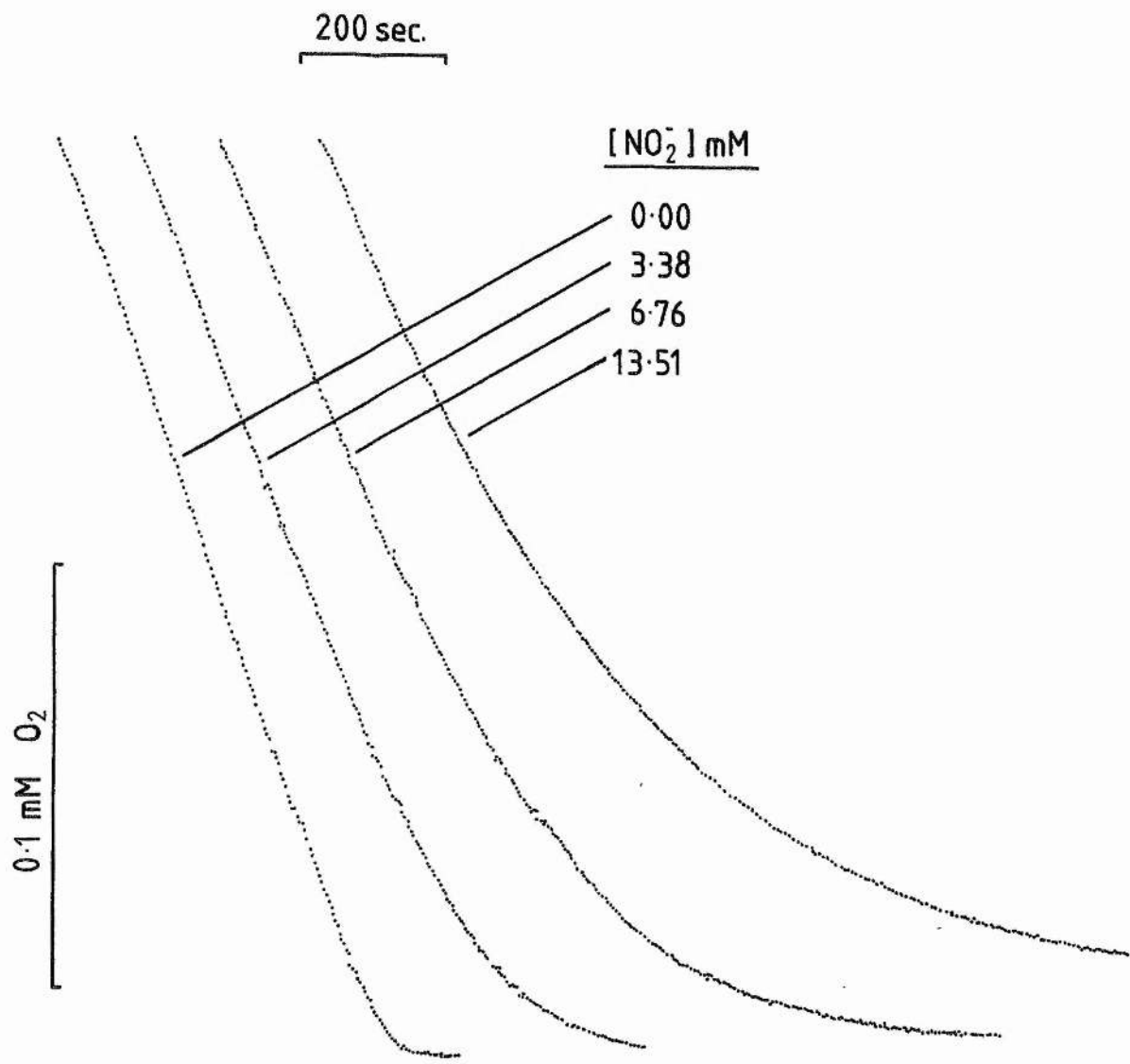


Figure 3.7

Effect of nitrite on oxygen electrode progress curves.

Computer recorded oxygen electrode traces for the consumption of oxygen by membranes with 34mM lactate as substrate in the presence and absence of nitrite at pH6.2. Protein concentration was 0.27mg ml⁻¹; temperature was 30°C. Membranes were suspended in 50mM Mes/KOH containing 2mM MgSO₄ (pH6.2).



within the concentration range easily measured using a Clark type oxygen electrode. The literature value of the K_m for oxygen is around 0.23 μM (Kita *et al.*, 1984b), which is too low to be accurately detected using a conventional oxygen electrode.

Progress curves such as those in Figure 3.7 were numerically differentiated (Chapter 2, Section 2.14.5), and the derivative data used to construct Hanes (s/v versus s) and Eadie-Hofstee (v versus v/s) plots (Figure 3.8a & b). Analyses of these plots (Segel, 1975; Chapter 2, Section 2.14.7) indicate that the oxidase reaction is cooperative with respect to oxygen binding in the presence of nitrite, and allowed estimations of V_{max} , K_m , and the apparent number of oxygen binding sites, n , to be made.

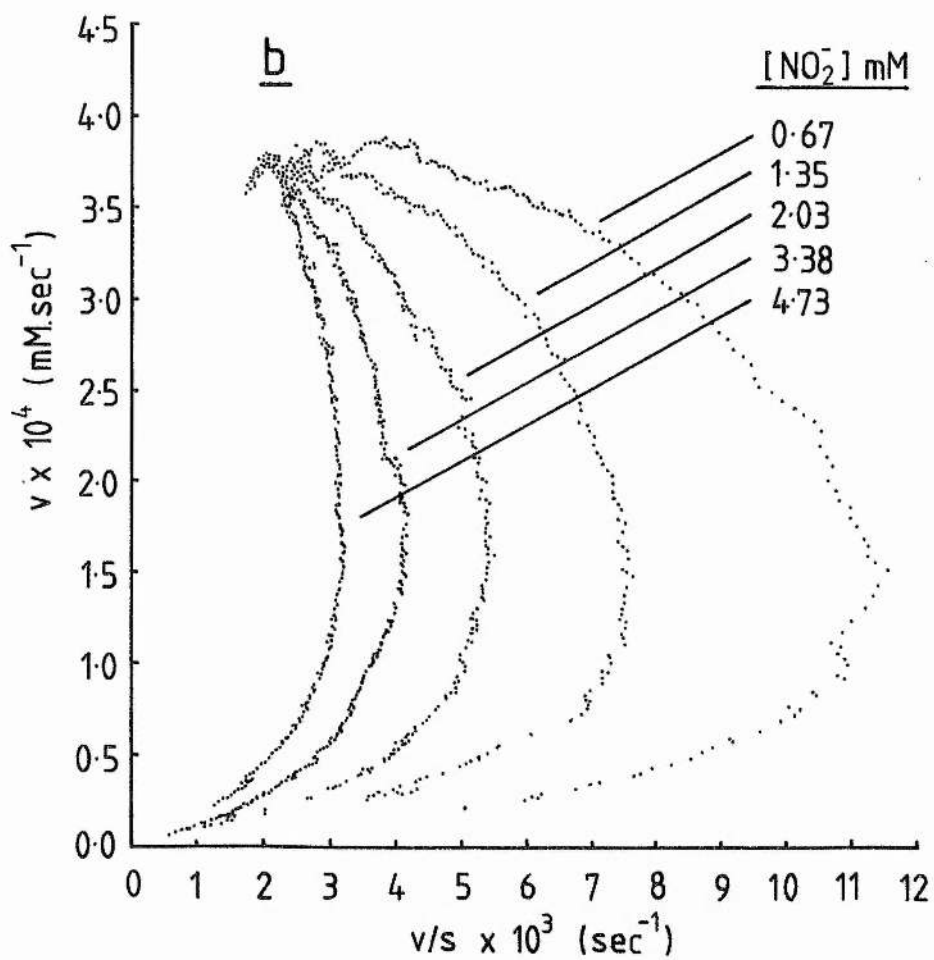
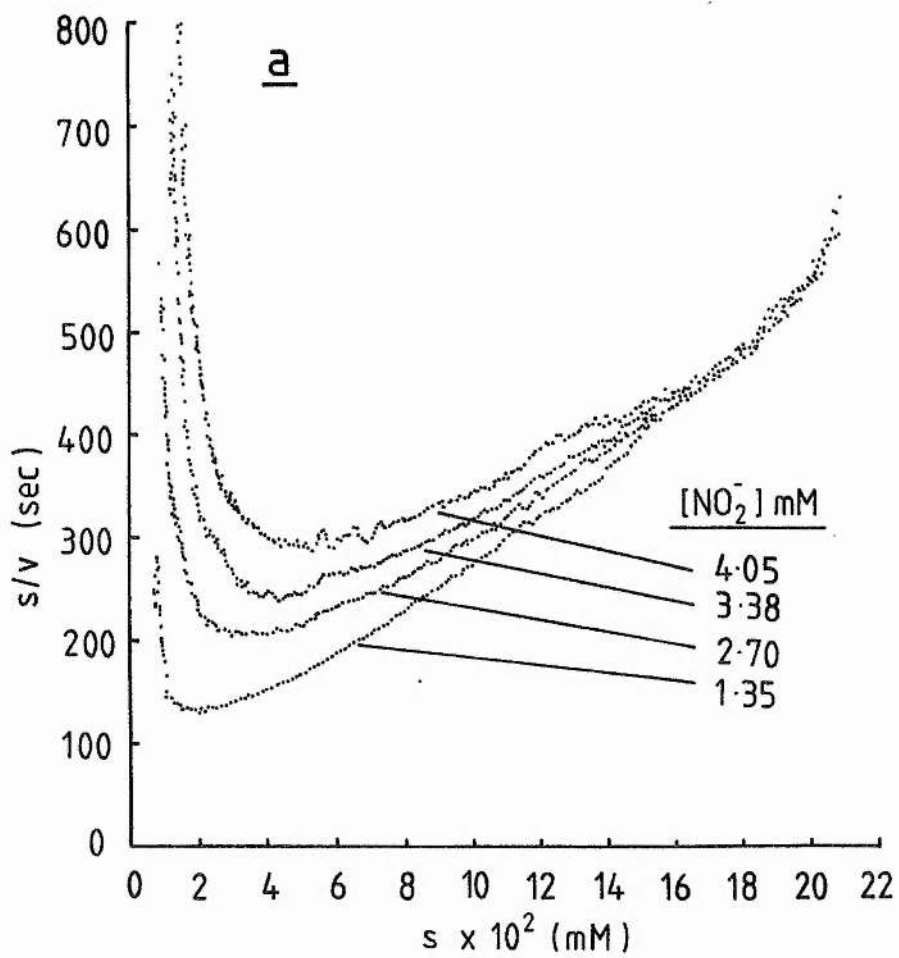
For example, in the case of the Eadie-Hofstee plot of Figure 3.8b at 1.35mM nitrite, the position of the peak on the ordinate is at $1.64 \times 10^{-4} \text{ mM sec}^{-1}$. The V_{max} can be estimated from the Hanes plot of Figure 3.8a as $3.92 \times 10^{-1} \text{ mM sec}^{-1}$. Application of Equation 2.2 (Chapter 2, Section 2.14.7) to these values enables the apparent number of oxygen binding sites to be calculated yielding a value of 1.72. Likewise, the peak position on the abscissa of the plot of Figure 3.8b at 1.35mM nitrite is 0.0076 sec^{-1} , and Equation 2.3 can be used to calculate the K_m , yielding a value of 36.1 μM . Similar results could be obtained by plotting the data as a Hill plot (not shown).

The convergence of the Eadie-Hofstee plots of Figure 3.8b and the tendency of the Hanes plots of Figure 3.8a to approach a single gradient at around 0.15mM oxygen indicates that increasing concentrations of nitrite increase the apparent K_m of the oxidase for

Figure 3.8

Kinetic analyses of oxygen electrode progress curves.

Hanes (a) and Eadie-Hofstee (b) plots for the nitrite inhibited oxidase reaction. Data were obtained from differentiated oxygen electrode progress curves recorded at pH6.0 in the presence of increasing concentrations of nitrite using 34mM lactate as reductant and with a protein concentration of 0.27mg ml⁻¹. Temperature, 30°C. Membranes were suspended in 50mM Mes/KOH (pH6.0) containing 2mM MgSO₄.



oxygen whilst having little effect on the V_{max} . Nitrite therefore appears to act as a competitive inhibitor of the oxidase reaction. Estimations of K_m were also made from the intercept of the 'linear' region of the Hanes plots on the abscissa and these values were similar to those determined from Eadie-Hofstee plots, albeit with more noise. The values determined from Eadie-Hofstee plots were therefore used in most of the analyses described herein.

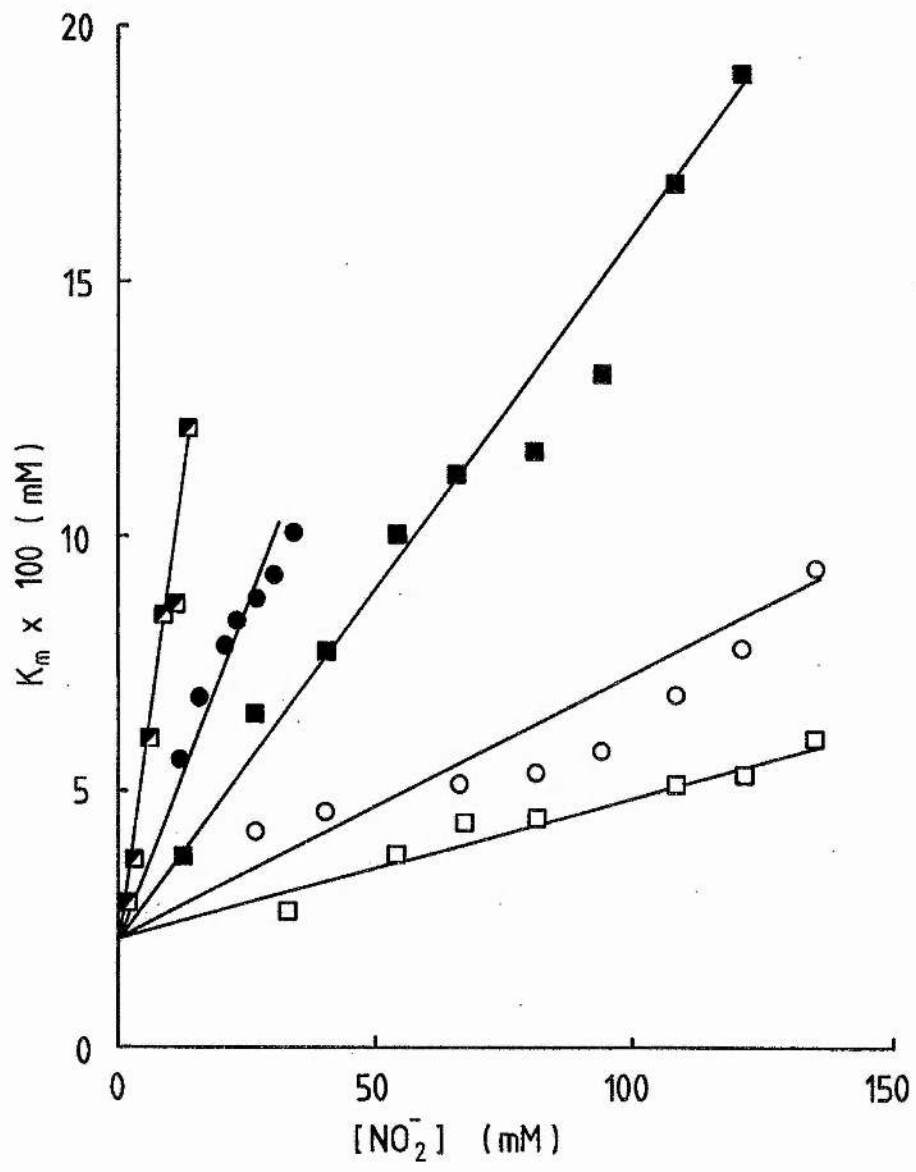
The concentration dependence of the nitrite inhibition and the cooperativity exhibited by the oxidase reaction were investigated in the pH range pH6.0-7.0. At each pH, the K_i was calculated by measuring the gradient of a plot of the apparent K_m for oxygen versus nitrite concentration (Figure 3.9). Extrapolation of these linear plots to zero inhibitor concentration at each pH indicated a K_m in the absence of nitrite of around 22uM throughout the pH range studied. This value conflicts with that of 0.23uM obtained by Kita *et al.* (1984b) using an oxygen electrode optimised to detect low oxygen tensions. The validity of the extrapolation of the K_m to zero inhibitor concentration is questionable, as the steady state kinetics of the oxidase reaction are complex. Estimations of the K_m in the absence of nitrite were highly variable because of the inability of the oxygen electrode to accurately measure very low oxygen tensions and the large size of the differentiating frames used compared to the size of the oxygen limited region of the progress curves. The K_m of cytochrome *bd* in the absence of nitrite was estimated to be between 1 and 6uM.

Sanchez-Crispin *et al.* (1979) determined a K_m for oxygen of 32uM for the cytochrome *bd* of *E.coli* membranes from cells grown

Figure 3.9

Plots of K_m versus nitrite concentration between pH6 and pH7.

K_i values were determined from analysis of the gradient of the plots of K_m versus nitrite concentration at each pH. \blacksquare — \blacksquare , pH6.2; \bullet — \bullet , pH6.4; \blacksquare — \blacksquare , pH6.6; \circ — \circ , pH6.6; \square — \square , pH6.8. Since $K_m = K_{m(i=0)}(1+i/K_i)$, in a plot of K_m versus i the K_i equals $K_{m(i=0)}/G$, where G is the slope of the graph. $K_{m(i=0)}$ was assumed to equal 22 μ M by extrapolation of the plots to zero inhibitor concentration. However, estimations of the K_m for oxygen in the absence of nitrite indicate a K_m between 1 and 6 μ M. This anomaly is discussed in the text. Depending on the required pH, membranes were suspended in 50mM Mes (pH6) or Tes (pH7). Intermediate pH's were obtained by using appropriate mixtures of these buffers and adjusting the pH with KOH or HCl prior to use. The buffers also contained 2mM $MgSO_4$.



anaerobically on nitrate. In such cells nitrite would have been produced by the functional nitrate reductase. An explanation for the high extrapolated K_m in the absence of nitrite in the above could be that nitrite reacts with cytochrome *bd* at concentrations below those at which competitive inhibition is observed in the studies reported herein, resulting in an increase of the K_m from around 0.23 μ M (Kita *et al.*, 1984b) to around 22-32 μ M. This suggests that the inhibition is more complex at very low nitrite concentrations.

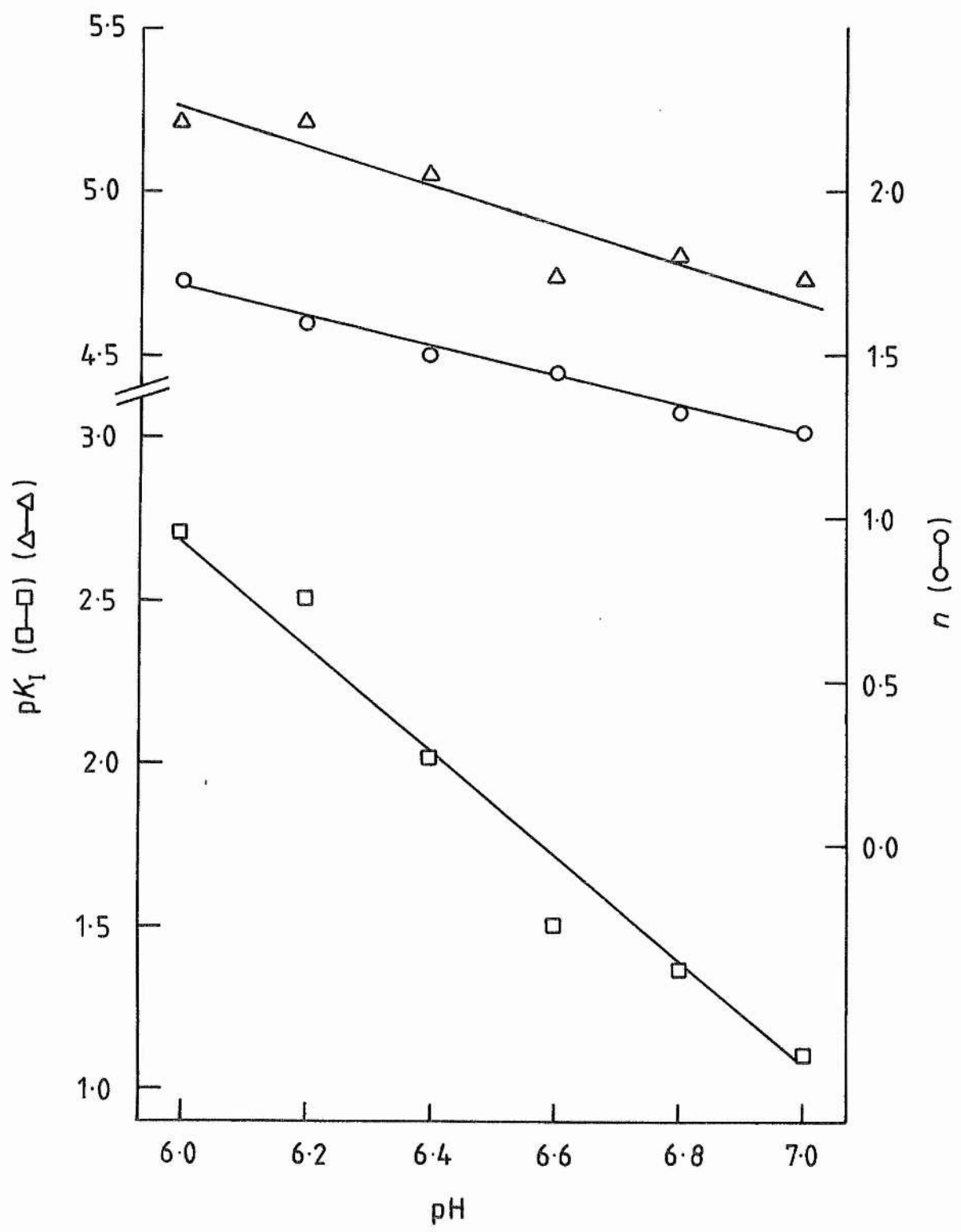
The K_i for nitrite increases from 1.95mM at pH6.0 to 78mM at pH7.0. Likewise, the pK_i (the negative \log_{10} of the K_i in moles l^{-1}) for nitrite decreases from 2.71 at pH6 to 1.1 at pH7 (Figure 3.10), and this variation is linear with respect to pH with a gradient of -1.7. However, if it is assumed that nitrous acid is the inhibitory species, then the K_i values for this species can be calculated from the K_i 's for nitrite by application of the Henderson-Hasselbach equation. The K_i for nitrous acid therefore increases from 4.6 μ M at pH6 to 18.4 μ M at pH7. The pK_i for nitrous acid decreases from 5.34 at pH6 to 1.1 at pH7, and this variation can be interpreted as being linear with respect to pH with a gradient of -0.7. These results suggest that if nitrite is the inhibitory species, then binding of the inhibitor is accompanied by binding of approximately 2 protons, and if nitrous acid is the inhibitory species, then binding of the inhibitor is accompanied by the binding of approximately 1 proton (Dixon, 1953).

In addition to perturbing the K_i of cytochrome *bd* for nitrite, pH also affects the apparent number of oxygen binding sites, n , in the presence of the inhibitor. The value of n increases linearly from 1.26

Figure 3.10

Effect of pH on the pK_i for nitrite and the apparent number of oxygen binding sites.

The effect of pH on the pK_i for nitrite (\square — \square). The effect of pH on the pK_i for nitrous acid (\triangle — \triangle). The effect of pH on the apparent number of oxygen binding sites, n (\circ — \circ). Data were obtained from analysis of oxygen electrode progress curves as described in the text. pH buffering was as for Figure 3.9.



at pH7 to 1.72 at pH6, with a gradient of -0.46 sites per pH unit (Figure 3.10). Extrapolation of the pH dependence of n to $n=1$ indicates that it may equal 1 at around pH7.5. However, the validity of such an extrapolation is questionable and it was not possible to measure n at pH7.5 because of the impotency of nitrite as an inhibitor at this pH.

3.9 Conclusions.

The anaerobic reactions of the *in situ* cytochrome *bd* with nitrite show kinetics which are dependent on the concentrations of protons, nitrite, and haem *d* in the reaction mixture. Two optically resolvable species are detected, a nitric oxide adduct to haem *d* and a nitric oxide adduct to haem b_{595} . These species result in major troughs in reduced *plus* nitrite *minus* reduced optical difference spectra at 630nm (haem *d*-NO) and 438nm (haem b_{595} -NO). Parallel e.p.r. experiments also indicate that two nitrosyl haem species are formed in the reaction between *in situ* cytochrome *bd* and nitrite (Chapter 4). The haem *d* species appears throughout the pH range used in this work, whereas the extent of the formation of haem b_{595} -NO increases with decreasing pH and is linked to an end point with a pK_a of around 7.3.

The effect of pH on the rate of formation of both haem *d*-NO and haem b_{595} -NO suggests that it is nitrous acid, rather than nitrite, which is the reactive species. In the reaction between nitrous acid and cytochrome *cd*₁ of *Pseudomonas aeruginosa*, two basic mechanisms have been proposed for the formation of nitric oxide (Kim & Hollocher, 1984). These involve general acid and electrophilic catalysis.

Consideration of such mechanisms allows two tentative models for the reaction between nitrous acid and cytochrome *bd* to be proposed. The first model involves general acid catalysis in the reaction between nitrous acid and both haems *d* and *b₅₉₅* (Figure 3.11). The second model involves haem *b₅₉₅* acting as an electrophilic catalyst in the formation of haem *d*-NO and general acid catalysis in the formation of haem *b₅₉₅*-NO (Figure 3.12). It should be noted that these models do not attempt to suggest the relative orientation of haems *b₅₉₅* and *d*.

In the first model (Figure 3.11), the ligand binding pocket of cytochrome *bd* with its haems *d* and *b₅₉₅* also contains two ionisable functional groups, one with a pK_a above 8.5 which is located close to the haem *d* (*dR*), and another with a pK_a of 7.3 which is located close to the haem *b₅₉₅* (*bR*). The formation of nitrosyl haems in this model can only proceed via a mechanism involving *dR* and *bR* as general acids in their protonated forms. The first nitrous acid to enter the haem pocket binds to haem *d* and is reduced to haem *d*-NO in a reaction involving *dR*-H as a general acid. Formation of haem *d*-NO prevents protonation or deprotonation of *bR* and therefore isolates it from the bulk phase pH. The second nitrous acid to enter the haem pocket can only be reduced at the haem *b₅₉₅* if its adjacent *bR* is protonated. Since the total concentration of protonated *bR* is determined and limited by the pH prior to reaction of nitrous acid with haem *d*, the extent of the formation of haem *b₅₉₅*-NO is linked to the pK_a of *bR*. In this model, the difference between the rates of formation of haem *d*-NO and haem *b₅₉₅*-NO is accounted for by the accessibility of the haem *d* relative to that of the haem *b₅₉₅*.

Figure 3.11

General acid catalysis model for the reaction of cytochrome bd with nitrous acid.

The ligand binding haem pocket with its haems *d* and *b₅₉₅* (labelled d^{2+} and b^{2+} , respectively) contains two ionisable functional groups, one with a pK_a above 8.5 (*bR*) and another with a pK_a of 7.3. Nitrous acid is assumed to be the reactive form of nitrite, and can only be reduced to NO in a reaction involving either *bR* or *dR* acting as general acids in their protonated forms. Only the ligand binding haems of the oxidase are shown for the sake of clarity. No protons apart from those associated with the functional groups *bR* and *dR* are involved in this model.

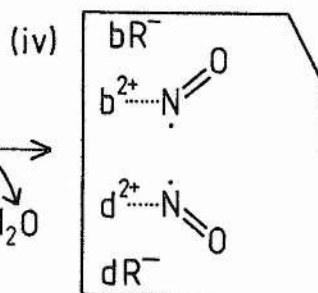
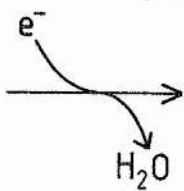
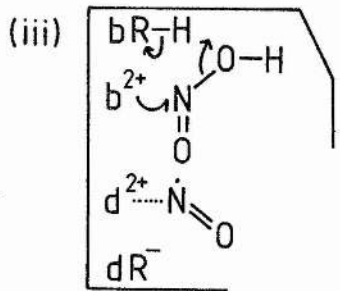
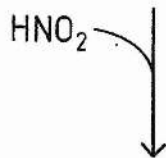
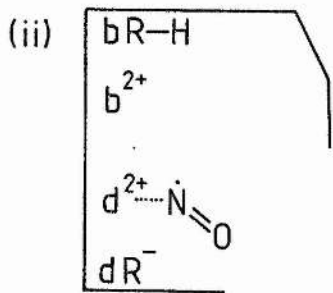
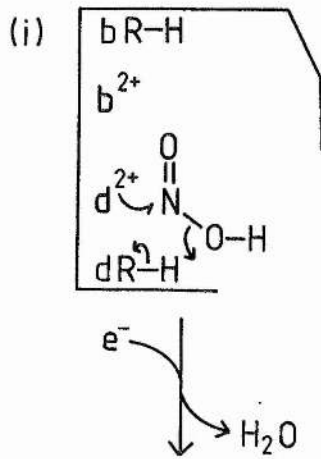
(a) pH < 7.3.

Nitrous acid enters the haem pocket and binds to haem *d*, which is the most accessible of the two haems (i). It is then reduced in a reaction involving *dR-H* as a general acid to form haem *d-NO* (ii). A second nitrous acid enters the haem pocket and binds to haem *b₅₉₅* (iii), and is reduced to form haem *b₅₉₅-NO* (iv) in a reaction involving *bR-H* as a general acid.

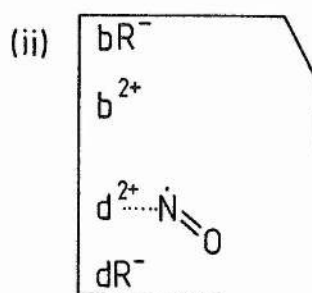
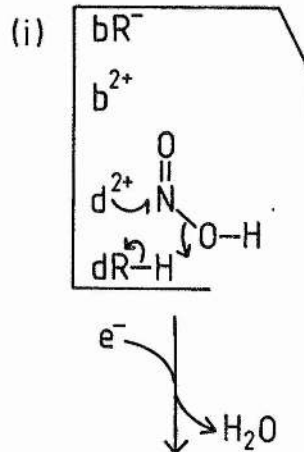
(b) pH > 7.3.

Only haem *d-NO* is formed in this pH range because only *dR-H* is available to act as a general acid. Obviously, the distinction between the formation and non formation of haem *b₅₉₅-NO* at pH 7.3 is arbitrary. The extent of formation of this species depends on the relative protonation of *bR* before reaction of nitrous acid with haem *d* (see text).

a pH < 7.3



b pH > 7.3



In the second model, haem b_{595} acts as an electrophilic catalyst in the reduction of nitrous acid at haem d (Figure 3.12), and a functional group (bR) with a pK_a of 7.3 acts as a general acid in the reduction of nitrous acid at haem b_{595} . The first nitrous acid to enter the haem pocket binds to haem d and is reduced to haem d -NO in a reaction involving haem b_{595} as an electrophilic catalyst. As in the previous model, formation of haem d -NO prevents protonation or deprotonation of bR and therefore isolates it from the bulk phase pH. The second nitrous acid to enter the haem pocket can only be reduced at the haem b_{595} if its adjacent bR is protonated. Again, since the total concentration of protonated bR is determined and limited by the pH prior to reaction of nitrous acid with haem d , the extent of the formation of haem b_{595} -NO is linked to the pK_a of bR. In this model, the difference between the rates of formation of haem d -NO and haem b_{595} -NO is accounted for both by the greater accessibility of the haem d relative to that of the haem b_{595} and by the difference in the two reaction mechanisms.

Nitrite inhibits the oxidase reaction catalysed by cytochrome bd and this inhibition is competitive with respect to oxygen. The K_i of the oxidase for nitrite is 78mM at pH7, and this compares to a value of 1.5mM for the K_i of cytochrome aa_3 for nitrite at pH7.4 (Paitian *et al.*, 1985). If nitrous acid is the inhibitory species in the case of cytochrome bd , then its K_i of 18.4uM at pH7 indicates that it is a potent inhibitor compared to cyanide and azide (Chapter 1, Table 1.2).

Kauffman *et al.* (1980) studied the inhibition of cytochrome bd catalysed oxidase activity by hydroxylamine in membranes from

Figure 3.12

Electrophilic and general acid catalysis model for the reaction of cytochrome bd with nitrous acid.

It is proposed that the haem pocket of the oxidase which contains haems *d* and *b₅₉₅* (labelled d^{2+} and b^{2+} , respectively) also contains a protonatable functional group, *bR*, with a pK_a of 7.3. Nitrous acid is assumed to be the reactive form of nitrite. It is reduced to form haem *d*-NO in a mechanism with haem *b₅₉₅* acting as an electrophilic catalyst. Formation of haem *b₅₉₅* proceeds with a mechanism involving *bR* acting as a general acid in its protonated form. Only the ligand binding haems of the oxidase are shown for the sake of clarity. In addition to the proton associated with *bR*, a proton is consumed in the reaction of haem *d* with nitrous acid.

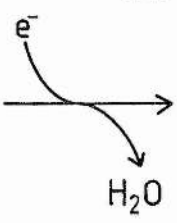
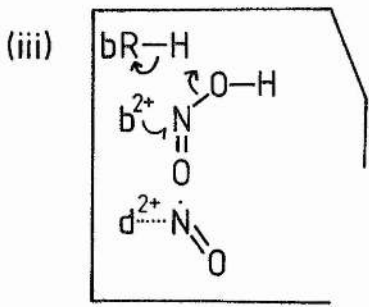
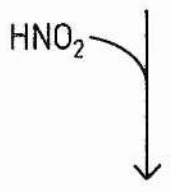
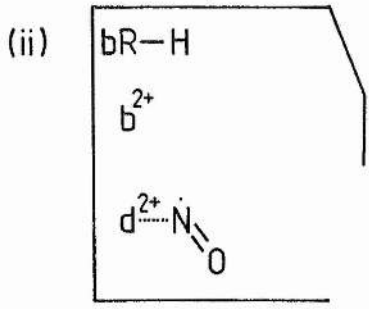
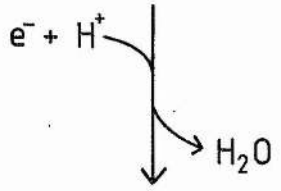
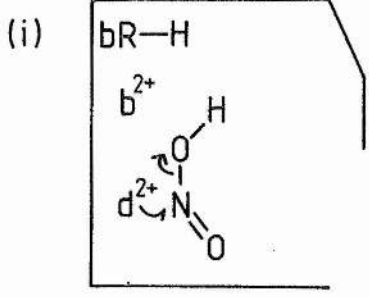
(a) $pH < 7.3$.

Nitrous acid enters the haem pocket and binds to haem *d*, which is the most accessible of the two haems (i). It is then reduced in a reaction involving haem *b₅₉₅* as an electrophilic catalyst to form haem *d*-NO (ii). A second nitrous acid enters the haem pocket and binds to haem *b₅₉₅* (iii), and is reduced to form haem *b₅₉₅*-NO (iv) in a reaction involving *bR*-H as a general acid.

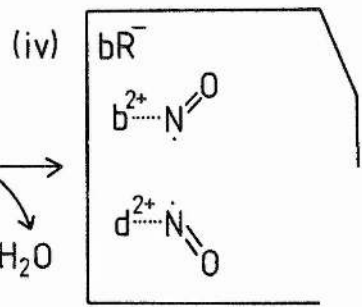
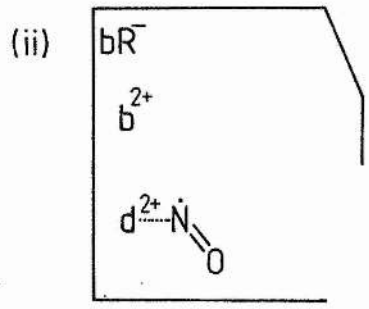
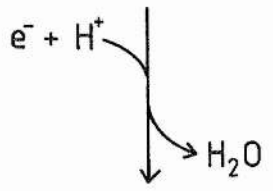
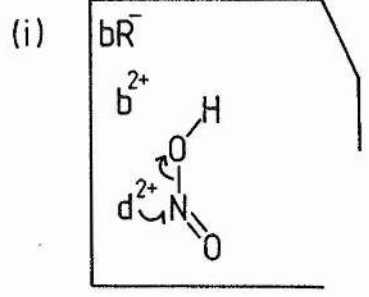
(b) $pH > 7.3$.

Nitrous acid reacts with haem *d* with haem *b₅₉₅* acting as an electrophilic catalyst, as in (a). Reaction of nitrous acid with haem *b₅₉₅* cannot proceed because functional group *bR* is unprotonated. As for the model of Figure 3.11, the distinction between the formation and non formation of haem *b₅₉₅*-NO at $pH 7.3$ is arbitrary.

a pH < 7.3



b pH > 7.3



Azotobacter vinelandii. These workers found that the spectrophotometrically detectable form of haem *d* under turnover conditions in the presence of hydroxylamine is haem *d*-NO and that under such conditions haem *b*₅₉₅ is partially reduced. The optical changes elicited by nitrite in membranes containing cytochrome *bd* are very similar to those produced by hydroxylamine. If the optical properties under steady state conditions in the presence of nitrite are similar to those in the presence of hydroxylamine, then nitrite inhibition may be due to the transient formation of haem *d*-NO. The NO ligand would have to be displaced by oxygen, perhaps via oxygen binding to haem *b*₅₉₅ to explain the competitive inhibition reported herein. Alternatively, the oxidase reaction may proceed via oxygen binding to haem *b*₅₉₅ with NO remaining on haem *d*. The behaviour of the apparent K_m with increasing nitrite concentration is consistent with the inhibition being due to a single nitrous acid reacting with a single oxygen binding site. It is notable that the effect of pH on the pK_i for nitrous acid is consistent with its binding being accompanied by that of a single proton, and this is consistent with the 'electrophilic' model for the formation of haem *d*-NO (Figure 3.12).

The cooperative steady state kinetics of the oxidase reaction suggest cooperativity between two oxygen binding centres. The decrease in the apparent number of substrate binding sites with increasing pH indicates that the affinity of one of these sites has a pronounced pH dependence; the optical data suggest that the ligand binding behaviour of haem *b*₅₉₅ is responsible for this effect. Extrapolation of the plot of the apparent number of oxygen binding sites, n , versus pH to $n=1$

indicates that this may occur at around pH7.5. If n does equal 1.0 at around pH7.5, then this can be interpreted mechanistically as meaning that haems d and b_{595} bind a single oxygen between them. Such a scheme would be reminiscent of cytochrome aa_3 , where oxygen is bound and reduced between haem a_3 and Cu_B . A model for the oxidase reaction in which oxygen acts as a bridging ligand will be discussed in Chapter 7.

At pH's below around 7.5, the optical and polarographic data point to a model for the oxidase which has two binding sites for oxygen which are in close proximity. The data presented herein indicate that these sites are haems d and b_{595} . The oxidase reaction would only be cooperative if the reaction cycle involves a mechanism which proceeds more rapidly when oxygen binds to both ligand binding haems. For example, the reaction cycle may involve binding of two oxygens (at haems d and b_{595}), their reduction to peroxide, and disproportionation leading to a residual bound oxygen and two molecules of water. Such a mechanism and its merits compared to other possibilities is described in Chapter 7.

There is no obvious physiological role for the observed cooperativity of the oxidase reaction. Indeed, a sigmoidicity of the v versus s curve for an oxidase could be detrimental to its efficiency, giving lower reaction rates at lower oxygen concentrations than an enzyme with an apparent number of sites, n , of 1.0. The effect is probably of purely mechanistic origin, and a result of the proximity of the two ligand binding haems of cytochrome bd .

CHAPTER FOUR

*Formation and sidedness with respect to the cytoplasmic membrane of
e.p.r. detectable nitrosyl cytochrome bd.*

4.1 Introduction.

It was concluded in Chapter 3 that nitrite reacts with ferrous cytochrome *bd*, resulting in the formation of nitric oxide adducts to its two putative ligand binding haems, haems *d* and *b₅₉₅*. Nitric oxide binding to ferrous haemoproteins is of particular interest because like oxygen, it binds to haems in a bent fashion and its unpaired electron makes it an effective spin label (Hori *et al.*, 1981; Morse & Chan, 1980). It is therefore possible that nitrosyl cytochrome *bd* is a good e.p.r. detectable analogue of oxygen ligated cytochrome *bd*. This chapter includes an e.p.r. study of the nitrosyl haem spectra formed following anaerobic reaction of lactate reduced *E.coli* EMG2 cytoplasmic membranes with nitrite.

Nitrosyl haemoproteins exhibit e.p.r. spectra with three major features (g_x , g_y , and g_z) centred around $g=2$ (Yonetani *et al.*, 1972; Henry & Banerjee, 1973). Of the enzymes able to catalyse the oxidase reaction, only nitrosyl cytochrome *aa₃* (Brudvig *et al.*, 1981) and nitrosyl cytochrome *cd₁* (Johnson *et al.*, 1980) have been extensively studied using e.p.r. Nitrosyl cytochrome *aa₃* exhibits a spectrum with g -values of 2.09 (g_x), 2.00 (g_z), and 1.97 (g_y) with the g_z feature split into a triplet of hyperfine structure. Each unit of the g_z hyperfine structure is itself split into a triplet of superhyperfine structure. The hyperfine structure is due to perturbation of the magnetic field at the ferrous haem iron by the nuclear spin of the exogenous distal ligand (the nitrosyl ^{14}N), whilst the superhyperfine structure is due to perturbation of the magnetic field by the nuclear spin of the endogenous proximal nitrogenous ligand (a histidyl ^{14}N ;

Stevens & Chan, 1981). Both the haems *c* and *d*₁ of cytochrome *cd*₁ appear to be able to bind nitric oxide at low pH (<7.0). Above pH7, only haem *d*₁ appears to be able to bind the ligand, resulting in the observation of an e.p.r. spectrum with *g*-values of 2.07 (*g*_x), 2.01 (*g*_z), and 1.96 (*g*_y) (Johnson *et al.*, 1980). In this case the *g*_z is again split into a triplet of triplets, indicating that the endogenous proximal ligand is nitrogenous. No study has been reported to date of the nitric oxide adducts to cytochromes *bd* or *b*₅₆₂-*o* of *E.coli*.

Cytochrome *bd* has been identified as a coupling site in the aerobic electron transport chain of *E.coli* (Miller & Gennis, 1985). To comprehend the molecular mechanism of the redox linked proton translocation across the cytoplasmic membrane, it is desirable to be able to determine the sidedness of the subunits and active sites of this oxidase. Antibodies and trypsin digestion have been used to determine that subunit I and the quinol oxidation site are oriented towards the outer surface of the cytoplasmic membrane (Miller & Gennis, 1985; Lorence *et al.*, 1988). No data is yet available on the sidedness of the ligand binding haems with respect to the cytoplasmic membrane, although a proposal consistent with the published H⁺/O₂ stoichiometries (Miller & Gennis, 1985) is that they are located on the cytoplasmic side of the membrane (Chapter 1, Section 1.4.4).

The sidedness of redox active and e.p.r. visible components in the mitochondrial inner membrane have been studied by investigating spin-spin (dipolar) interactions between individual intrinsic redox centres and membrane impermeant extrinsic paramagnetic probes (Case & Leigh, 1976; Ohnishi *et al.*, 1985). When paramagnetic ions such as

nickel(II), gadolinium(II), and dysprosium(III) are allowed to approach to within 30\AA of an intrinsic e.p.r. visible centre, they elicit enhancement of its spin lattice relaxation rate ($1/T_1$) and broadening of the intrinsic e.p.r. signal (Case & Leigh, 1976; Blum *et al.*, 1981). Of the three probes used extensively to date, dysprosium(III) has proved to be the most successful due to its very fast spin lattice relaxation rate ($1/T_1$) and the position of its principal g-value at around $g=14$, which renders it unlikely to overlap with the e.p.r. resonances of the intrinsic redox centres under investigation (Blum *et al.*, 1981). However, this e.p.r. spectrum has a long high field 'tail' which can distort spectral baselines of the spectra of some centres recorded at high instrument gain. The most useful property of dysprosium(III) is its ability to enhance the spin lattice relaxation rate ($1/T_1$) of the intrinsic e.p.r. centre. The distance dependence of this effect is most readily quantified in terms of dependence of the descriptive parameter $P_{1/2}$ (the power for half saturation) on the probe concentration. The effect of dysprosium(III) as a paramagnetic probe complexed with EDTA on the e.p.r. properties of nitrosyl cytochrome *bd* is reported in this chapter in order to determine the sidedness of its ligand binding haems with respect to the cytoplasmic membrane.

This chapter contains an investigation of the formation of nitrosyl cytochrome *bd* using e.p.r. spectroscopy. These studies complement those reported using optical spectroscopy in Chapter 3. The sidedness with respect to the cytoplasmic membrane of the nitric oxide adducts to the putative ligand binding haems of the oxidase are also

reported using the dysprosium(III) paramagnetic probe technique.

4.2 Formation of nitrosyl cytochrome *bd*.

Figure 4.1 shows the effect of nitrite on the e.p.r. spectrum at 30K of lactate reduced membranes from anaerobically grown *E.coli* EMG2. Noticeable in the baseline spectrum (Figure 4.1, top) prior to addition of nitrite are features at $g=2.000$, 2.021 , and 2.081 . The broad peak around $g=2.081$ and the broad trough around $g=2.000$ are attributable either to the cavity signal of the Bruker ER200D or to copper present in the cytoplasmic membrane preparation. The sharp peak-trough at $g=2.000$ is due to free radicals present in the lactate reduced membrane preparation, probably flavin or semiquinone radicals. The other feature of the baseline is a peak at $g=2.021$ which appears with peak-trough at around $g=1.930$ (not shown). These features are due to iron-sulphur centres (Ingledeu, 1983); the $g=2.021$ and $g=1.930$ features probably correspond to the g_z and g_{xy} resonances of centre FR1 of fumarate reductase (Simpkin, 1985). To clarify analysis of the changes in the e.p.r. spectrum of these membranes following addition of nitrite, the baseline spectrum of Figure 4.1 (top) was subtracted from e.p.r. spectra recorded following addition of nitrite.

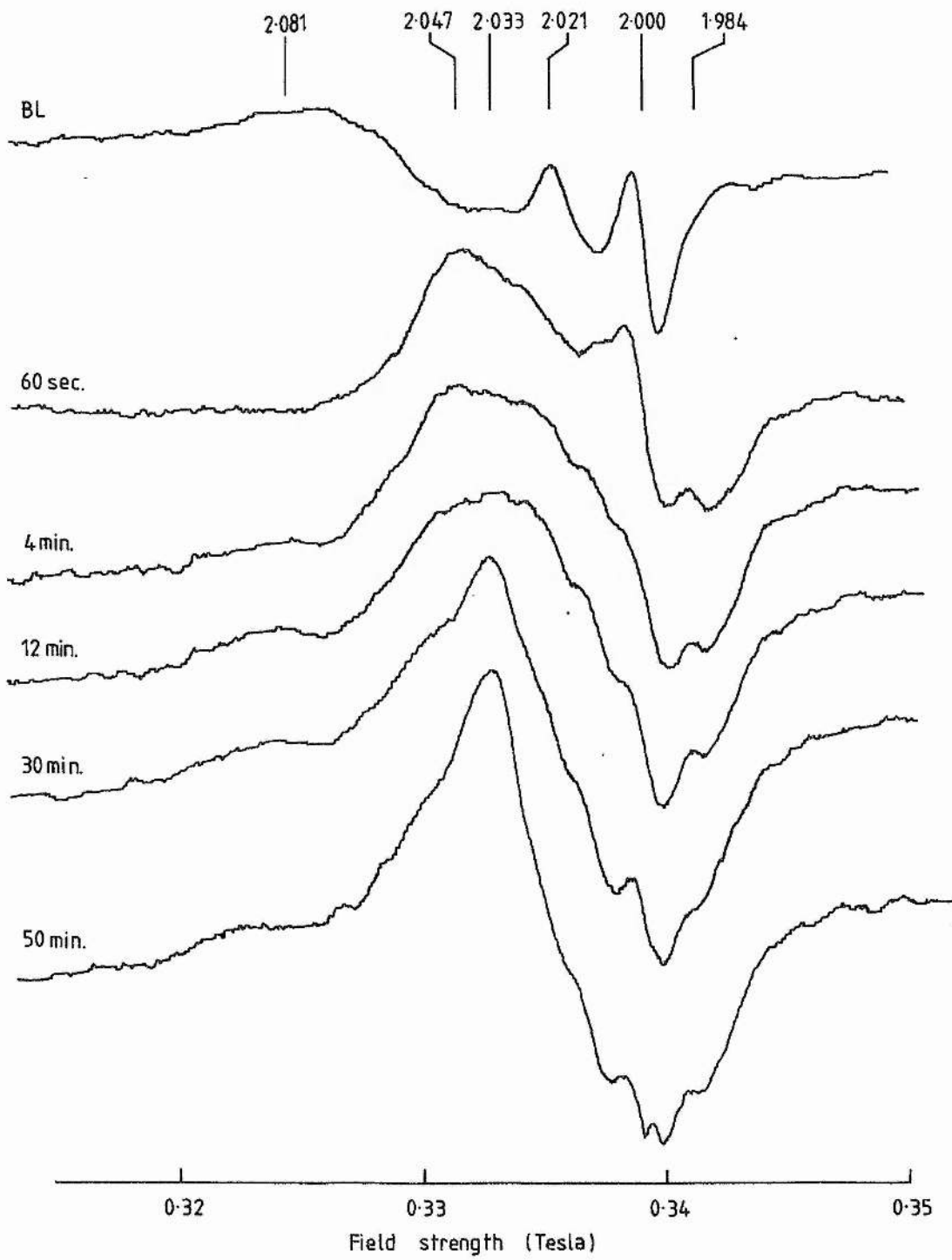
Since, on the basis of optical difference spectra (Chapter 3), cytochrome *bd* is the only detectable ligand binding haemoprotein in the membranes used in this work, any nitrosyl haem signals detected following reaction with nitrite can be attributed to nitric oxide adducts to its ligand binding haems.

Two changes are apparent in the spectrum following reaction with

Figure 4.1

Formation of nitroxide haem adducts to ferrous cytochrome bd.

Membranes suspended in 50mM Bes/KOH containing 2mM MgSO₄ (pH7, 40mg ml⁻¹ protein) were incubated anaerobically in the presence of 10mM lactate at 30°C. Sodium nitrite was then added to a concentration of 10mM. E.p.r. spectra were recorded using a signal averager (Model 4202, Princeton Applied Research) interfaced to the Bruker ER200D e.p.r. spectrometer). BL, spectrum of a sample prepared prior to addition of nitrite. This baseline was recorded using the digital signal averager and was subtracted from the spectra recorded after addition of nitrite. The other spectra in this figure were recorded of samples withdrawn from the incubation at the specified times after initiation of the reaction. Spectrometer settings: temperature, 30K; microwave power, 2mW; field modulation intensity, 10G_{pp}; instrument gain, 5 x 10⁴. g-values are indicated by the bars and numbers above the upper spectrum.



10mM nitrite for 60 seconds (Figure 4.1). Firstly, the intensity of the free radical signal at $g=2.0$ transiently increases. Secondly, a broad peak appears at $g=2.047$ and a trough appears at $g=1.984$. These features are attributable to the g_x ($g_x=2.047$) and g_y ($g_y=1.984$) of the spectrum of a nitrosyl haem. Comparison of this spectrum with those of a range of haemoproteins (Yonetani *et al.*, 1972; Henry & Banerjee, 1973) suggests that the g_z of the spectrum should appear between the g_x and g_y , but is unresolved in the 60 second spectrum of Figure 4.1.

Two research groups (Yoshimura *et al.*, 1979; Morse & Chan, 1980) have studied the temperature dependence of the e.p.r. spectrum of model nitrosyl compounds and nitrosyl haemoproteins. These workers have concluded that most ligand binding haemoproteins exhibit two distinct e.p.r. spectra due to two nitric oxide adducts to the same haem with two conformations at the haem iron with respect to the haem plane in a temperature dependent equilibrium. Morse & Chan, (1980) classified these two species as a low temperature species, Type I, and a high temperature species, Type II. In the Type I species, the iron atom is displaced towards the proximal (endogenous) haem ligand, whereas in the Type II species, it is displaced towards the nitrosyl nitrogen (Figure 4.2). The nitrosyl haem features of the 60 second spectrum of Figure 4.1 resemble those of a Type II nitrosyl haem spectrum.

After four minutes reaction with nitrite, the free radical signal at $g=2.0$ subsides and what can tentatively be assigned as a triplet of nitrogen hyperfine structure can be discerned centred at $g=2.015$ (g_z).

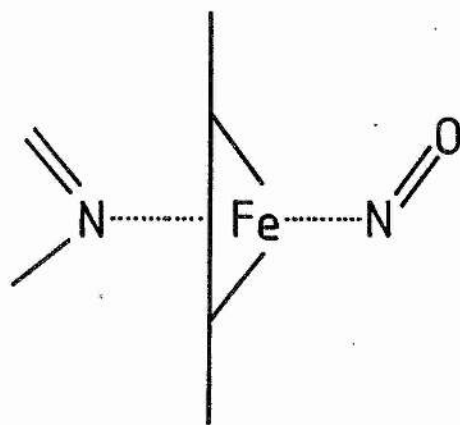
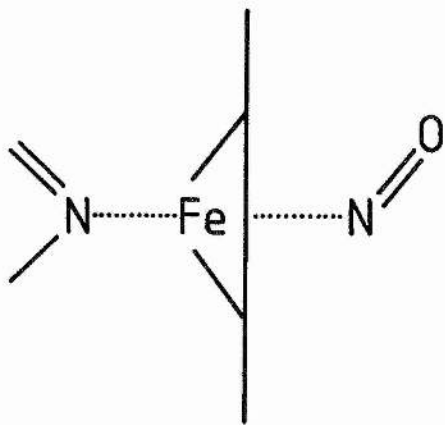
*Figure 4.2**Conformations of Type I and Type II nitrosyl haems.*

Model for the Type I and Type II nitrosyl haem species discussed in the text copied from Morse & Chan (1980). The diagram shows the equilibrium between species predominating at low temperatures (I) and high temperatures (II) in base-ferrohaem·NO complexes exhibiting temperature dependent e.p.r. spectra. Vertical line represents the porphyrin plane. The displacements of iron from the haem plane are in the range 0.07-0.11Å in model systems. In addition, the Fe-N-O bond angle of a typical Type I nitrosyl haem (Mb-NO, low temperature) is 110°, whilst that of a Type II haem (Mb-NO, high temperature) is 145°.

I



II



The hyperfine coupling constant, A_z , appears to be around 15.5 Gauss (1.55mT), a value typical of a Type II nitrosyl haem (Morse & Chan, 1980). However, the possibility exists that the hyperfine structure is due to changes in the 'baseline' elicited by nitrite, with changes in the $g=2.0$ and $g=2.021$ regions of this spectrum causing the changes attributed to hyperfine splitting of the nitrosyl haem g_2 . The absence of any superhyperfine structure in the 4 minute spectrum suggests that the proximal (endogenous) haem ligand may not be nitrogenous. However, it is not unusual for superhyperfine structure to be unresolved in spectra of nitrosyl haemoproteins which have a nitrogenous proximal ligand. This is the case in myoglobin (Yonetani *et al.*, 1972) and haemoglobin (Henry & Banerjee, 1973).

Additional changes are observed after four minutes, the peak at $g=2.047$ becomes broader and moves upfield, and a broad peak at $g=2.081$ becomes discernable. These observations are consistent with the formation of a Type I nitrosyl haem species (Morse & Chan, 1980). The spectrum also suggests that there is an equilibrium between a Type I and a Type II nitrosyl haem species. Comparison of the spectra with the optical data of Chapter 3 (Figure 3.1) suggests that the Type I and Type II nitrosyl haem species formed at pH7 during the first few minutes of the reaction with nitrite are attributable to the formation of nitrosyl haem *d*. The composite spectrum due to nitrosyl haem *d* is similar to the spectra reported for a number of nitrosyl haemoproteins, including myoglobin, haemoglobin, cytochrome *c*, and catalase (Yonetani *et al.*, 1972; Henry & Banerjee, 1973). The g -values of nitrosyl haem *d*, in the nomenclature of Yonetani *et al.* (1972),

appear to be $g_x=2.081$, $g_y=2.047$, $g_z=2.015$, and $g=1.984$. The g_x , g_y , and g_z refer to the Type I species, whereas the g refers to the Type II g_x . The Type II g_y contributes to the trough at $g=1.984$, and the g_z is between the g_x and g_y , but is unresolved.

Between 12 and 30 minutes after initiation of the reaction with nitrite, a new peak develops at $g=2.033$, which obscurs the nitrogen hyperfine observed in the g_z region of the 4 and 12 minute spectra. This peak is attributable to the formation of a second nitrosyl haem quite distinct from nitrosyl haem *d*. This species is further developed in the 50 minute spectrum. Comparison of Figure 4.1 with the data of Chapter 3 (Figure 3.1) indicates that this second nitrosyl haem corresponds to nitrosyl haem *b₅₉₅*. Its lineshape is relatively axial, with g_x at $g=2.033$ and g_y and g_z at around $g=2.0$. The region of the spectrum where the hyperfine structure of the g_z resonance would be expected to occur is complicated by overlap with the residual free radical signal discussed above. However, an apparent triplet is discernable which has a coupling constant (A_z) of around 14 Gauss (1.4mT) centred on an apparent g_z of 1.997. The spectrum of nitrosyl haem *b₅₉₅* has a lineshape similar to that of nitrosyl thyroid peroxidase (Lukat *et al.*, 1988) and imidazole-haemin-NO in a DMSO glass (Kon & Kataoka, 1969). However, the spectrum is quite distinct from those of other peroxidases such as Horseradish peroxidase, cytochrome *c* peroxidase (Yonetani *et al.*, 1972) and mushroom peroxidase (Lukat *et al.*, 1988). The spectrum of nitrosyl haem *b₅₉₅* resembles a Type II spectrum, and there appears to be no Type I / Type II equilibrium, as is observed in the nitrosyl haem *d*

spectrum. All the above comparisons are with low temperature (<77K) spectra of nitrosyl haemoproteins. The nitrosyl haem *b₅₉₅* spectrum is similar to the room temperature spectra of nitrosyl cytochrome *c*, nitrosyl myoglobin, and nitrosyl haemoglobin (Henry & Banerjee, 1973).

The rate at which these nitrosyl haems are formed can be increased by incubating membranes with lactate and nitrite at pH6 for 10 minutes at 30°C (Figure 4.3). These spectra were recorded at 15K. The nitrosyl haem *b₅₉₅* spectrum clearly dominates at low microwave power (Figure 4.3 top), whereas the spectrum of nitrosyl haem *d* dominates at high microwave power (Figure 4.3, bottom). Clearly, the two nitrosyl haem species exhibit very different behaviour with respect to increasing microwave power. The intensity of all e.p.r. spectra increase with increasing microwave power until saturation becomes apparent. This phenomenon arises because the rate at which spins are promoted to their excited state exceeds their rate of relaxation. Thus, in Figure 4.3, the nitrosyl haem *b₅₉₅* spectrum appears to be more easily saturated than the nitrosyl haem *d* spectrum. The spin lattice relaxation rate ($1/T_1$) of the excited state of nitrosyl haem *d* is therefore more rapid than that of nitrosyl haem *b₅₉₅*. The saturation characteristics of the nitrosyl haem adducts to cytochrome *bd* are described in more detail in the next section.

4.3 Temperature and microwave power dependence of the nitrosyl cytochrome *bd* e.p.r. signals.

The temperature dependencies of the three major features of the nitrosyl cytochrome *bd* e.p.r. spectrum are shown in Figure 4.4. These

Figure 4.3

Low temperature nitrosyl cytochrome bd spectra.

E.p.r. spectra recorded at 15.5K of nitrite treated lactate reduced membranes (37mg ml⁻¹ protein). Membranes were suspended in 50mM Mes/KOH (pH6) containing 50uM CCCP (to collapse any vesicle Δ pH), 2mM MgSO₄, and 50mM sodium lactate and were incubated anaerobically for 10 minutes. Sodium nitrite (50mM) was then added and after a further 10 minutes incubation the membranes were transferred to an e.p.r. tube and were rapidly frozen. Spectrometer settings: temperature, 15.5K; field modulation intensity, 10G_{pp}; instrument gain, 4 x 10⁴. g-values are indicated by the numbers and bars above the upper spectrum.

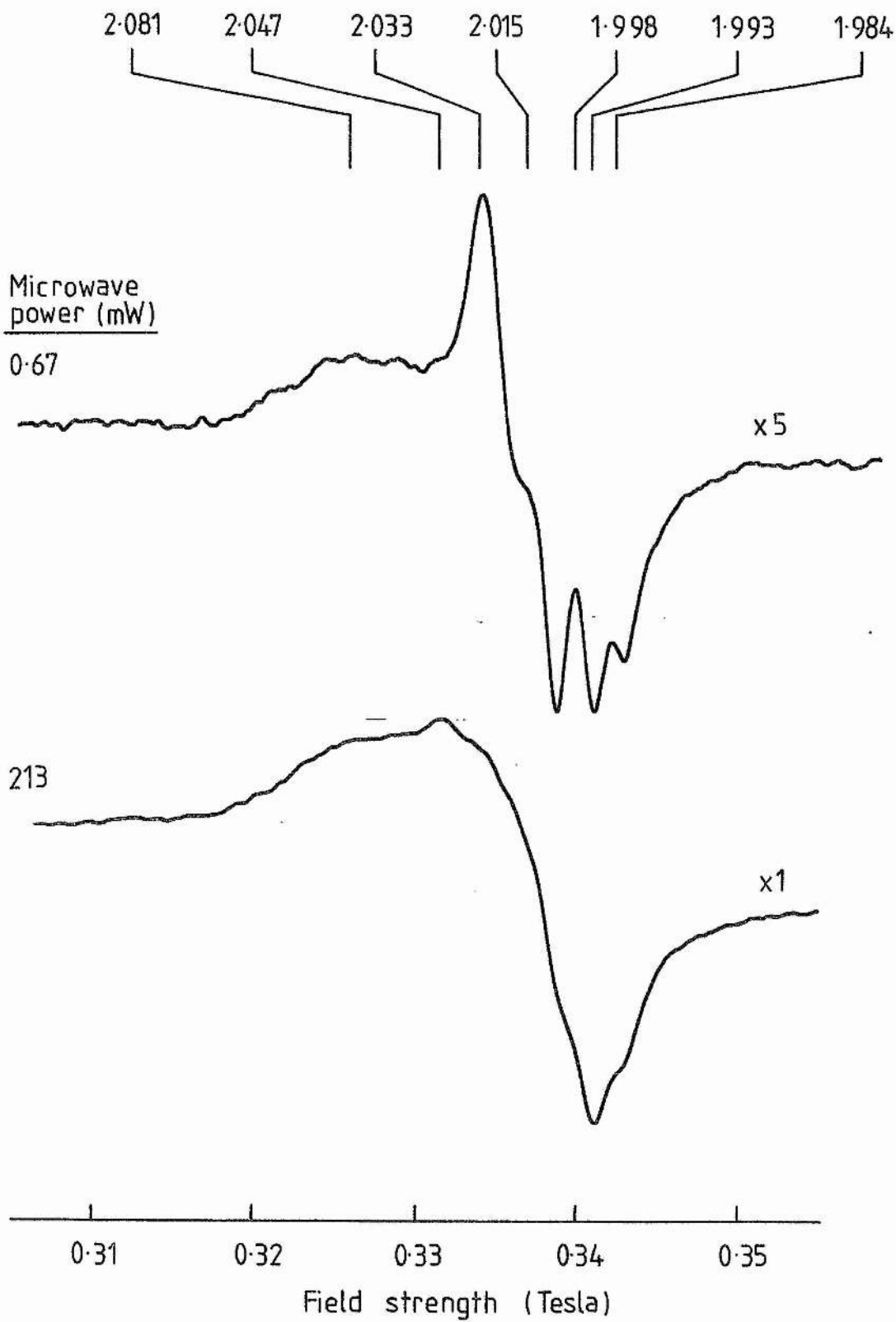
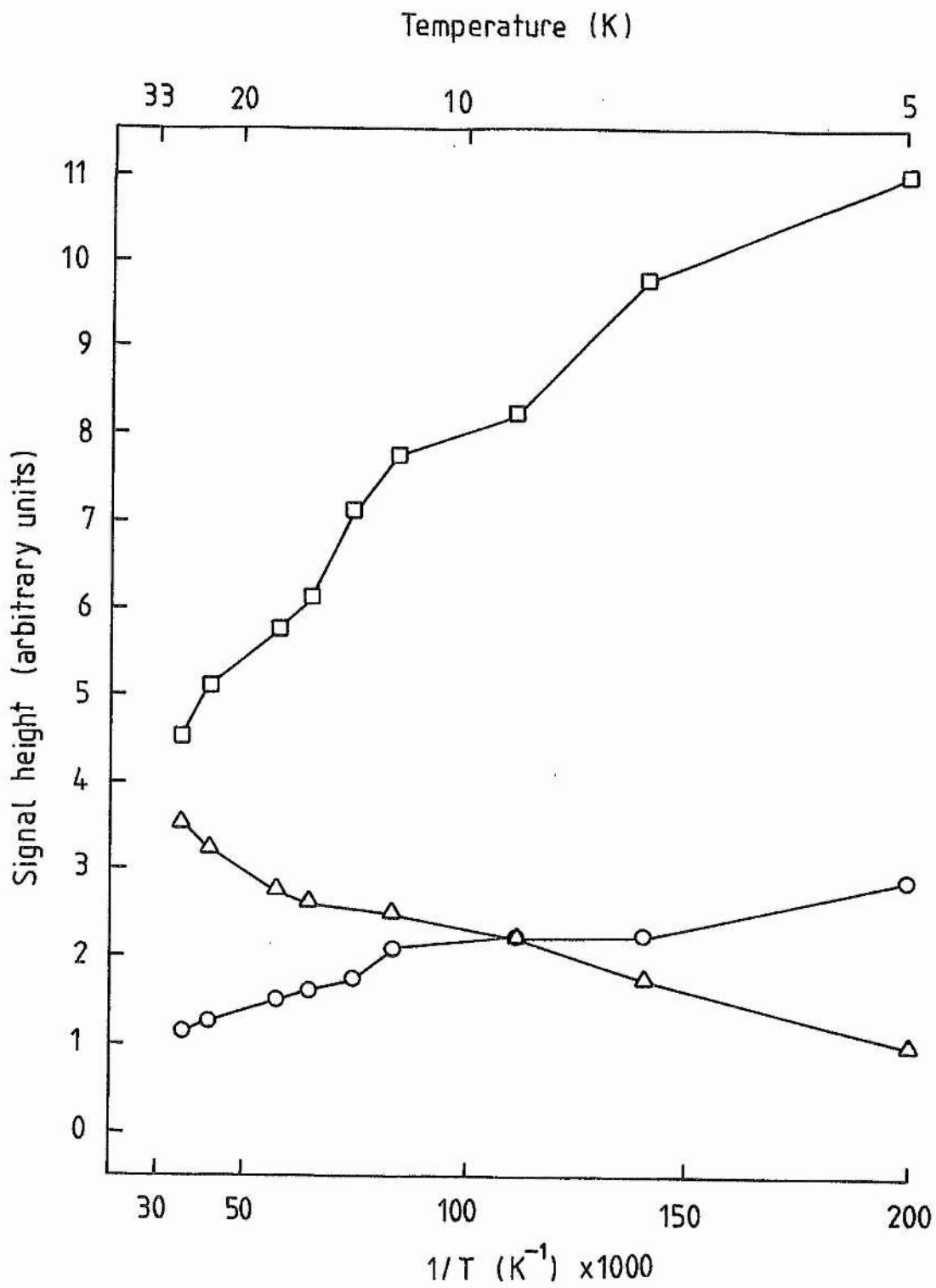


Figure 4.4

Temperature dependence of the nitrosyl cytochrome bd spectrum.

Signal height was plotted versus reciprocal temperature for a sample prepared as for Figure 4.3. \bigcirc — \bigcirc , the $g=1.984$ signal; \triangle — \triangle , the $g=2.033$ signal; \square — \square , the $g=2.081$ signal. Spectrometer settings: microwave power 3.38mW; field modulation intensity, 10G_{pp}; sample protein concentration, 37mg ml⁻¹.



features, the $g=2.081$ peak, the $g=2.033$ peak, and the $g=1.984$ trough exhibit distinct temperature dependencies. Both the $g=2.081$ peak and the $g=1.984$ trough increase in intensity with decreasing temperature, whilst the $g=2.033$ feature decreases in intensity with decreasing temperature. These results are consistent with the nitrosyl haem *d* species being responsible for $g=2.081$ and $g=1.984$ features of the spectrum. The increase in intensity of the $g=2.033$ feature with increasing temperature is consistent with the nitrosyl haem *b₅₉₅* spectrum being saturated at the microwave power used in the temperature range of Figure 4.4. The difference in the gradient between the temperature dependencies of the $g=2.081$ and $g=1.984$ features indicates that the g_y and g_z of the spectrum of nitrosyl haem *b₅₉₅* also contribute in this region of the spectrum.

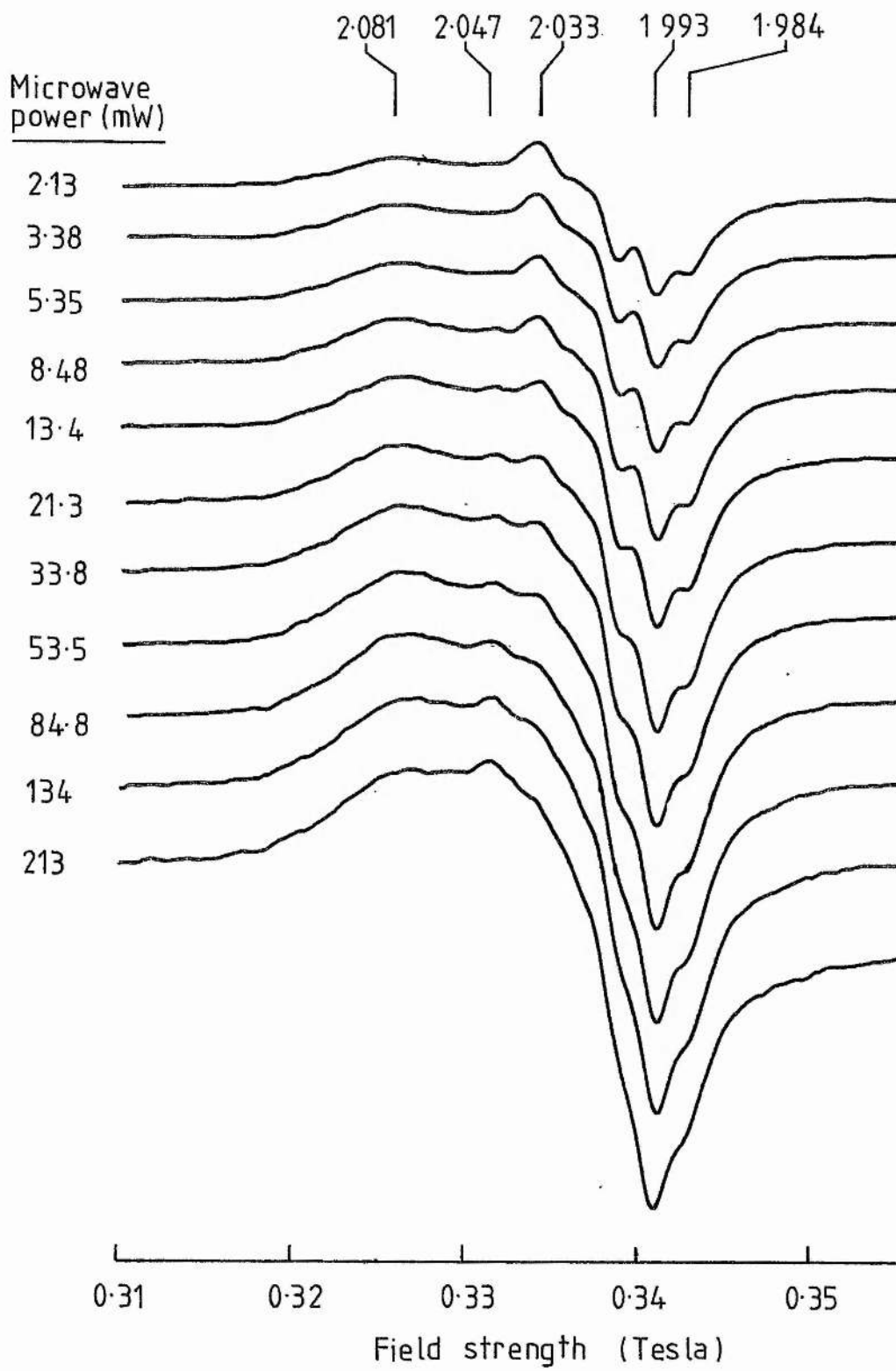
Figure 4.5 shows the effect of increasing microwave power on the features of the e.p.r. spectrum of nitrosyl cytochrome *bd*. At high microwave power, only the g_x , g_z , and g_y of the nitrosyl haem *d* spectrum are readily discernable (the g_z occurs on the downslope of the g_y trough). With decreasing microwave power, the features of the nitrosyl haem *d* spectrum become smaller, whilst the features of the nitrosyl haem *b₅₉₅* spectrum and g_z nitrogen hyperfine and/or the free radical signal appear and become relatively larger. Below about 53mW, the g_z of nitrosyl haem *d* is supplanted by the g_x of the nitrosyl haem *b₅₉₅* spectrum, and the $g=1.993$ trough begins to become complicated by the desaturation of the haem *b₅₉₅* g_z nitrogen hyperfine and/or the free radical signal at $g=2.0$.

The effect of increasing microwave power can be quantified by

Figure 4.5

Effect of increasing microwave power on the e.p.r. spectrum of nitrosyl cytochrome bd.

Spectra were recorded of a sample prepared as for Figure 4.3, but with the microwave powers indicated and at a temperature of 13.4K. g-values are indicated by the numbers above the upper spectrum. Spectrometer settings: field modulation intensity, 10G_{pp}; instrument gain, 5 x 10⁴. g-values are indicated by the numbers and bars above the upper spectrum. Protein concentration, 37mg ml⁻¹.



plotting the intensities of the features of Figure 4.5 versus microwave power and such plots are illustrated in Figure 4.6. It is clear from the figure that the microwave power dependence of the $g=2.033$ feature is quite distinct from those of the $g=2.081$ and $g=1.984$ features of the nitrosyl cytochrome *bd* spectrum.

Saturation profiles such as those in Figure 4.6 can be described quantitatively by the following equation (Barber *et al.*, 1982):

$$S = k\sqrt{P} / [1 + P/P_{1/2}]^{0.5b} \quad \dots\dots\dots 4.1$$

where k is a constant relating to the concentration of the species responsible for the e.p.r. spectral features under investigation; P is the microwave power; and b is the inhomogeneity parameter which varies from 1.0 to 4.0 for inhomogeneously and homogeneously broadened lines, respectively. The saturation parameter, $P_{1/2}$, is the microwave power required for half saturation and is defined quantitatively as the microwave power at which the following condition is met (Ohnishi *et al.*, 1982):

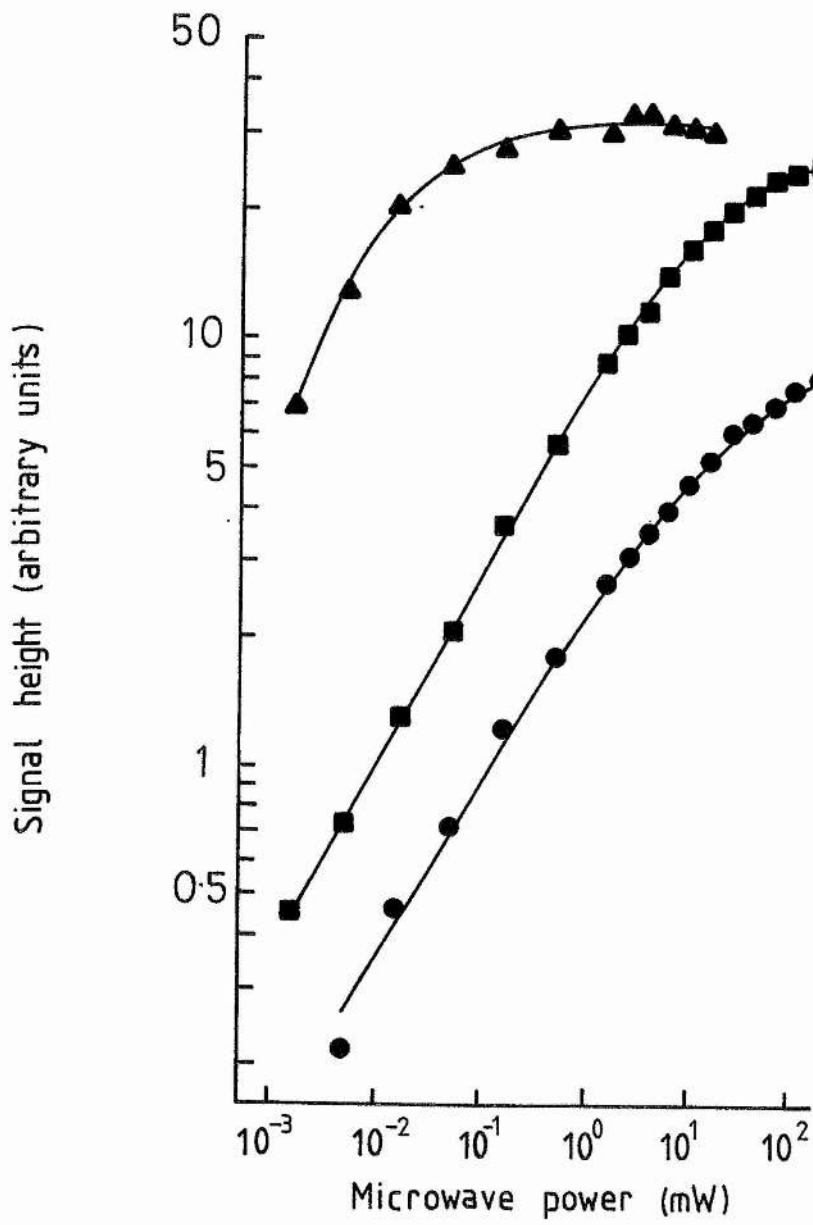
$$\gamma^2 T_1 T_2 H_{1/2}^2 = 1 \quad \dots\dots\dots 4.2$$

where γ is the magnetogyric ratio; T_1 and T_2 are the spin-lattice and spin-spin relaxation times, respectively; $H_{1/2}$ is the microwave magnetic field corresponding to the $P_{1/2}$. The $P_{1/2}$ can be determined from plots of signal height versus microwave power by extrapolation of the linear region of the saturation profile with increasing microwave

Figure 4.6

Saturation profiles of the three major features of the nitrosyl cytochrome *bd* spectrum.

The effect of microwave power on the three major features of the cytochrome *bd* nitrosyl haem spectrum of a sample prepared as for Figure 4.3. ●—●, the $g=2.081$ peak had a $P_{1/2}$ of 19.4mW; ■—■, the $g=1.984$ trough had a $P_{1/2}$ of 18.6mW; ▲—▲, the $g=2.033$ peak had a $P_{1/2}$ of 0.12mW. Protein concentration, 37mg ml⁻¹. Spectrometer settings: temperature, 12K; field modulation intensity, 10G_{pp}; instrument gain, 4 x 10⁴.



power and determining the point at which the signal height is half that expected for an unsaturated signal. The $P_{1/2}$ values determined at 12K for the saturation profiles of Figure 4.6 are 19.4, 18.6, and 0.12mW for the $g=2.081$, $g=1.984$, and $g=2.033$ features of the cytochrome *bd* nitrosyl haem spectrum.

Figure 4.7 shows the effect of temperature on the $P_{1/2}$'s of the three major features of the nitrosyl cytochrome *bd* e.p.r. spectrum. The $g=2.081$ and $g=1.984$ features of the nitrosyl haem spectrum both exhibit a $T^{1.7}$ dependence of the $P_{1/2}$ on temperature, whereas the $g=2.033$ feature exhibits a $T^{2.2}$ dependence of the $P_{1/2}$ on temperature. These dependencies are both sufficiently close to a T^2 dependence to be characteristic of a phonon bottleneck (direct) relaxation mechanism (Gayda *et al.*, 1976).

Overall, the major features of the nitrosyl cytochrome *bd* e.p.r. spectrum can be resolved on the basis of their temperature and microwave power dependencies. The features of the nitrosyl haem *d* spectrum get larger with decreasing temperature and are relatively difficult to saturate, whereas the major feature of the nitrosyl haem *b₅₉₅* spectrum gets larger with increasing temperature and is relatively easy to saturate.

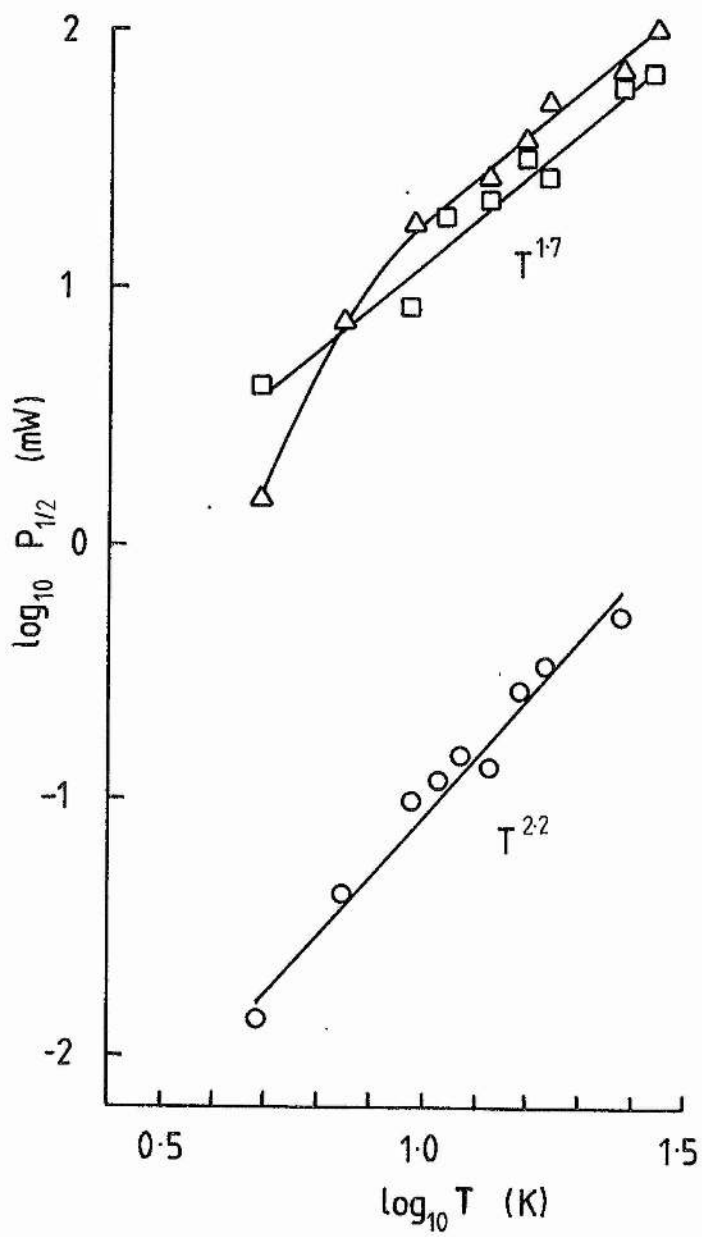
4.4 Use of dysprosium as an exogenous paramagnetic probe.

As described in Section 4.1, exogenous paramagnetic probes have been used to determine the sidedness of e.p.r. visible prosthetic groups of membrane bound electron transport proteins. These probes have also been used to estimate the radii of a number of proteins with

Figure 4.7

*Temperature dependence of the $P_{1/2}$'s of the three major features of the nitrosyl cytochrome *bd* spectrum.*

Data were obtained from spectra recorded of a sample prepared as for Figure 4.3. \triangle — \triangle , the dependence of the $g=2.081$ $P_{1/2}$ on temperature appeared biphasic. Above 8K, there was a $T^{1.7}$ dependence, below 8K, the relaxation tended towards a T^4 dependence. \square — \square , the dependence of the $g=1.984$ $P_{1/2}$ on temperature; there was a $T^{1.7}$ dependence. \circ — \circ , the dependence of the $g=2.033$ $P_{1/2}$ on temperature; there was a $T^{2.2}$ dependence. Spectrometer settings: microwave frequency, 9.59GHz; field modulation intensity, 10G_{pp}. Sample protein concentration was 37mg ml⁻¹.



e.p.r. visible prosthetic groups (Blum *et al.*, 1981; Blum *et al.*, 1983). Such studies have enabled the distance dependent dipolar interactions between dysprosium and a paramagnetic prosthetic group to be characterised. Blum *et al.* (1981) studied the effects of dysprosium complexed with EDTA, hydroxy-EDTA, and nitrate on the $P_{1/2}$'s of the e.p.r. spectrum of a number of bacterial iron-sulphur proteins. It was found that increasing concentrations of DyEDTA and DyNO₃ increased the $P_{1/2}$'s of the features of iron-sulphur protein spectra in a linear manner, whereas Dy-hydroxy-EDTA had no effect. DyEDTA, Dy-hydroxy-EDTA, and DyNO₃ have overall negative, neutral, and positive charges in the physiological pH range. This behaviour indicates that the dysprosium effects are elicited via binding of the complexes to the surface of the proteins rather than via interactions with a uniform dispersion of probe complexes. The nature of the binding sites for the EDTA and nitrate complexes is unknown. Dysprosium(III) complexed with EDTA was used in the work reported herein, this complex has been found to be the most powerful probe in the published work described above.

The linear effect of DyEDTA concentration on the $P_{1/2}$ of an endogenous e.p.r. centre can be explained as follows (Blum *et al.*, 1983). The binding of DyEDTA is assumed to be associated with a dissociation constant which is much greater than the range of probe concentrations used in a typical experiment. Under these circumstances, the fraction of possible probe binding sites occupied is proportional to the probe concentration. Each probe molecule bound to the surface elicits an increase in the $P_{1/2}$ which is proportional

to r^{-6} , where r is the distance between the probe and the endogenous e.p.r. centre. The effect of each bound DyEDTA is additive, and therefore the effect of the probe concentration on the $P_{1/2}$ is linear.

The studies of Blum *et al.* (1981) on the effect of increasing DyEDTA concentration on the $P_{1/2}$ of a number of iron-sulphur proteins has allowed these workers to propose the following empirical relationship between the $P_{1/2}$ and the effective protein radius:

$$\Delta P_{1/2} \text{ (mW mM}^{-1}\text{)} = 4.12 \times 10^8 r^{-6} \exp(-12.5/T) \quad \dots\dots\dots 4.3$$

where $\Delta P_{1/2}$ is the concentration dependence of the $P_{1/2}$, r is the interatomic distance (\AA), and T is the temperature (K).

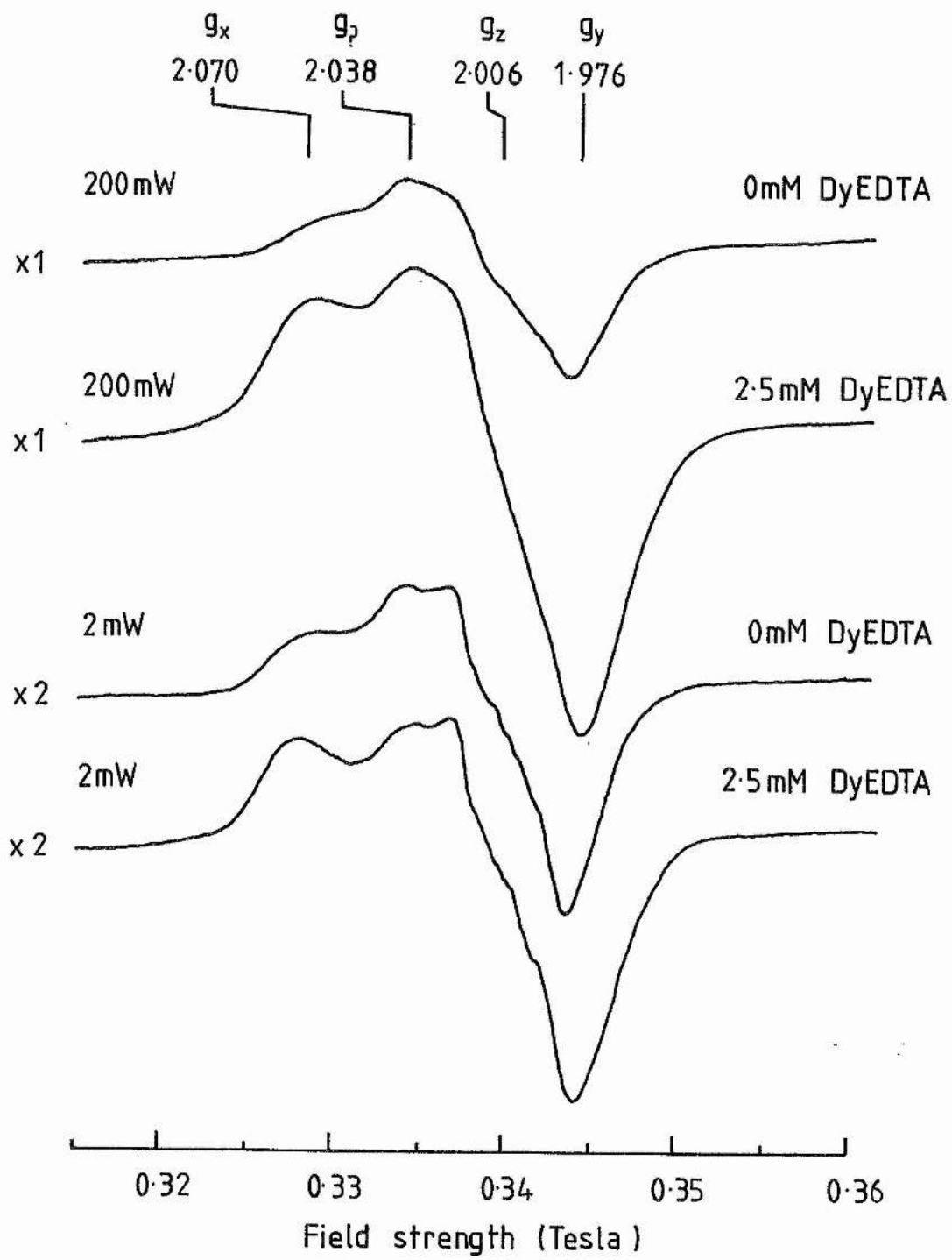
To test the validity of Equation 4.3 for the experimental conditions and e.p.r. spectrometer used in this work, the effect of increasing probe concentration was determined on the e.p.r. saturation behaviour of myoglobin nitroxide. Figure 4.8 shows e.p.r. spectra in the $g=2$ region at 15K of nitrosyl myoglobin in the presence and absence of 2.5mM DyEDTA. The spectrum in the absence of DyEDTA is identical to that reported for nitrosyl myoglobin by Henry & Banerjee (1973). Noticeable in the spectra of Figure 4.8 recorded at low microwave power (2mW) are peaks at $g=2.070$ (g_x), 2.038 (g_z), and a trough at $g=1.976$ (g_y). The g_z features of these spectra occur at around $g=2.006$, and constitute a triplet of unresolved hyperfine structure due to the nuclear spin of the ^{14}N of the NO ligand.

The spectrum recorded in the absence of DyEDTA at high microwave power (200mW) is clearly smaller compared to the spectrum recorded in

Figure 4.8

E.p.r. spectra of nitrosyl myoglobin and the effect of DyEDTA on these spectra.

Nitrosyl myoglobin samples were prepared as follows: 1ml of 10mg ml⁻¹ myoglobin (horse heart, in a 50mM Bes/KOH buffer, pH7) was reduced using a few grains of sodium dithionite in a 1.5ml Eppendorf tube. Sodium nitrite was then added to a final concentration of 50mM, and the nitrosyl haem species was allowed to develop for 10 minutes prior to transferring 0.5ml of the sample to an e.p.r. tube. The sample was then rapidly frozen. The figure also shows spectra recorded in the presence of 2.5mM DyEDTA. Spectrometer settings: temperature, 15K; field modulation intensity, 5G_{pp}; instrument gain, 5 x 10⁴. g-values are indicated by the numbers and bars above the upper spectrum.



its presence. This difference is attributable to microwave power saturation of the spectrum in the absence of DyEDTA. In the presence of 2.5mM DyEDTA, the microwave power saturation is clearly relieved, and the signal becomes larger. Figure 4.9 shows the effect of increasing probe concentration on saturation profiles of the g_y trough of spectra such as those in Figure 4.8.

Figure 4.10 shows the effect of DyEDTA concentration on the $P_{1/2}$'s of the three major components of the nitrosyl myoglobin spectrum. The $P_{1/2}$'s for each feature are almost identical and can be fitted to a single gradient on the plot of Figure 4.10. This gradient, the $\Delta P_{1/2}$, is 15.1 mW mM^{-1} . The distance calculated between the Dy^{3+} and the $\text{Fe}^{2+}\text{-NO}$ using Equation 4.3 is 15.1 \AA . Subtraction of the radius of the EDTA complex (5 \AA , Blum *et al.*, 1980) indicates that the effective radius of myoglobin is 10.1 \AA . This value is consistent with the literature value of 11.4 \AA (calculated from the hydrodynamic properties of myoglobin; Blum *et al.*, 1983). This control study of nitrosyl myoglobin is important, because in the studies of the *in situ* nitrosyl cytochrome *bd* described below, the dysprosium effect is measured for features of e.p.r. spectra with slightly different g -values. In the case of nitrosyl myoglobin, all the features of the e.p.r. spectrum appear to originate from the same distance under the protein surface.

4.5 Dysprosium effect on the nitrosyl cytochrome *bd* spectrum.

Nitrosyl haem spectra of *E.coli* membrane samples containing various concentrations of DyEDTA are illustrated in Figure 4.11. These

Figure 4.9

Effect of DyEDTA on the saturation profiles of nitrosyl myoglobin.

The effect of signal microwave power on the depth of the $g=1.976$ trough was investigated in the presence of various concentrations of DyEDTA at 15K. Saturation profiles are shown for samples prepared as for Figure 4.8 containing the following concentrations of DyEDTA: 0mM (◆—◆), 2.5mM (▲—▲), 7.5mM (■—■), and 10mM (●—●). The $P_{1/2}$ values determined for these concentrations of DyEDTA were 3.6mW, 68mW, 115mW, and 152mW, respectively. Spectrometer settings: field modulation intensity, 5G_{pp}; instrument gain, 5×10^4 ; temperature 15K.

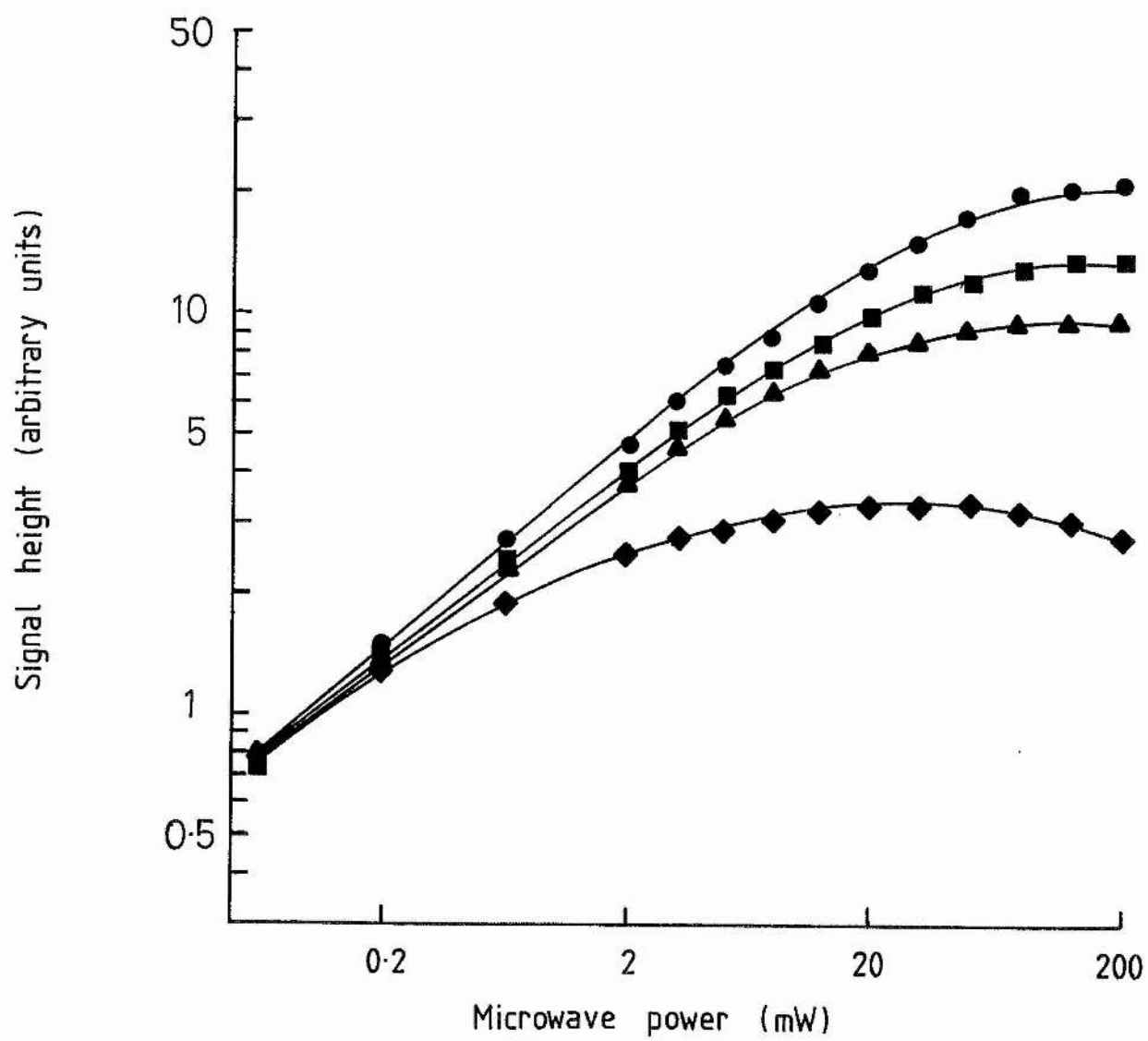
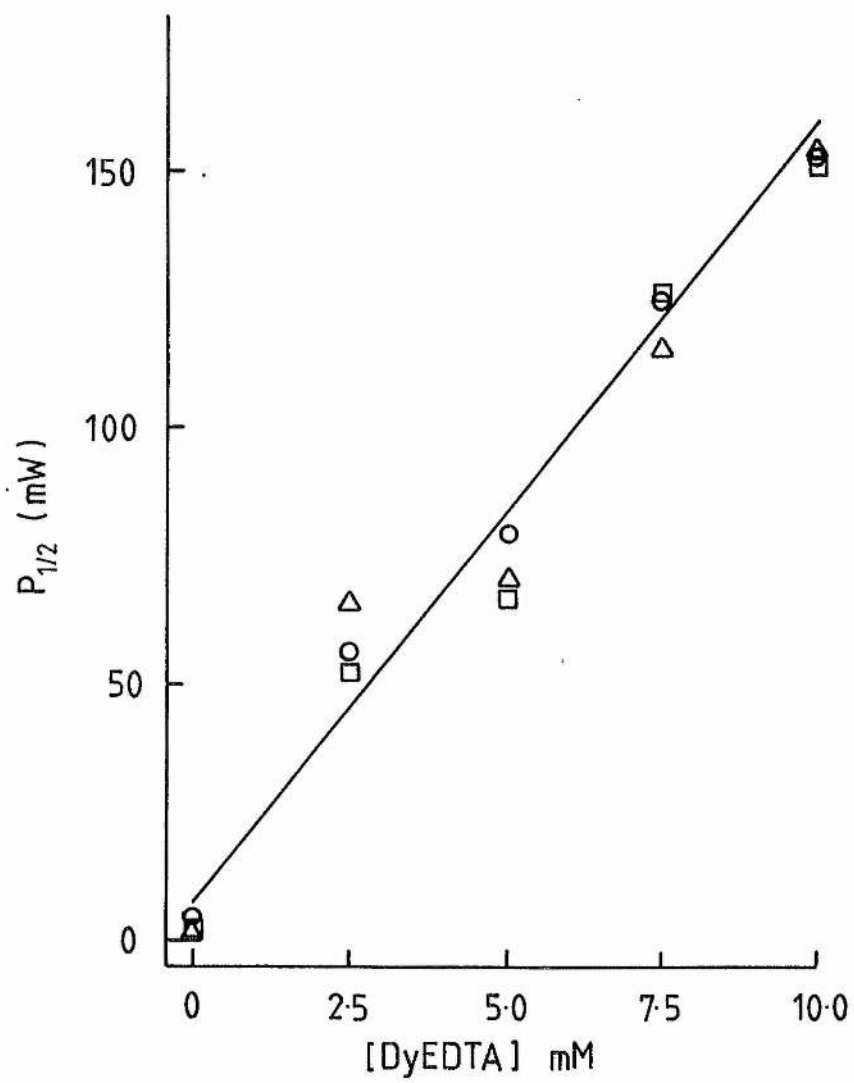


Figure 4.10

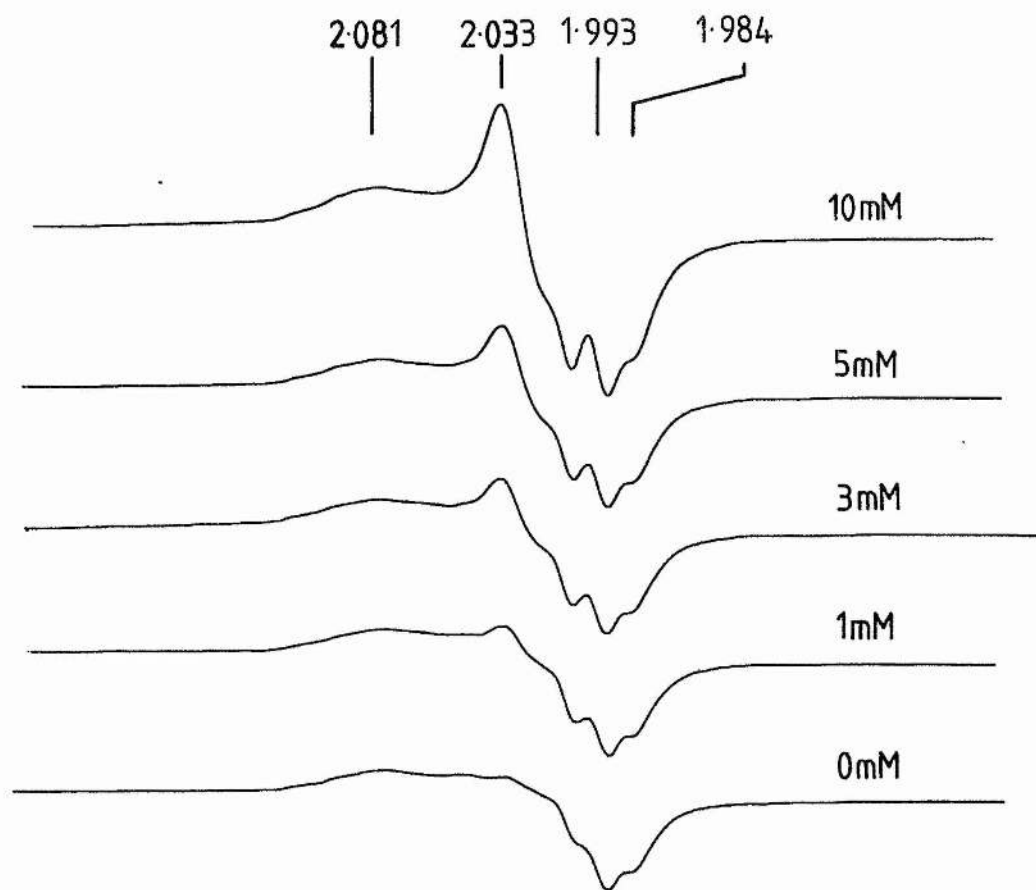
Effect of DyEDTA concentration on the $P_{1/2}$'s of the nitrosyl myoglobin spectral features.

The effect of DyEDTA concentration on the $P_{1/2}$'s of the g_x , g_z , and g_y of the nitrosyl myoglobin spectrum. \square — \square , g_x ; \circ — \circ , g_z ; and \triangle — \triangle , g_y . $P_{1/2}$'s were determined from saturation profiles such as those in Figure 4.9. The $\Delta P_{1/2}$'s of the three major features of the spectrum are all around 15.1 mW mM^{-1} .



*Figure 4.11**Effect of DyEDTA on the nitrosyl cytochrome bd spectrum.*

E.p.r. spectra of nitrite reacted membranes in the $g=2$ region in the presence of 0, 1, 3, 5, and 10mM DyEDTA. Samples were prepared as for Figure 4.3. Spectrometer settings: temperature 15K; microwave power, 21.3mW; field modulation intensity, 10G_{pp}; instrument gain, 2×10^4 . Protein concentration was 37mg ml⁻¹. g -values are indicated by the numbers and bars above the upper spectrum.



spectra clearly show that increasing probe concentrations cause relief from microwave power saturation.

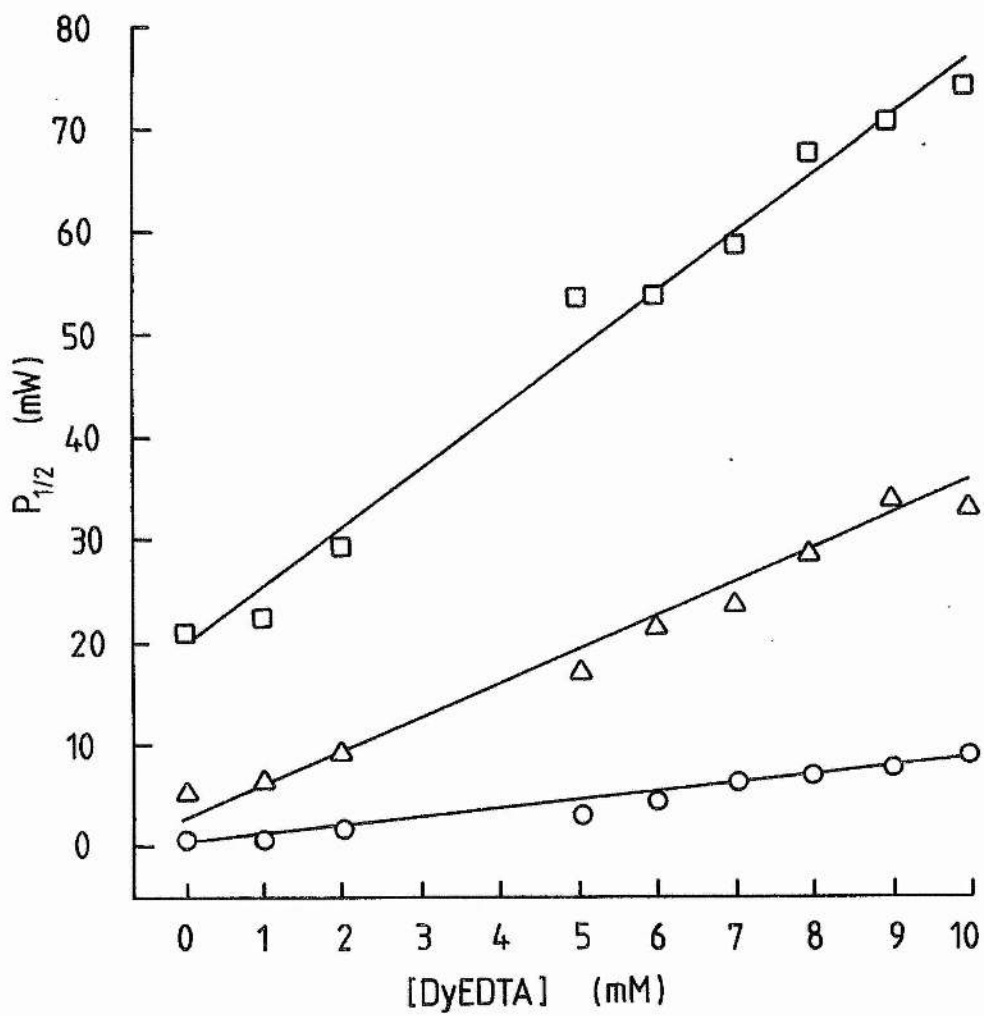
Figure 4.12 shows the effect of increasing DyEDTA concentration on the $P_{1/2}$ values of the three major features of the nitrosyl cytochrome *bd* spectrum. The $\Delta P_{1/2}$ values of these features at 15K are 5.69mW mM^{-1} , 3.04mW mM^{-1} , and 0.874mW mM^{-1} for the $g=2.081$, 1.984 , and 2.033 features, respectively. Use of Equation 4.3 allows the distances between the dysprosium ion and the haem centres responsible for the features of the spectra to be calculated as 17.8\AA , 19.7\AA , and 24.3\AA for the $g=2.081$, 1.984 , and 2.033 features, respectively. These distances have to be corrected for the fact that the DyEDTA only has access to one side of the membrane bound cytochrome *bd*. Ohnishi *et al.* (1982) suggests that the calculated distances should be corrected by multiplying them by 0.7. If the radius of the DyEDTA complex (5\AA ; Blum *et al.*, 1980) is then subtracted from the corrected membrane distances, the below membrane surface distance estimations are 7.4\AA , 8.8\AA , and 12.0\AA for the $g=2.081$, 1.984 , and 2.033 features, respectively.

In order to confirm that the dysprosium(III) ion itself is responsible for the above effects, the effect of lanthanum(III) complexed with EDTA on the e.p.r. spectrum of nitrosyl cytochrome *bd* was investigated. Lanthanum(III) is a diamagnetic control and its complex with EDTA should bind to the surface of the protein in the same way as DyEDTA. Increasing concentrations of LaEDTA have no effect on the saturation behaviour or the lineshape of the nitrosyl cytochrome *bd* e.p.r. signal.

Figure 4.12

*Effect of DyEDTA concentration on the $P_{1/2}$'s of the nitrosyl cytochrome *bd* spectral features.*

The concentration dependence of the effect of DyEDTA on the $P_{1/2}$'s of the three major features of the nitrosyl cytochrome *bd* spectrum in membranes at 15K. \square — \square , the $g=2.081$ component had a dependence of 5.69mW mM^{-1} ; \triangle — \triangle , the $g=1.984$ component had a dependence of 3.04mW mM^{-1} ; \circ — \circ , the $g=2.033$ component had a dependence of 0.874mW mM^{-1} . $P_{1/2}$ data were obtained from saturation profiles such as those shown in Figure 4.6 with samples prepared in the presence of increasing concentrations of DyEDTA. Sample protein concentration, 37mg ml^{-1} .



It can be concluded from the above data that the oxygen binding site of cytochrome *bd* is located towards the inner aspect of the cytoplasmic membrane. Haems *d* and *b₅₉₅* appear to be located at approximately 8 and 12Å° below the surface of the protein on the cytoplasmic side of the membrane, respectively.

4.6 The nitrosyl haem spectrum of nitrite treated whole cells.

The e.p.r. spectrum of nitrite treated whole cells in the $g=2$ region is qualitatively different from that of membranes (Figure 4.13b). The broad peak at $g=2.081$ is smaller relative to the peak at $g=2.033$ and the trough at $g=1.984$. This probably reflects the much lower specific concentration of cytochrome *bd* in whole cells compared to membranes. The nitrosyl haem spectrum of whole cells cannot be unequivocally assigned to cytochrome *bd*, as other ligand binding haemoproteins are likely to contribute to the spectrum. These include the periplasmic nitrite reductase cytochrome *c₅₅₂* (Lin & Kuritzkes, 1987) and the cytoplasmic hydroperoxidase haemoprotein *b-590* (Poole *et al.*, 1986).

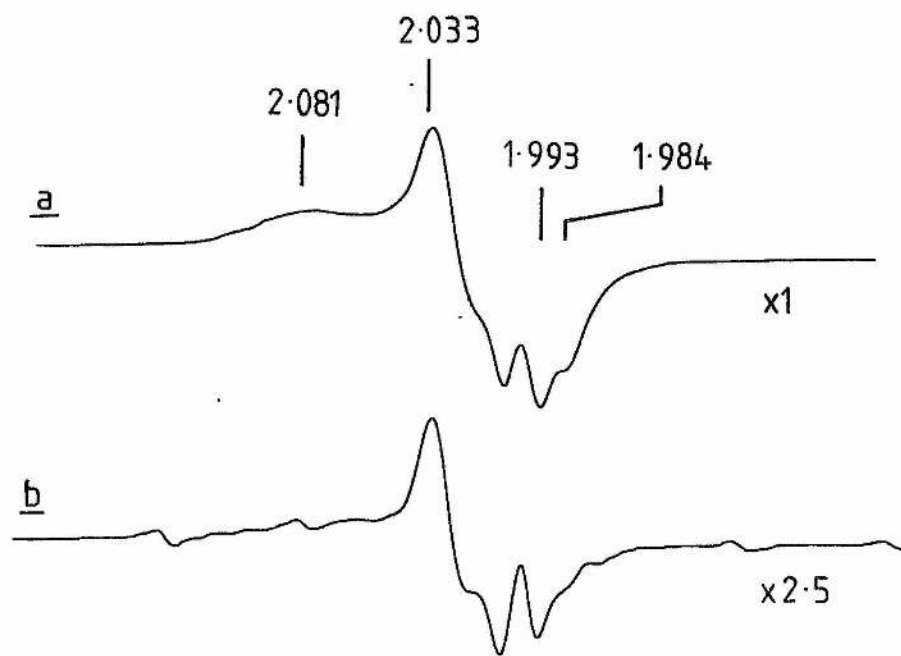
4.7 The effect of DyEDTA on the whole cell nitrosyl haem spectrum.

If the distances calculated in Section 4.5 reflect the distances of the nitrosyl haems from the inner surface of the membrane, then it should be possible to determine their distances from the outer surface of the membrane. However, as described above, the nitrosyl haem spectrum of whole cells is likely to be a composite of the spectra due to a number of nitrosyl haemoproteins, and therefore any distance

Figure 4.13

Comparison of nitrosyl haem spectra of membranes and whole cells.

Samples were prepared using membranes (a) or whole cells (b) as described for Figure 4.3. Spectrometer settings: temperature, 15K; field modulation intensity, 10G_{pp}; instrument gain, 2 x 10⁴. Protein concentrations: membranes (a), 37mg ml⁻¹; whole cells (b), 82mg ml⁻¹. g-values are indicated by the numbers and bars above the upper spectrum.



estimations are unlikely to be accurate.

The success of experiments using DyEDTA as a paramagnetic probe in whole cells depends on the permeability of the periplasm to the EDTA complex. The diameter of the porin pores of the outer (periplasmic) membrane of *E.coli* has been estimated to be around 11Å and the upper permeant solute molecular weight limit has been estimated as around 600 daltons (Nikaido & Vaara, 1987). The diameter of the DyEDTA complex used as a paramagnetic probe in this work has been estimated to be 10Å (Blum *et al.*, 1980), and its molecular weight is 431 (ignoring its degree of protonation). Thus, the complex should be able to diffuse into the periplasm.

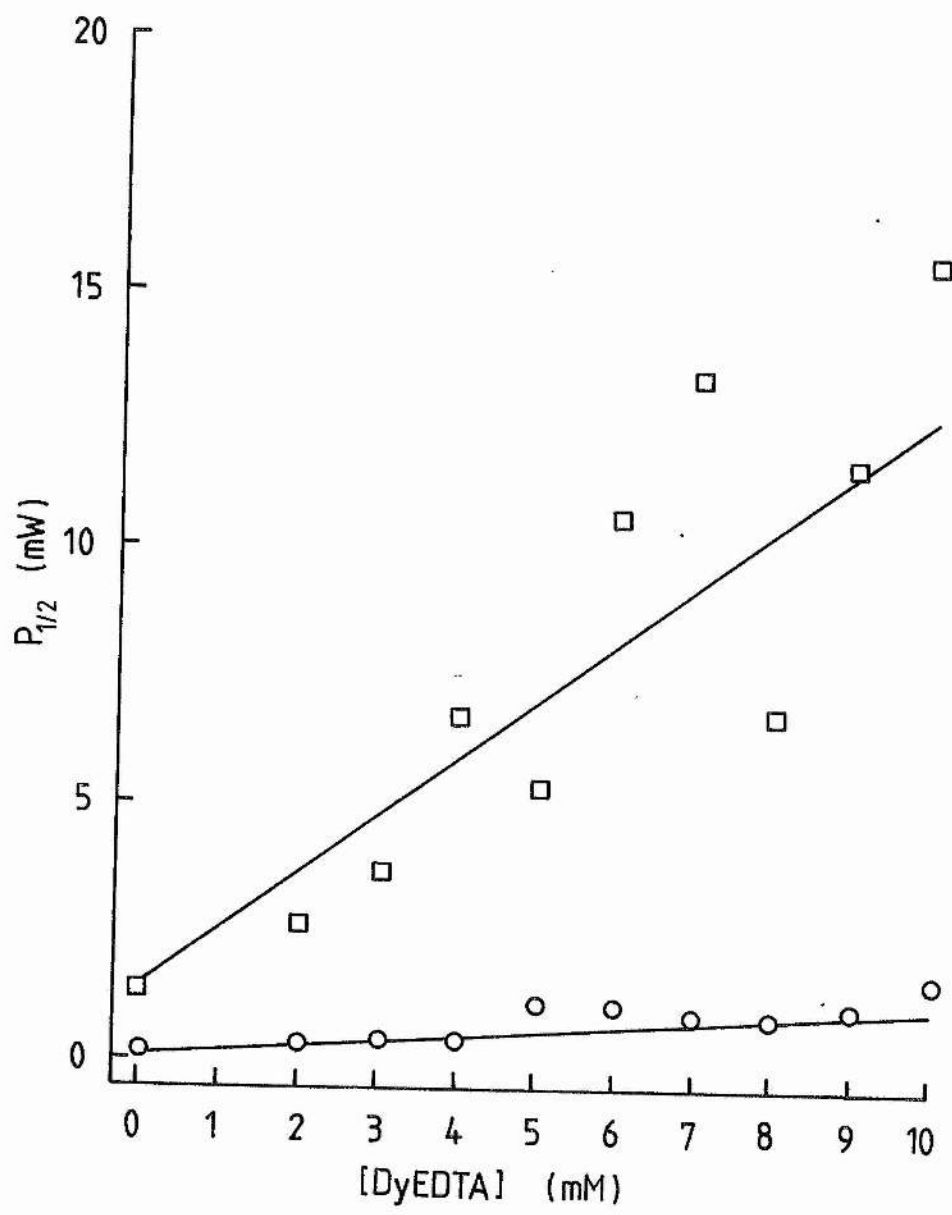
The effect of DyEDTA concentration on the two major features of the whole cell nitrosyl haem spectrum is illustrated in Figure 4.14. The $\Delta P_{1/2}$'s of the $g=2.033$ peak and $g=1.984$ trough are 0.10 and 1.26, respectively. Use of Equation 4.3 allows the distance between the dysprosium ion and the haem centres responsible for the features of the spectrum to be calculated as 34.5 and 22.0Å for the $g=2.033$ peak and $g=1.984$ trough, respectively. Correction of these values as described in Section 4.5 results in below membrane surface distance estimations of 19.2 and 11.0Å for the $g=2.033$ and $g=1.984$ features, respectively.

The estimates for the depths below the outer surface of the cytoplasmic membrane of the two haems responsible for the whole cell nitrosyl haem spectrum are based on the assumption that the only species contributing to this spectrum are membrane bound. However, both periplasmic and cytoplasmic ligand binding haemoproteins will

Figure 4.14

Effect of DyEDTA concentration on the $P_{1/2}$'s of the nitrosyl haem spectral features of whole cells.

The concentration dependence of the effect of DyEDTA on the $P_{1/2}$'s of the two major features of the nitrosyl haem spectrum of whole cells at 15K. \square — \square , the $g=1.984$ signal; \circ — \circ , the $g=2.033$ signal. In both cases, there is no significant dependence of the $P_{1/2}$ on DyEDTA concentration. $P_{1/2}$ data were obtained from saturation profiles such as those in Figure 4.6. Sample protein concentration, 43mg ml^{-1} protein.



also have reacted with nitrite in the experiments reported herein. The $\Delta P_{1/2}$'s and resultant distances are therefore averages for the effect of this probe on the spectra of all the nitrosyl haems formed following treatment of whole cells with nitrite. No dysprosium effect should be observable on the e.p.r. spectra of the cytoplasmic nitrosyl haemoproteins, whilst a major effect is presumably elicited on the spectra of periplasmic haemoproteins. Thus, the distance estimates determined using nitrite treated whole cells are questionable. However, the results are consistent with those of Section 4.5 and support the proposal that the oxygen binding site of cytochrome *bd* is located towards the inner aspect of the cytoplasmic membrane. Moreover, the results indicate that the periplasm is permeable to the DyEDTA complex.

4.8 Conclusions.

The data presented herein show that reaction of *in situ* cytochrome *bd* with nitrite results in the formation of two distinct nitrosyl haem species detectable by e.p.r. The kinetics of formation of these species are broadly similar to the kinetics of formation of the optically detectable nitrosyl haem species described in Chapter 3. The first species to form in the reaction at pH7 is nitrosyl haem *d*, which has an e.p.r. spectrum similar to those of nitrosyl myoglobin (Henry & Banerjee, 1973), nitrosyl cytochrome *c*, nitrosyl catalase (Yonetani *et al.*, 1972), and nitrosyl cytochrome *cd*₁ (Johnson *et al.*, 1980). Its spectrum is quite distinct from that of nitrosyl cytochrome *aa*₃ (Brudvig *et al.*, 1980).

The ligand binding haems of *in situ* cytochrome *bd* are located towards the inner surface of the cytoplasmic membrane. The two species responsible for the components of the haem-NO signal are located at different depths below the protein surface. These findings are consistent with a model for the oxidase involving two oxygen binding sites (haems *d* and *b₅₅₈*). Haem *d* appears to be located at about 12Å° below the surface of the membrane, whilst haem *b₅₅₈* appears to be located about 8Å° below the surface of the membrane.

These studies bear interesting comparison with those carried out on mitochondrial cytochrome *aa₃* by Ohnishi *et al.* (1985). Haem *a₃* is located towards the middle of the inner mitochondrial membrane, and haem *a* is located towards the outer surface of the membrane. Estimations of distances between the two sides of the membrane and haems *a* and *a₃* are complicated by the known projections of cytochrome *aa₃* into the two phases of the mitochondrion. Such projections are also likely to complicate the distance estimations in the cytochrome *bd* system.

No information is available on the position of the haem *b₅₅₈* of cytochrome *bd* on the basis of the experiments reported herein, but it is likely to be located towards the outer surface of the *E.coli* cytoplasmic membrane, as is the quinol oxidation site (Chapter 1, Section 1.4.4). It was not possible to study the effect of DyEDTA on the e.p.r. spectrum of haem *b₅₅₈* because its e.p.r. characteristics are not amenable to its study using this technique (it has an attenuated low spin ferric haem signal; Chapter 5).

Overall, the data presented herein supports a model for

cytochrome *bd* with two oxygen binding sites, haems *d* and *b₅₉₅*, which are both located towards the inner aspect of the cytoplasmic membrane.

CHAPTER FIVE

*Electron paramagnetic resonance spectroscopy of the in situ oxidised
cytochrome bd.*

5.1. Introduction.

It was concluded in Chapter 1 that the published assignments of e.p.r. signals to the constituent haems of cytochrome *bd* remain equivocal. In this chapter, the e.p.r. signals observed in a membrane preparation of *E.coli* containing cytochrome *bd* as the major cytochrome component are described with a view to clarifying, substantiating, or ameliorating the assignments of e.p.r. signals published to date.

Of the three haem components present in cytochrome *bd*, haems *d* and *b₅₉₅* have been implicated in oxygen binding on the basis of their ligand binding behaviour (Chapter 1, Section 1.4.7). The optical spectrum of haem *b₅₉₅* is also typical of a high spin haem *b*. Such ligand binding haems tend to be five coordinate and high spin (Wood, 1984), and in other enzymes able to bind oxygen species they exhibit high spin ferric haem signals with an intense g_{xy} around $g=6$ (the g_z of such spectra are minor features and occur around $g=2$; Palmer, 1985). The ligand binding haems of cytochrome *b_{562-o}* (Hata *et al.*, 1985; J.C. Salerno, B. Bolgiano, & W.J. Ingledew, unpublished results) and cytochrome *aa₃* exhibit high spin ferric haem signals (Aasa *et al.*, 1976), although the e.p.r. of these enzymes is complicated by antiferromagnetic coupling between the high spin ferric haem and a high potential cupric copper. Other ligand binding enzymes which exhibit high spin ferric haem e.p.r. signals include thyroid peroxidase (Lukat *et al.*, 1988), horseradish peroxidase (Young & Seigel, 1987), spinach catalase (Hirasawa *et al.*, 1987), metmyoglobin (Young & Seigel, 1987), and methaemoglobin (Peisach *et al.*, 1969). It would therefore not be surprising if the two putative ligand binding

haems of cytochrome *bd* also exhibit high spin ferric haem e.p.r. signals.

As described in Chapter 1 (Section 1.4.6), Hata *et al.* (1985) assigned low spin ferric haem signals at $g=2.3$ (g_y) and $g=2.5$ (g_z) observed in their membrane and purified preparations to haem *d*. These values of g_y and g_z are very similar to those exhibited by model low spin (six coordinate) chlorin compounds (Stolzenberg *et al.*, 1981). The only other cytochrome containing a ligand binding haem *d* to have been extensively studied by e.p.r. is cytochrome *cd*₁ of *Pseudomonas aeruginosa* (Walsh *et al.*, 1979; Gudat *et al.*, 1973). In this enzyme, the oxidised haem *d*₁ has an e.p.r. spectrum with features at $g=2.52$ (g_z), 2.42 (g_y), and 1.73 (g_x) (Muhoberac & Wharton, 1983). However, there is m.c.d. evidence indicating that haem *d*₁ undergoes an unusual high to low spin transition on oxidation, and this raises the possibility the oxidised haem picks up a sixth ligand from the protein (Walsh *et al.*, 1979). However, whilst there are similarities between the optical spectra of haems *d* and *d*₁, there are major differences in the structures of their respective porphyrins. Haem *d* has been identified as a chlorin derivative of protoporphyrin IX with one reductively dihydroxylated pyrrole (Timkovich *et al.*, 1985). Haem *d*₁, on the other hand, is a porphyrindione (Chang *et al.*, 1986), a structure with ketone groups in two adjacent pyrrole rings which is quite distinct from that of haem *d*. Another dissimilarity between these two enzymes is that cytochrome *bd* functions as an oxidase, whereas the primary function of cytochrome *cd*₁ is dissimilatory nitrite reduction (Yamanaka, 1964). However, the latter is also able

to catalyse the four electron reduction of oxygen to water (Timkovich & Robinson, 1979). Synthetic five coordinate chlorin complexes exhibit axial high spin ferric haem e.p.r. signals (Stolzenberg *et al.*, 1981), and it would therefore be surprising if ferric haem *d* does not also exhibit a high spin ferric haem signal. There is therefore little basis upon which to expect the e.p.r. behaviour of the haem *d* of cytochrome *bd* to be similar to that of the haem *d*₁ of cytochrome *cd*₁.

Haems *b* present in cytochromes not involved in ligand binding exhibit low spin ferric haem signals. One group of such cytochromes, including cytochromes *b*₅ and *b*₂ exhibit e.p.r. spectra with *g*-values in the range $g_x > 1.34 < g_y < g_z < 3.03$ (Walker *et al.*, 1984). Another group is characterised by a peculiar e.p.r. signal with a $g_z > 3.3$ as the sole observable spectral feature (the *g*_{*y*} and *g*_{*z*} of such haems are too broad to be observed). This group includes the haems *b*₅₆₂ and *b*₅₆₆ of mitochondrial complex III (Salerno, 1984), and haem *b*₅₆₃ of cytochrome *b*_{6f} (Bergstrom, 1985). The haems of these two enzymes have roles central to the redox reactions of quinol species in their respective electron transport chains, as does haem *b*₅₅₈ of cytochrome *bd*. Haem *b*₅₅₈ has an optical spectrum typical of a low spin haem *b* (Koland *et al.*, 1984). It is therefore likely that the haem *b*₅₅₈ of cytochrome *bd* has a low spin ferric haem signal in its native, six coordinate state, not an axial high spin signal as reported by Hata *et al.* (1985).

In this chapter, an *in situ* e.p.r. study of the cytochrome *bd* is reported using a cytoplasmic membrane preparation from *E.coli* strain EMG2 grown anaerobically on glycerol with fumarate as respiratory oxidant. The effects of redox potential, pH, and the ligands oxygen,

CO and cyanide are reported with a view to assigning the observed e.p.r. signals to the haems present in cytochrome *bd*.

5.2. E.p.r. of oxidised *in situ* cytochrome *bd*.

Figure 5.1 shows e.p.r. spectra of oxidically oxidised membranes in both the $g=6$ and $g=3$ regions. There is an intense g_{xy} of an axial high spin ferric haem at $g=6$ (g_{xy}), whilst the g_z of a low spin ferric haem is observed at around $g=3.3$. The $g=3.3$ signal has an asymmetric 'ramp' type lineshape similar to those reported for haem b_{566} of mitochondrial complex III (Salerno, 1984) and haem b_{563} of cytochrome b_{56} (Salerno *et al.*, 1983). The prominent signal at $g=4.3$ is due to ferric iron of low symmetry which is not specifically associated with protein (Blumberg, 1967). The low spin ferric chlorin signals observed by Hata *et al.* (1985) with g -values of 2.3 and 2.5 are observed in oxidised membranes (not shown), but at very low intensities compared to the signals observed by Hata *et al.* (1985) in membranes from aerobically grown cells. However, membranes from aerobically grown *E.coli* strain FUN4/pNG2, which overexpresses cytochrome *bd* 8 to 10 fold compared to anaerobically grown EMG2, do exhibit readily observable low spin ferric chlorin signals around $g=2.3$ and $g=2.5$ (Section 5.9).

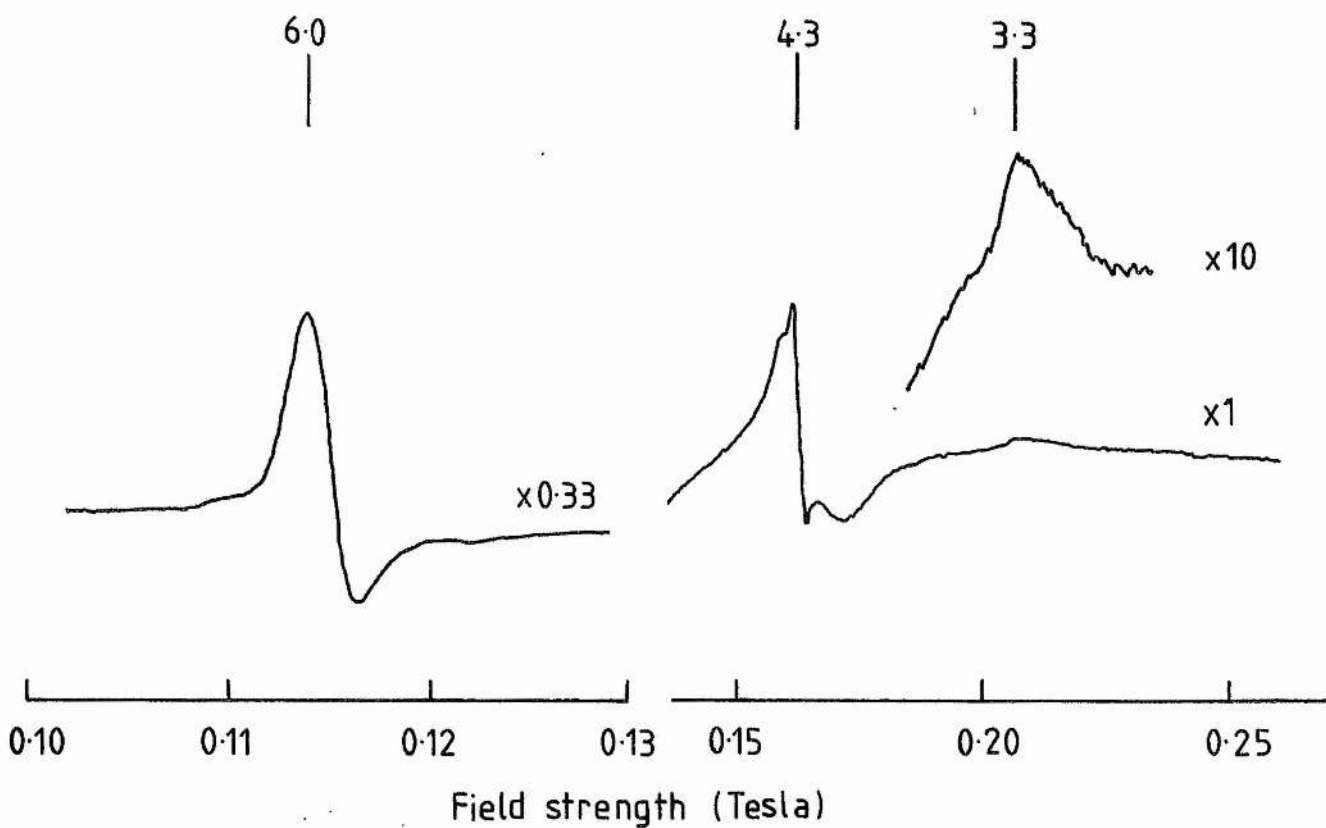
5.3. E.p.r. spectra of high spin ferric haems.

Of the three haems present in cytochrome *bd*, haems *d* and b_{595} would be expected to have high spin ferric haem signals on the basis of their putative role in ligand binding. The e.p.r. spectrum of the

Figure 5.1

E.p.r. spectra of air oxidised membranes from fumarate grown cells.

Approximately 0.5mls of *E.coli* membranes (protein concentration, 25mg ml⁻¹) were placed in a 3mm internal diameter quartz e.p.r. tube and were vigorously aerated using a coiled stainless steel wire. Membranes were suspended in a 100mM Tes/KOH buffer (pH7) containing 2mM MgSO₄. Spectrometer settings: temperature, 5K; field modulation intensity, 10G_{pp}; microwave power, 20mW; instrument gain, 2.5x10⁴. g-values are indicated by numbers above the spectrum.



in situ cytochrome *bd* around $g=6$ was therefore further investigated by poisoning membranes anoxically at appropriate redox potentials. The published E_{m7} 's, based on optical redox potentiometry, of haems *d* and *b₅₉₅* are 280 and 150mV, respectively (Reid & Ingledew, 1979). Figure 5.2 shows the e.p.r. spectra of membranes poised anoxically at 380 and 200mV. Comparison of these spectra with the oxically oxidised spectrum of Figure 5.1 indicates that there are major differences between the e.p.r. lineshapes of anoxically and oxically oxidised membranes. These will be described in Section 5.6.

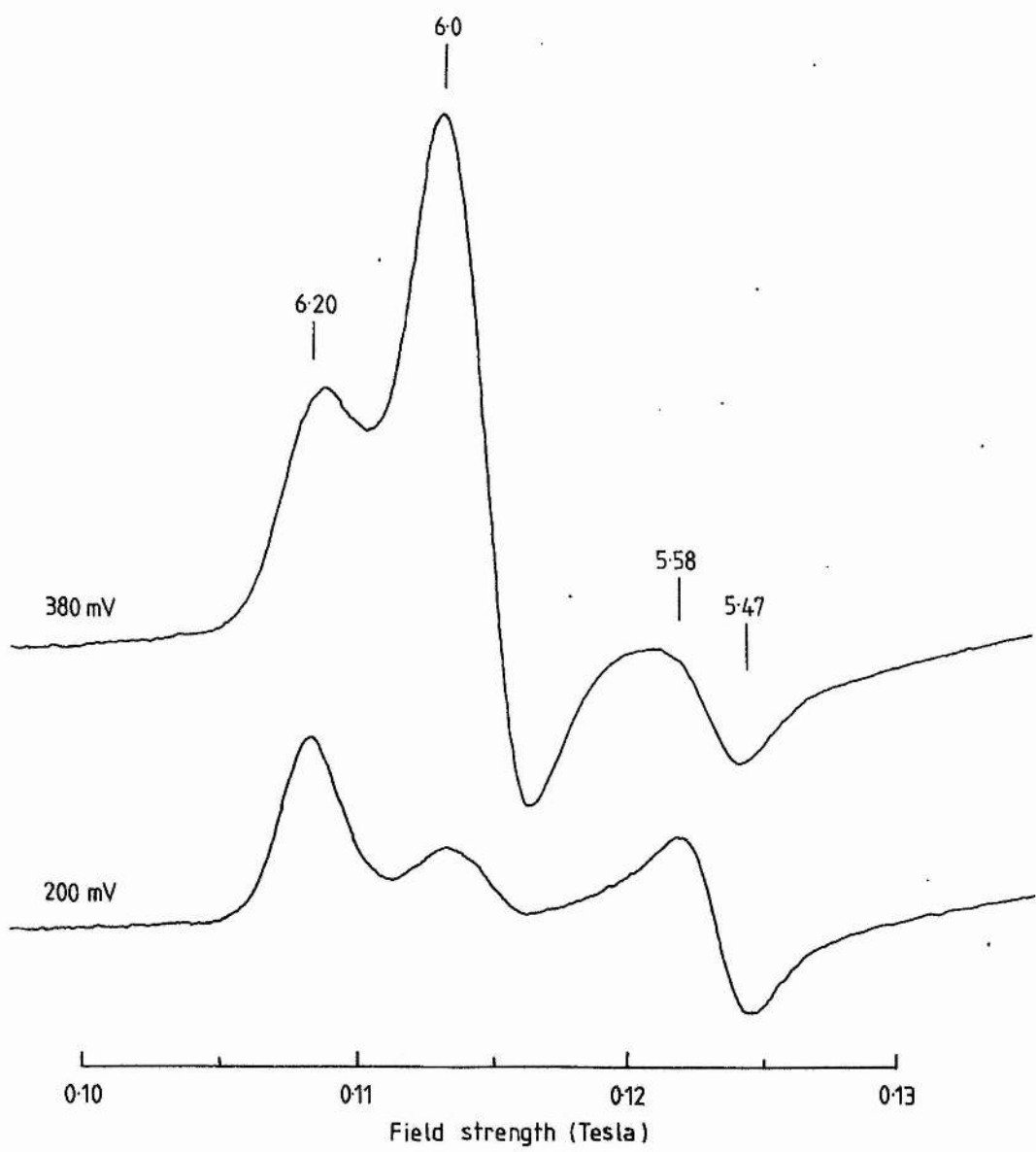
Noticeable in the high potential (380mV) spectrum of Figure 5.2 are peaks at around $g=6.2$, 6.0, and 5.6. This spectrum is consistent with the presence of both axial and rhombic ferric haem signals. In the low potential (200mV) spectrum the central axial signal (peak at $g=6.0$) has almost titrated out, resulting in a spectrum dominated by the features of the rhombic signal at around $g=6.2$ and 5.6. Truncated double integrations (Aasa *et al.*, 1976) of the two spectra in Figure 2 indicate that the spin intensity of the 200mV spectrum in the $g=6$ region is approximately half that of the 380mV spectrum. The species responsible for the rhombic and axial high spin ferric haem signals are therefore present in approximately equal concentrations in cytoplasmic membranes containing cytochrome *bd*.

Noticeable in Figure 5.2 is a significant difference in the lineshape of the rhombic haem signal between the 380 and 200mV spectra. Its apparent g_y moves downfield and the intensity of its g_y peak-trough decreases when the axial haem is oxidised. Truncated double integrations indicate that the apparently smaller size of the

Figure 5.2

E.p.r. spectra of redox poised membranes.

E.p.r. samples of *E.coli* membranes were withdrawn from an anaerobic redox titration vessel after being poised at 200 and 380mV (see methods). Membranes were suspended in a 100mM Tes/KOH buffer (pH7) containing 2mM MgSO₄. Spectrometer settings: temperature, 6K; field modulation intensity, 10G_{pp}, microwave power 20mW; instrument gain, 5x10⁴; protein concentration, 27mg ml⁻¹. The positions of g-values are indicated in the Figure by vertical bars.



rhombic g_y peak-trough in the high potential spectrum is not due to loss of rhombic haem spin intensity. A haem-haem interaction between the axial and rhombic haems would explain this lineshape change, resulting in a subpopulation of the rhombic haem with an altered g_y when the axial haem becomes oxidised. This explanation of the lineshape change of the rhombic haem is supported by simulations of the e.p.r. lineshapes of the two high spin ferric haems (Section 5.5).

The above results are consistent with an assignment of the axial and rhombic high spin ferric haem signals to haems *d* and *b₅₉₅*, respectively. However, consideration of other results presented herein is required to strengthen these assignments.

5.4. Redox potentiometry of the e.p.r. signals.

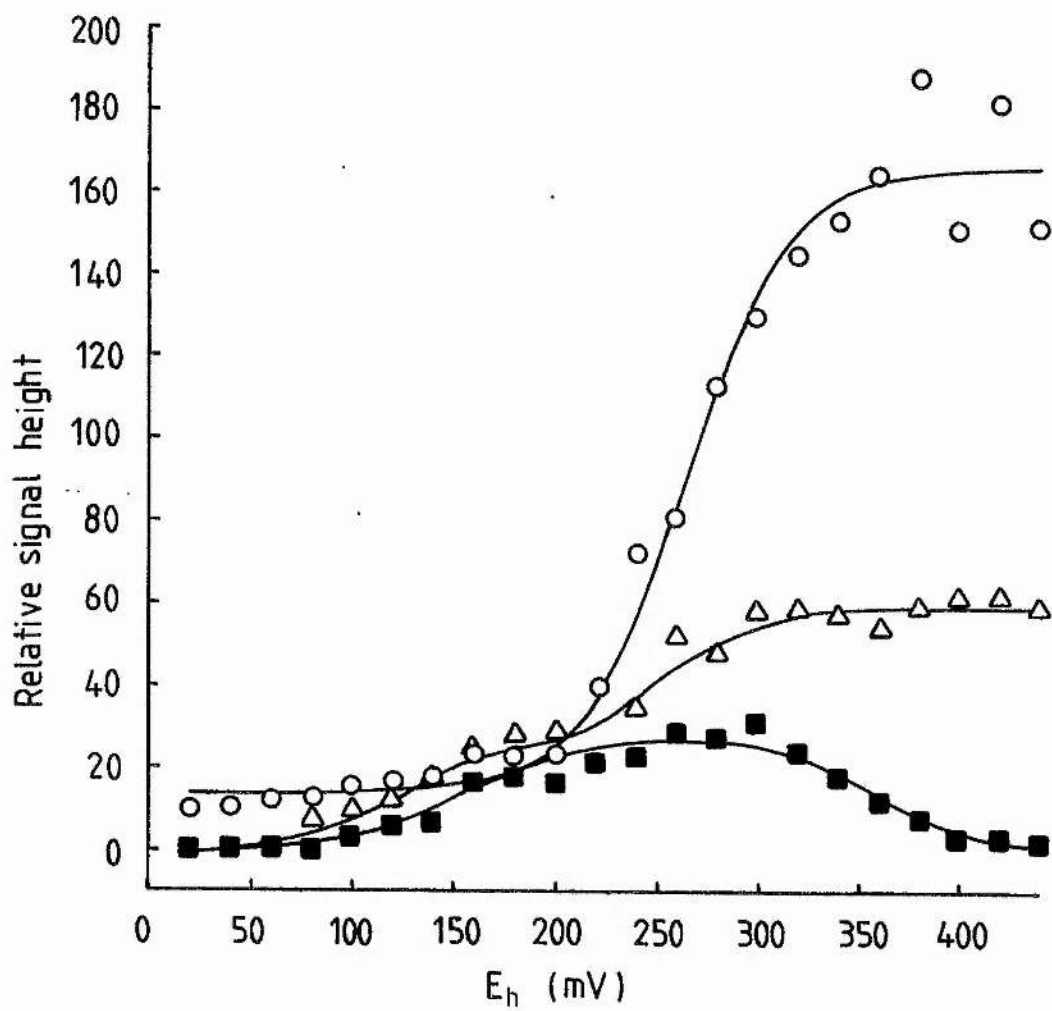
The behaviour of the high spin ferric haem signals was further probed by redox potentiometry (Figure 5.3). The axial feature of the spectrum titrates with an E_{m7} of 260mV, whilst the two rhombic haem features, the low field peak and the high field peak-trough show apparently anomalous behaviour. With increasing E_h , the rhombic high spin spectral features appear with an E_{m7} of around 154mV, but the high field rhombic peak-trough gets smaller again at higher potentials. The analysis of these changes is complicated by spectral overlap with the putative second (minor) rhombic component and the broad peak-trough of the central axial component of the spectra.

The difference in the e.p.r. lineshape in the rhombic g_y region between samples poised at 380mV and 200mV (Figure 5.2) and the behaviour of this feature in potentiometric redox titrations can be

Figure 5.3

Redox titration of the $g=6$ region of the e.p.r. spectrum.

Data from spectra recorded under the conditions of Figure 2 were plotted. Solid lines represent the $n=1$ fits of the data to the Nernst equation using single or multiple components (see text). \triangle — \triangle low field peak. \circ — \circ central peak-trough. \blacksquare — \blacksquare high field peak-trough.



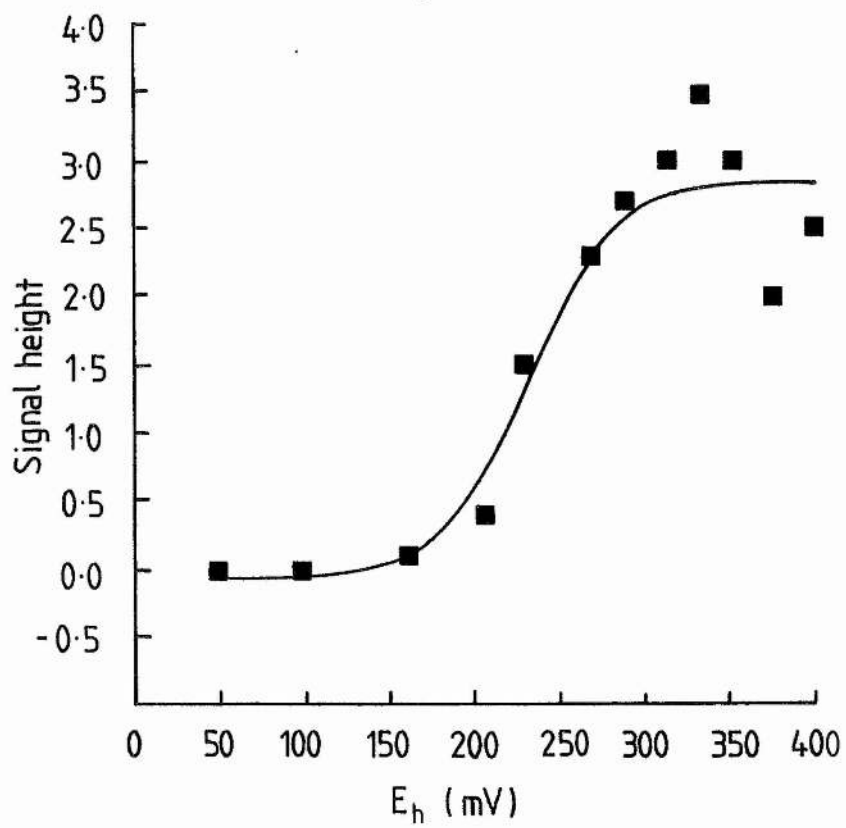
explained if there are two rhombic components in the high potential spectrum. One of these would correspond to the rhombic component observed in the 200mV spectrum (the low potential component; Figure 5.2), and the other would be derived from this component, appearing at higher redox potentials (the high potential component) as a result of the interaction of the rhombic species with the axial species. A small difference in the position of the g_y 's of these two rhombic components would result in the high potential component cancelling out the low potential component leading to an apparently smaller rhombic g_y feature in the spectra recorded at high redox potentials. However, this lineshape transition of the rhombic signal is not complete upon full oxidation of the axial haem, and there is also some variability in its extent between different batches of membranes. This explanation for the lineshape change of the rhombic species at high potentials is supported by simulation of the e.p.r. spectrum of fully anoxically oxidised membranes (Section 5.5). The potentiometric behaviour of the axial and rhombic high spin ferric haem signals supports their assignment to haems *d* and *b₅₉₅*, respectively (see Section 5.10).

The other major haem signal in e.p.r. spectra of oxidised membranes containing cytochrome *bd* is the g_z of a low spin ferric haem observed at $g=3.3$. Analysis of the behaviour of this spectral feature is complicated by its low intensity and the low temperatures necessary for its observation (5K). This signal titrates with an E_{m7} of around 226mV (Figure 5.4), a value intermediate between those of the two high spin haem species, as would be expected for the haem *b₅₅₈* of

Figure 5.4

Redox titration of the $g=3.3$ low spin ferric haem signal.

The size of the $g=3.3$ feature of the e.p.r. spectrum was plotted against redox potential. The data were obtained from spectra recorded at 5K using samples under the conditions of Figure 5.2. The solid line represents an $n=1$ fit of the data to the Nernst equation (see text).



cytochrome *bd* on the basis of published potentiometric titrations (Lorence *et al.*, 1984a; Reid & Ingledew, 1979). The $g=3.3$ signal can be assigned to haem b_{558} (see Section 5.10).

5.5. Simulation of the anoxically oxidised spectrum around $g=6$.

A good fit to the experimental lineshape of fully oxidised cytochrome *bd* in the $g=6$ region can be obtained by computer simulation (Figure 5.5). This fit is obtained using a total axial spin concentration that is equal to the total rhombic spin concentration, as indicated by the value of the double integrals in the high spin region of the 380mV and 200mV spectra. The simulation is a composite of three components, one axial and two rhombic. Of the two rhombic components, one, a high potential component must be derived from the other, a low potential component to maintain a total rhombic to axial ratio of 1:1. The low potential rhombic component corresponds to the major rhombic component of the simulation (component (b), Figure 5.5), whilst the high potential rhombic component corresponds to the minor component rhombic component of the simulation (component (c), Figure 5.5). The high potential rhombic component can be attributed to a subpopulation of haem b_{595} which interacts with haem *d*.

5.6. Effect of oxygen on the high spin ferric haem signal around $g=6$.

Oxygen affects the anoxically oxidised cytochrome *bd* and results in the spectral lineshape shown in Figure 5.6 in the $g=6$ region of the e.p.r. spectrum. No differences are observed between the spectra of air oxidised membranes and those of anoxically oxidised membranes to

Figure 5.5

Simulation of the anoxically oxidised spectrum in the g=6 region.

Experimental and simulated e.p.r. spectra of membranes poised at 380mV. Sample and instrument conditions were as for Figure 5.2. The lower trace is a simulation obtained by adding three different components in suitable proportions. The g-values, linewidths, and relative weights of these components are:

(a): (5.97, 5.96, 2.0), (0.2400, 0.1800, 0.3000) mT, 0.50;

(b): (6.25, 5.54, 2.0), (0.1215, 0.1480, 0.3000) mT, 0.33;

(c): (6.24, 5.67, 2.0), (0.1215, 0.1480, 0.3000) mT, 0.17.

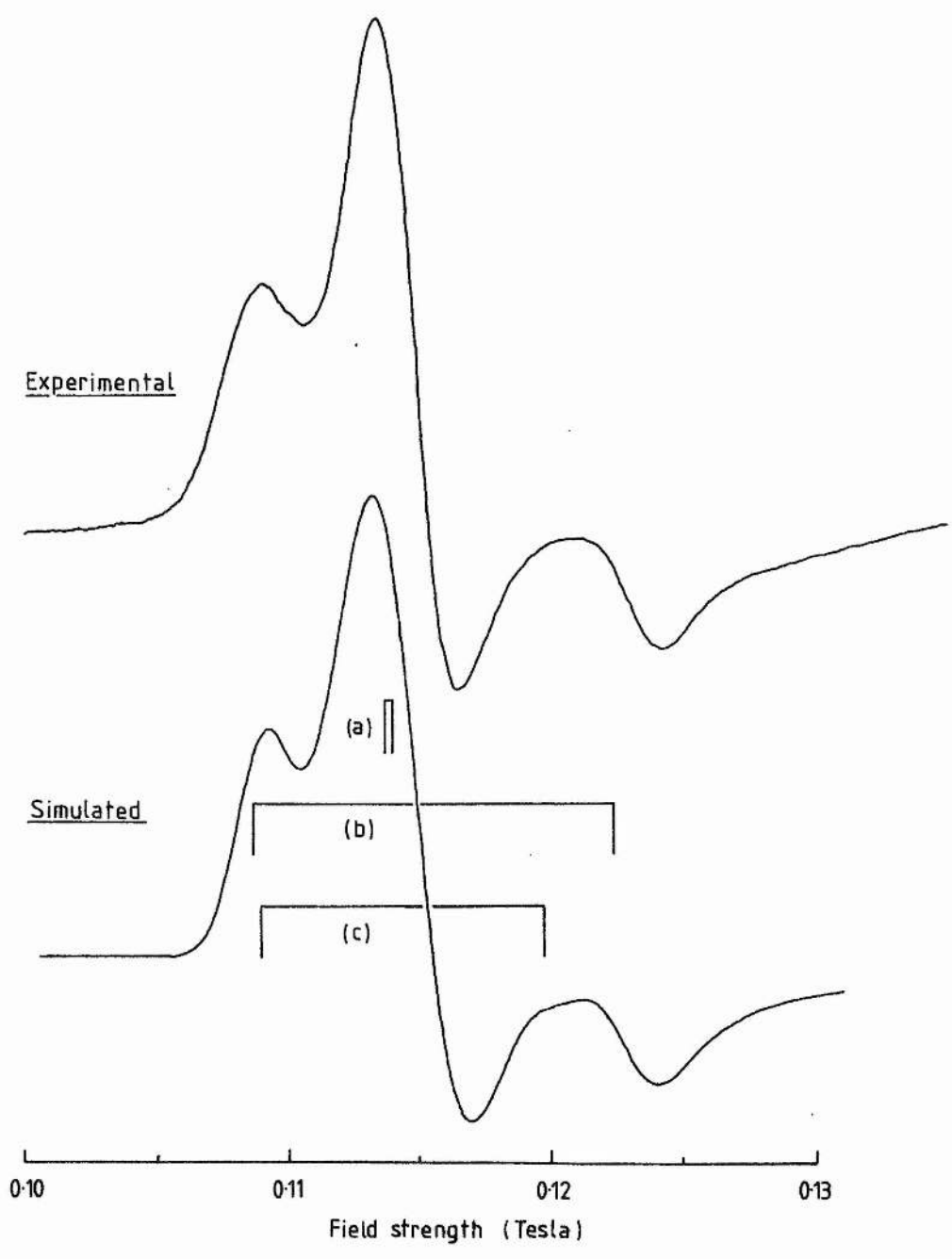


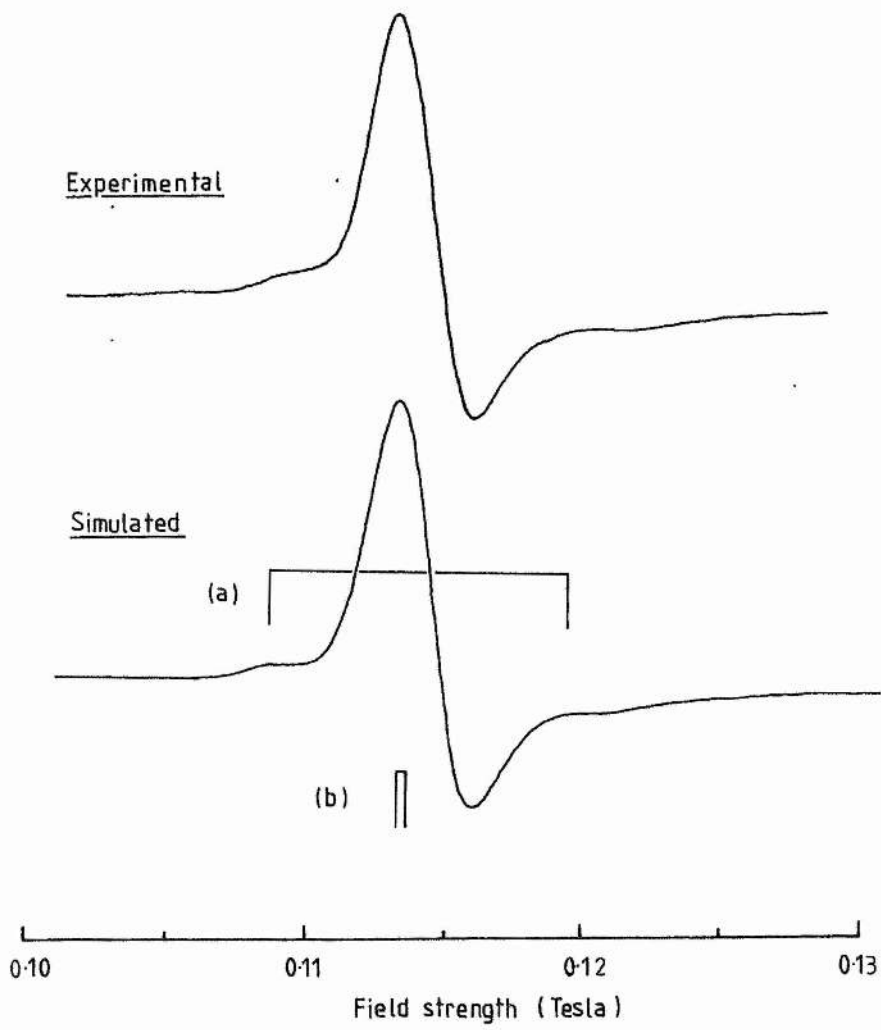
Figure 5.6

Simulation of the oxically oxidised spectrum in the $g=6$ region.

Experimental and simulated e.p.r. spectra of oxically oxidised membranes. Sample and instrument conditions were as for Figure 5.1. The lower trace is a simulation obtained by adding two different components in suitable proportions. The g -values, linewidths, and relative weights of these components are:

(a): (6.24, 5.67, 2.0), (0.1215, 0.1480, 0.3000) mT, 0.14;

(b): (5.97, 5.96, 2.0), (0.1800, 0.1200, 0.3000) mT, 0.86.



which oxygen has been introduced or peroxide added. Oxygen clearly results in a transition in overall lineshape from a mixture of rhombic and axial high spin ferric haem (Figure 5.5) to a lineshape that is predominantly axial high spin with only a minor rhombic component (Figure 5.6). This effect of oxygen on the fully ferric cytochrome is unusual, and is consistent with oxygen binding to fully oxidised cytochrome *bd*. However, there is prior evidence showing that the optical spectrum of oxidised cytochrome *bd* is perturbed by oxygen (see Section 5.11).

Truncated double integrations of spectra of oxically and anoxically oxidised membranes in the $g=6$ region indicate that their relative spin concentrations are approximately equal. This suggests that both the haem *d* and the haem b_{595} are e.p.r. visible under oxically oxidising conditions. This contrasts with the data of Hata *et al.* (1985) who observed that the low spin ferric chlorin signals (the $g=2.3$ and $g=2.5$ spectral features which they attributed to haem *d*) were attenuated under oxidic conditions, suggesting that haem *d* was largely e.p.r. silent under these conditions. The finding that there is no loss of spin intensity in the $g=6$ region in oxically oxidised membranes suggests that oxygen perturbs the e.p.r. spectrum of haem b_{595} resulting in a transition of its lineshape from rhombic to axial.

Only two components are necessary to simulate the lineshape of oxically oxidised membranes (Figure 5.6). These correspond to a major axial component with narrower linewidths than the anoxic axial component and a minor rhombic component corresponding to the minor, high potential rhombic component in the anoxic simulation

(component (c), Figure 5.5). Although only two components were used in the simulation, it is possible to simulate two major axial components attributable to the haem *d* and haem *b₅₉₅* with very similar or identical *g*-values.

5.7. Effect of carbon monoxide and cyanide.

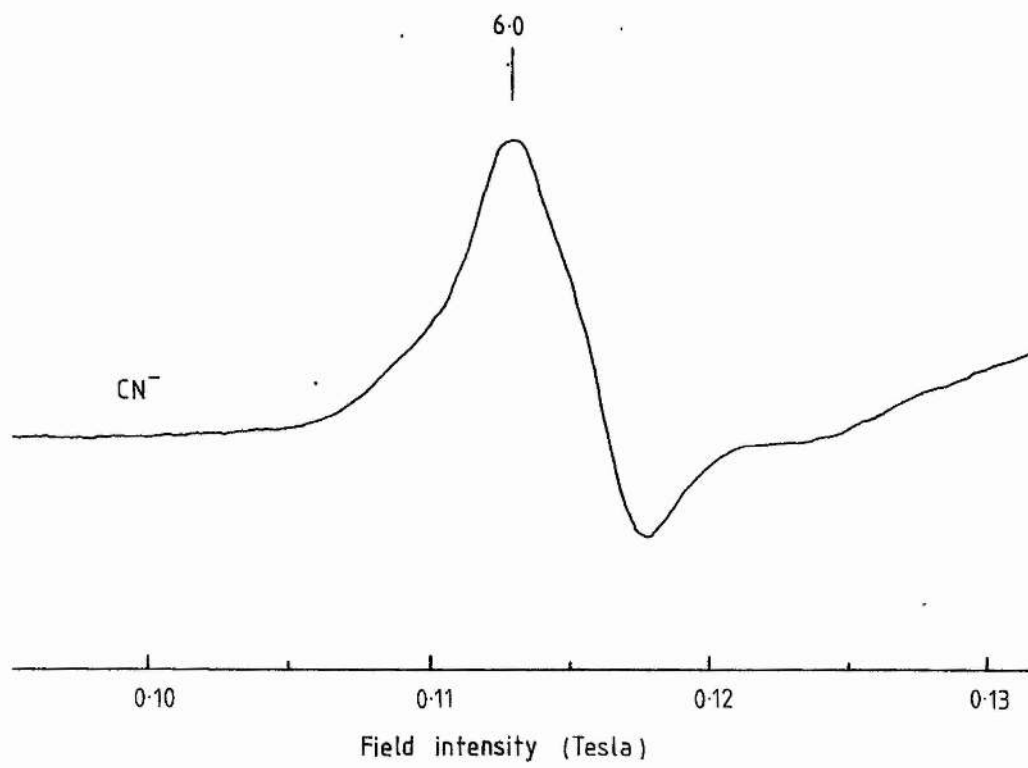
Carbon monoxide causes diminution of the axial component of the e.p.r. spectrum around $g=6.0$. In redox titrations of membranes in the presence of CO, only a minor axial component is observed, and the species that titrates corresponds to the low potential rhombic component reported herein. E.p.r. spectra of samples poised at high potentials in the presence of CO therefore have lineshapes very similar to that of the 200mV spectrum in Figure 5.2. The rhombic features of such spectra titrate with an E_{m7} of 150mV, whilst the central axial feature remains small and unchanged up to an E_h of 400mV. CO therefore binds to haem *d* and raises its E_{m7} to greater than 400mV (the highest potential of the titration). The effect of CO on the low spin haem *b₅₅₅* signal was not determined, because of the very low intensity of this feature in typical spectra and the low temperatures necessary for its observation. The E_{m7} of this haem is not perturbed by CO in optical redox titrations (Lorence et al., 1984a).

Cyanide causes a major change in the spectral lineshape in the $g=6.0$ region (Figure 5.7). These changes are observed following oxidation of reduced ($E_h=0mV$) membranes in the presence of 10-25mM cyanide under anoxic conditions. The intensity of the high spin signal is reduced compared to the intensities of oxically and anoxically

Figure 5.7

*Effect of cyanide on the anoxically oxidised spectrum
in the $g=6$ region.*

The cyanide adduct to the membrane bound cytochrome *bd* was prepared as follows. Membranes (suspended in a 100mM Bes/KOH buffer containing 2mM MgSO₄, pH7.0; protein concentration, 27 mg ml⁻¹) were poised anoxically at 0mV in the presence of 10mM KCN and were then oxidised to 400mV using potassium ferricyanide as oxidant. Samples were then withdrawn into e.p.r. tubes. Spectrometer settings: temperature, 10K; field modulation intensity, 20G_{pp}, microwave power 20mW; instrument gain, 8x10⁴.



oxidised spectra. The lineshapes of both the rhombic and axial components of the spectrum are altered. The central axial component clearly becomes slightly rhombic upon cyanide binding. An additional low spin signal is observed in cyanide treated membranes at $g=2.96$ corresponding to a cyanide adduct to ferric haem *d*. This feature is very weak in spectra of cyanide treated EMG2 membranes, but it is larger in membranes from FUN4/pNG2 (Section 5.9).

5.8. Effect of pH on the high spin spectrum.

pH affects the spectral lineshape of the e.p.r. spectrum of oxically oxidised membranes (Figure 5.8). The relative size of the rhombic g_x component compared to the axial g_{xy} increases with increasing pH, and this lineshape change titrates with a pK_a of around 8.0. The data suggests that there is a pH dependent equilibrium between the rhombic and axial components of the aerobic spectrum, and that this lineshape change is a result of changes in the geometry of the haem b_{595} .

5.9. E.p.r. spectra of membranes from *E.coli* FUN4/pNG2.

A spectrum of oxically oxidised membranes from *E.coli* FUN4/pNG2 is shown in Figure 5.9. Noticeable in this spectrum are intense signals at $g=6.0$, $g=4.3$, and $g=1.98$. The $g=6.0$ and $g=4.3$ signals have been assigned in the above to the high spin ferric haems of cytochrome *bd* and to adventitious iron, respectively. The feature around $g=1.98$ is probably attributable to HiPIP type iron-sulphur centres, although the g_z of the high spin ferric haem may also make a minor contribution

Figure 5.8

Effect of pH on the oxically oxidised spectral lineshape.

Membranes were suspended in buffers of appropriate pH (50mM total buffer concentration, 30mg ml⁻¹ protein), samples were transferred to e.p.r. tubes and these were then vigorously aerated with a stainless steel wire. Spectrometer settings were as for Figure 2. *Inset:* a plot of the ratio of the intensity of the rhombic g_x to that of the axial g_{xy} versus pH.

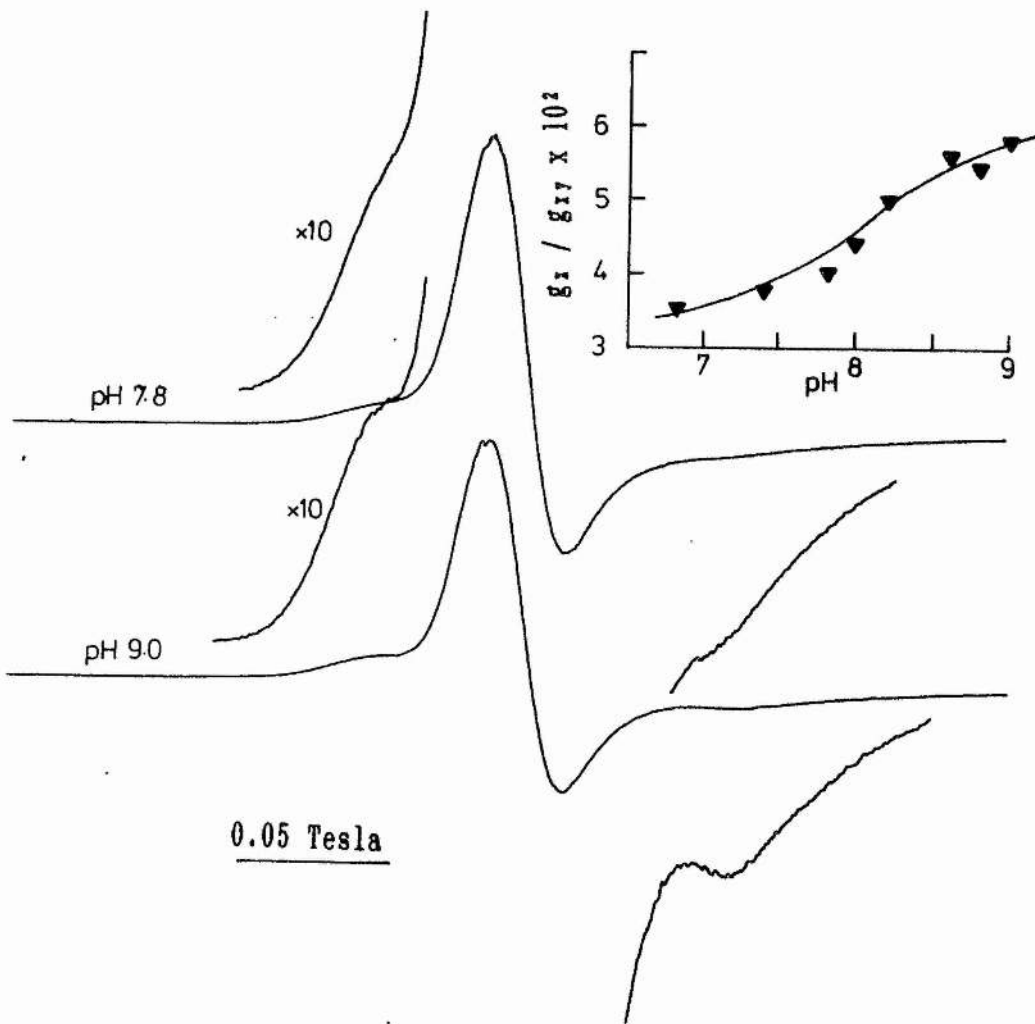
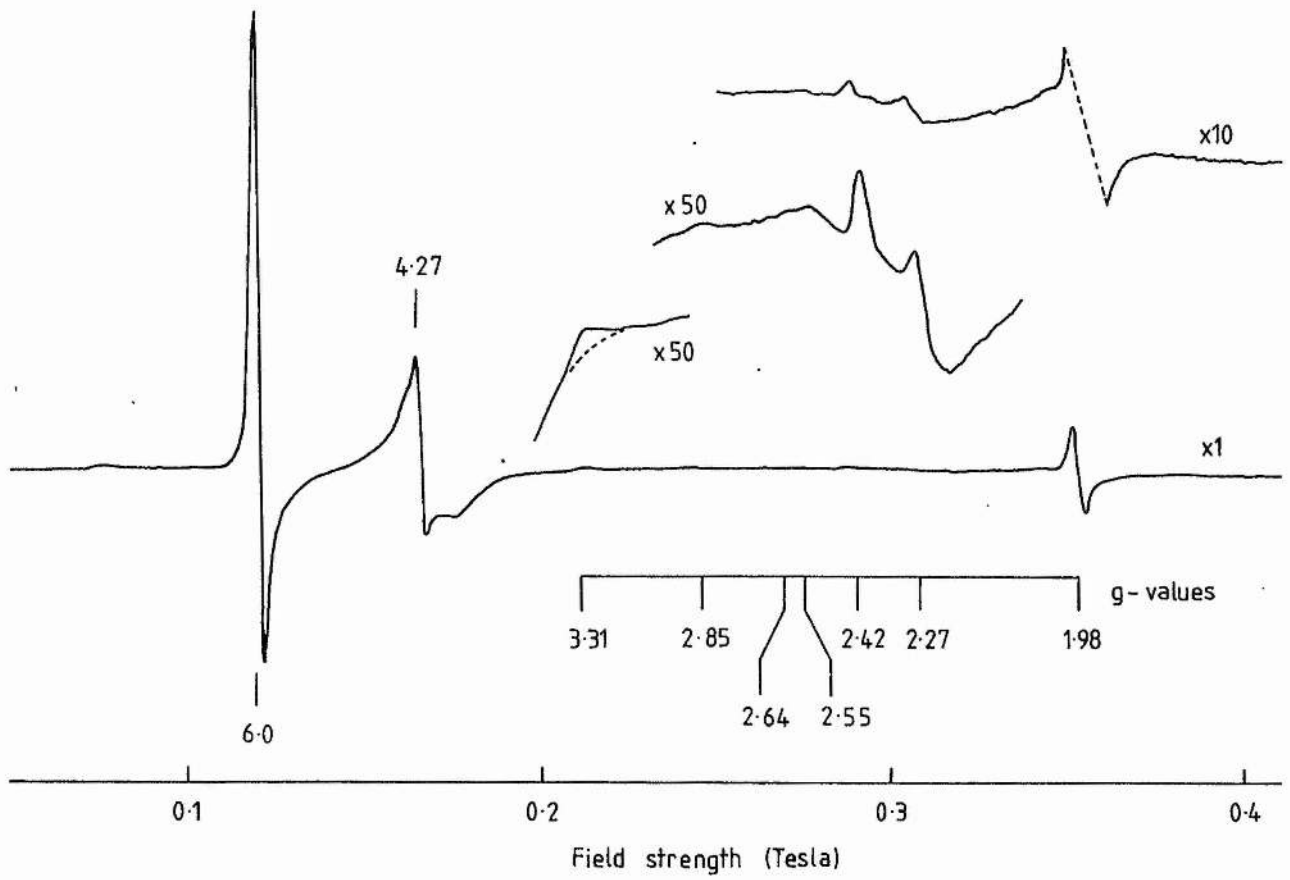


Figure 5.9

E.p.r. spectrum of membranes from E.coli FUN4/pNG2.

Approximately 0.5mls of *E.coli* membranes (protein concentration, 45mg ml⁻¹) were placed in a 3mm internal diameter quartz e.p.r. tube and were vigorously aerated using a coiled stainless steel wire. Membranes were suspended in a 100mM Tes/KOH buffer (pH7) containing 2mM MgSO₄. Spectrometer settings: temperature, 10K; field modulation intensity, 20G_{pp}; microwave power, 20mW; instrument gain, 4x10³. *g*-values are indicated by bars above and below the spectrum.



to this feature.

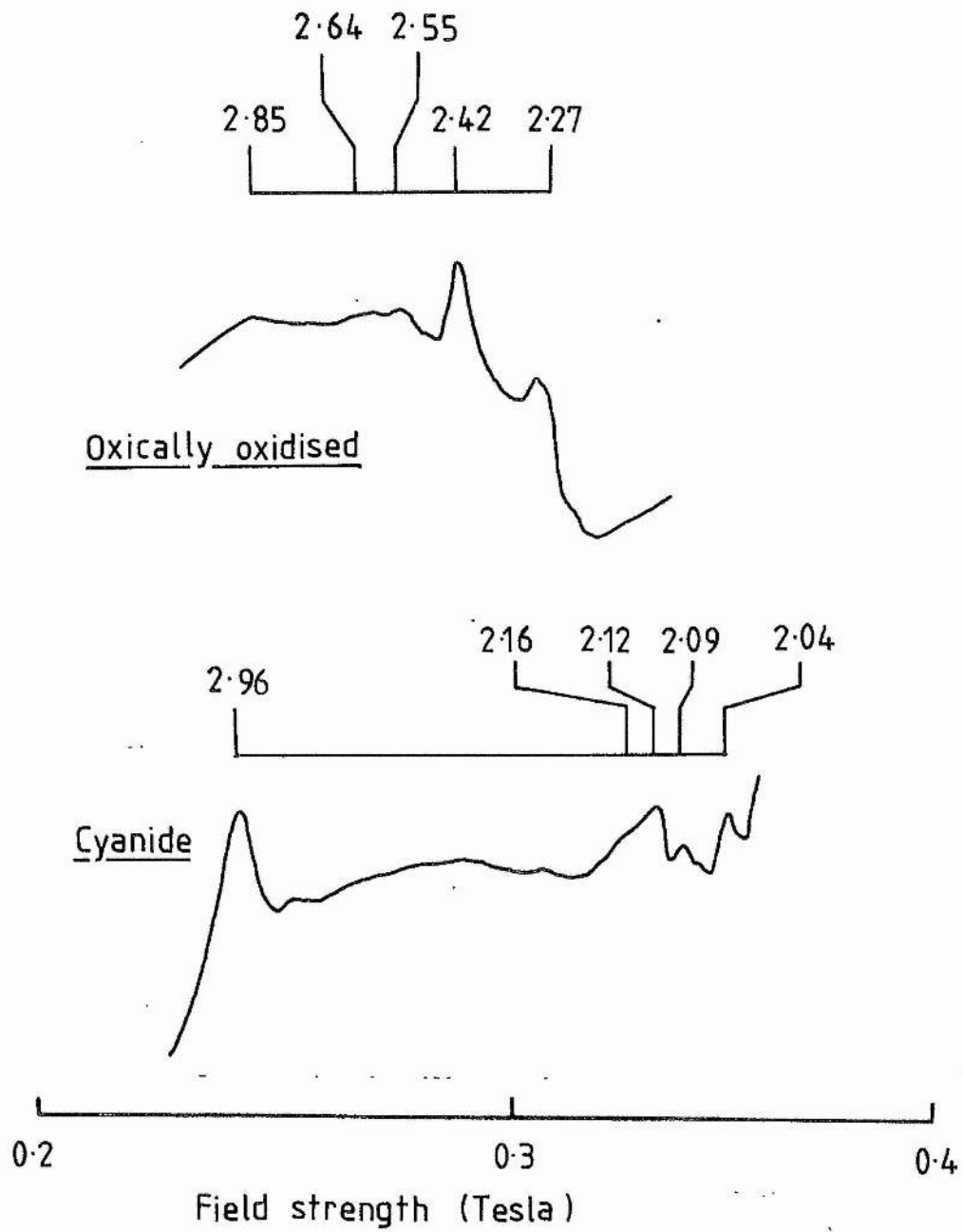
Considerable amplification of the high field region of the spectrum is necessary before further features become observable. The g_z and g_y of the low spin ferric chlorin (haem *d*) observed by Hata *et al.* (1985) are clearly visible at $g=2.42$ and $g=2.27$, respectively. The g_x of this haem is not observed in the sweep width of Figure 5.9, or is too broad to be resolved. The g_z of the haem *b₅₅₈* is also observed at $g=3.31$. The intensity of this feature in Figure 5.9 is smaller than in Figure 5.1 because of the higher temperature used to record the spectrum in Figure 5.9. Minor features in the spectrum of Figure 5.9 are observed at $g=2.85$, 2.64, and 2.55, and these are attributable to unidentified low spin ferric haems present in the membrane preparation at much lower concentrations than those responsible for the other spectral features.

Figure 5.10 shows e.p.r. spectra of membranes from *E.coli* FUN4/pNG2 oxidised in the presence of cyanide. The low spin ferric haem signals present in spectra of cyanide treated membranes are quite distinct from those observed under oxically oxidising conditions. An intense g_z feature is observed at $g=2.96$, and additional features due to low spin ferric haem(s) are observed between $g=2.16$ and 2.04. The features at the high field end of the cyanide spectrum are complex, and probably include the g_y of the $g=2.96$ signal. Judging by the effect of cyanide on both the components of the high spin ferric haem signal of cytochrome *bd*, (Section 5.7) it is possible that there are two low spin ferric haem signals attributable to cyanide adducts to both haem *d* and haem *b₅₉₅* in the spectrum of Figure 5.10. The data

Figure 5.10

Effect of cyanide on the low spin ferric haem spectrum of membranes from E.coli FUN4/pNG2.

The oxically oxidised sample was prepared as for Figure 5.9. The cyanide sample was prepared by anoxically oxidising reduced $E_h=0\text{mV}$ membranes to 400mV in the presence of 10mM KCN . Membranes were suspended in 100mM Bes/KOH buffer ($\text{pH}7$) containing 2mM MgSO_4 and were reduced or oxidised using dilute solutions of sodium dithionite and potassium ferricyanide, respectively. Protein concentration of both samples: 45mg ml^{-1} . Spectrometer settings: temperature, 10K ; field modulation intensity, 20G_{pp} ; microwave power, 20mW ; instrument gain, cyanide- 1×10^5 , oxically oxidised- 2×10^5 . g-values are indicated by bars above the spectra.



suggest that the loss of signal intensity observed in the $g=6.0$ region in the presence of cyanide is due to the formation of one, or possibly two, low spin ferric cyanide adducts to cytochrome *bd*.

5.10. Assignments of the ferric haem e.p.r. signals to the components of cytochrome bd.

The assignment of the axial high spin ferric haem signal to haem *d* is based on its potentiometric and ligand binding behaviour. This signal has an E_{m7} of 260mV, which is raised to above 400mV in the presence of CO, as has been reported for haem *d* on the basis of optically monitored redox titrations (Lorence *et al.*, 1984a). The assignment is strengthened by comparison with the e.p.r. signals of other haemoproteins able to bind oxygen species and five coordinate model chlorin complexes (Section 5.1). The effect of cyanide on the axial high spin signal suggests that this ligand binds to haem *d*.

The assignment of the rhombic high spin ferric haem signal to haem *b₅₉₅* is based on the similarity of its E_{m7} to the published values for this centre (Lorence *et al.*, 1984a), and this assignment is in agreement with that of Hata *et al.* (1987). The optical spectrum of haem *b₅₉₅* is typical of a high spin haem *b* (Lorence *et al.*, 1986), so the observation of a high spin e.p.r. signal attributable to this haem is much as expected. CO has been shown to bind to both haem *b₅₉₅* and haem *d* on the basis of photochemical action spectra (Edwards *et al.*, 1981) and optically followed CO binding titrations (Chapter 6). However, in potentiometric redox titrations followed optically (Lorence *et al.*, 1984a) and by e.p.r., CO has little effect on the E_{m7}

of haem *b₅₉₅*, suggesting that it binds to the haem with low affinity. However, the data is also consistent with CO binding to the oxidised haem *b₅₉₅* with an affinity similar to that for its binding to the reduced haem, although this would represent very unusual ligand binding behaviour. Alternatively, the tendency of CO to raise the E_{m7} of haem *b₅₉₅* may be offset by an interaction energy with the ferrous carbonmonoxy haem *d* which results in a tendency to lower the E_{m7} of this haem.

The assignment of the low spin ferric haem signal at $g=3.3$ is based on its potentiometric behaviour and comparison with the e.p.r. signals attributable to other haems *b* involved in the redox reactions of quinol species (Section 5.1). This signal is similar to those of haem *b₅₆₆* of mitochondrial complex III (Salerno, 1984) and haem *b₅₆₃* of chloroplast cytochrome *b_{6f}* (Salerno *et al.*, 1983). The $g=3.3$ signal has very low intensity compared to the high spin ferric haem signals because of the broadness of its e.p.r. *absorption* spectrum and its low transition probability (Salerno, 1984; J.C. Salerno, personal communication). The low spin $g=3.3$ signal was not reported by Hata *et al.* (1985), and these workers assigned the axial high spin species to haem *b₅₅₈*.

The reported E_{m7} 's of haem *b₅₅₈* from aerobically and anaerobically grown cells differ (Lorence *et al.*, 1984a; Reid & Ingledew, 1979), and this may be due to differences in the phospholipid composition of the cytoplasmic membrane. The E_{m7} of haem *b₅₅₈* has also been reported to be sensitive to detergents in purified preparations (Lorence *et al.*, 1984b). It is possible to speculate that

differences in membrane phospholipid composition in aerobically grown cells also result in a subpopulation of haem *b₅₅₈* being high spin, resulting the high spin haem *b₅₅₈* reported by Hata *et al.* (1985).

5.11. Conclusions.

The anoxically oxidised cytochrome *bd* of *E.coli* exhibits a high spin e.p.r. signal which is similar to that observed in partially reduced cytochrome *aa₃* (Aasa *et al.*, 1976). In cytochrome *aa₃*, the high spin signal has been assigned to a total of three components attributable to sub-populations of haem *a₃*. In the work reported herein, there is clear evidence, based on potentiometric and ligand binding behaviour, that there are two ferric haems responsible for the high spin signals from anoxically oxidised cytochrome *bd* from anaerobically grown *E.coli* EMG2, haems *d* and *b₅₉₅*. In the fully oxidised cytochrome, haem *b₅₉₅* is present as a mixed population of two rhombic high spin species with slightly different *g*-values, whilst haem *d* is present as a single axial species. The data indicate that there is a haem-haem interaction between haem *b₅₉₅* and haem *d*, indicating that they are in close proximity. On the basis of the double integrations of the spectra in the *g*=6.0 region, it can be concluded that haems *b₅₉₅* and haem *d* are present in the cytochrome *bd* complex in an 1:1 ratio. This contrasts with the data of Lorence *et al.* (1986) which suggests that the cytochrome contains two haems *d* per haem *b₅₉₅*.

The assignments of the high spin signals attributable to cytochrome *bd* have to be reconciled with the effect of aerobiosis on

the e.p.r. spectrum. The optical data of Poole *et al.* (1983a) suggests that the oxically oxidised cytochrome has an oxygen ligated haem *d*, the d_{650} species. These workers also proposed that the first spectrophotometrically detectable intermediate formed in the reaction of fully reduced cytochrome *bd* with oxygen is the d_{650} species and that this species is oxygen ligated ferrous haem *d*, which is e.p.r. silent. However, the data reported herein indicate that there is no loss of spin intensity in the $g=6$ region of e.p.r. spectra upon aerobiosis of anoxically oxidised membranes. There is potentiometric evidence that oxygen affects fully oxidised cytochrome *bd*. Pudek & Bragg (1976b) found that the d_{650} 'oxidised' species does not appear at high redox potentials under anoxic conditions unless aliquots of H_2O_2 solution or oxygen saturated water are added. Hendler & Schragar (1979) carried out redox titrations under oxic (aerobic) conditions and were able to study the potentiometric behaviour of the d_{650} species. At potentials above around 330mV, the intensity of the 650nm absorbance was found to be level at about one third of its maximum. Its intensity dropped sharply to zero at 330mV, and then increased with decreasing potential until a maximum was reached at around 100mV. Hence, there appear to be two forms of the d_{650} species, one ferrous and one ferric.

The effect of oxygen on haem *d* results in a change in the haem b_{595} lineshape; this change is a manifestation of the interaction between the two high spin haems in the presence of oxygen. The effect of pH on the relative heights of the axial and rhombic components of the oxically oxidised high spin spectrum indicates that within the

active site of the cytochrome *bd* there exists an ionisable group with a pK_a of around 8. The presence of an ionisable group with a pK_a in this region has already been proposed on the basis of the optical changes elicited by nitrite at different pH's (Chapter 3). This ionisable group is associated with haem *b₅₉₅* and affects the relative concentrations of the axial and rhombic forms of this centre under oxidic conditions.

The effect of cyanide on the e.p.r. properties of cytochrome *bd* is to perturb the high spin e.p.r. spectrum of both haems *b₅₉₅* and *d*. Cyanide also elicits the formation of at least one and possibly two low spin ferric haem species. Published optical data (Chapter 1) indicates that cyanide binds to both haems *b₅₉₅* and *d*, and the e.p.r. data, although not conclusive, is also consistent with cyanide binding to these two haems.

In this chapter, the spectral features of e.p.r. spectra of membranes from anaerobically grown *E.coli* have been assigned to the haem components of cytochrome *bd*. Haems *d* and *b₅₉₅* exhibit high spin e.p.r. signals, and haem *b₅₅₈* exhibits a low spin e.p.r. signal. The data indicates that haems *d* and *b₅₉₅* are present in the cytochrome *bd* complex in a 1:1 ratio. The effect of oxygen, E_h , and pH on the high spin e.p.r. signals indicates that there is a haem-haem interaction between haems *d* and *b₅₉₅*. The data presented herein supports a model for cytochrome *bd* with two oxygen binding sites, haem *d* and haem *b₅₉₅*.

CHAPTER SIX

*Reactions of the in situ cytochrome bd with carbon monoxide
and oxygen.*

6.1. Introduction.

As described in Chapter 1, carbon monoxide binds to reduced cytochrome *bd* and this results in marked changes in its optical absorption spectrum. In the reduced *plus CO minus reduced* difference spectrum of the purified oxidase, there are major peaks at 420nm and 642nm, and major troughs occur at 430nm, 444nm, and 622nm (Miller & Gennis, 1983; Kita *et al.*, 1984b). Similar features are observed in CO difference spectra of membranes and whole cells containing cytochrome *bd* as the major ligand binding haemoprotein (Rice & Hempfling, 1978; Poole & Chance, 1981). It was suggested in Chapter 1 (Section 1.4.7.2) that the most appropriate assignment of these Soret features is as follows: the peak at 420nm and the trough at 430nm are due to CO binding to haem *b₅₉₅*, whilst the features at 444nm, 626nm, and 642nm are due to ligand binding to haem *d*. This chapter contains an optical study of the CO concentration dependence of the formation of the adducts responsible for the features present in difference spectra of cytoplasmic membranes from anaerobically grown *E.coli* EMG2.

The inhibition of oxidase activity elicited by CO and its photodissociability have been exploited to determine photochemical action spectra of a variety of oxidases (Castor & Chance, 1959). This technique has allowed identification of haems *d* and *b* as sites of the oxidase reaction in aerobically grown *E.coli*. These two haems can be identified as haem *b₅₅₅* of cytochrome *b_{562-o}* and haem *d* of cytochrome *bd*. Edwards *et al.* (1981) recorded a photochemical action spectrum of aerobically grown *E.coli* cells using a tunable dye laser as a high intensity light source. A band was observed at 592nm which was

attributed to photorelief of CO inhibited respiration by photodissociation of the ligand from haem b_{595} . Thus, it is possible that both haems d and b_{595} are associated with the oxygen binding site of cytochrome bd . In this chapter the effect of CO as an inhibitor of the oxidase reaction catalysed by cytochrome bd is reported with a view to determining the nature of the inhibition of the oxidase reaction and the apparent number of oxygen binding sites involved.

The studies reported herein on the CO binding properties of cytochrome bd complement those on the reaction of nitrite with the oxidase which results in formation of NO adducts to haems d and b_{595} (Chapters 3 & 4). Since nitric oxide binds to haems in a bent fashion and CO binds in a linear fashion, comparison of the reactions of nitrite and CO with cytochrome bd may reveal differences in the immediate environment of the two putative ligand binding haems of the oxidase.

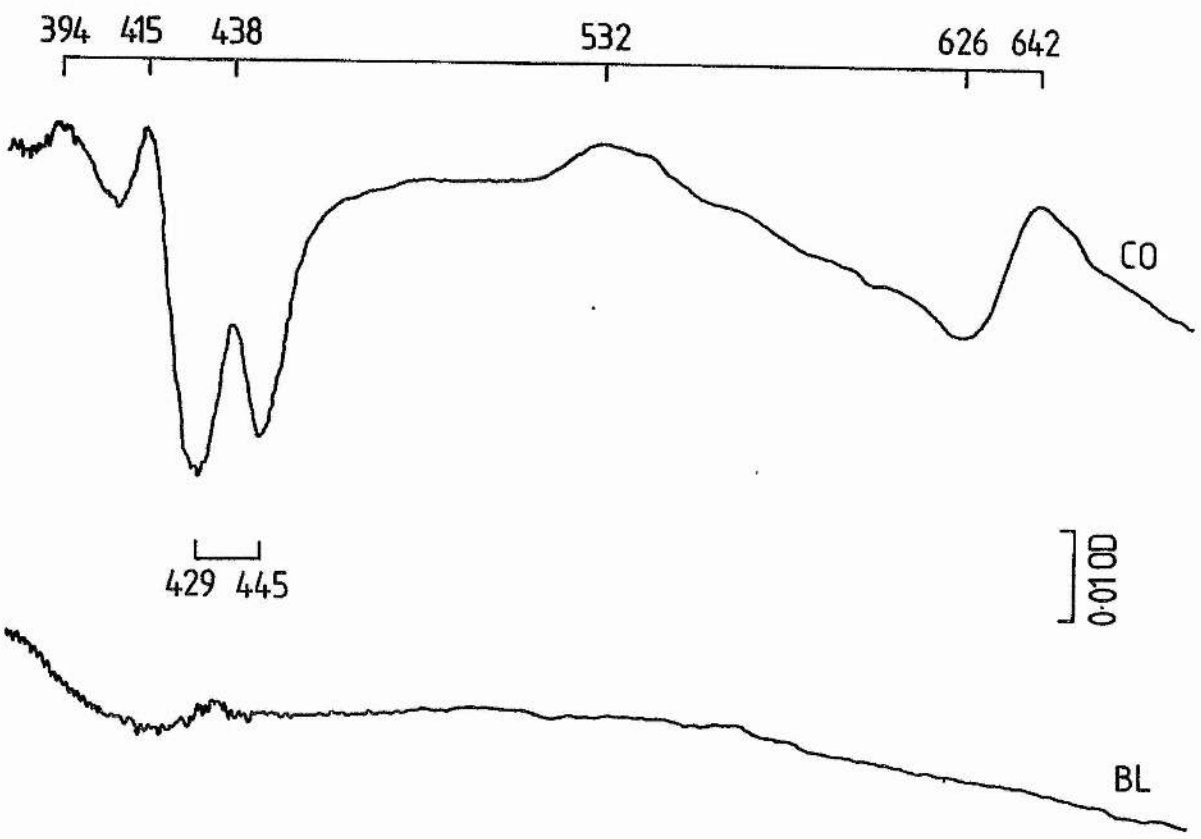
6.2. Carbon monoxide binding to cytochrome bd .

Figure 6.1 shows a room temperature reduced *plus* CO *minus* reduced difference spectrum of the cytoplasmic membrane preparation used in this work (dithionite was used as reductant). Noticeable therein are peaks at 394nm, 415nm, 438nm, 532nm, and 642nm, and troughs at 429nm, 445nm, and 626nm. This spectrum is almost identical to that of purified cytochrome bd (Miller & Gennis, 1983; Kita *et al.*, 1984b). Kranz & Gennis (1983) showed that cytochrome b_{562-o} synthesis is repressed under conditions favouring synthesis of cytochrome bd , and the spectrum of Figure 6.1 shows no major features in the haem b alpha

Figure 6.1

Reduced plus CO minus reduced spectrum of membranes from anaerobically grown E.coli EMG2.

A baseline (BL) was recorded of dithionite reduced *minus* dithionite reduced membranes (5.7mg ml^{-1} protein). CO to a final concentration of $15\mu\text{M}$ (bound *plus* unbound) was added to the sample cuvette by injection of CO saturated buffer (bubbled at 30°C , 0.859mM CO).. This was achieved by injecting an appropriate volume of CO saturated buffer into the sample cuvette. A reduced *plus* CO *minus* reduced spectrum was recorded. The spectrum was recorded at room temperature (approx. 22°C). Membranes were suspended in a 50mM Mes/KOH buffer (pH7) containing 2mM MgSO_4 . Appropriate wavelengths are indicated by bars above and below the spectrum.



region attributable to the CO difference spectrum of cytochrome *b₅₆₂-o* (Poole *et al.*, 1979; Kita *et al.*, 1984a). Thus, cytochrome *bd* appears to be the only detectable ligand binding haemoprotein in membranes from anaerobically grown *E.coli* EMG2.

As described above, the features of the spectrum of Figure 6.1 at 415nm and 429nm can be assigned to the CO difference spectrum of haem *b₅₉₅*, whilst the features at 445nm, 626nm, and 642nm can be assigned to the CO difference spectrum of haem *d*. There are no features in the haem *b* alpha region corresponding to perturbation of the haem *b₅₉₅* alpha band by CO. This may be because CO has little effect on the alpha band of this haem; the band is, in any case, a minor feature of the reduced *minus* oxidised spectrum of the purified oxidase (Lorence *et al.*, 1986; Chapter 1, Figure 1.4).

The optical changes elicited by CO were further characterised by titration of membranes with CO saturated buffer and recording difference spectra (with lactate reduced membranes in the reference cuvette) in the haem *d* alpha region and the Soret.

6.3. Titration of the optical changes in the haem *d* alpha region elicited by CO.

Figure 6.2 shows CO difference spectra in the haem *d* alpha region (600-700nm) recorded in the presence of increasing concentrations of CO. The optical changes are virtually complete at a CO concentration of around 1 μ M, indicating that haem *d* has a very high affinity for CO. The effect of increasing CO concentration on the extent of formation of carbonmonoxy haem *d* is shown in Figure 6.3. At low concentrations,

Figure 6.2

Effect of CO on the 600-700nm region of the reduced plus CO minus reduced difference spectrum of E.coli membranes.

A suspension of membranes (protein concentration, 6.6mg ml^{-1}) at pH7 (50mM Tes/KOH, 2mM MgSO_4) was split into two cuvettes. Sodium lactate (27mM) was used to reduce both cuvettes, and a baseline was recorded (0). Aliquots of CO saturated buffer (bubbled at 30°C ; 0.859mM CO) were then added, and the spectra were recorded 2 minutes after each addition. Incubation at each CO concentration for longer than 2 minutes had no effect on the spectra. Concentrations of CO are total concentrations (bound plus unbound) after each addition. Aliquots of buffer were added to the reference cuvette at each addition. The experiment was carried at room temperature.

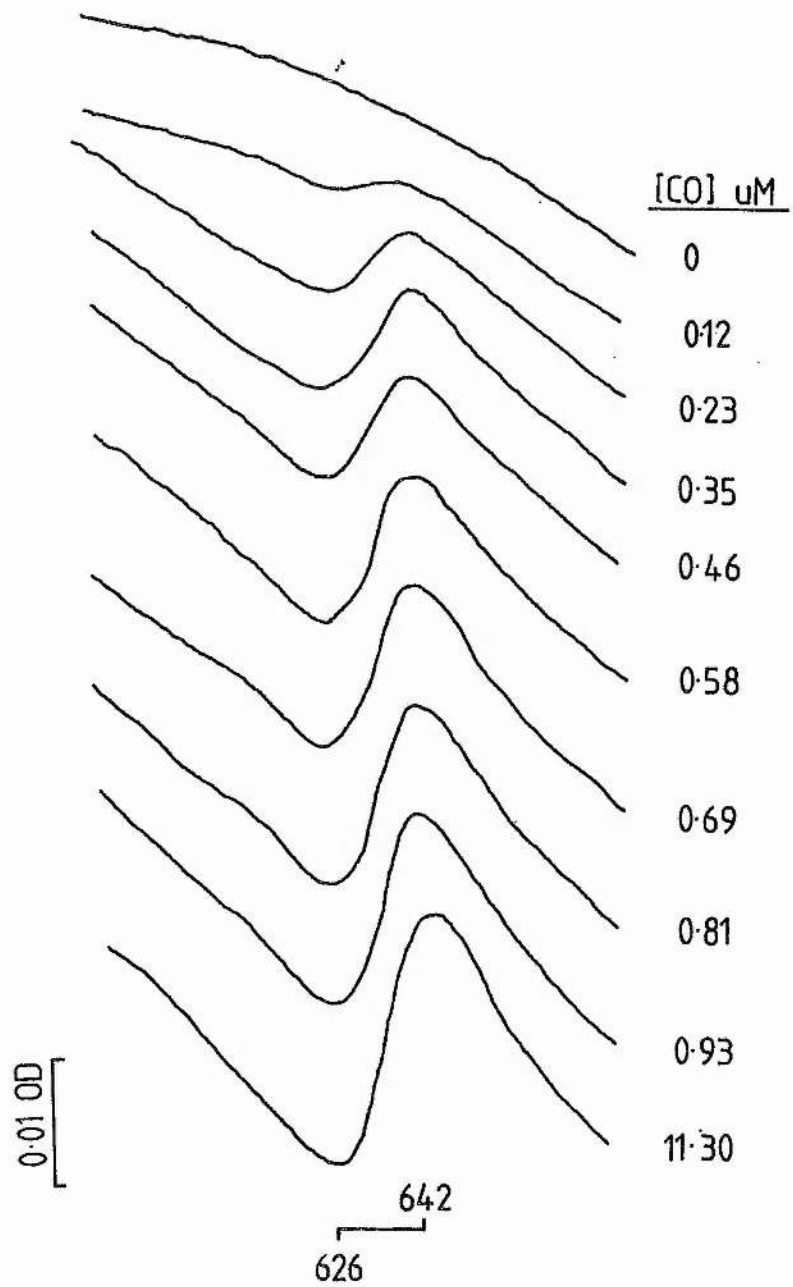
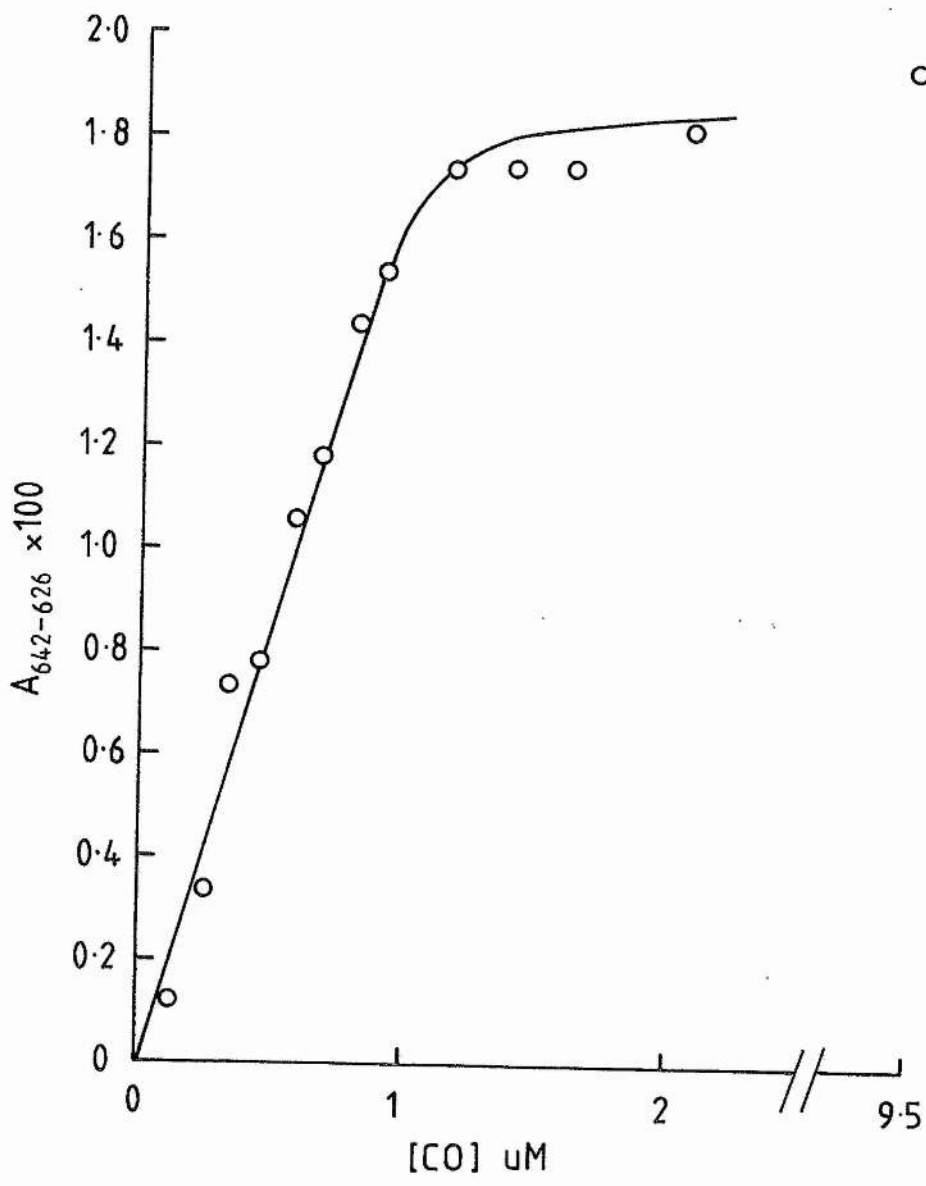


Figure 6.3

*Effect of CO concentration on the extent of the absorbance difference
between 626nm and 640nm.*

The absorbance difference between 626nm and 640nm were plotted versus CO concentration (bound plus unbound). Data were obtained from spectra such as those in Figure 6.2.



the extent is linearly dependent on the CO concentration (Figure 6.3), and the transition from the CO binding to the CO saturated regions of the titration curve is sharp. This indicates that the K_d of haem *d* for CO is too low to be determined using the experimental technique employed herein (see legend of Figure 6.2 for details).

The end-point of the titration can be estimated as the CO concentration (bound plus free) where the linear region of the plot, if extrapolated, equals the maximum absorbance difference between 642nm and 626nm in the titration. The CO concentration at this point was thus estimated to be 1.2 μ M; this corresponds to a haem *d* concentration of 0.18nmol (mg protein)⁻¹. Using a millimolar extinction coefficient of 12.6 for the wavelength pair 622-642nm (Kita *et al.*, 1984b), the haem *d* concentration can be calculated from the peak-trough absorbance difference at the end point of the titration to be 0.23nmol (mg protein)⁻¹. The difference between these two concentration values is probably due to the effect of light scattering on the effective path length, resulting in a slight overestimation of the haem *d* concentration calculated on the basis of the published extinction coefficient.

The high affinity of haem *d* for CO may partly explain the unusual behaviour of cytochrome *bd* following photolysis of the CO adduct at low temperatures compared to cytochrome *b₅₆₂-o* and cytochrome *a_{a3}*. When CO treated cells containing cytochrome *bd* are photolysed in the absence of oxygen, no photolysis of CO from haem *d* is detected (Poole & Chance, 1981) unless the photolysis is carried out at temperatures close to that of liquid helium (<20K; Poole *et al.*, 1982b). A major

difference between the oxygen binding site of cytochrome *bd* and those of cytochrome *aa₃* and cytochrome *b₅₆₂-o* appears to be the presence of copper in the latter two oxidases (Wikstron *et al.*, 1981; Kita *et al.*, 1984a; J.C. Salerno, B. Bolgiano, & W.J. Ingledew, unpublished results). Copper present in the ligand binding pocket of cytochrome *aa₃* is able to trap photodissociated CO, and thus slow its recombination of this ligand with haem *a₃* (Alben *et al.*, 1981).

6.4. Titration of the optical changes in the Soret elicited by CO.

Figure 6.4 shows the effect of increasing CO concentration on reduced *plus* CO *minus* reduced spectra in the Soret. The concentration dependencies of the features in the Soret due to haems *b₅₉₅* and *d* are clearly different. At low CO concentration, a peak-trough develops at 436-442nm with an end point at around 1μM CO (bound *plus* free). At higher concentrations, a second trough appears at 428nm with a peak at 416nm. The concentration dependencies of these changes can be studied by plotting the absorbance differences between the wavelength pairs 416-406nm and 436-442nm *versus* the concentration of CO (Figure 6.5). The differences between these wavelength pairs can be assigned to haems *d* (436-442nm) and *b₅₉₅* (416-406nm).

The formation of the species responsible for the 436nm peak and the 442nm trough reaches an end point at a total CO concentration of approximately 1μM, and this spectral change is almost complete before the 416nm peak begins to become apparent. These observations strengthen the assignment of the 436-442nm peak trough to haem *d*.

The haem *d* concentration can be estimated as in the previous

Figure 6.4

Effect of CO on the Soret region of the reduced plus CO minus reduced difference spectrum of E.coli membranes.

Titration of the changes in the Soret region of reduced *plus* CO *minus* reduced spectra of membranes. A suspension of membranes (protein concentration 3.3mg ml^{-1}) at pH7 in 50mM Tes/KOH containing 2mM MgSO_4 was split into two cuvettes. Sodium lactate (27mM) was used to reduce both cuvettes. A baseline was recorded (BL). Concentrations of CO are total (bound *plus* unbound) after each addition. CO concentrations were increased by adding aliquots of CO saturated buffer as for Figure 6.2. Aliquots of buffer were added to the reference cuvette at each addition.

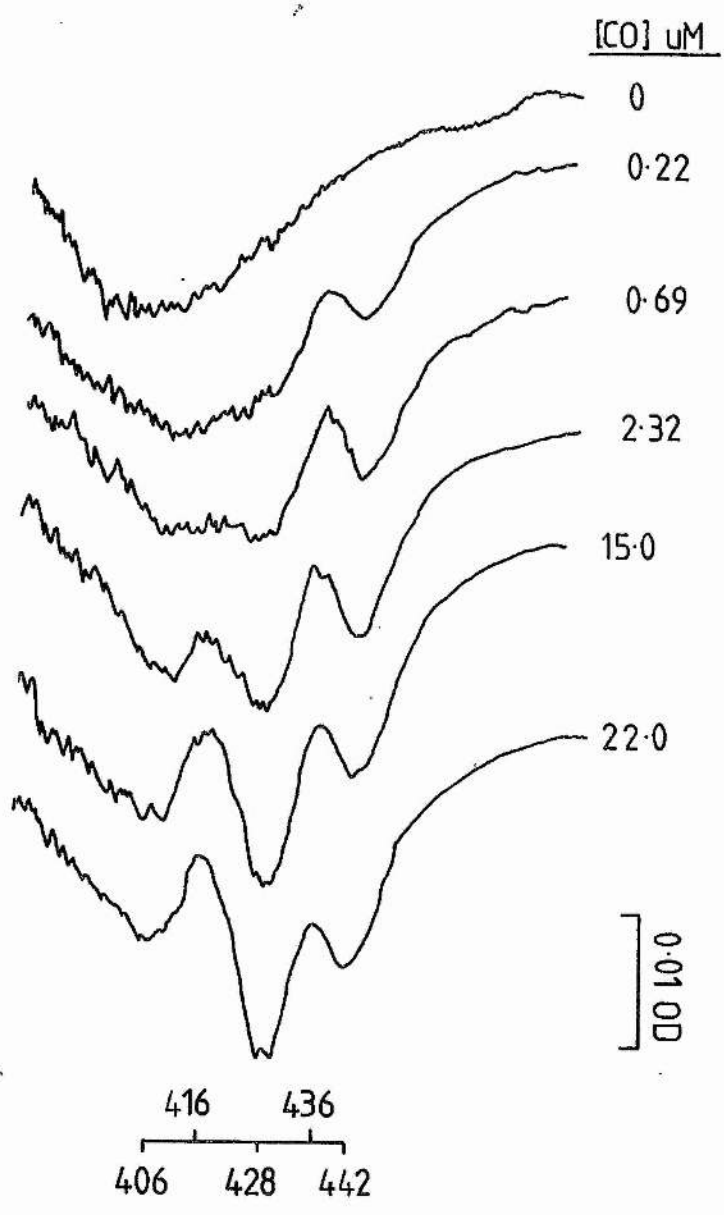
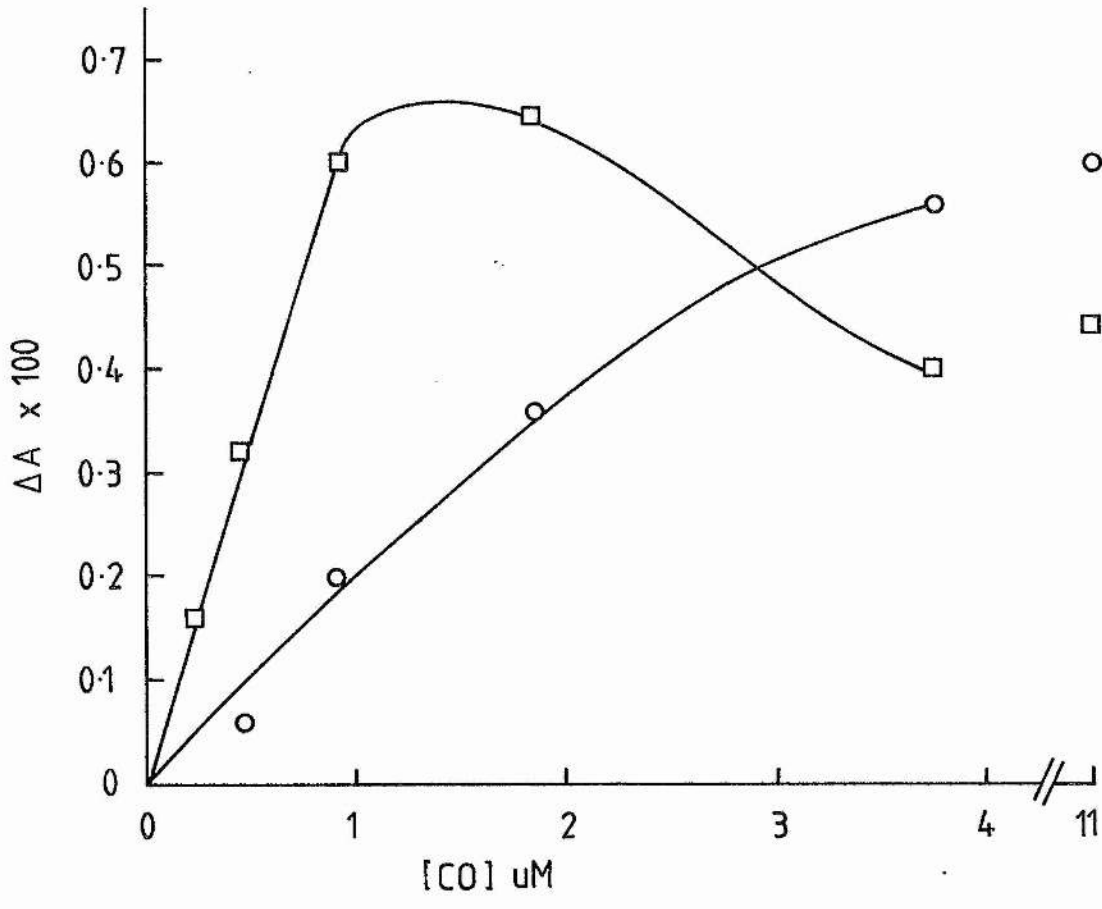


Figure 6.5

Effect of CO concentration on the extent of the absorbance changes in the Soret.

Effect of CO concentration on the extent of the absorbance changes in the Soret. Data were obtained from spectra such as those in Figure 6.4. \square — \square absorbance difference between 436nm and 442nm.
 \circ — \circ absorbance difference between 415nm and 406nm.



section as $0.30\text{nmol (mg protein)}^{-1}$ which is higher than that estimated on the basis of the titration of the changes in the haem *d* alpha region. There are a number of potential reasons for this anomaly. Firstly, the absorbance difference between the wavelength pair 436-442nm may be interfered with by the formation of the trough at 428nm attributable to CO binding to haem *b₅₉₅*. Secondly, the performance of the spectrophotometer used in this work in the Soret is not as good as in the 500-700nm region, resulting in a lower signal to noise ratio than in the former spectral region. Overall, the concentration of haem *d* calculated from the titration of the Soret features of reduced cytochrome *bd* are not inconsistent with the assignment of the peak at 436nm and the trough at 442nm to haem *d*.

At higher CO concentrations ($>1\mu\text{M}$), a second CO adduct is formed which is detected in the difference spectrum as a peak at 416nm and a trough at 428nm. Inspection of the titration curve (using the wavelength pair 416-406nm) corresponding to this species in Figure 6.5 indicates that the haem responsible has a much lower affinity for CO than haem *d*. The K_d of this haem can be estimated as being around 1.5-2.5 μM by simple inspection of Figure 6.5.

At CO concentrations above 1.3 μM , the intensity of the Soret features attributable to haem *d* decline as the features attributable to haem *b₅₉₅* become more apparent. This phenomenon is likely to be an artifact due to interference of the 436-442nm peak-trough by the 428nm trough due to carbonmonoxy haem *b₅₉₅*.

Overall, the CO binding titrations reported above show that haem *d* has a very high affinity for CO ($K_d \ll 1\mu\text{M}$), whereas haem *b₅₉₅*

has a lower affinity (K_d approx. 1.5-2.5 μ M). Unfortunately, the sensitivity of the technique used to obtain the titration data (see legend to Figure 6.2) was not great enough for the data to be subjected to Hill plot analysis for accurate estimation of the K_d 's of haems *d* and *b₅₉₅* for CO.

6.5. Effect of carbon monoxide on oxygen consumption in membranes.

The effect of CO on oxygen electrode progress curves recorded using the microcomputer interface described in Chapter 2 (Section 2.14) is illustrated in Figure 6.6. CO reversibly inhibits the oxidase reaction catalysed by cytochrome *bd* in membranes from anaerobically grown *E.coli* EMG2 and allows analysis of the steady state kinetics of the oxidase reaction by raising the K_m for oxygen to within the usable concentration range of a Clark type oxygen electrode.

Progress curves such as those in Figure 6.6 were numerically differentiated (Chapter 2, Section 2.14.5), and the derivative data used to construct Eadie-Hofstee plots (v versus v/s ; Figure 6.7) and Hanes plots (s/v versus s ; not shown). These plots were analysed as described in Chapter 2 (Section 2.14.7) and Chapter 3 (Section 3.8). Inspection of the Eadie-Hofstee plots of Figure 6.7 reveals that, in addition to affecting the K_m of the oxidase reaction, the V_{max} becomes smaller with increasing concentrations of CO. Also, the plots suggest that the apparent number of oxygen binding sites, n , becomes smaller with increasing CO concentration. The effect of increasing CO concentrations on the apparent number of oxygen binding sites, n will

Figure 6.6

Effect of CO on oxygen electrode progress curves.

Computer recorded oxygen electrode traces for the consumption of oxygen by membranes (0.44mg ml^{-1} protein) with 39mM sodium lactate as substrate in the presence of increasing concentrations of CO at pH7 (50mM Tes/KOH containing 2mM MgSO_4). Increasing concentrations of CO were achieved by injecting appropriate volumes of CO saturated buffer (0.859mM at 30°C) into the unstirred oxygen electrode chamber filled with air saturated buffer. A hypodermic syringe was used to do this with a needle sufficiently long to reach the bottom of the chamber from the ground glass stopper and capillary portal. The latter were both located at the top of the chamber. Careful injection of CO saturated buffer resulted in displacement of air saturated buffer from the chamber which exited via the gap between the hyperdermic needle and the inside wall of the capillary portal.

A potential error exists in the method used to determine the CO concentration used in the experiments reported herein. The final CO and oxygen concentrations were calculated on the assumption that no CO saturated buffer is displaced during its injection into the incubation vessel. An error introduced by displacement of CO from the incubation vessel would result in minor errors in any calculated K_m 's, and larger errors in estimations of V_{max} . No errors should be introduced into estimates of the apparent number of oxygen binding sites. A very large error (approx. 50%) in the calculated CO concentration would need to be present to account for the results reported in the text.

200 sec.

[CO] mM

0.07

0.13

0.20

0.34

0.1 mM O₂

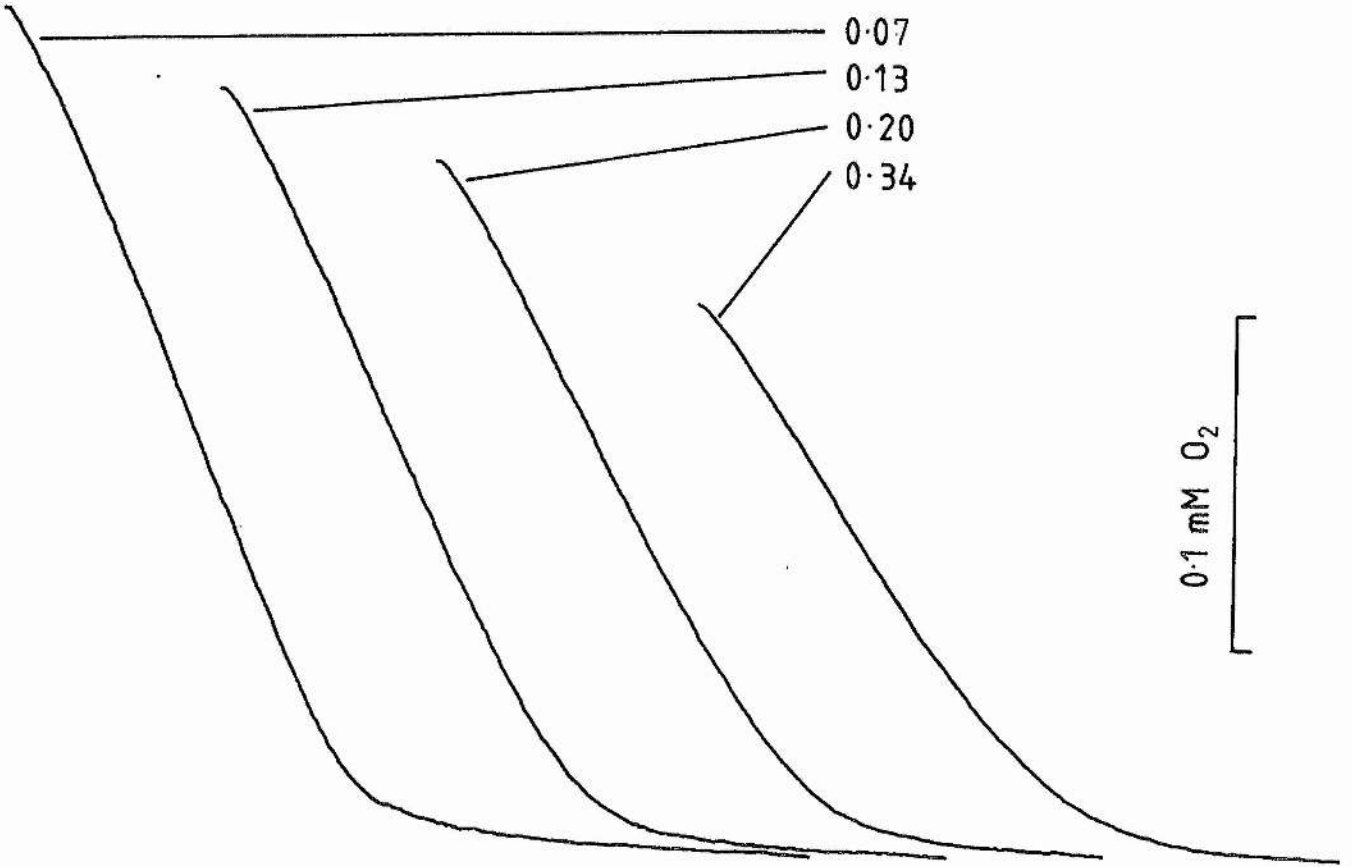
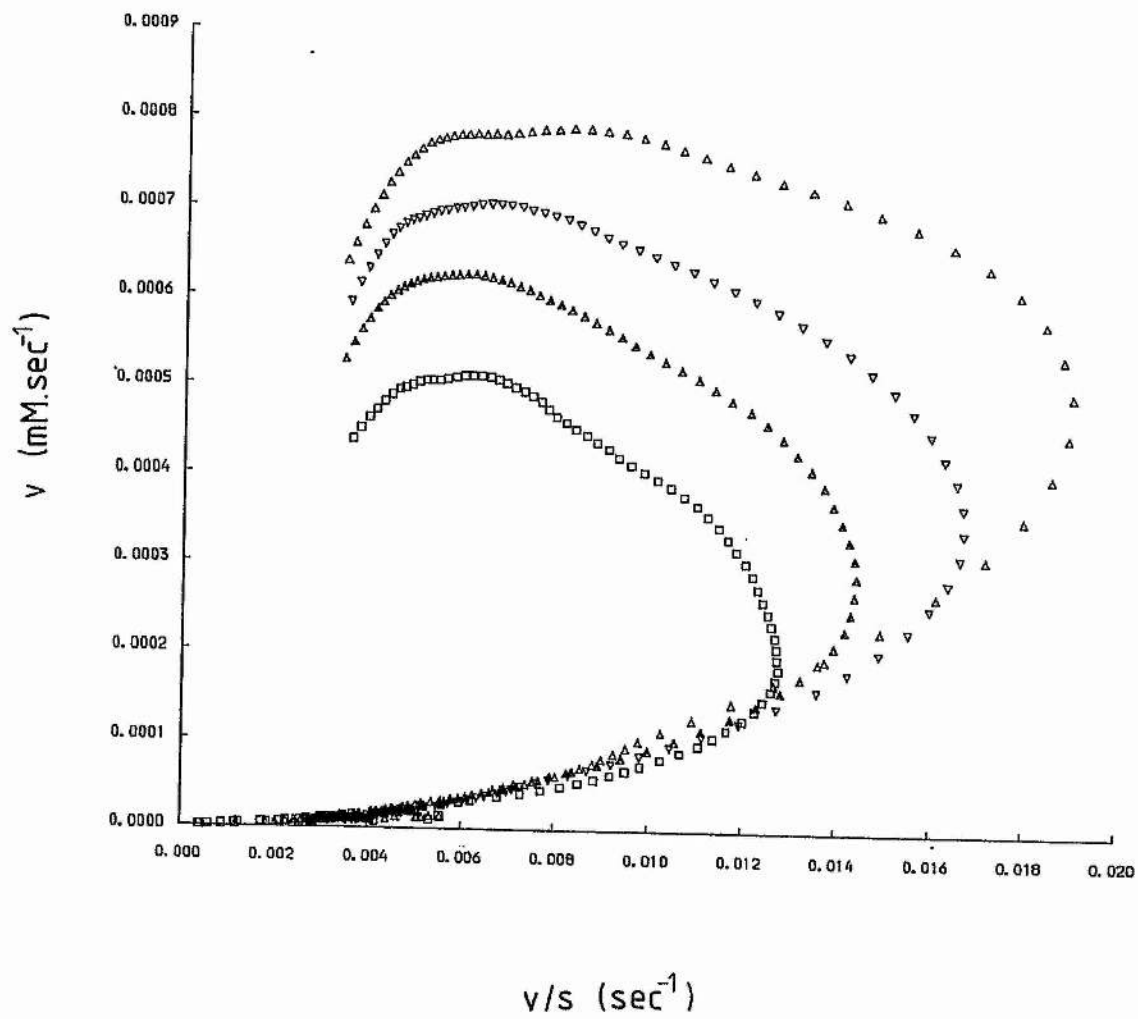


Figure 6.7

Eadie-Hofstee plots for the inhibition of the oxidase reaction by CO.

Data were obtained from differentiated oxygen electrode progress curves such as those in Figure 6.7. CO concentrations; \triangle — \triangle 0.067mM, ∇ — ∇ 0.135mM, \blacktriangle — \blacktriangle 0.202mM, \square — \square 0.337mM.



be discussed in more detail later.

The effect of CO on both the K_m and the V_{max} suggests that the inhibition elicited by the ligand is of the mixed type (Cornish-Bowden, 1979). Figure 6.8 shows the linear effects of CO concentration on both the apparent K_m of the oxidase reaction for oxygen, and its apparent V_{max} . In the case of mixed inhibition, the ligand is able to bind to both the unligated oxidase and the oxidase-oxygen complex (intermediate).

Mixed inhibition can be described by two inhibitor binding constants, one for inhibitor binding to the unligated enzyme (K_i), and one for inhibitor binding to the enzyme-substrate complex (K_i'). In the case of cytochrome *bd* catalysed oxygen consumption, K_i describes the binding of CO to the unligated reduced oxidase, whereas K_i' describes the binding of CO to the enzyme substrate complex. The values of K_i and K_i' can be determined by plotting K_m/V_{max} versus [CO] and $1/V_{max}$ versus [CO], respectively (Cornish-Bowden, 1979). In both cases, the value of the respective inhibitor binding constant corresponds to the negative of the CO concentration value at the intercept of the plot on the abscissa. The values of K_i and K_i' can thus be estimated as 9 μ M and 1.28mM, respectively (Figure 6.9). An attractive interpretation of these values is that they refer to CO binding to haem *d* and *b₅₉₅* under turnover conditions, respectively.

6.6. Effect of CO on the cooperativity of the oxidase reaction catalysed by *in situ* cytochrome *bd*.

The effect of increasing CO concentration on the apparent number

Figure 6.8

Effect of increasing CO concentration on the kinetic parameters K_m and V_{max} .

Kinetic parameters were determined from Eadie-Hofstee (Figure 6.7) and Hanes plots (not shown) as described in Chapter 3 (Section 3.7). ■—■, effect of [CO] on K_m . ●—●, effect of [CO] on V_{max} . Oxygen electrode progress curves were recorded as for Figure 6.6.

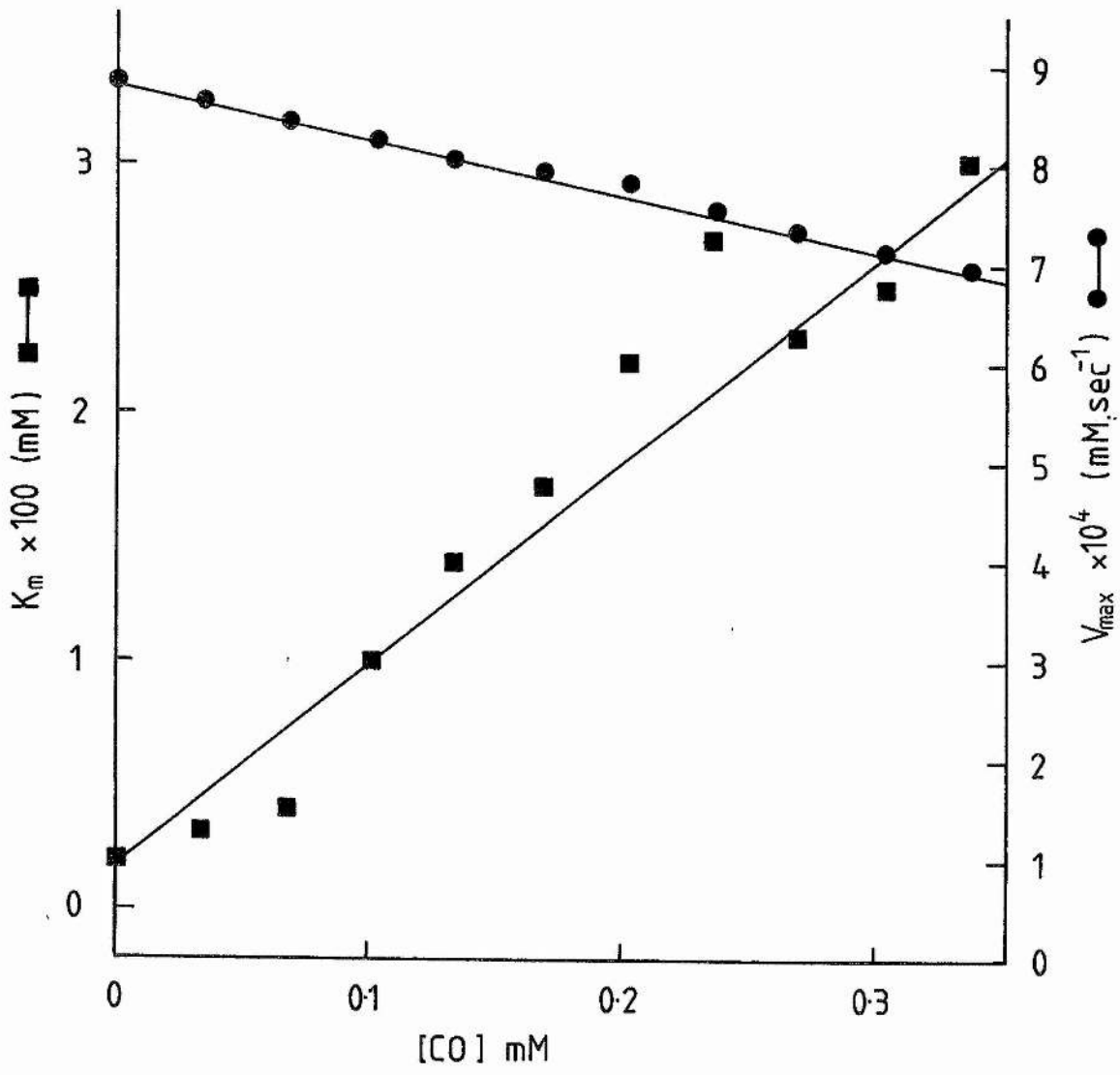
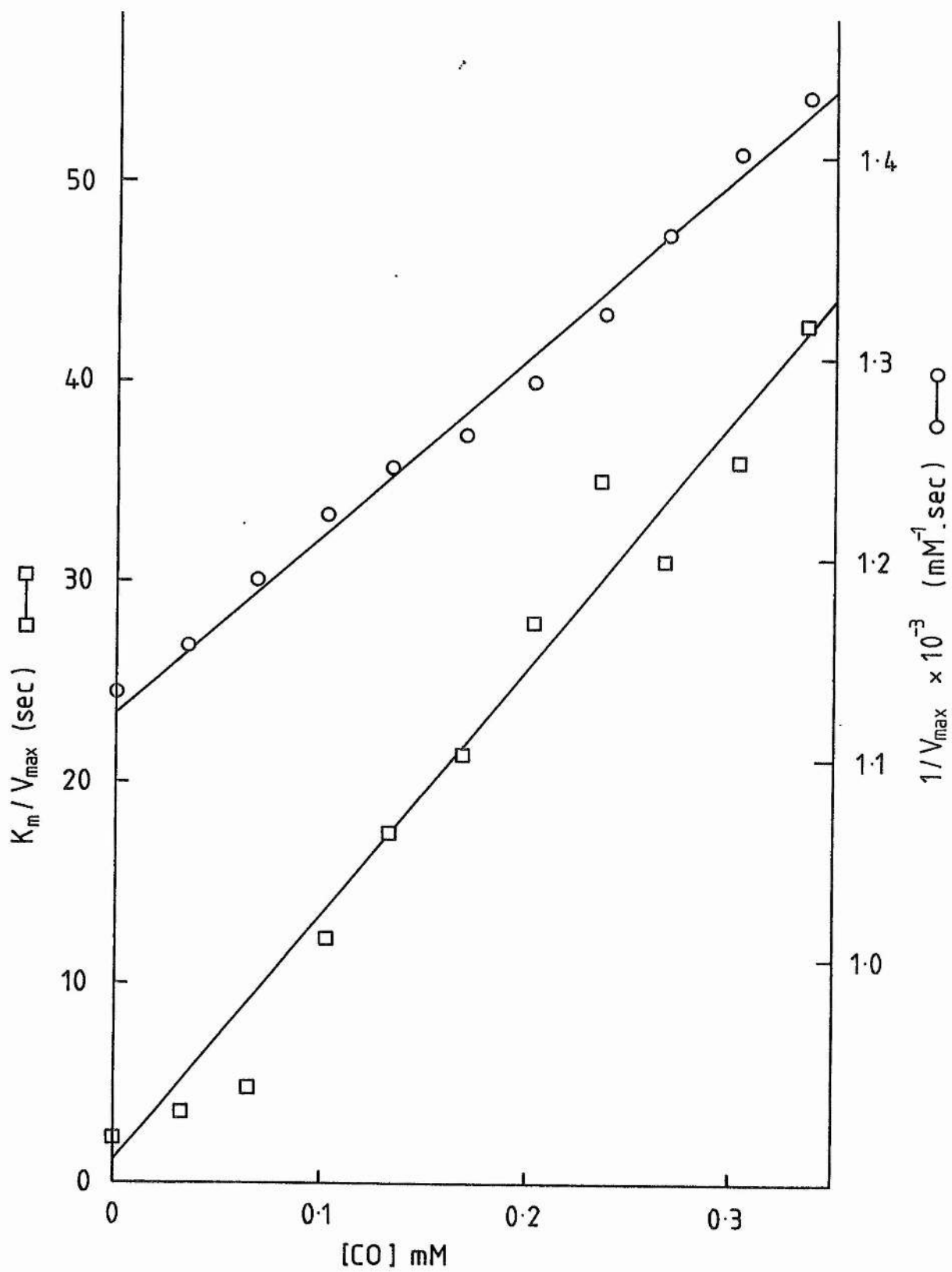


Figure 6.9

Kinetic analyses of CO inhibition of oxidase activity.

Plots of $1/V_{\max}$ versus $[CO]$ (\bigcirc — \bigcirc) and K_m/V_{\max} versus $[CO]$ (\square — \square). Data obtained from Eadie-Hofstee (Figure 6.7) and Hanes plots (not shown) obtained under the conditions outlined in Figure 6.6. K_i values were determined by extrapolation of a line fitted by linear regression to the experimental data to the abscissa (see text).



of oxygen binding sites, n , was further investigated by plotting the derivative data as a series of Hill plots (Figure 6.10). These clearly show that the apparent number of sites decrease with increasing CO concentration, and that the values determined from such plots in terms of the estimates of K_m and n are close to those derived from Eadie-Hofstee and Hanes plots. The effect of increasing CO concentration on the apparent number of oxygen binding sites, n , is illustrated in Figure 6.11 (n values determined from Eadie-Hofstee plots). At high CO concentrations, n tends towards a value of approximately 1.3, whilst at low CO concentrations n reaches a maximum value of around 2.78. However, the n values calculated from oxygen electrode traces in the absence of and at low CO concentrations are likely to be overestimations because of the low K_m for oxygen under these conditions.

The effect of increasing CO concentration on n is intriguing. A possible explanation for this phenomenon is that the oxidase reaction in the absence of CO involves binding of oxygen cooperatively to both haems d and b_{595} . As the CO concentration is increased, haem d , which has a high affinity for CO, becomes progressively blocked, and the reaction proceeds via oxygen binding to haem b_{595} (which has a relatively low affinity for CO), and therefore tends kinetically towards involving only a single oxygen binding site. A possible oxidation-reduction scheme for the oxidase reaction in the presence of high CO concentrations is discussed in detail in Section 6.8.

Figure 6.10.

Effect of CO concentration on the gradient of Hill plots of derivative data.

Hill plots were constructed from the derivative data from the oxygen electrode progress curves such as those in Figure 6.6. Values of V_{max} were obtained from Hanes plots (not shown). \triangle — \triangle , 0.067mM CO, $V_{max} = 8.41 \times 10^{-4} \text{mM sec}^{-1}$. ∇ — ∇ , 0.135mM CO, $V_{max} = 8.03 \times 10^{-4} \text{mM sec}^{-1}$. \blacktriangle — \blacktriangle , 0.202mM CO, $V_{max} = 7.81 \times 10^{-4} \text{mM sec}^{-1}$. \square — \square , 0.337mM CO, $V_{max} = 6.99 \times 10^{-4} \text{mM sec}^{-1}$. The n values calculated from the gradients of the plots are 2.46, 1.67, 1.47, and 1.38 for CO concentrations of 0.067, 0.135, 0.202, and 0.337mM, respectively. The values of K_m estimated from the values $[O_2]$ at $\log_{10} v/(V_{max}-v)=0$ were 0.023, 0.025, 0.028, and 0.031mM for CO concentrations of 0.067, 0.135, 0.202, and 0.337mM, respectively. These values are roughly comparable to those calculated from Eadie-Hofstee and Hanes plots.

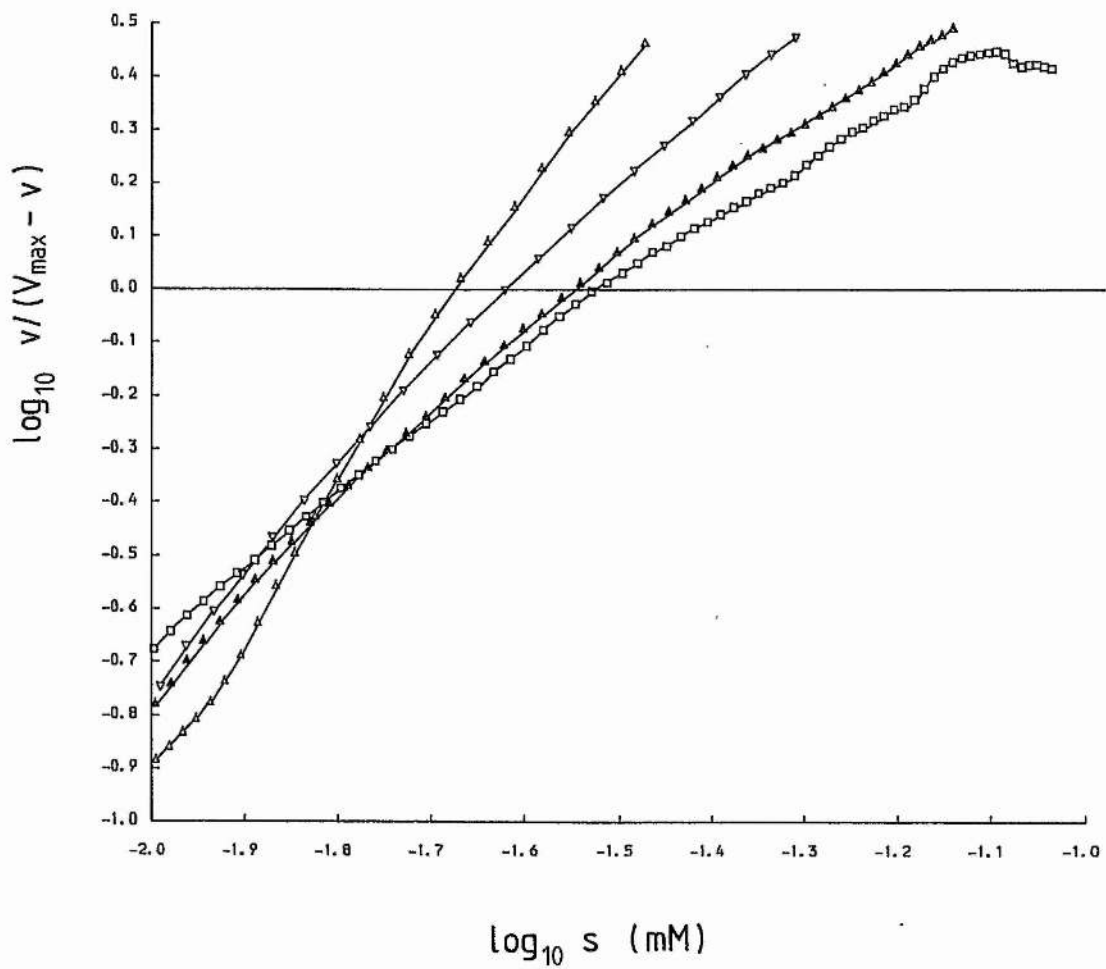
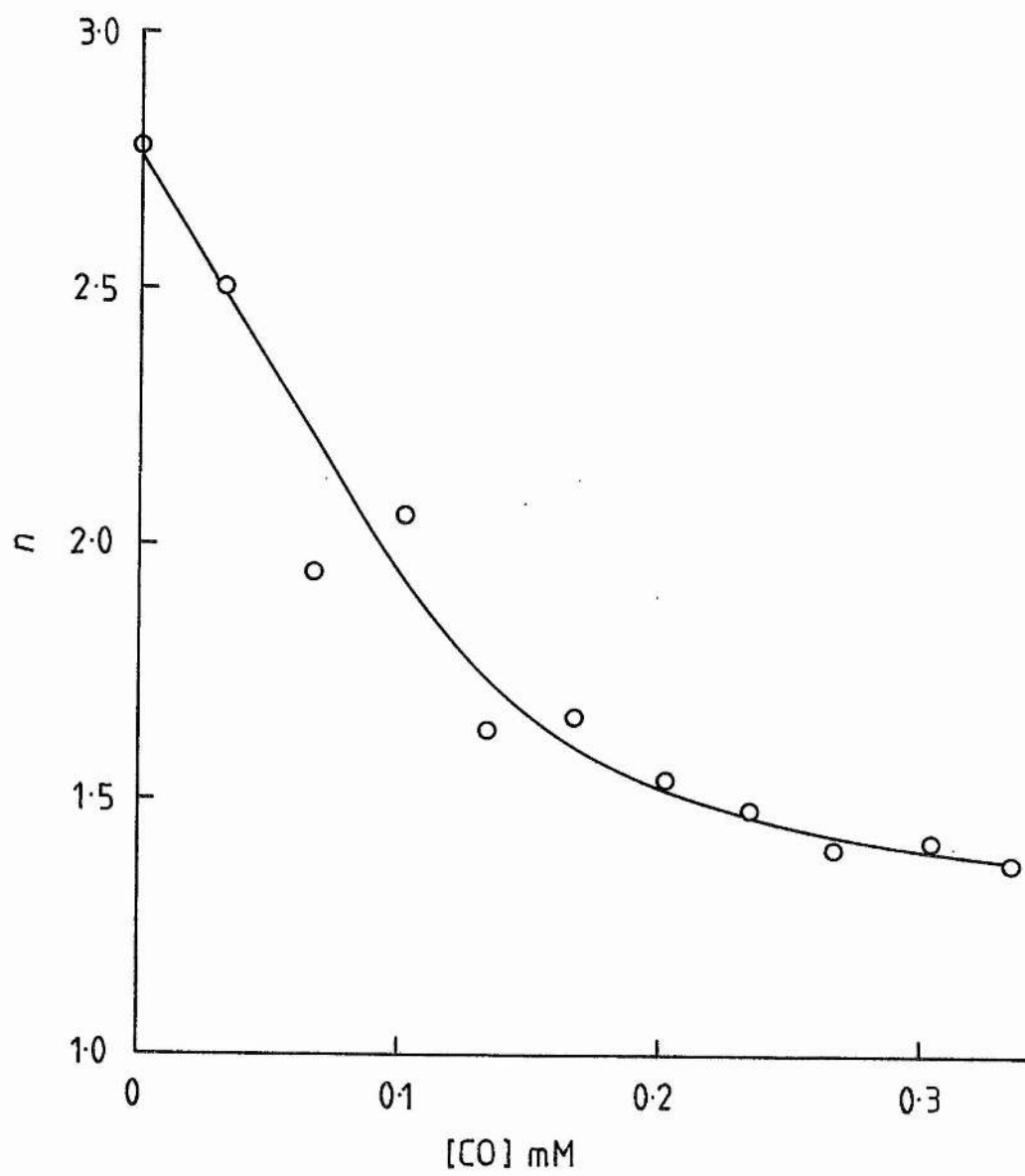


Figure 6.11

Effect of increasing CO concentration on the apparent number of oxygen binding sites, n .

Values of n were determined from analysis of Eadie-Hofstee plots (Figure 6.6) as described in Chapter 2 (Section 2.14.7).



6.7. Use of higher derivatives of oxygen electrode progress curves to analyse the oxidase reaction catalysed by cytochrome *bd*.

Because of the constraints imposed on the use of higher derivatives of oxygen electrode traces by the transference of noise to higher derivatives (Chapter 2, Section 2.14.8), it was not possible to routinely use second and third derivatives to determine kinetic parameters. However, occasionally traces were recorded which were exceptionally 'clean' and these could be analysed by calculating second and third derivatives. Figure 6.12a shows an oxygen electrode progress curve recorded in the presence of 0.202mM CO and its derivatives plotted versus time. Noticeable are the prominent peak of the second derivative and the peak-trough of the third derivative. Figure 6.12b shows the derivative data plotted versus oxygen concentration and also shows a Hanes plot of the first derivative data. As described in Chapter 2 (Section 2.14.8), the K_m of the oxidase for oxygen can be estimated from the oxygen concentration at the peak of the second derivative and the intercept of the third derivative with the abscissa (assuming that the reaction is cooperative; Chapter 2, Section 2.14.8). The K_m can thus be estimated as 0.022mM which corresponds exactly to the estimate determined from the Hanes plot of Figure 6.12b.

Unfortunately, differentiation of more typical traces resulted in spurious peaks and troughs in the second and third derivatives. However, when oxygen electrode traces with good signal to noise ratios can be obtained, analysis using higher derivatives provides an interesting alternative to the use of the more traditional Hanes and

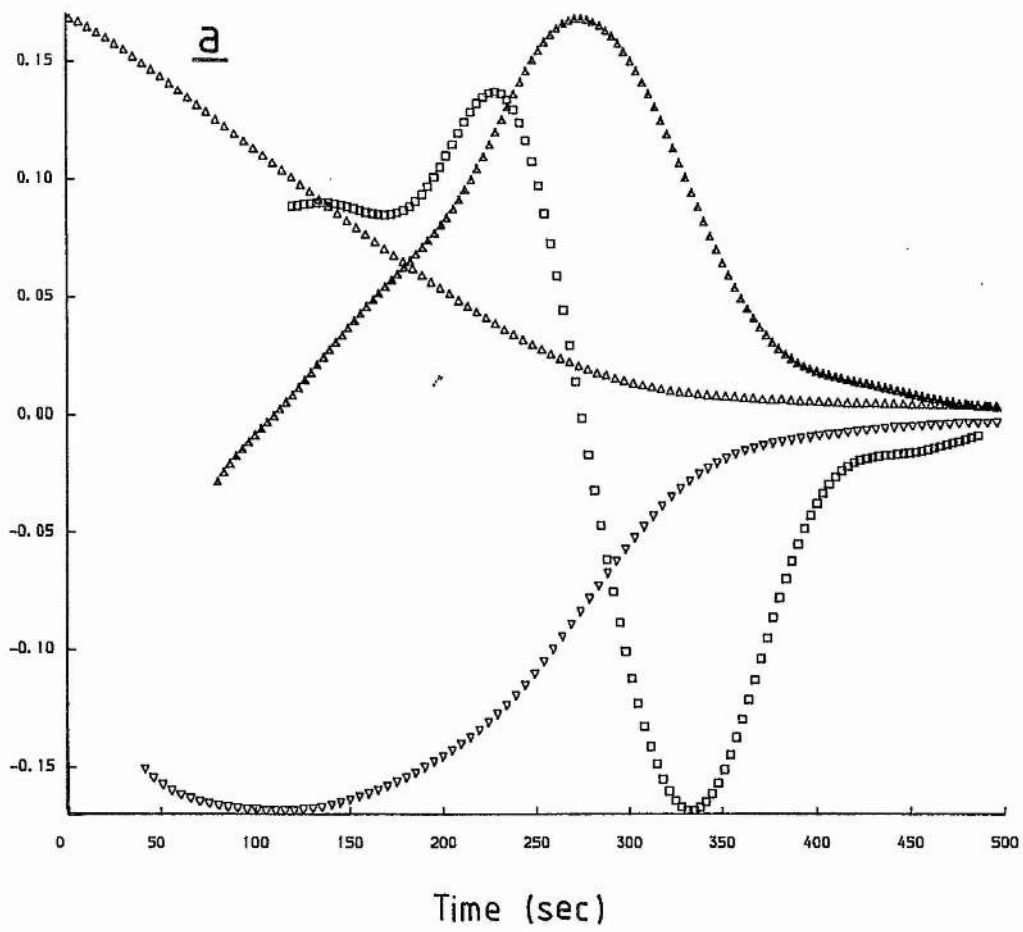
Figure 6.12

Higher derivatives of a CO inhibited oxygen electrode progress curve.

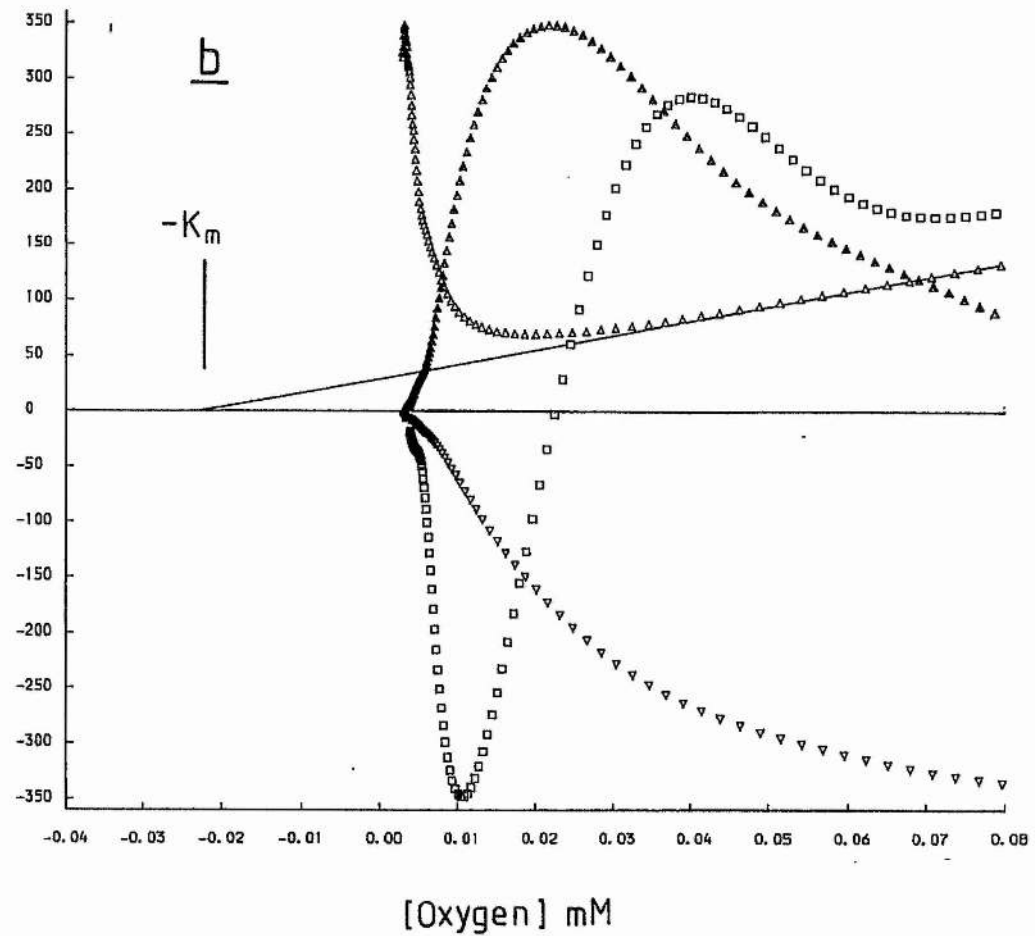
Second and subsequent derivatives of an oxygen electrode progress curve recorded in the presence of 0.202mM CO under the experimental conditions of Figure 6.6 were obtained as described in Chapter 2 (Section 2.14.8).

- (a) Plots of derivatives *versus* time. \triangle , progress curve (intensity $\times 1$). ∇ , first derivative (intensity $\times 2.69 \times 10^2$). \blacktriangle , second derivative (intensity $\times 4.24 \times 10^4$). \square , third derivative (intensity $\times 4.11 \times 10^6$).
- (b) Plots of derivatives *versus* oxygen concentration. \triangle , Hanes plot (s/v *versus* s) of first derivative data (intensity $\times 1$). ∇ , first derivative (intensity $\times 5.58 \times 10^5$). \blacktriangle , second derivative (intensity $\times 8.78 \times 10^7$). \square , third derivative (intensity $\times 8.51 \times 10^9$).

Derivative intensity



Derivative intensity



Eadie-Hofstee plots for the determination of the oxidase K_m .

6.8. Conclusions.

The two putative ligand binding haems of cytochrome *bd* have markedly different affinities for CO. Haem *d* has a very high affinity for this ligand ($K_d \ll 1 \mu M$), whereas haem *b₅₉₅* has a lower affinity (K_d approx. 1.5-2.5 μM). Reaction of CO with haem *d* results in formation of a trough at 626nm and a peak at 642nm in the reduced *plus* CO *minus* reduced difference spectrum. The concentration dependence of the formation of the 445nm trough in the Soret region of this spectrum indicates that this feature is due to the effect of CO on the Soret band of haem *d*. Reaction of CO with haem *b₅₉₅* results in the formation of a major peak-trough in the Soret at 415-429nm, but no major features are detected in the region around the alpha band of this haem (595nm). Overall, given that cytochrome *bd* is the major ligand binding haemoprotein present in membranes from *E.coli* EMG2 grown anaerobically with fumarate as respiratory oxidant, the results of the optical CO titrations confirm the assignment of the features of the CO difference spectrum suggested in Chapter 1 (Section 1.4.7.2).

The lower affinity of haem *b₅₉₅* for CO compared to that of haem *d* parallels the lower rate of reaction of nitrite with this haem observed in Chapter 3. A possible reason for this may be that the first CO molecule to enter the haem pocket binds to haem *d*, resulting in steric hindrance of subsequent ligand binding to haem *b₅₉₅*. Alternatively, an amino acid side chain located on the distal side of haem *b₅₉₅* may sterically hinder binding of CO to this haem, as is the

case in haemoglobin and myoglobin (Collman *et al.*, 1976). This side chain may function as the general acid possibly involved in the reaction of nitrite with haem *b₅₉₅* (Chapter 3, Section 3.9).

The mixed inhibition elicited by CO on the oxidase reaction catalysed by cytochrome *bd* suggests that CO is able to bind to both the unligated and the oxygen ligated oxidase. As is the case with the optical studies of CO binding, two K_i values were determined, K_i and K_i' , possibly corresponding to CO binding to haem *d* and haem *b₅₉₅*, respectively. K_i was found to be 9 μ M and K_i' was found to be 1.28mM. The mixed inhibition is in contrast to the data presented in Chapter 3 which indicates that nitrite acts as a competitive inhibitor of the oxidase reaction.

The reduced number of oxygen binding sites, n , at high CO concentrations suggests that one of the haems becomes blocked, and on the basis of the estimated K_i and K_a values this haem can be identified as haem *d*. Under these conditions, the oxidase reaction would have to proceed via a mechanism involving oxygen binding to haem *b₅₉₅*. A model for such a mechanism is proposed below. At low CO concentrations, a mechanism involving oxygen binding to both haems *d* and *b₅₉₅* is indicated. As suggested in Chapter 3, the reaction cycle may involve binding of two oxygens (at haems *d* and *b₅₉₅*), their reduction to peroxide, and disproportionation leaving a residual bound oxygen and two molecules of water. Such a mechanism and its merits compared to other possibilities is described in Chapter 7.

Kauffman *et al.* (1980) studied the effect of CO on the optical spectrum of the haem *d* alpha band region in membranes containing

cytochrome *bd* from *A. vinelandii* under turnover conditions and found that only ferrous carbonmonoxy haem *d* (from its alpha band at 636nm) and haem *d** (from the incomplete formation of the band at 636nm) could be detected as major intermediates. A small shoulder at around 670nm indicated that haem *d*₆₈₀ was also present as a minor species in the presence of CO. No haem *d*₆₅₀ was detected under turnover conditions in the presence of CO. The results of Kauffman *et al.* (1980) therefore indicate that haem *d* has a high affinity for CO under turnover conditions, a finding which is consistent with the data reported herein. In the photodissociation experiments (recording of photochemical action spectra) of Castor and Chance (1959) and Edwards *et al.* (1981), the inhibition of oxidase activity elicited by CO is far from complete. Thus, the absence of haem *d*₆₅₀ and the incomplete inhibition of oxidase activity suggests that in the presence of CO oxygen may bind initially to haem *b*₅₉₅ rather than haem *d*.

The results discussed above suggest that an alternative oxidation-reduction cycle not involving the *d*₆₅₀ intermediate operates in the presence of CO. A tentative scheme for such a cycle is illustrated in Figure 6.13. In this model, ubiquinol is assumed to react in much the same way as indicated in Chapter 1 (Section 1.4.9; Figure 1.5). As described above, Kauffman *et al.* (1980) were only able to identify the following intermediates: haem *d**, haem *d*₆₈₀ and the CO adduct to haem *d* corresponding to the adduct to the fully reduced enzyme. In Figure 6.13, intermediate (i) corresponds to the CO adduct to the haem *d* of the fully reduced oxidase. In the model, the K_i and K_i' observed under turnover conditions are assumed to correspond to CO

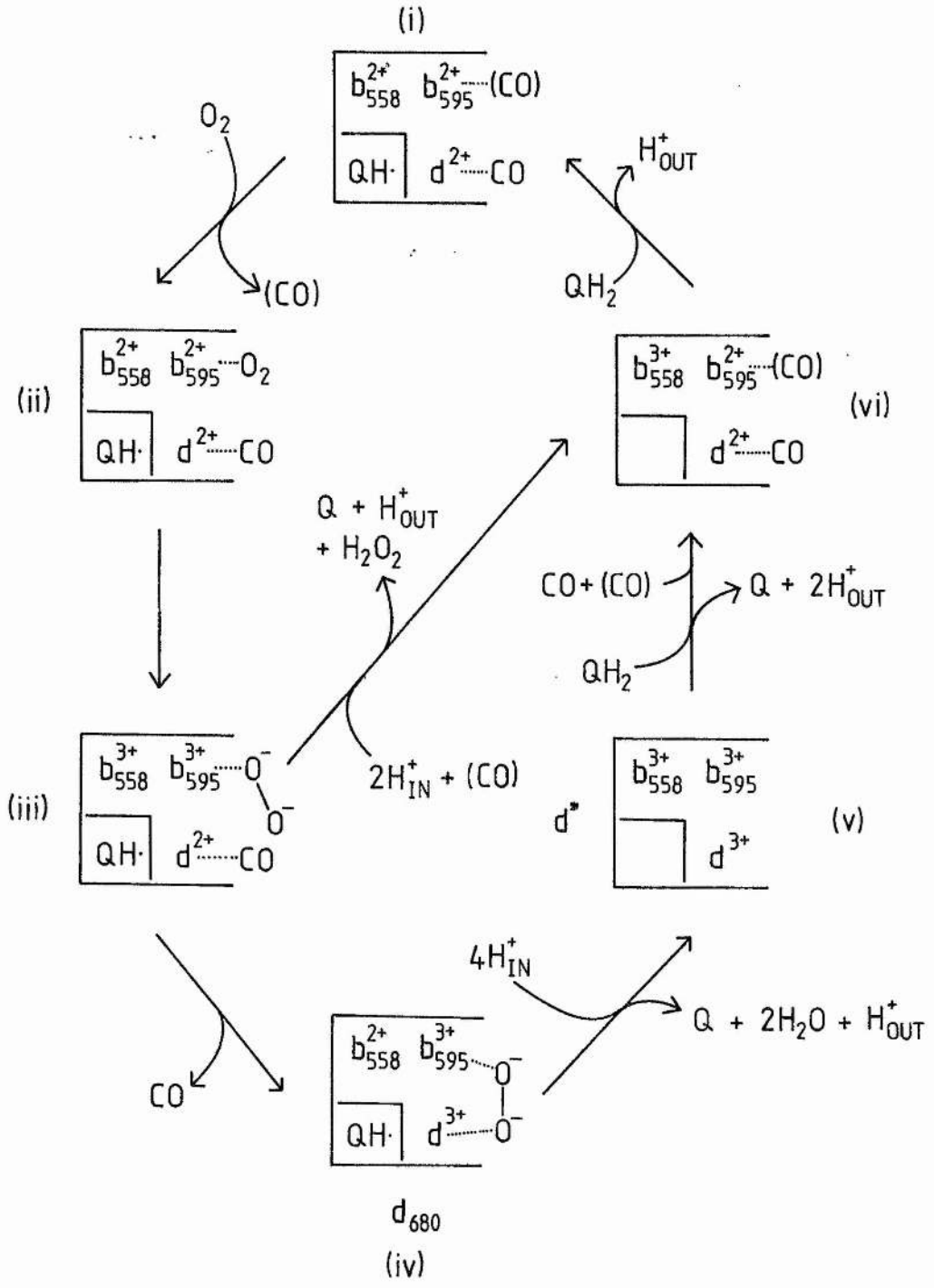
Figure 6.13

*Oxidation-reduction cycle of the reaction between cytochrome bd and oxygen
in the presence of CO.*

A tentative model for the oxidase reaction of cytochrome bd in the presence of CO. The following reactions are proposed to occur:

- (i)-(ii) The fully reduced, CO ligated enzyme (i) reacts with oxygen resulting in formation of an oxygen adduct to haem b_{595} (ii). CO molecules in parentheses may not bind under turnover conditions because of the relatively high K_d and K_i' corresponding to CO binding to haem b_{595} .
- (ii)-(iii) The bound oxygen becomes reduced to peroxide by electron transfer from haems b_{558} and b_{595} , whilst CO remains bound to ferrous haem d .
- (iii)-(iv) The peroxide displaces the CO from haem d , resulting in formation of the peroxy adduct, haem d_{680} . The peroxide may bridge between haems b_{595} and d .
- (iv)-(v) The remaining available electrons (from haem b_{558} and a putative bound semiquinone reduce the peroxide to water, resulting in the formation of the fully oxidised d^+ intermediate.
- (v)-(vi)-(i) The oxidase is reduced and ligated by CO, and then further reduced to form intermediate (i).
- (iii)-(vi) In this step the peroxide dissociates from the enzyme rather than undergoing further reduction to water.

See text for further details. Abbreviations are as for Figure 1.5 (Chapter 1).



binding to haems *d* and *b₅₉₅*, respectively. Thus, the fully reduced enzyme is expected to have a CO molecule bound to haem *d*, whereas the higher K_i' suggests that CO is less likely to be bound to haem *b₅₉₅*. Oxygen reacts with the reduced carbonmonoxy cytochrome *bd* and binds preferentially in this case to haem *b₅₉₅*, forming intermediate (ii). Electron transfer then takes place from haem *b₅₅₈* and haem *b₅₉₅*, resulting in reduction of the bound oxygen to peroxide (intermediate (iii)). This peroxy adduct to haem *b₅₉₅* displaces the CO from haem *d* which then transfers an electron back to haem *b₅₉₅*, resulting in the formation of the haem *d₆₃₀* species (intermediate (iv)). The bound peroxide then becomes reduced to water by electron transfer from ferrous haem *b₅₅₈* and the bound semiquinone, resulting in formation of the haem *d** 'invisible' intermediate (intermediate (v)). Reduction and binding of CO then occurs, regenerating intermediate (i) via intermediate (vi). A 'short cut' is also shown in the scheme whereby peroxide can be released from intermediate (iii), resulting in formation of intermediate (vi).

Although the scheme presented in Figure 6.13 is speculative, it is consistent with the high affinity of haem *d* for CO reported herein, and the optical observations of Kauffman *et al.* (1980) which indicate that the haem *d₆₃₀* intermediate (oxy ferrous haem *d*) is not observed under turnover conditions in the presence of CO. An intriguing possibility raised by the model and discussed in Chapter 7 is that the two putative ligand binding haems of the oxidase are able to act as a binuclear centre of the oxidase reaction in much the same way as is observed in the cytochrome *aa₃* system (Nacqui *et al.*, 1986). If a

peroxy adduct to haem b_{595} exists and is able to displace CO from ferrous haem d , then it is possible that ligands such as peroxide and oxygen are able to bridge between the two haems in much the same way as these ligands appear able to bridge between haem a_3 and Cu_B in cytochrome aa_3 .

The model of Figure 6.13 also appears to account for the decrease in the apparent number of oxygen binding sites in the presence of CO. It represents a limiting case where high concentrations of CO may result in the oxidase reaction proceeding via oxygen binding initially to haem b_{595} rather than to haem d , and is a limiting case where $n=1$.

Overall, the data presented herein confirms that cytochrome bd has two ligand binding sites, haem d and haem b_{595} . Further, the steady state kinetics of oxygen reduction do not appear to be consistent with a single reaction mechanism, suggesting that there may be two mechanisms of the oxidase reaction, one involving a single ligand binding site and one involving two ligand binding sites. These possibilities will be further discussed in Chapter 7.

DISCUSSION

CHAPTER SEVEN

Discussion.

7.1 Ligand binding to haems *d* and *b₅₉₅*.

Lorence *et al.* (1986) concluded on the basis of CO binding titrations that cytochrome *bd* has two ligand binding haems *d*, in addition to the high spin haem *b₅₉₅*. However, the e.p.r. quantitations of the half reduced and fully oxidised *in situ* oxidase indicate that haems *d* and *b₅₉₅* are present in an equimolar ratio (Chapter 5, Meinhardt *et al.*, 1989). This, and the evidence for ligand binding to both haems *d* and *b₅₉₅*, and the unlikelihood of an oxidase having three ligand binding haems indicates that cytochrome *bd* has a single ligand binding haem *d* and a single ligand binding haem *b₅₉₅*. The optical, polarographic, and e.p.r. data indicate that these centres are close enough to experience haem-haem interactions in the form of cooperative oxygen binding and perturbation of the ferric haem *b₅₉₅* lineshape upon oxidation of haem *d*.

It can be concluded that, rather than having two distinct ligand binding haem pockets, the oxidase has a single such pocket accommodating both haems *d* and *b₅₉₅*. The enzyme appears to be able to bind two ligands such as CO and NO in this pocket at the same time. Cytochrome *aa₃*, on the other hand, has a ligand binding haem pocket containing haem *a₃* and Cu_B, but appears to be able to bind only a single ligand in this pocket. Cu_B is able to bind CO, but only after this ligand has been photolysed off the haem *a₃* (Alben *et al.*, 1981). Thus, in cytochrome *bd* the ligand binding haem pocket must have a more open conformation than in cytochrome *aa₃*, with a greater distance between the two metal centres. As will be discussed in Section 7.3, the ability of the pocket to bind two ligands suggests that a possible

reaction scheme for the oxidase reaction may involve oxygen binding to both haem *d* and haem *b₅₉₅* at the same time, or binding of a single oxygen between these two haems.

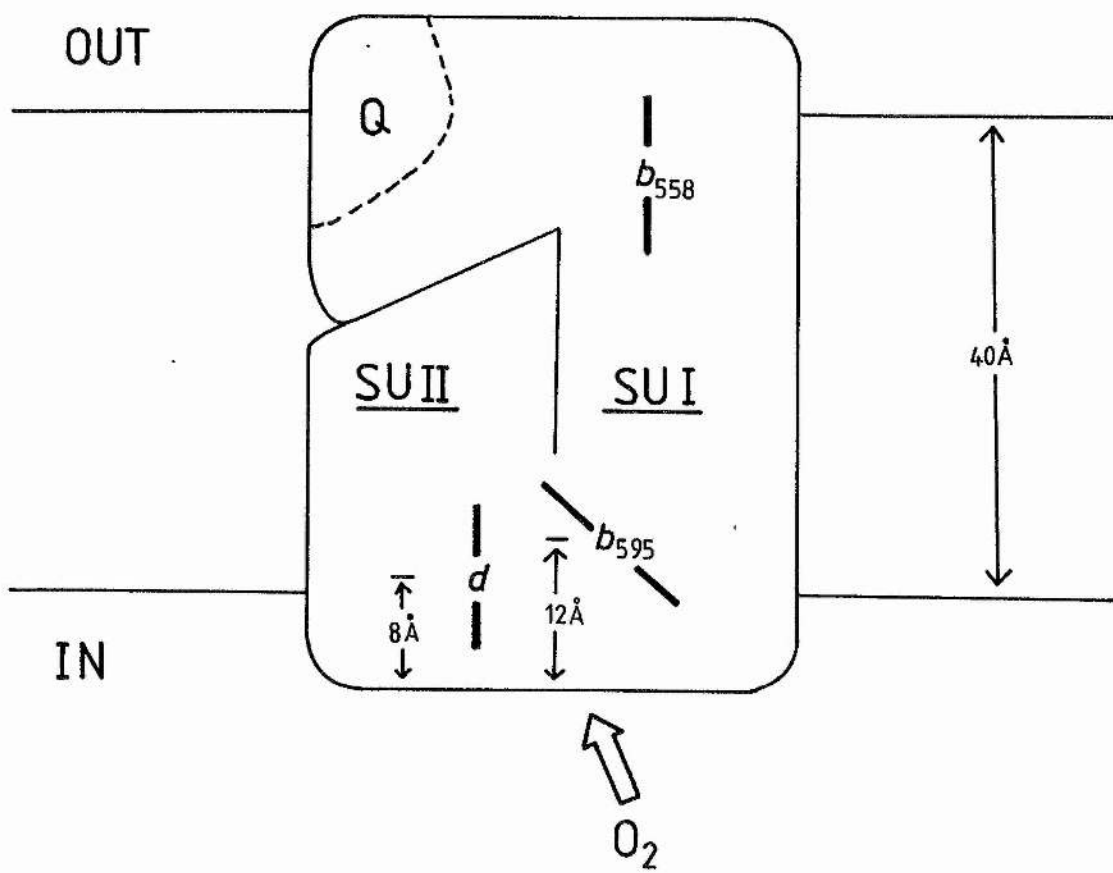
7.2. *The arrangement of the oxidase in the cytoplasmic membrane.*

In Chapter 4, it was concluded that haems *d* and *b₅₉₅* of cytochrome *bd* are located at 8 and 12Å° below the inner surface of the cytoplasmic membrane, respectively. Since the dysprosium probe technique used to estimate these distances is of low resolution, it can be concluded that the ligand binding haems of cytochrome *bd* are located at approximately the same distance below the surface of the protein on the inner side of the cytoplasmic membrane. This is a comparatively shallow location compared to the situation in cytochrome *aa₃*, where haem *a₃* is located towards the centre of the membrane. Whilst the latter oxidase pumps protons across the mitochondrial inner membrane (one proton is pumped across the membrane per electron used in the reduction of oxygen; Wikstrom *et al.*, 1981) and oxidises a hydrophilic electron donor (cytochrome *c*) on the outer surface of the mitochondrial membrane, cytochrome *bd* does not pump protons and oxidises hydrophobic ubiquinol within the membrane bilayer. This may explain the comparative closeness of the ligand binding haems of the *in situ* cytochrome *bd* to the inner surface of the cytoplasmic membrane. Figure 7.1 shows a schematic arrangement of the ligand binding haems of cytochrome *bd* in the *E.coli* cytoplasmic membrane.

Green *et al.* (1988) determined the amino acid sequences of the two subunits of cytochrome *bd* and used the Kyte-Doolittle algorithm

*Figure 7.1**Arrangement of cytochrome bd in the cytoplasmic membrane.*

Structural model based on that presented in Chapter 1 (Section 1.4.4; Figure 1.2) showing the orientation of the haems of cytochrome *bd* with respect to the cytoplasmic membrane. The orientations of the haems with respect to the membrane plane are arbitrary, but are supported by preliminary studies of the e.p.r. spectra of oriented multilayers of membranes from cytochrome *b₅₆₂-0* deficient, cytochrome *bd* overexpressing *E.coli* strain FUN4/pNG2 (J.C.Salerno & W.J.Ingledew, unpublished results). Haems *d* and *b₅₉₅* are shown in the figure in a single ligand binding haem pocket able to accommodate one or two molecules of oxygen.



(Kyte & Doolittle, 1982) to estimate that the subunits I and II of cytochrome have a maximum of seven and eight membrane spanning alpha helical segments, respectively.

The amino acid sequences of subunits I and II of cytochrome *bd* contain a total of 6 and 4 histidines, respectively. Kyte-Doolittle analyses of the sequences indicate that in Subunit I, four of these are located on the periplasmic side of the cytoplasmic membrane and two are located on the cytoplasmic side. Two of the four periplasmic histidine residues are likely to be involved in haem *b₅₅₈* ligation, whereas it is possible that one or two of the periplasmic histidines are involved in ligation of haem *d* and/or haem *b₅₉₅*. Subunit II has two periplasmic histidines and two cytoplasmic histidines, and one or two of the cytoplasmic histidines are likely to be involved in haem *b₅₉₅* and haem *d* ligation. As they are high spin, each of the two ligand binding haems of cytochrome *bd* requires only a single endogenous haem ligand, so that a maximum of two histidines is required for haem ligation on the cytoplasmic side of the membrane. Although the locations of the histidine residues have been considered in the above, it is possible that other residues are also involved in haem ligation, such as methionine and lysine.

7.3. Potential models for the oxidase reaction.

In cytochrome *aa₃*, the binuclear haem *a₃* and Cu_B centre is thought to rapidly transfer two electrons to a bound oxygen, resulting in a peroxide adduct to this oxidase. Whereas the oxygen adduct to cytochrome *bd* is stable at room temperature (Poole *et al.*, 1983a), the oxygen adduct to cytochrome *aa₃* is very short lived and unstable at

room temperature (Naqui et al., 1986). The data presented in Chapters 3 and 6 of this thesis suggest that the oxidase reaction catalysed by cytochrome *bd* is able to proceed via two mechanisms involving either a single or two oxygen binding sites.

The accepted functional model for the haem a_3 / Cu_B centre of cytochrome aa_3 has oxygen binding and being reduced between these two centres, followed by a concerted two electron transfer resulting in a bound peroxide. Subsequent one or two electron reductions result in the reduction of the bound peroxide to two molecules of water (Naqui et al., 1986). A mechanism similar to this could operate in cytochrome *bd*, and such a scheme is illustrated in Figure 7.2. Such a model would account for steady state oxidase kinetics with an apparent single oxygen binding site.

In the 'bridging oxygen' model of Figure 7.2, oxygen binds initially to haem *d* forming the haem d_{6s0} intermediate, which then accepts two electrons, one from haem *d* and one from haem b_{595} , to form the haem d_{6s0} intermediate with a peroxide bound between haems *d* and b_{595} . A second two electron reduction results in the production of two molecules of water. As far as the redox states of the intermediates are concerned, this model is identical to that presented in Chapter 1 (Section 1.4.9; Figure 1.5), although the latter accounts for the role of the oxidase as a coupling site in the *E.coli* aerobic respiratory chain.

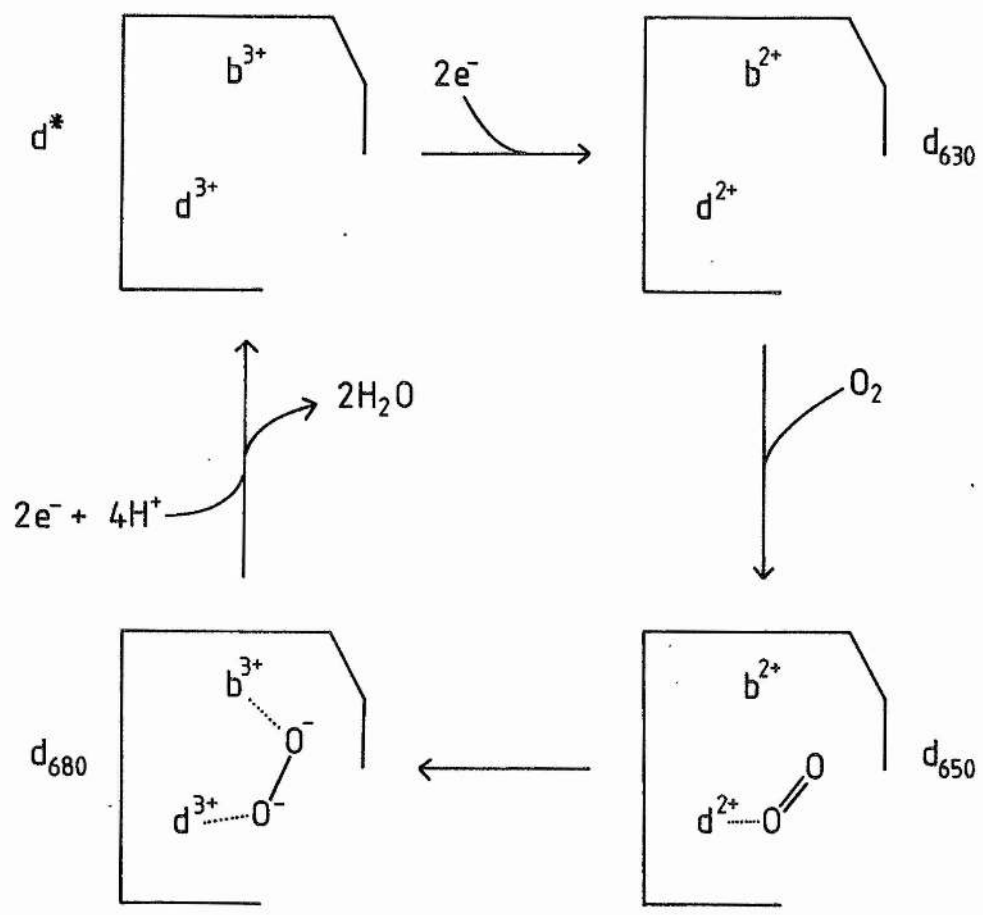
To account for the data of Chapters 3 and 6, a second model can be proposed in which two molecules of oxygen bind to the oxidase, one to haem *d* and one to haem b_{595} , followed by a total four electron

DISCUSSION

Figure 7.2

'Bridging oxygen' model for the oxidase reaction.

Only the ligand binding haems of the oxidase are shown in this figure. See text for details. For the sake of clarity, possible redox states of haem *b₅₅₈* and ubiquinol species are omitted, as are the sources and destinations of the protons involved in the redox cycle. See Figure 1.5 and Figure 6.13 for details of how ubiquinol and haem *b₅₅₈* may behave under turnover conditions.



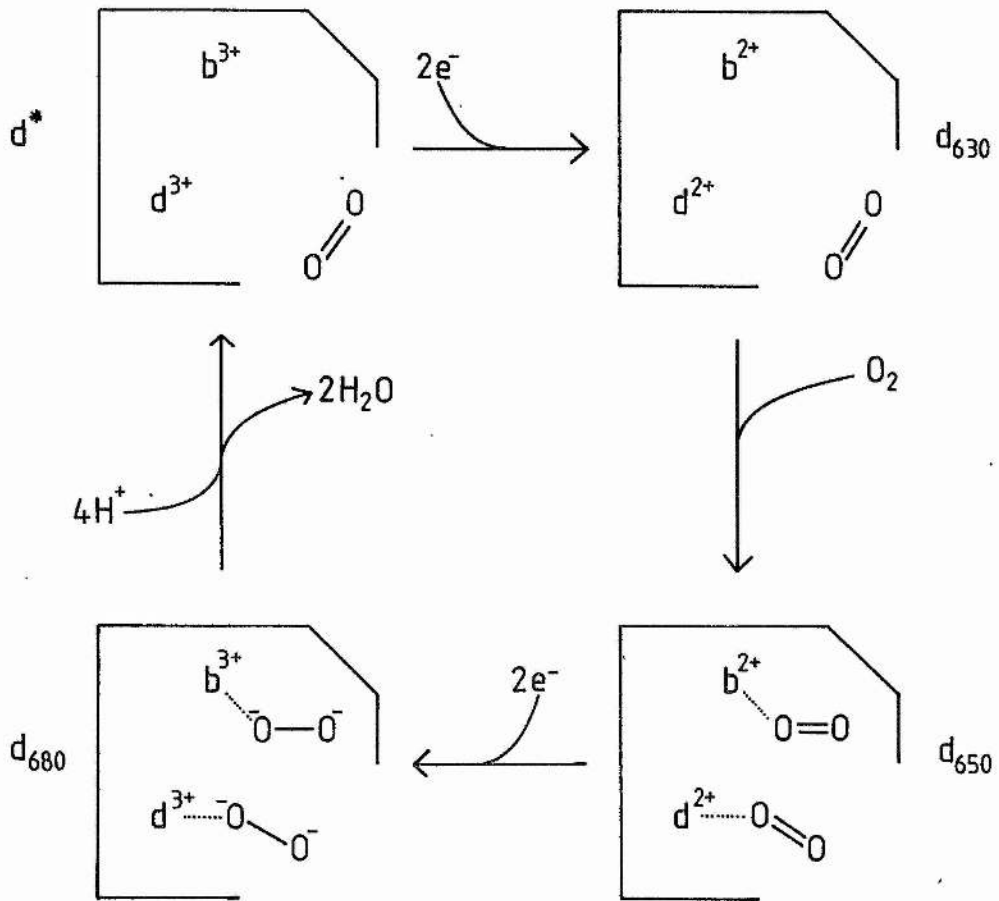
transfer to form an intermediate with peroxides bound at both haems (Figure 7.3). Subsequent disproportionation and protonation results in a residual oxygen and two molecules of water. Such a mechanism could result from a more open conformation of the ligand binding haem pocket, allowing the easy entry of two molecules of oxygen. On the basis of the data of Chapter 3, such an open conformation may occur at pH's below around 7.5.

In the 'disproportionation' model of Figure 7.3 two molecules of oxygen bind initially to haem *d* and haem *b₅₉₅*, resulting in the haem *d₆₅₀* intermediate. The bound oxygens are then reduced by a total of four electrons, from haems *d*, *b₅₉₅*, and *b₅₅₈*, and a bound ubiquinol species (ubisemiquinol or ubiquinol), resulting in a haem *d₆₈₀* intermediate with two bound peroxides. Disproportionation and protonation then results in a residual oxygen and two molecules of water.

The two models described above both have intermediates corresponding to the optically detectable species described by Poole and coworkers (Chapter 1; Section 1.4.7.3). The haem *d₆₅₀* intermediate is e.p.r. silent (Kumar *et al.*, 1985; Poole *et al.*, 1983a), whereas the haem *d₆₈₀* intermediate is e.p.r. visible with a rhombic high spin signal attributable to ferric haem *b₅₉₅* whilst no high spin signal is observed corresponding to the ferric haem *d* of the *d₆₈₀* intermediates of the models. An explanation for this which is consistent with the models described in the above is that the haem *d* of the *d₆₈₀* species is low spin. Hata *et al.* (1987) observed a low spin e.p.r. signal at $g=2.15$ in their low temperature ligand exchange experiments which they

*Figure 7.3**'Disproportionation' model for the oxidase reaction.*

Only the ligand binding haems of cytochrome *bd* are shown in this model. See text for details. For the sake of clarity, possible redox states of haem *b₅₅₈* and ubiquinol species are omitted, as are the sources and destinations of the protons involved in the redox cycle. See Figure 1.5 and Figure 6.13 for details of how ubiquinol and haem *b₅₅₈* may behave under turnover conditions.



attributed to superoxide ligated to ferrous haem *d*. The $g=2.15$ signal appeared in parallel with the rhombic high spin haem b_{595} signal. Consideration of the models described above suggests, however, that there is concerted electron transfer (2 or $4e^-$) from (and via) both haems b_{595} and haem *d* to bound oxygen and that the $g=2.15$ signal observed by Hata *et al.* (1987) may be due to a low spin peroxy adduct to ferric haem *d*. However, a $g=2.15$ signal wasn't observed in the peroxide treated membranes used in this work. The $g=2.3$ and 2.5 observed herein were very much less intense than those observed by Hata *et al.* (1985, 1987).

To account for the cooperativity observed in Chapters 3 and 6, the above reaction schemes would have to function concurrently since the apparent number of oxygen binding sites, n , is generally between one and two. The effect of pH on the nitrite inhibition of oxidase activity observed in Chapter 3 suggests that the conformation of the oxidase favouring the $n=2$ reaction becomes more favourable at pH's less than 7.5.

7.4 Future prospects.

Further work is required to verify or ameliorate the models described above. Studies involving low temperature ligand exchange experiments in combination with e.p.r., m.c.d., and Resonance Raman spectroscopies would allow further characterisation of the intermediates of the oxidase reaction. Investigations of the optically detectable intermediates under turnover conditions, particularly in the Soret and haem b_{595} alpha band regions could provide further

DISCUSSION

information on the role of haem b_{595} .

The structural information available to date on the spatial organisation of the redox centres and the subunits of cytochrome bd is very much sparser than that available on the cytochrome aa_3 system (Naqui *et al.*, 1986; Wikstrom *et al.*, 1981). Some of the approaches used in delineating the spatial arrangements of the redox centres of the latter oxidase may prove fruitful in the study of cytochrome bd . A large amount of structural information about the spatial disposition of the redox centres of cytochrome aa_3 has been obtained by studying the dipolar interactions between its redox active centres (for example, see Mascarenhas *et al.*, 1983; Ohnishi *et al.*, 1982; Boelens *et al.*, 1984; Goodman & Leigh, 1985). These studies have exploited the effects of a relatively fast relaxing e.p.r. visible centre such as ferric haem a on a relatively slow relaxing centre such as nitrosyl ferrous haem a_3 or Cu_B . The application of such techniques to cytochrome bd could provide an estimate of the distance between the nitrosyl haems and haem b_{595} . EXAFS has also provided estimates of the distances in the cytochrome aa_3 system, and this technique may also be able to provide information on the cytochrome bd system.

BIBLIOGRAPHY

BIBLIOGRAPHY

BIBLIOGRAPHY

- Aasa, R., Albracht, S.P.J., Falk, K., Lanne, B., & Vanngard, T. (1976). *Biochimica et Biophysica Acta*, 422, 260-272.
- Alben, J.O., Moh, P.P., Fiamingo, F.G., & Altschuld, R.A. (1981). Cytochrome oxidase (a_3) haem and copper observed by low temperature Fourier transform infrared spectroscopy of the CO complex. *Proceedings of the National Academy of Science USA*, 78, 234-237.
- Anraku, Y. & Gennis, R.B. (1987). The aerobic respiratory chain of *Escherichia coli*. *Trends in Biochemical Sciences*, 12, 262-266.
- Arima, K. & Oka, T. (1965). Cyanide resistance in *Achromobacter*: Induced formation of cytochrome a_2 and its role in cyanide resistant respiration. *Journal of Bacteriology*, 90, 734-743.
- Ashcroft, J.R. & Haddock, B.A. (1975). Synthesis of alternative membrane-bound redox carriers during aerobic growth of *Escherichia coli* in the presence of potassium cyanide. *Biochemical Journal*, 148, 349-352.
- Au, D.C.-T., Lorence, R.M., & Gennis, R.B. (1985). Isolation and characterisation of an *Escherichia coli* mutant lacking the cytochrome o terminal oxidase. *Journal of Bacteriology*, 161, 123-127.

BIBLIOGRAPHY

- Barber, D., Parr, S.R., & Greenwood, C. (1976). Some spectral and steady-state kinetic properties of *Pseudomonas* cytochrome oxidase. *Biochemical Journal*, 157, 431-438.
- Barber, M.J., Salerno, J.C., & Siegel, L.M. (1982). Magnetic interactions in milk xanthine oxidase. *Biochemistry*, 21, 1648-1656.
- Barrett, J. (1956). The prosthetic group of cytochrome *a*₂. *Biochemical Journal*, 64, 626-639.
- Bergstrom, J. (1985). The EPR spectrum and orientation of cytochrome *b*-563 in the chloroplast thylakoid membrane. *FEBS Letters*, 183, 87-90.
- Blum, H., Leigh, J.S., & Ohnishi, T. (1980). Effect of dysprosium on the spin lattice relaxation time of cytochrome *c* and cytochrome *a*. *Biochimica et Biophysica Acta*, 626, 31-40.
- Blum, H., Cusanovich, M.A., Sweeney, W.V., & Ohnishi, T. (1981). Magnetic interactions between dysprosium complexes and two iron-sulphur proteins. *Journal of Biological Chemistry*, 256, 2199-2206.
- Blum, H., Bowyer, J.R., Cusanovich, M.A., Waring, A.J., & Ohnishi, T. (1983). Spin lattice relaxation rates of iron-sulphur proteins

BIBLIOGRAPHY

- and haem proteins affected by dysprosium complexes and temperature. *Biochimica et Biophysica Acta*, 748, 418-428.
- Blumberg, W.E. (1967). The e.p.r. of high spin Fe^{3+} in rhombic fields. In *Magnetic resonance in Biological Systems*, pp. 119-133. Edited by A. Ehrenberg, B.G. Malmstrom, & T. Vanngard. Pergamon Press, Oxford.
- Boelens, R., Rademaker, H., Wever, R., & Van Gelder, B.F. (1984). The cytochrome c oxidase-azide-nitric oxide complex as a model for the oxygen binding site. *Biochimica et Biophysica Acta*, 765, 196-209.
- Brudvig, G.W., Stevens, T.H., & Chan, S.I. (1980). Reactions of nitric oxide with cytochrome aa₃. *Biochemistry*, 19, 5275-5285.
- Butler, W.L. (1979). Fourth derivative spectra. *Methods in Enzymology*, 56, 501-515.
- Carter, K. & Gennis, R.B. (1985). Reconstitution of the ubiquinone dependent pyruvate oxidase system of *Escherichia coli* with the cytochrome o terminal oxidase complex. *Journal of Biological Chemistry*, 260, 10986-10990.
- Case, G.D., & Leigh, J.S. (1976). Intramitochondrial positions of cytochrome haem groups determined by dipolar interactions with

BIBLIOGRAPHY

- paramagnetic cations. *Biochemical Journal*, 160, 769-783.
- Castor, L.N. & Chance, B. (1959). Photochemical determinations of the oxidases of bacteria. *Journal of Biological Chemistry*, 234, 1587-1592.
- Chance, B., Graham, N., & Legallais, V. (1975). Low temperature trapping method for cytochrome oxidase oxygen intermediates. *Analytical Biochemistry*, 67, 552-579.
- Chang, C.K., Timkovich, R., & Wu, W. (1986). Evidence that haem d_1 is a 1,3-porphyrindione. *Biochemistry*, 25, 8447-8453.
- Chappell, J.B. (1964). The oxidation of citrate, isocitrate, and cis-aconitate by isolated mitochondria. *Biochemical Journal*, 90, 225-237.
- Coll, J. (1982). *The BBC Microcomputer: User Guide*, pp204, pp426.
Published by The British Broadcasting Corporation, London.
- Collman, J.P., Brauman, J.I., Halbert, T.R., & Suslick, K.S. (1976). Nature of O_2 and CO binding to mettaloporphyrins and haem proteins. *Proceedings of the National Academy of Sciences USA*, 73, 3333-3337.
- Cole, J.A. (1982). Independent pathways for the anaerobic reduction of

BIBLIOGRAPHY

- nitrite to ammonia by *Escherichia coli*. *Biochemical Society Transactions*, 10, 476-478.
- Cornish-Bowden, A. (1979). *Fundamentals of Enzyme Kinetics*, pp16-38. Butterworths, London.
- Degn, H. & Wohlrab, H. (1971). Measurement of steady-state values of respiration rate and oxidation levels of respiratory pigments at low oxygen tensions. *Biochimica et Biophysica Acta*, 245, 347-355.
- Dixon, M. (1953). The effect of pH on the affinities of enzymes for substrates & inhibitors. *Biochemical Journal*, 55, 161-170.
- Dutton, P.L. (1978). Redox potentiometry: determination of midpoint potentials of oxidation-reduction components of biological electron transfer systems. *Methods in Enzymology*, 54, 411-435.
- Edwards, C., Beer, S., Siviram, A., & Chance, B. (1981). Photochemical action spectra of bacterial *a* and *o* type oxidases using a dye laser. *FEBS Letters*, 128, 205-207.
- Finlayson, S.D. & Ingledew, W.J. (1985). Cytochrome *bd* of *Escherichia coli*: its isolation and study by electron paramagnetic resonance spectroscopy. *Biochemical Society Transactions*, 13, 632-633.
- Gayda, J., Gibson, J.F., Cammack, R., Hall, D.O., & Mullinger, R.

BIBLIOGRAPHY

- (1976). Spin relaxation and exchange interaction in a 2-iron, 2-sulphur protein. *Biochimica et Biophysica Acta*, 434, 154-163.
- Gennis, R.B. (1987). The cytochromes of *Escherichia coli*. *FEMS Microbiology Reviews*, 46, 387-399.
- Goodman, G. & Leigh, J.S. (1985). Distance between the visible copper and cytochrome *a* in beef heart cytochrome oxidase. *Biochemistry*, 24, 2310-2317.
- Green, G.N. & Gennis, R.B. (1983). Isolation and characterisation of an *Escherichia coli* mutant lacking cytochrome *d* terminal oxidase. *Journal of Bacteriology*, 154, 1269-1275.
- Green, G.N., Kranz, R.G., Lorence, R.M., & Gennis, R.B. (1984). Identification of subunit I as the cytochrome *b₅₅₈* component of the cytochrome *d* terminal oxidase complex of *Escherichia coli*. *Journal of Biological Chemistry*, 259, 7994-7997.
- Green, G.N., Lorence, R.M., & Gennis, R.B. (1986). Specific overproduction and purification of the cytochrome *b₅₅₈* component of the cytochrome *d* complex from *Escherichia coli*. *Biochemistry*, 25, 2309-2314.
- Green, G.N., Fang, H., Lin, R., Newton, G., Mather, M., Georgiou, C.D., & Gennis, R.B. (1988). The nucleotide sequence of the *cyd*

BIBLIOGRAPHY

- locus encoding the two subunits of the cytochrome *d* terminal oxidase complex of *Escherichia coli*. *Journal of Biological Chemistry*, 263, 13138-13142.
- Gudat, J.C., Singh, J., & Wharton, D.C. (1973). Cytochrome oxidase from *Pseudomonas aeruginosa*: purification and some properties. *Biochimica et Biophysica Acta*, 292, 376-390.
- Haddock, B.A., Downie, J.A., & Garland, P.B. (1976). Kinetic characterisation of the membrane-bound cytochromes of *Escherichia coli* grown under a variety of conditions by using a stopped-flow dual-wavelength spectrophotometer. *Biochemical Journal*, 154, 285-294.
- Hata, A., Kirino, Y., Matsuura, K., Itoh, S., Hiyama, T., Konishi, K., Kita, K., & Anraku, Y. (1985). Assignment of ESR signals of *Escherichia coli* terminal oxidase complexes. *Biochimica et Biophysica Acta*, 810, 62-72.
- Hata-Tanaka, A., Matsuura, K., Itoh, S., & Anraku, Y. (1987). Electron flow and haem-haem interaction between cytochromes *b*-558, *b*-595, and *d* in a terminal oxidase of *Escherichia coli*. *Biochimica et Biophysica Acta*, 893, 289-295.
- Hendler, R.W. & Schragar, R.I. (1979). Potentiometric analysis of *Escherichia coli* cytochromes in the optical absorbance range of

BIBLIOGRAPHY

- 500nm to 700nm. *Journal of Biological Chemistry*, 254, 11288-11299.
- Henry, Y. & Banerjee, R. (1973). Electron paramagnetic studies of nitric oxide haemoglobin and its derivatives: isolated subunits and nitric oxide hybrids. *Journal of Molecular Biology*, 73, 469-482.
- Hirasawa, M., Gray, K.A., Shaw, R.W., & Knaff, D.B. (1987). Spectroscopic properties of spinach catalase. *Biochimica et Biophysica Acta*, 911, 37-44.
- Hori, H., Ikeda-Saito, M., & Yonetani, T. (1981). Single crystal EPR of myoglobin nitroxide. Freezing induced reversible changes in the molecular orientation of the ligand. *Journal of Biological Chemistry*, 256, 7849-7855.
- Hubbard, J.A.M., Hughes, M.N., & Poole, R.K. (1983). Nitrite, but not silver, ions induce spectral changes in *Escherichia coli* cytochrome *d*. *FEBS letters*, 164, 241-243.
- Ingledeu, W.J. (1983). The electron transport chain of *Escherichia coli* grown anaerobically with fumarate as terminal electron acceptor: an electron paramagnetic study. *Journal of General Microbiology*, 129, 1651-1659.

BIBLIOGRAPHY

- Johnson, M.K., Thomson, A.J., Walsh, T.A., Barber, D., & Greenwood, C. (1980). Electron paramagnetic resonance studies on *Pseudomonas* nitrosyl nitrite reductase: Evidence for multiple species in the electron paramagnetic resonance spectra of nitrosyl haemoproteins. *Biochemical Journal*, 189, 285-294.
- Jones, C.W. (1973). The inhibition of *Azotobacter vinelandii* terminal oxidases by cyanide. *FEBS Letters*, 36, 347-350.
- Kauffman, H.F., DerVartanian, D.V., Van Gelder, B.F., & Wampler, J. (1975). EPR studies on cytochrome components in phosphorylating particles of *Azotobacter vinelandii*. *Journal of Bioenergetics*, 7, 215-221.
- Kauffman, H.F. & Van Gelder, B.F. (1973a). The respiratory chain of *Azotobacter vinelandii*: spectral properties of cytochrome *d*. *Biochimica et Biophysica Acta*, 305, 260-267
- Kauffman, H.F. & Van Gelder, B.F. (1973b). The respiratory chain of *Azotobacter vinelandii*: the effect of cyanide on cytochrome *d*. *Biochimica et Biophysica Acta*, 314, 276-283.
- Kauffman, H.F. & Van Gelder, B.F. (1974). The respiratory chain of *Azotobacter vinelandii*: the effect of cyanide in the presence of substrates. *Biochimica et Biophysica Acta*, 333, 218-227.

BIBLIOGRAPHY

- Kauffman, H.F., Van Gelder, B.F., & DerVartanian, D.V. (1980). Effect of ligands on cytochrome *d* from *Azotobacter vinelandii*. *Journal of Bioenergetics and Biomembranes*, 12, 265-277.
- Kim, C. & Hollocher, T.C. (1984). Catalysis of nitrosyl transfer reactions by a dissimilatory nitrite reductase (cytochrome *cd₁*). *Journal of Biological Chemistry*, 259, 2092-2099.
- Kita, K., Yamato, I., & Anraku, Y. (1978). Purification and properties of cytochrome *b₅₆₆* in the respiratory chain of aerobically grown *Escherichia coli* K12. *Journal of Biological Chemistry*, 253, 8910-8915.
- Kita, K., Konishi, K., & Anraku, Y. (1984a). Terminal oxidases of *Escherichia coli* aerobic respiratory chain: purification and properties of cytochrome *b₅₆₂-o* complex from cells in the early exponential phase of aerobic growth. *Journal of Biological Chemistry*, 259, 3368-3374.
- Kita, K., Konishi, K., & Anraku, Y. (1984b). Terminal oxidases of *Escherichia coli* aerobic respiratory chain: purification and properties of cytochrome *b₅₅₈-d* complex from cells grown with limited oxygen and evidence of branched electron carrying systems. *Journal of Biological Chemistry*, 259, 3375-3381.
- Knopp, J.A. & Longmuir, I.S. (1972). Intracellular measurement of

BIBLIOGRAPHY

- oxygen by quenching of fluorescence of pyrenebutyric acid. *Biochimica et Biophysica Acta*, 279, 393-397.
- Koland, J.G., Miller, M.J., & Gennis, R.B. (1984). Potentiometric analysis of the purified cytochrome *d* terminal oxidase complex from *Escherichia coli*. *Biochemistry*, 23, 1051-1056.
- Kon, H. & Kataoka, N. (1969). Electron paramagnetic resonance of nitric oxide-protohaem complexes with some nitrogenous base. Model systems of nitric oxide haemoproteins. *Biochemistry*, 8, 4757-4762.
- Konishi, K., Ouchi, M., Kita, K. & Horikoshi, I. (1986). Purification and properties of a cytochrome *b₅₆₀-d* complex, a terminal oxidase of the aerobic respiratory chain of *Photobacterium phosphoreum*. *Journal of Biochemistry*, 99, 1227-1236.
- Kranz, R.G. & Gennis, R.B. (1983). Immunological characterisation of the cytochrome *o* terminal oxidase of *Escherichia coli*. *Journal of Biological Chemistry*, 258, 10614-10621.
- Kranz, R.G. & Gennis, R.B. (1984a). Immunological investigation of the distribution of cytochromes related to the two terminal oxidases of *Escherichia coli* in other Gram negative bacteria. *Journal of Bacteriology*, 161, 709-713.

BIBLIOGRAPHY

- Kranz, R.G. & Gennis, R.B. (1984b). Characterisation of the cytochrome *d* terminal oxidase complex of *Escherichia coli* using polyclonal and monoclonal antibodies. *Journal of Biological Chemistry*, 259, 7998-8003.
- Kumar, C., Poole, R.K., Salmon, I., & Chance, B. (1985). The oxygen reaction of the cytochrome *d* terminated respiratory chain of *Escherichia coli* at sub-zero temperatures: kinetic resolution of two high spin cytochromes. *FEBS Letters*, 190, 227-231.
- Kyte, J. & Doolittle, R.F. (1982). A simple method for displaying the hydropathic character of a protein. *Journal of Molecular Biology*, 157, 105-132.
- Lakshminarayanaiah, N. (1976). *Membrane Electrodes*, pp328-333. Academic Press, New York.
- Lawford, H.G. & Haddock, B.A. (1973). Respiration driven proton translocation in *Escherichia coli*. *Biochemical Journal*, 136, 217-220.
- Lessler, M.A. & Brierley, G.P. (1969). Oxygen electrode measurements in biochemical analysis. *Methods of Biochemical Analysis*, 17, 1-29.

BIBLIOGRAPHY

- Lin, E.C.C. & Kuritzkes, D.R. (1987). Pathways for anaerobic electron transport. In *Escherichia coli and Salmonella typhimurium cellular and molecular biology*, I, pp170-200. Edited by Ingraham, J., Low, K.B., Magasanik, B., Schaechter, M., Umberger, H.E., & Neidhart, F.C. American Society for Microbiology, Washington DC.
- Longmuir, I.S. (1957). Respiration rate of rat liver cells at low oxygen concentrations. *Biochemical Journal*, 65, 378-382.
- Lorence, R.M., Green, G.N., & Gennis, R.B. (1984a). Potentiometric analysis of the cytochromes of an *Escherichia coli* mutant strain lacking the cytochrome *d* terminal oxidase complex. *Journal of Bacteriology*, 157, 115-121.
- Lorence, R.M., Miller, M.J., Borochoy, A., Faiman-Weinberg, R., & Gennis, R.B. (1984b). Effects of pH and detergent on the kinetic and electrochemical properties of the purified cytochrome *d* terminal oxidase complex of *Escherichia coli*. *Biochimica et Biophysica Acta*, 790, 148-153.
- Lorence, R.M., Koland, J.G., & Gennis, R.B. (1986). Coulometric and spectroscopic analysis of the purified cytochrome *d* complex of *Escherichia coli*: Evidence for the identification of "cytochrome *a*₁" as cytochrome *b*₅₉₅. *Biochemistry*, 25, 2314-2321.
- Lorence, R.M., Carter, K., Green, G.N., & Gennis, R.B. (1987).

BIBLIOGRAPHY

- Cytochrome *b₅₅₈* monitors the steady state redox state of the ubiquinone pool in the aerobic respiratory chain of *Escherichia coli*. *Journal of Biological Chemistry*, 262, 10532-10536.
- Lorence, R.M., Carter, K., Gennis, R.B., Matsushita, K., & Kaback, H.R. (1988). Trypsin proteolysis of the cytochrome *d* complex of *Escherichia coli* selectively inhibits ubiquinol oxidase activity while not affecting *N,N,N',N'*-tetramethylphenylenediamine oxidase activity. *Journal of Biological Chemistry*, 263, 5271-5276.
- Lowry, O.H.; Rosenbrough, N.J.; Farr, A.L.; & Randall, R.J. (1951). Protein determination with the Folin phenol reagent. *Journal of Biological Chemistry*, 191, 265-275.
- Lukat, G.S., Jabro, M.N., Rodgers, K.R., & Goff, H.M. (1988). Electron paramagnetic resonance spectroscopy of thyroid peroxidase. *Biochimica et Biophysica Acta*, 954, 265-270.
- Mascarenhas, R., Wei, Y., Scholes, C.P., & King, T.E. (1983). Interaction in cytochrome *c* oxidase between cytochrome *a₃* ligated with nitric oxide and cytochrome *a*. *Journal of Biological Chemistry*, 258, 5348-5351.
- Matsushita, K., Patel, L., & Kaback, H.R. (1984). Cytochrome *o* type oxidase from *Escherichia coli*. Characterisation of the enzyme and mechanism of electrochemical proton gradient generation.

BIBLIOGRAPHY

- Biochemistry*, 23, 4703-4714.
- Meinhardt, S.W., Gennis, R.B., & Ohnishi, T. (1989). EPR studies of the cytochrome *d* complex of *Escherichia coli*. *Biochimica et Biophysica Acta*, in the press.
- Meyer, D.J. (1973). Interaction of cytochrome oxidases *aa₃* and *d* with nitrite. *Nature New Biology*, 245, 276-277.
- Miller, M.J. & Gennis, R.B. (1983). The purification and characterisation of the cytochrome *d* terminal oxidase complex of the *Escherichia coli* aerobic respiratory chain. *Journal of Biological Chemistry*, 258, 9159-9165.
- Miller, M.J., & Gennis, R.B. (1985). The cytochrome *d* complex is a coupling site in the aerobic respiratory chain of *Escherichia coli*. *Journal of Biological Chemistry*, 260, 14003-14008.
- Miller, M.J., Hermondson, M., & Gennis, R.B. (1988). The active form of the cytochrome *d* terminal oxidase complex of *Escherichia coli* is a heterodimer containing one copy of each of the two subunits. *Journal of Biological Chemistry*, 263, 5235-5240.
- Moodie, A.D. & Ingledew, W.J. (1988). Photochemical evidence for cytochrome *b₅₉₅* of *Escherichia coli* *bd*-oxidase binding and reducing O₂. *European Bioenergetics Conference Short Reports*, 5,

BIBLIOGRAPHY

97.

Morse, R.H. & Chan, S.I. (1980). Electron paramagnetic resonance studies of nitrosyl ferrous haem complexes. Determination of an equilibrium between two conformations. *Journal of Biological Chemistry*, 255, 7876-7882.

Muhoberac, B.B. & Wharton, D.C. (1983). Electron paramagnetic resonance study of the interaction of some anionic ligands with oxidised *Pseudomonas* cytochrome oxidase. *Journal of Biological Chemistry*, 258, 3019-3027.

Naqui, A., Chance, B., & Cadenas, E. (1986). Reactive oxygen intermediates in biochemistry. *Annual Reviews of Biochemistry*, 55, 137-166.

Nicholls, D.G. (1982). *Bioenergetics: an introduction to the chemiosmotic theory*, pp107. Academic Press, London.

Nikaido, H. & Vaara, M. (1987). Outer membrane. In *Escherichia coli and Salmonella typhimurium cellular and molecular biology*, I, pp7-22. Edited by Ingraham, J., Low, K.B., Magasanik, B., Schaechter, M., Umberger, H.E., & Neidhart, F.C. American Society for Microbiology, Washington DC.

Ohnishi, T., Blum, H., Harmon, H.J., & Hompo, T. (1982). Location of

BIBLIOGRAPHY

- Rieske iron-sulphur cluster in the mitochondrial membrane. In *Electron transport and oxygen utilisation*, pp387-393. Edited by Ho, C. Elsevier North Holland Inc.
- Ohnishi, T., Harmon, H.J., & Waring, A.J. (1985). Electron paramagnetic resonance studies on the spacial relationship of redox components in cytochrome oxidase. *Biochemical Society Transactions*, 13, 607-611.
- Oshino, R., Oshino, N., Tamura, M., Kobilinsky, L., & Chance, B. (1972). A sensitive bacterial luminescence probe for O₂ in biochemical systems. *Biochimica et Biophysica Acta*, 273, 5-17.
- Paitian, N.A., Markossian, K.A. & Nalbandyan, R.M. (1985). The effect of nitrite on cytochrome oxidase. *Biochemical and Biophysical Research Communications*, 133, 1104-1111.
- Palmer, G. (1985). The electron paramagnetic resonance of metalloproteins. *Biochemical Society Transactions*, 13, 548-560.
- Peisach, J., Blumberg, W.E., Wittenberg, B.A., Wittenberg, J.B., & Kampa, L. (1969). Haemoglobin A: An electron paramagnetic resonance study of the effects of interchain contacts on the haem symmetry of high-spin and low-spin derivatives of ferric alpha chains. *Proceedings of the National Academy of Sciences USA.*, 63, 934-939.

BIBLIOGRAPHY

- Peterson, L.C. (1983). Determination of Michaelis parameters from differentials of progress curves. *Biochemical Journal*, 215, 589-595.
- Poole, R.K. (1983). Bacterial cytochrome oxidases: a structurally and functionally diverse group of electron transfer proteins. *Biochimica et Biophysica Acta*, 726, 205-243.
- Poole, R.K. (1988). Bacterial cytochrome oxidases. In *Bacterial energy transduction*, pp231-291. Edited by Anthony, C. Academic Press, London.
- Poole, R.K., Waring, A.J., & Chance, B. (1979). The reaction of cytochrome *o* in *Escherichia coli* with oxygen. Low temperature kinetic and spectral studies. *Biochemical Journal*, 184, 379-389.
- Poole, R.K. & Chance, B. (1981). The reaction of cytochrome *o* in *Escherichia coli* K12 with oxygen. Evidence for a spectrally and kinetically distinct cytochrome *o* in cells from oxygen limited cultures. *Journal of General Microbiology*, 126, 277-287.
- Poole, R.K., Scott, R.I., & Chance, B. (1981). The light-reversible binding of carbon monoxide to cytochrome *a₁* in *Escherichia coli* K12. *Journal of General Microbiology*, 125, 431-438.

BIBLIOGRAPHY

- Poole, R.K., Baines, B.S., Hubbard, J.A.M., M.N. Hughes, & Campbell, N.J. (1982a). Resonance Raman spectroscopy of an oxygenated intermediate species of cytochrome oxidase *d* from *Escherichia coli*. *FEBS Letters*, 150, 147-150.
- Poole, R.K., Sivaram, A., Salmon, I., & Chance, B. (1982b). Photolysis at very low temperatures of CO-ligated cytochrome oxidase (cytochrome *d*) in oxygen limited *Escherichia coli*. *FEBS Letters*, 141, 237-241.
- Poole, R.K., Kumar, C., Salmon, I., & Chance, B. (1983a). The 650nm chromophore in *Escherichia coli* is an 'Oxy-' or oxygenated compound, not the oxidised form of cytochrome oxidase *d*: an hypothesis. *Journal of General Microbiology*, 129, 1335-1344.
- Poole, R.K., Salmon, I., & Chance, B. (1983b). The reaction with oxygen of cytochrome oxidase (cytochrome *d*) in *Escherichia coli* K12: optical studies of intermediate species and cytochrome *b* oxidation at sub-zero temperatures. *Journal of General Microbiology*, 129, 1345-1355.
- Poole, R.K., Baines, B.S., Curtis, S.J., Williams, H.W., & Wood, P.M. (1984). Haemoprotein *b*-590 (*Escherichia coli*); redesignation of a bacterial 'cytochrome *a*₁'. *Journal of General Microbiology*, 130, 3055-3058.

BIBLIOGRAPHY

- Poole, R.K., Baines, B.S., & Appleby, C.A. (1986). Haemoprotein *b-590* (*E.coli*), a reducible catalase and peroxidase: evidence for its close relationship to hydroperoxidase I and "cytochrome *a₁ b*" preparation. *Journal of General Microbiology*, 132, 1525-1539.
- Poole, R.K., & Ingledew, W.I. (1987). Pathways of electrons to oxygen. In *Escherichia coli and Salmonella typhimurium cellular and molecular biology*, I, pp170-200. Edited by Ingraham, J., Low, K.B., Magasanik, B., Schaechter, M., Umberger, H.E., & Neidhart, F.C. American Society for Microbiology, Washington DC.
- Poole, R.K. & Williams, H.D. (1987). Proposal that the function of the membrane-bound cytochrome *a₁*-like haemoprotein (cytochrome *b-595*) in *Escherichia coli* is a direct electron donation to cytochrome *d*. *FEBS Letters*, 217, 49-52.
- Poole, R.K. & Williams, H.D. (1988). Formation of the 680nm-absorbing form of the cytochrome *bd* oxidase complex of *Escherichia coli* by reaction of hydrogen peroxide with the ferric form. *FEBS Letters*, 231, 243-246.
- Pudek, M.R. & Bragg, P.D. (1974). Inhibition by cyanide of the respiratory chain oxidases of *Escherichia coli*. *Archives of Biochemistry and Biophysics*, 164, 682-693.
- Pudek, M.R. & Bragg, P.D. (1976a). Trapping of an intermediate in the

BIBLIOGRAPHY

- oxidation-reduction cycle of cytochrome *d* in *Escherichia coli*.
FEBS Letters, 62, 330-333.
- Pudek, M.R. & Bragg, P.D. (1976b). Redox potentials of the cytochromes in the respiratory chain of aerobically grown *Escherichia coli*.
Archives of Biochemistry and Biophysics, 174, 546-552.
- Reid, G.A. & Ingledew, W.J. (1979). Characterisation and phenotypic control of the cytochrome content of *Escherichia coli*.
Biochemical Journal, 182, 465-472.
- Rice, C.W., & Hempfling, W.P. (1978). Oxygen-limited continuous culture and respiratory energy conservation in *Escherichia coli*.
Journal of Bacteriology, 134, 115-124.
- Salerno, J.C. (1984). Cytochrome electron spin resonance line shapes, ligand fields, and components stoichiometry in ubiquinol-cytochrome *c* oxidoreductase. *Journal of Biological Chemistry*, 259, 2331-2336.
- Salerno, J.C., McGill, J.W., & Gerstle, G.C. (1983). The electron paramagnetic resonance spectra of partially purified cytochrome *b₆f* complex from spinach. *FEBS Letters*, 162, 257-261.
- Sanchez-Crispin, J.A., Dubourdieu, M., & Chippaux, M. (1979). Localisation and characterisation of cytochromes from membrane

BIBLIOGRAPHY

- vesicles of *Escherichia coli* K-12 grown in anaerobiosis with nitrate. *Biochimica et Biophysica Acta*, 547, 198-210.
- Scott, R.I. & Poole, R.K. (1982). A re-examination of the cytochromes of *Escherichia coli* using fourth order finite difference analysis: their characterisation under different growth conditions and accumulation during the cell cycle. *Journal of General Microbiology*, 128, 1685-1696.
- Segel, I.H. (1975). *Enzyme kinetics: Behavior and analysis of steady state enzyme systems*. pp353. Wiley Interscience, New York.
- Shipp, W.S. (1972). Cytochromes of *Escherichia coli*. *Archives of Biochemistry and Biophysics*, 150, 459-472.
- Simpkin, D. (1985). *The anaerobic fumarate reductase of Escherichia coli: a study of its prosthetic groups*. Doctoral thesis, University of St.Andrews, pp150.
- Smith, A.T., Hill, S., & Anthony, C. (1988). The purification and characterisation of the cytochrome d terminal oxidase complex of *Klebsiella pneumoniae* and determination of its oxygen affinity: proposal of a physiological role during microaerobic nitrogen fixation. *Fifth European Bioenergetics Conference, Short Reports*, 5, pp99.

BIBLIOGRAPHY

- Sokal, R.R. & Rohlf, F.J. (1981). *Biometry*. pp468. W.H. Freeman & Co., San Fransisco.
- Stevens, T.H., & Chan, S.I. (1981). Histidine is the axial ligand to cytochrome a₃ in cytochrome c oxidase. *Journal of Biological Chemistry*, 256, 1069-1071.
- Stolzenberg, A.M., Strauss, S.H., & Holm, R.H. (1981). Iron(II,III)-chlorin and isobacteriochlorin complexes. Models of haem prosthetic groups in nitrite and sulphite reductases. *Journal of the American Chemical Society*, 103, 4673-4778.
- Timkovich, R., Cork, M.S., Gennis, R.B., & Johnson, P.Y. (1985). Proposed structure of haem d, a prosthetic group of bacterial terminal oxidases. *Journal of the American Chemical Society*, 107, 6069-6075.
- Timkovich, R. & Robinson, M.K. (1979). Evidence for water as the product for oxygen reduction by cytochrome cd. *Biochemical and Biophysical Research Communications*, 88, 649-655.
- Vanderkooi, J.M., Maniara, G., Green, T.J., & Wilson, D.F. (1987). An optical method for measurement of dioxygen concentration based upon quenching of phosphorescence. *Journal of Biological Chemistry*, 262, 5476-5482.

BIBLIOGRAPHY

- Walker, F.A., Reis, D., & Balke, V.L. (1984). Models of cytochrome *b*. EPR studies of low-spin iron(III) tetraphenylporphyrins. *Journal of the American Chemical Society*, 106, 6888-6898.
- Wallace, J. & Young, I.G. (1977). Role of quinones in electron transport to oxygen and nitrate in *Escherichia coli*: studies with a *ubiA*⁻ and *menA*⁻ double quinone mutant. *Biochimica et Biophysica Acta*, 461, 84-100.
- Walsh, T.A., Johnson, M.K., Greenwood, C., Barber, D., Springall, J.P., & Thomson, A.J. (1979). Some magnetic properties of *Pseudomonas* cytochrome oxidase. *Biochemical Journal*, 177, 29-39.
- Wikstrom, M., Krab, K., & Saraste, M. (1981). *Cytochrome oxidase. A synthesis*. Published by Academic Press, London.
- Williams, H.D. & Poole, R.K. (1987). The cytochromes of *Acetobacter pasteurianus* NCIB 6428. Evidence of a role for a cytochrome *a*₁-like haemoprotein in electron transfer to cytochrome *d*. *Journal of General Microbiology*, 133, 2461-2472.
- Wilson, D.F., Rumsey, W.L., Green, T.J., & Vanderkooi, J.M. (1988). The oxygen dependence of mitochondrial oxidative phosphorylation measured by a new optical method for measuring oxygen concentration. *Journal of Biological Chemistry*, 263, 2712-2718.

BIBLIOGRAPHY

- Wittenberg, B.A. & Wittenberg, J.B. (1985). Oxygen pressure gradients in isolated cardiac myocytes. *Journal of Biological Chemistry*, 260, 6548-6554.
- Wood, P.M. (1984). Bacterial proteins with CO-binding *b*- or *c*- type haem: functions and absorption spectroscopy. *Biochimica et Biophysica Acta*, 768, 293-317.
- Wray, J.L. & Filner, J.L. (1970). Structural and functional relationships of enzyme activities induced by nitrate in Barley. *Biochemical Journal*, 119, 715-725.
- Yamanaka, T. (1964). Identity of *Pseudomonas* cytochrome oxidase with *Pseudomonas* nitrite reductase. *Nature*, 204, 253-255.
- Yang, F., Yu, L., Yu, C., Lorence, R.M., & Gennis, R.B. (1986). Use of an azido-ubiquinone derivative to identify subunit I as the ubiquinol binding site of the cytochrome *d* terminal oxidase complex of *Escherichia coli*. *Journal of Biological Chemistry*, 261, 14987-14990.
- Yonetani, T., Yamamoto, H., Erman, J.E., Leigh, J.S., & Reed, G.H. (1972). Electromagnetic properties of haemoproteins: optical and electron paramagnetic resonance characteristics of nitric oxide derivatives of metalloporphyrin-apohaemoprotein complexes. *Journal of Biological Chemistry*, 247, 2447-2455.

BIBLIOGRAPHY

- Yoshimura, T., Ozaki, T., Shintani, Y., & Watanabe, H. (1979). Electron paramagnetic resonance of nitrosylprotohaem dimethyl ester complexes with imidazole derivatives as model systems for nitrosylhaemoproteins. *Archives of Biochemistry and Biophysics*, 193, 301-313.
- Young, L.J. & Seigel, L.M. (1987). On the reactions of ferric haem proteins with nitrite and sulphite. *Biochemistry*, 27, 2790-2800.